Australian Geomechanics Volume 61 No 1 MARCH 2026

ISSN 0818-9110

AUSTRALIAN GEOMECHANICS

JOURNAL AND NEWS OF THE AUSTRALIAN GEOMECHANICS SOCIETY ISSN 0818-9110

VOLUME 61: NO.1 MARCH 2026

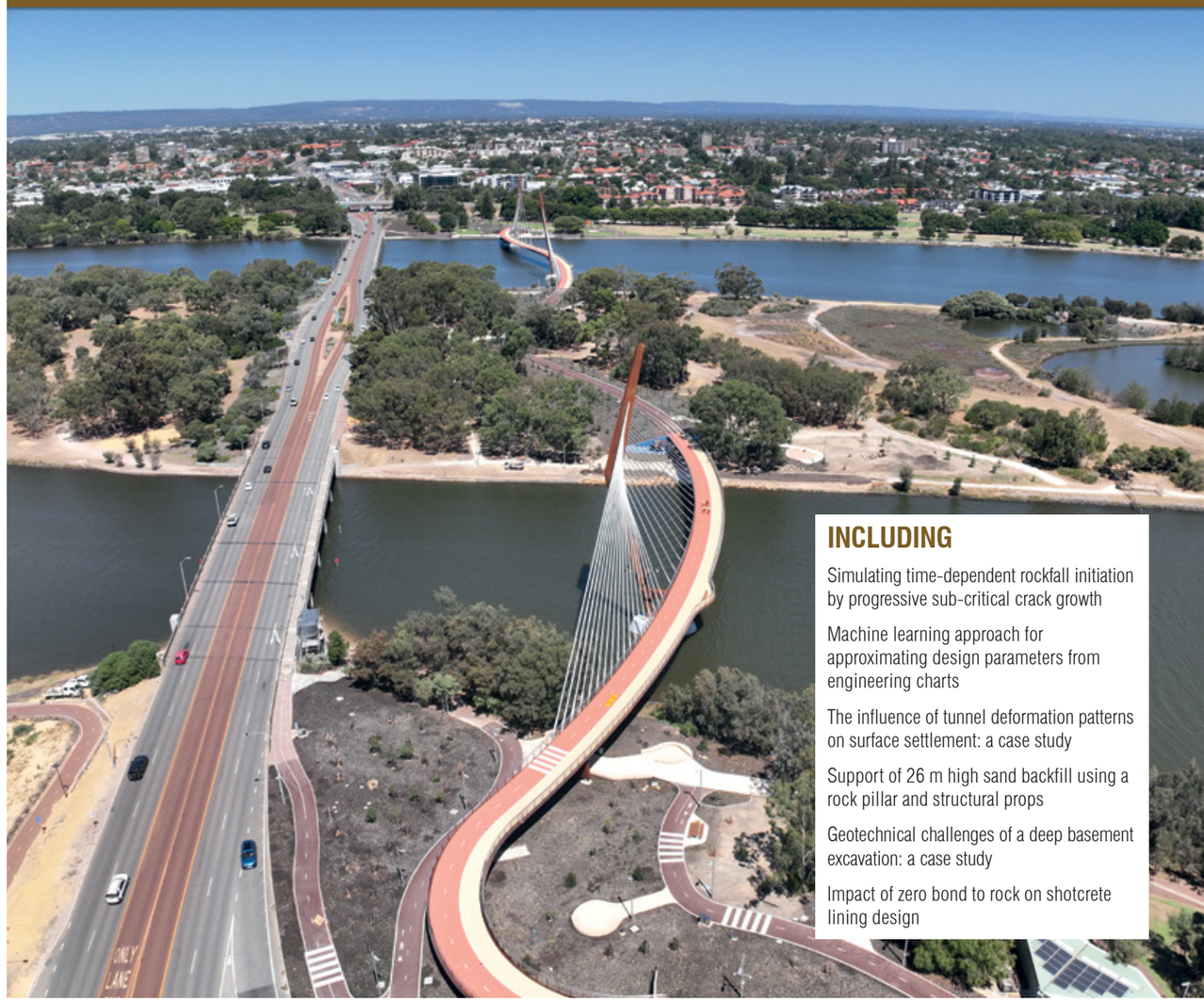

INCLUDING

AUSTRALIAN GEOMECHANICS SOCIETY

A technical society of
ENGINEERS AUSTRALIA

Reducing geotechnical uncertainty

INSITU GEOTECH SERVICES

reducing geotechnical uncertainty

COMPREHENSIVE RANGE OF
IN SITU TESTING, SAMPLING
AND GEOTECHNICAL SERVICES

mick@insitu.com.au mark@insitu.com.au

0407 467 025 **0437 824 776**

ISO 9001 Quality Management Systems CERTIFIED FS787470

ISO 45001 Occupational Health and Safety Management CERTIFIED OHS787471

insitu.com.au

BRISBANE | MELBOURNE | SYDNEY | HOBART | PERTH | TOWNSVILLE | PNG

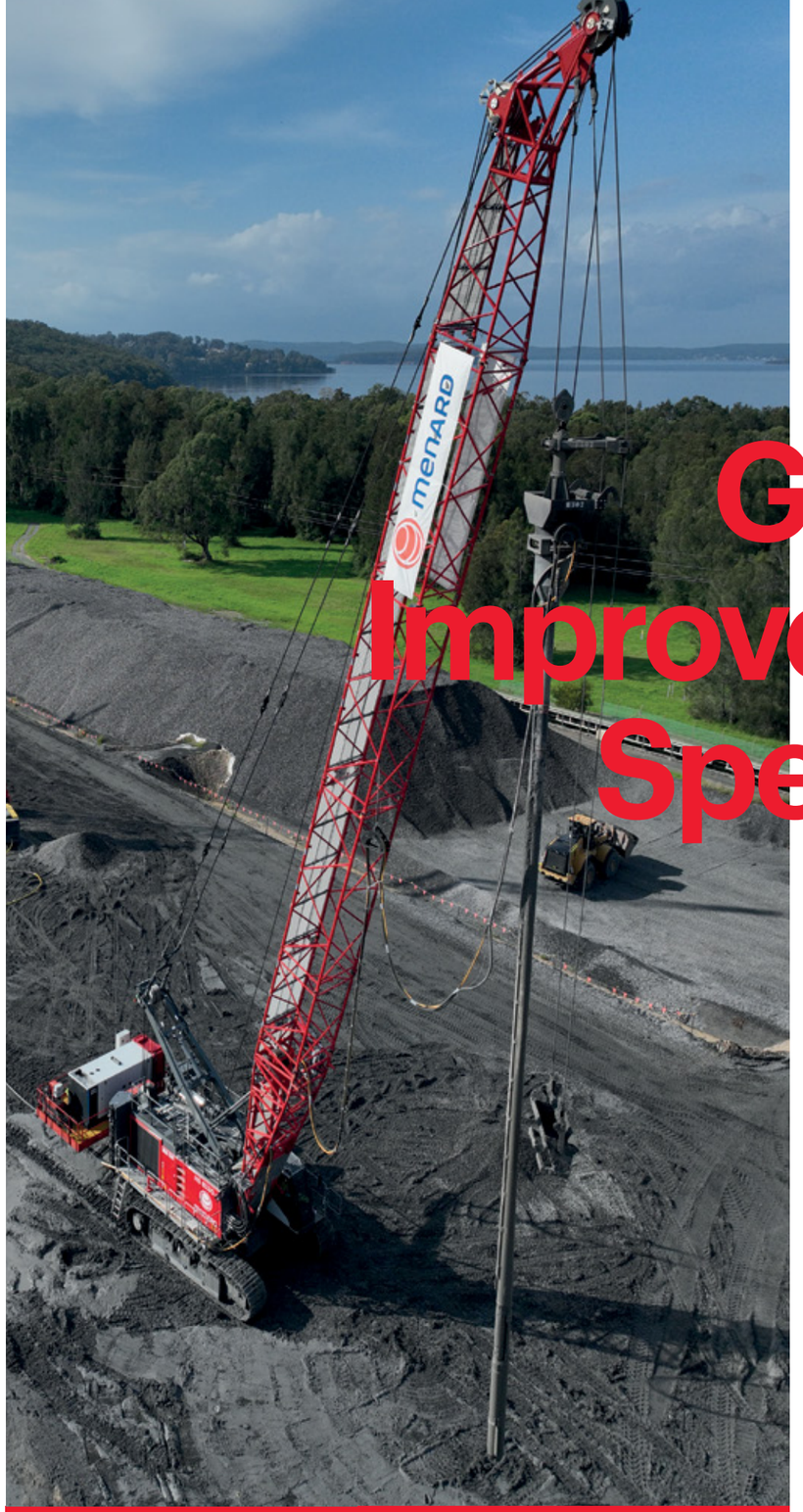

Eraring Tailings Dam, New South Wales

Menard delivers innovative ground improvement solutions to the dams, tailings, and mining sectors across Australia. At the Eraring Tailings Dam, Menard mitigated undrained and seismic liquefaction risks through precision-installed Vibro Stone Columns, staged earthworks, and real-time instrumentation, achieving an increase in factor of safety above industry recommendations. The Design & Construct delivery model, combined with tailored solutions, also reduced CO_2 emissions by 84% compared to conventional alternatives.

Ground Improvement Specialist

CMC
Stone Columns
Vertical Drains
Mass Soil Mixing
Dynamic Compaction
Soil Mixing
High Energy Impact Compaction (HEIC)
Menard Vacuum™
Rapid Impact Compaction (RIC)
Slurry Walls
Jet Grouting
Dynamic Replacement
Bi-modulus Columns
Compaction Grouting
Vibrocompaction
Anchoring
Rock Grouting
Micropiling

Visit menardoceania.com.au

Sydney (head office) +61 2 9491 7100
Brisbane +61 428 829 275
Melbourne +61 407 926 767
Adelaide +61 407 926 767
Perth +61 450 402 239
Auckland (NZ) +64 22 541 6134

At Menard, we are leaders in our industry and have a proven track record in delivering small and large ground improvement works, in this case for the tailings and dam industry. With over 25 different techniques, Menard can deliver the right solution for your project.

menard

AUSTRALIAN GEOMECHANICS

JOURNAL AND NEWS OF THE AUSTRALIAN GEOMECHANICS SOCIETY

VOLUME 61: NO.1 MARCH 2026

AUSTRALIAN GEOMECHANICS SOCIETY

Published by

**Australian Geomechanics Society Limited,
National Secretariat**

**PO Box 7, The Gap, QLD 4061
T: 07 3705 5971**

ISSN 0818-9110

ENGINEERS AUSTRALIA

**Australian Geomechanics Society Limited
is a technical society of Engineers Australia.**

Cover image: Boorloo Bridge, Perth, Western Australia
Image: Causeway Link Alliance, 2025.
Story: Matthieu Duong and Su Kwong Tan

Cable-stayed pedestrian and cyclist bridge crossing the Swan River in Perth, Western Australia, shown here adjacent to the existing Causeway corridor. The curved deck alignment and pylon geometry reflect traditional heritage elements such as the digging sticks and boomerang, acknowledging local cultural narratives expressed through form. From a geotechnical perspective, the riverine alluvial setting is characterised by spatially variable soils and elevated groundwater, and construction in or near water influenced foundation selection, installation methodology and deformation control. Geotechnical design and construction staging focused on serviceability performance and control of construction-related ground movements and groundwater conditions. Conceptually, the bridge substructure relies on piled foundations, while the approach embankments are supported by ground improvement using rigid inclusions combined with preloading or surcharging to manage settlement.

CONTENTS

TECHNICAL PAPERS

[All papers have been refereed in accordance with the full HERDC review process, unless stated otherwise]

AUSTRALIAN GEOMECHANICS SOCIETY BOARD OF DIRECTORS, NATIONAL STAKEHOLDERS GROUP, MEDIA AND ADMIN SUPPORT

TITLE	NAME	EMAIL
BOARD OF DIRECTORS		
Mr	Timothy THOMPSON *Director, Chair of Board*	chair@geomechanics.org.au
Dr	David LACEY *Director*	dlacey@fsg-geotechnics.com.au
Dr	Amir SHAHKOLAHI *Director*	amir@globalsynthetics.com.au
Ms	Joanna SYLVESTER *Director*	joanna.sylvester@ghd.com
Dr	Ali PARSA-PAJOUH *Director*	aparsa@jkgeotechnics.com.au
Mr	Darren PAUL *Appointed Director*	darren.paul@wsp.com
NATIONAL STAKEHOLDERS GROUP		
Dr	Davide GUCCIONE *Newcastle Chapter Chair*	davide.guccione@newcastle.edu.au
Mr	Mehdi TAMADON *New South Wales Chapter Chair*	mehdi.tamadon@ghd.com
Mr	Jared PRIDDLE *Queensland Chapter Chair*	jpriddle@fsg-geotechnics.com.au
Ms	Lauren AMATO *South Australia & Northern Territory Chapter Chair*	lauren.amato@arup.com
Dr	Ashley DYSON *Tasmania Chapter Chair*	ashley.dyson@utas.edu.au
Dr	Yuqi TAN *Victoria Chapter Chair*	yuqit@atcwilliams.com.au
Mr	Eddy YONG *Western Australia Chapter Chair*	per@geomechanics.org.au
Prof	Muhammad SHAZZAD HOSSAIN *ISSMGE Australian Representative*	muhammad.hossain@uwa.edu.au
Dr	Robert BERTUZZI *ISRM Australian Representative*	robert.bertuzzi@psm.com.au
Ms	Megan PACKER *IAEG Australian Representative*	megan.packer@psm.com.au
Dr	Hugo E ACOSTA MARTINEZ *Editor, Australian Geomechanics*	editor@geomechanics.org.au
INVITED MEMBERS, GENERAL MANAGER		
Mrs	Natalie QUINLISK *Women in AGS Chair*	natalie.quinlisk@jacobs.com
Mrs	Emilia STOCKS *NZGS Chair*	chair@nzgs.org
Mr	Jon GIBBS *AGS General Manager*	operations@geomechanics.org.au
MEDIA AND ADMIN SUPPORT		
Ms	Sara LANESMAN *Advertisement, Australian Geomechanics*	lanesman@optusnet.com.au
Mr	James ROBINSON *Web Support*	support@geomechanics.org.au

VIEW FROM THE CHAIR

MARCH 2026

I concluded some issues ago that these 'View from the Chair' pieces get read by few people. Like most printed pages, there is no feedback loop for immediate gratification or validation to see thumbs up (or thumbs down), but I have occasionally received a message from an AGS colleague or friend (all over 45 years of age) with a question or compliment, which I always appreciate. While I have collected a little more verbal feedback (with emphasis on 'a little'), I recall receiving about 6 total emails or texts relating to what I have written in 8 total 'View from the Chair' editorials for the journal over two years. So my documented feedback has been about 0.75 communications per editorial – the stuff of journalistic dreams - and I would guess based on smelling the air that the average readership would be in the low double figures, perhaps 25 to 50 readers, on average, per editorial. Because several of the pieces have been about AGS governance and strategy – inherently boring topics for most engineers, which I have acknowledged - preparing them has helped me to organise, and to refine my own thinking in a way that wouldn't have happened otherwise. The pieces might just be too long, or they might suffer from too few images of cracked foundations, or not enough paleo-channels, or too many hyphens and too many conjunctions. But I have really enjoyed and have found value in writing what admittedly at times has felt like a personal journal entry relating to my profession. While I may submit more editorials in the future – and the occasional technical paper – this will be my last as the AGS National Chair, hence the above reflection.

On a few occasions I have learned or re-learned that a presentation should start with a summary for the audience of what they're about to hear. So in presentation format, you may be about to read about Engineers Australia (EA), politics in the United States, infrastructure in New York City, China, back to EA and the AGS.

In representation of the AGS, I attended EA's Forums meeting in March 2025 along with representatives of the EA-affiliated learned societies and colleges. For one of the sessions involving around 70 people, we were separated by tables and asked to identify the biggest challenges facing the engineering profession(s). My table discussed climate change, infrastructure resilience, an inadequate supply of future engineers, and one person mentioned the lack of engineers in positions of decision making. I think that last concern deserves consideration and does have relevance, but as ideas from all tables converged, and votes were tabulated, I was surprised to see that the need for more engineers in positions of decision-making (or 'at the table') was getting pushed from all directions and shifted up to become recognised as our biggest challenge. I had/have my doubts about this and shared my opinion through a microphone that while I think the issue should be on the list, it felt a bit self-indulging to see it at the top.

My high school years in Las Vegas coincided with a lot of local debate relating to Yucca Mountain, a site on federal land roughly 125 km north which in 1987 had been proposed by the federal government as a disposal location for nuclear fuel and high-level radioactive waste. In 1994, and then as a second year Civil Engineering student at Purdue University, I first learned about someone calling-out the lack of leaders educated as engineers in the United States Congress. Norman Augustine was the CEO of Lockeed Martin at the time, and he coupled this observation with commentary about the interactions between engineering and society. He also popularised an expression that 'For every scientific (or engineering) action, there is an equal and opposite social reaction'. I counted six of 535 members of the United States Congress with an engineering degree (the AI tells me now that it was actually nine). There was also a PhD physicist and a handful of other scientists, but the overall limited number of engineers and scientists in political leadership - who ultimately made decisions of far-reaching technical consequence - was curious to me. In 1995 with a few days free from study, I drove from Indiana to Washington DC where extended family offered me a bed and warm meals in support of a visit to the US Congress. I had called in advance and aimed to meet as many of the engineers as possible along with my two non-engineer Nevada state senators. For good measure I also contacted the physicist and another scientist.

The three engineers I ultimately spoke to or corresponded with were all proud of their educational background and readily agreed to the need for more technically minded leaders. John Hostettler (R-IN) had previously made public statements about how his degree in mechanical engineering enabled him to pursue working solutions to problems that others might not see. He welcomed me into his office, which I remain appreciative of, and I asked him about the complexities of social and environmental challenges, and what insight his preparation as an engineer could provide to a scenario like Yucca Mountain. For the sake of transparency, I wasn't then nor am now opposed to nuclear energy – Purdue has its own very small reactor on campus and I had friends who studied it – but the emotions were high, and the 'not in my backyard' effect was strong. Still in the wake of a partial reactor meltdown in 1979 at Three Mile Island in Pennsylvania and the Chernobyl accident in 1986, the public was understandably concerned about safety and it permeated the culture. From Mr. Burns in an episode of the Simpsons: 'Homer, your bravery and quick thinking have turned a potential Chernobyl into a mere Three Mile Island.' The Yucca Mountain debate included not just Nevada, but every state with rail lines where the waste would be transported to Nevada, and the politics reached local television screens between repeats of 'Cheers' to educate everyone on just how unsafe the whole plan was. Or on just how safe. Public safety depended on which ad came up. Our conversation was friendly and I got a better sense of how he engaged with colleagues on matters of technical and policy importance. While I don't think Hostettler had previously implied that engineers can fix anything, I had started to wonder if having more engineers at the table of the Yucca Mountain debates would make any difference at all. And if there were more engineers, would it be a good thing if they all lined up on one side of the issue, likely in support? And if I disagreed with the social politics of an engineer, would I still want to support them for public office?

I spoke on the phone with Joe Skeen (R-NM) and corresponded with Jay C. Kim (R-CA), both with engineering degrees. I also spoke with two scientists: Vern Ehlers (R-MI) in his office and Roscoe Bartlett (R-MD) over the phone. To avoid doubt, 'R' is for 'Republican' and a trend was apparent. Eight of the nine representatives with engineering degrees at the time were Republican. I was also able to meet my home senators Harry Reid (D-NV) and Richard Bryan (D-NV) in their respective offices, knowing in advance that both were representing their Nevada state constituents in adamant opposition to the federal government's plans for Yucca Mountain. To avoid doubt again, the 'D' is for 'Democrat'. My suspicion after speaking with them all was that the problem might not be too few engineers and scientists in the US Congress – I did in my conversations hear from most about their engagement with a lot of technical advisors at different levels of government. By the way, Churchill popularised the expression that scientists should be 'on tap, not on top'. Perhaps the problem was too many lawyers. But then a legislature is there to make laws, so why be surprised at so many lawyers? Thirty years later, the number of members of the US Congress with an engineering degree is not much different: the AI tells me in 2026 that it is now ten.

From early 2002 to mid-2004 I spent most of my days logging boreholes somewhere around New York City. I worked in many wonderful neighbourhoods that I would not have sought out at the time if not sent there for a geotechnical investigation. This included a couple of months in 2003 working on the Upper East Side and East Harlem for the Second Avenue Subway Project. One day after finishing I attended a public consultation session for the project and observed members of the public use their right to 2 or 3 minutes to post questions or ridicule a panel of representatives from the project (one member of the public just called them all idiots and didn't post a question, which is what the consultation process enables there and obviously here and in many places and is probably a healthy outlet, if peaceful). Construction of Phase 1 started some years later in 2007, and 2.9 km of tunnel with three new stations opened in 2017.

If you work in or around the Civil Engineering profession in New York City, it is inevitable that you will learn about Robert Moses. Starting as the Parks Commissioner in 1934, and never publicly elected to anything, Moses accumulated a gargantuan amount of administrative power over some decades and drove public works projects at an extraordinary pace. While he didn't want to acknowledge some instances of shifting project plans to address the concerns of the wealthy or well-positioned, he prided himself on not shifting, and on a willingness to construct projects where they best served the public, regardless of who was affected. And therein was the controversy, because undeniably, lower income residents living in dense apartment blocks tended to feel the disruption of his projects most often. Un-checked by New York City mayors and New York State governors as they recognised he held more public sway than they usually did, having steered highways through the hearts of several thriving and often immigrant communities, he finally was stopped in 1971 when trying to build an elevated ten lane highway across Lower Manhattan.

Moses was incredibly energetic and very skilled at overcoming barriers, and at 'getting things done'. An online map entitled 'Achievements of Robert Moses' can clarify the scale of what he did, noting that he had a preference for bridges over tunnels, as he liked visible monuments. While not an engineer himself, he saw the work of engineers in particular as being at the forefront of unquestionable progress. The power of Moses was critically dissected in a 1974 Pulitzer Prize winning book of more than 1300 pages. 'The Power Broker' by Robert Caro is critical reading for modern New York City history and became one of the most influential books for city planning in the United States shortly after publication. Sub-titled 'Robert Moses and the Fall of New York', the final assessment of Moses was clear to anyone reading the cover. He was an unpleasant person in many regards, but if there was corruption, it was related to the creative wielding of administrative power, and not the lining of his own pockets or those of others with public money. He 'got things done' as an authoritarian with little regard for community consultation and difference of opinion. So, in the last quarter of the 20th century, he became a benchmark in the United States for how not to undertake public works.

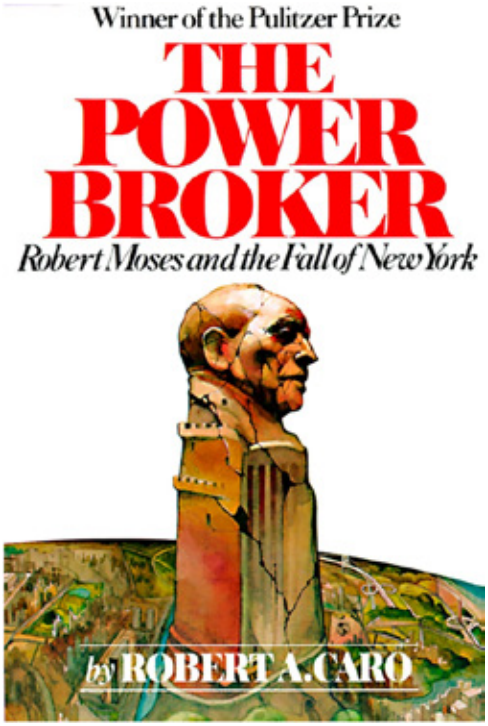

In the years following the 11 September attacks, Robert Moses started getting a new look. Despite the human tragedy, a lot of people still questioned why the rebuilt One World Trade Centre didn't open until 2014. And why the Second Avenue Subway – with the Phase 1 design commencing in 2001 – required 16 years for those 2.9 km and three stations to be constructed. The expression 'Robert Moses is rolling in his grave' became commonplace in the media while I lived there up through 2006, and the debate about his legacy in New York City – which includes public parks and pools and Lincoln Center for the Arts and many things that survive beyond highways through communities – has been reborn and is far from settled.

Occasionally I am involved with a project here in Australia that is on the fast track and that struggles to get boreholes or CPTs into the ground at a reasonable time, such that a design must contend with seemingly more uncertainty than the normal uncertainty, making for a whole lot of uncertainty that has to be communicated on time, no delays, because the project, after all, is on the fast track. I realise that communicating my frustration here is a form of preaching to the choir – of probably 25

to 50 singers – but with age I admit to also becoming more sympathetic to more aspects of the legacy of Robert Moses… as well as to accounts of construction progress in China as a direct competitor to the United States.

The rates of construction in China over the last decades are undeniably remarkable. A book that describes it well, and that got a lot of attention in the United States in late 2025 is 'Breakneck: China's Quest to Engineer the Future' by Dan Wang, a Canadian of Chinese origin who attended university in the United States and returned to China for a job shortly before Covid. A short list of notable accomplishments (there are many many more) include:

- From 2003 to 2013, Shanghai added as much subway track as all active track exists in New York City. (I looked at Wikipedia and found reference to a sub-period of this timeframe that included expanding the network from 65 km in 2003 to over 400 km in 2010, with the large majority of expansion as tunnel. Compare 335 km in seven Shanghai years to 2.9 km in ten New York City years, or arguably 16 New York City years)
- Within a few decades, China has constructed the longest high speed rail network in the world, ten times the combined length of Spain (second in world) and Japan (third in world).
- One of China's poorer provinces Guizhou has built 45 of the world's 100 highest bridges.

Wang labels China as 'an engineering state' while the United States is 'a lawyerly society'. Of specific interest to the topic at hand: in 2002 all nine members of the Politburo Standing Committee (effectively the head of the Chinese Communist Party and therefore the national leadership) were educated as engineers. Leaders with a preparation in engineering – with varying specialties including infrastructure, manufacturing and aerospace - had become a tradition during the Premiership of Deng Xiaoping in the late 20th Century.

The last bullet point above is revealing for a few reasons. I have never been there, but understand from Wang that Guizhou is very mountainous so high bridges are to be expected. But some of the bridges haven't achieved much, and could be compared to several 'bridges to nowhere' that occasionally appear in the United States and in locations that make no economic sense other than to bring an expensive project to a politician's backyard. So China isn't immune to some of the same political drivers that infect western expenditures. And probably to a much greater degree than Moses, China likes monuments. Around all the roads, bridges, and trains, visitors are still advised not to drink tap water anywhere in China. Water treatment plants don't make good monuments, so the engineering state appears not to have prioritised them in the recent decades of growth.

Despite periodic protests, including during Covid when the population tired of what came to be perceived as government-excess while the world re-opened around it, China has been able to maintain 'the consent of the governed' as Wang refers to it in several chapters of the book, because the government has largely delivered. China objectively has many challenges/problems, but the people can feel the many many accomplishments, and overall economic vitality. While the starting point of the United States around the turn of the century was quite different, I would agree with Wang's observation that the United States government in this time has largely not delivered for its people. And these decades coincided with the export of massive amounts of manufacturing (and manufacturing capability, which Wang distinguishes) from the United States to China. Consumers in the United States benefitted, but we're seeing the long-term price. While Wang doesn't diverge from the main points of his book, I will momentarily digress in joining the many people who find some connection between these trends and the current state of politics in the United States, the fault of both the 'R' people and the 'D' people.

To be sure, Wang sees the competition between the 'engineering state' and the 'lawyerly society' as not yet decided, if it has to be. And he thinks that for the benefit of their respective populations, each country should try to be more like the other. Wang provides other examples of where the engineering and also scientist leaders of China didn't make the best decisions, sometimes with enormous consequences, and he explains how the 'lawyerly society' – with all its lawyers and attention to rights – had built-in mechanisms to prevent similar outcomes. He also points to some countries in Western Europe that have found a more effective balance between environmental reviews, public consultation, and 'getting things done'.

I recognise a distinction to be made between arguing for more engineers as political leaders, and more engineers at the table where decisions are made, perhaps as organisational leaders at varying levels. On some occasions the argument is in the interest of balance, and of ensuring that an analytical mind is present. Especially when in the public interest as in the case of decisions relating to planning and infrastructure, I am in full agreement with this need, even if I don't believe it to be the number one challenge facing our profession. Raj Aseervatham, EA's former President

who was present at the 2025 Forums meeting (and was also a guest later in May at an AGS National meeting in Brisbane) wrote a related article for 'Create' on 'Why more engineers should be leaders' in which he cites a career experience when he felt some engineers were too focused on their expertise, and less inclined 'to engage more willingly and deeply on the human or societal problem, not just the technical.' I like the anecdote because it hints at the responsibility of engineers to engage, rather than the responsibility of everyone else to engage engineers.

The argument for more engineers in leadership 'to get things done' (full-stop) is perilous unless society is on board and open to the occasional ten lane elevated highway across Lower Manhattan. The United States needs to build more for its people but the argument is best made not so much by engineers as by justifiably frustrated tax payers.

From so much of the discussion in the early chapters of Wang's book - it lacks an index so I couldn't easily search ahead – I anticipated a discussion of Robert Moses and 'The Power Broker'. It arrived in Chapter 7 with the heading 'Learning to Love Engineers'. For Wang, calling 'The Power Broker' monumental would be an understatement. Some of the bad decisions Moses made are undeniable, but the book is now dated. It played a part in the consolidation of 'the lawyerly society' and it helped to teach people in the United States 'to fear and loathe engineers'. Wang is not an engineer, but writers like him will be hugely influential in shifting, if not correcting, perceptions in a way that engineers won't so easily.

Australia is obviously not the United States, and per capita, Australia has built more infrastructure in recent decades. Compulsory voting probably is to credit for moderating the pendulum swings, but the pendulum still swings in its own way around different cities and states. Like most cities that win an Olympics, Brisbane - the new lighthouse of Australian culture - is adjusting to what will be required to deliver, as what worked to execute a large project just a few years ago won't work now. More effective at accelerating construction schedules than just engineers who 'get things done' will be a fixed deadline that everyone can see hovering over the river. Many engineers are already rightly and necessarily engaged and embedded in this process, but there's a lot of staring at that deadline (And some boreholes need to get moving).

To their credit, in September 2025 Engineers Australia, partnering with the Australian Academy of Technological Sciences and Engineering (ATSE), Consult Australia, Science and Technology Australia (STA) and the Australian Council of Engineering Deans (ACED), launched the Parliamentary Friends of Engineering. From the press release, 'the group provides a platform for parliamentarians to engage directly with engineers, universities and research organisations to develop solutions to some of the country's most pressing challenges, making their insights essential for informed policymaking.'

I've been honoured to serve as the National Chair for the AGS over the last two years and a bit. Working mostly with our now General Manager Jon Gibbs and the collective national leadership, I've also been honoured to lead our transition to a new public company limited by guarantee. We've had a number of bumps along the way and I've learned things about organisational and not-for-profit leadership – sometimes through my own mistakes – that I could not have so readily learned through other avenues in my career.

Our small learned society of roughly 3,000 people offers engagement within the profession and beyond. Not just observant of where I might have done something more effectively, I've noted many differing personalities within our membership and chapters: some people struggle to make decisions, some put low relevance minutia ahead of a bigger picture, some have little economic awareness, and some don't like any conflict. Like any organisation, really, but there are opportunities to work on these things.

For the last two years we have been actively sending our chapter leaders, international society vice presidents and representatives, our journal editor, and invited members to the AICD course on 'Governance Foundations for Not-for-Profit Directors'. And we are developing policies and procedures around the constitution to sustain the new organisation. I believe we are doing our part in helping many of our members to grow as leaders and are very much aligned with EA's vision for the profession, which we still hope can be expanded to formally recognise engineering geologists in the future.

As part of our strategic development, we held our first ever all-day strategy session in Brisbane on 6 February with an independent consultant. I want to thank Jon for arguing in favour of an invitation list that extended beyond our Board to include our National Stakeholders Group and a few others. Two days before the event I learned that all five of my predecessors in the National Chair role had confirmed attendance:

David Lacey: 2022-2023

Nina Levy: 2020-2021

Stephen Fityus: 2018-2019

Hugo Acosta-Martinez: 2016-2017

Darren Paul: 2014-2015

In chatting with Jon after the event, I appreciated from him how rare it is for any organisation to have 12 years of six consecutive leaders in the same room… for all sorts of reasons (we both laughed). My last honour would be observing the engagement of all five of those predecessors with AGS Limited as I conclude my time as Chair.

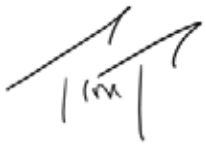

TIM THOMPSON

National Chair, Australian Geomechanics Society

2026 AUSTRALIAN GEOMECHANICS SOCIETY BOARD OF DIRECTORS, NATIONAL STAKEHOLDERS GROUP AND ADMIN SUPPORT

BOARD OF DIRECTORS

TIM THOMPSON
Director, Chair of Board

Tim is a geotechnical engineer with EDG Consulting in Brisbane. After graduating from Purdue University in 1997, Tim was a Peace Corps volunteer in Panama where he taught land surveying to high school students. He worked in New York City and London prior to moving to Brisbane in December 2009. Tim launched the Queensland Geotechnical Database with Jared Priddle of FSG in 2017. He is currently undertaking part-time research with the University of Queensland and was the AGS Queensland Chair in 2016-2017.

DAVID LACEY
Director

David is a principal geotechnical engineer with FSG Geotechnics + Foundations (FSG) in Brisbane. After attending The University of Sydney and graduating with both a Bachelor of Civil Engineering (Geotechnical) and Bachelor of Science (Geophysics), David relocated to Brisbane for work in 2006. During his full-time geotechnical consultant career, David undertook a part-time PhD research project at The University of Queensland which was completed in 2016. David was the recipient of Engineers Australia's QLD and National 'Young Professional Engineer of the Year' award in 2016 and has also received the AGS' Don Douglas Youth Fellowship. David has served on the local organising committee for multiple international technical conferences - including ANZ2023 (Cairns), 20th ICSMGE (Sydney), 10th YGPC (Noosa) and 11th YGPC (Queenstown) – whilst also being a member of the AGS QLD Chapter's committee since 2012. David has served upon the AGS' national executive since 2020, and will conclude his term and depart the AGS' inaugural Board of Directors in late March 2026.

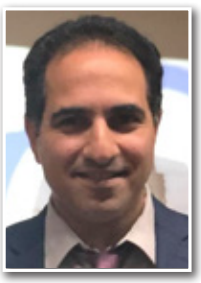

AMIR SHAHKOLAHI
Director

Amir is the National Technical Manager at Global Synthetics and a Fellow of Engineers Australia. He holds a PhD in geosynthetics/geotechnical engineering, master's degree in environmental engineering, and bachelor's degree in civil engineering. With over 25 years of experience in geosynthetics, geotechnical, and pavement engineering, Amir has worked extensively as a designer, project manager, researcher, and technical lead, and has authored more than 100 publications and technical documents on various geosynthetic applications such as soft soil stabilisation, reinforced structures and embankments, erosion control, stormwater drainage, waterproofing and barrier systems, landfill design, sustainability, etc.

He currently serves on numerous national and international committees, including as a director of the Australian Geomechanics Society, Industry Board member of the Australian Pavement Research Hub, elected Council Member of the International Geosynthetics Society (IGS), Chair of the International Geosynthetics Society (IGS) Asia Pacific Regional Committee, and member of the IGS Technical Committees TC-R (Reinforcement) and TC-RRA (Roads, Railways, and Airports). He is also the representative of Engineers Australia in Standards Australia Technical Committee CE-020 (Geosynthetics), members of ASTM and ISO technical committees for geosynthetics and sustainability, and guest lecturer at five Australian universities..

JOANNA SYLVESTER
Director

Joanna is an enthusiastic engineering geologist, a native Novocastrian and mother of two young boys. She graduated from the University of Newcastle with a Combined Bachelor of Science/Bachelor of Arts degree, and a subsequent Masters of Engineering Science through UNSW. She has 18 years consulting and 7 years leadership experience with GHD - currently as Manager of the Northern NSW Rail and Geotechnics teams.

Joanna's professional focus is mine subsidence, slope stability, 3D geological modelling, and integrating new technologies to improve outcome. She has a keen interest in developing emerging geotechnics professionals in a diverse, supportive and technically interesting way - and continuing to foster an increase in women and diversity in our industry.

ALI PARSA-PAJOUH
Director

Ali is a Senior Associate Geotechnical Engineer with over 20 years of experience spanning both academia and industry. He earned his PhD in Geotechnical Engineering from UTS in 2014, with an industry-sponsored research focus on soft soil improvement. His expertise covers a broad range of geotechnical disciplines, including numerical modelling, soil-structure interaction, ground improvement, deep excavation, retaining structures, slope stability, and the application of AI in geotechnical practice. Ali leads the design team at JK Geotechnics. Ali has been actively involved in R&D programs addressing complex geotechnical challenges. He is a member of several industry advisory boards, including the UTS Transport Research Centre. Since joining the AGS Sydney Chapter committee in 2016, Ali has held several leadership roles, including Coordinator of the Sydney Chapter Symposium (2018 to 2021) and Chair of the Sydney Chapter (2022–2023). Following his election to the AGS Board of Directors, Ali also chairs the AGS Digital Transformation Working

Party. He represents Australia on the ISSMGE Technical Committee for Numerical Methods (TC103).

DARREN PAUL
Appointed Director

Darren is a technical director in engineering geology at WSP Australia with over 25 years' experience. He has had a nearly 20 year involvement with AGS as a member of the Victorian chapter committee and the national committee, including the role of national chair in 2014/2015. He leads the AGS course on landslide risk assessment and has maintained involvement in supporting emerging professionals as a mentor at the Young Geotechnical Professionals Conference and chair of the ISSMGE Young Geotechnical Engineers Conference in 2021. Darren is currently co-chair of the committee to update the AGS guidelines for landslide risk management.

Darren's professional interests include landslides and landslide risk management, risk and uncertainty in geotechnical engineering, engineering geological models and ground characterisation for large projects and planning for geohazards.

NATIONAL STAKEHOLDERS GROUP CHAPTER CHAIRS

DAVIDE GUCCIONE
Newcastle (NSW) Chapter Chair

Davide holds both a Master's and a Bachelor's degree in Civil Engineering from the University of Parma in Italy. He received his PhD in Civil Engineering from the University of Newcastle in 2021, where he is currently continuing his research in rockfall-related projects. Davide has won several early career awards, including the AGS NSW Research Award in 2020, the D. H. Trollope Medal in 2022, and the 1st Runner-Up Prize for the NSW Young Geomechanical Professionals' Night in 2024. He is currently an ARC Industry Fellow in collaboration with Rocscience.

Davide's areas of expertise include rock mechanics, rockfall analysis, rock fragmentation, slope monitoring, and photogrammetry.

Since joining the AGS in 2020, Davide has been an active member of the Newcastle Chapter, contributing significantly as a committee member since 2022. In 2024, he was nominated as Secretary, and in 2025, he took on the role of Chair.

JARED PRIDDLE
Queensland Chapter Chair

Jared is a geotechnical engineer at FSG, where he has spent most of his career after graduating from QUT in 2012. He has extensive experience in investigation, design, and construction for both major and minor projects, with capabilities spanning geotechnical investigation, interpretation and modelling, earthworks, slopes, soft ground, piling, retaining structures, and temporary works. Jared has served on the QLD Chapter committee since 2017 and is the co-founder and developer of the Queensland Geotechnical Database (qgd.org.au), reflecting his strong interest in GIS, data management, and automation.

LAUREN AMATO
South Australia and Northern Territory Chapter Chair

Lauren is a geotechnical engineer at Arup Adelaide with over six years of experience working on major infrastructure projects in Adelaide and interstate. She has extensive expertise in managing and undertaking site investigations, soil and rock slope assessments, foundation design, retaining wall design, earthworks analysis, and construction phase support.

Actively involved with the Australian Geomechanics Society (AGS), Lauren served as Secretary of the South Australian and Northern Territory Chapter in 2023 and 2024. She established the Women of AGS sub-committee in South Australia to promote and support women in geomechanics, reflecting her passion for diversity and inclusion. As Chair for 2025–2026, Lauren is committed to enhancing AGS's collaboration with industry and advancing the geotechnical engineering profession in the region.

MEHDI TAMADON
Sydney/NSW Chapter Chair

Mehdi is a geotechnical engineer and team leader at GHD in Sydney Geotechnics and Tunnels Group, with over 15 years' experience. His skills include numerical modelling, soil-structure interaction, deep excavation, deep foundations, and slope stability assessment and design. He has also served as the geotechnical lead designer for infrastructure projects across NSW and Victoria.

Since joining the Australian Geomechanics Society (AGS) committee in 2019, Mehdi has actively contributed to the Sydney chapter, including serving as the Annual Sydney Symposium coordinator and Sydney Chapter Secretary.

ASHLEY DYSON
Tasmania Chapter Chair

Ashley is a geotechnical engineer and academic at the University of Tasmania (UTAS), whose research focuses on developing computational and probabilistic methods for slope stability analysis, landslides, and offshore engineering. His work considers practical risk mitigation and resilience strategies for the benefit of the Tasmanian community, especially in relation to debris flow and landslide hazards.

Prior to joining UTAS in 2021, Ashley completed a post-doctoral research fellowship with the Geotechnical and Hydrogeological Engineering Research Group (GHERG) at Federation University Australia, where his research address large open-pit mine stability and rehabilitation. He completed his PhD in 2020, developing probabilistic frameworks to assess the stability of open-cut mines with highly spatially variable geotechnical properties.

Ashley joined the committee of the Tasmanian chapter in 2021, serving as the secretary for three years and was elected to be chair in 2026. He also currently serves on the ISSMGE technical committee TC304 (Engineering Practice of Risk Assessment and Management).

YUQI TAN
Victoria Chapter Chair

Yuqi is a geotechnical and dam engineer with proven experience in tailings and embankment investigation, design, construction and operation. He worked on facilities in Australia, Asia and South America. Yuqi is passionate about collaboration between industry bodies. He served multiple roles with AGS and ANCOLD in the past years.

Yuqi has been on the AGS Victoria committee since 2018 and is currently serving as the chair of the AGS Victoria Chapter.

EDDY YONG
Western Australia Chapter Chair

Eddy is a geotechnical engineer with Aurecon in Perth. He earned a Bachelor of Engineering and Commerce from the University of Western Australia and has since spent almost all his career working in Western Australia. His interests are in multidisciplinary infrastructure, energy and resources projects, bringing geomechanics to inform design decisions, manage uncertainty and deliver great outcomes. He is passionate about the positive impact engineers and geologists can have on society.

A strong advocate for the geomechanics profession, Eddy sees it as both a rewarding career and a supportive professional community. He has been involved in the Western Australia chapter since 2019 and is actively committed to advancing the AGS. Eddy was nominated and elected as WA Chapter Chair in 2025.

INTERNATIONAL SOCIETIES REPRESENTATIVES

MUHAMMAD SHAZZAD HOSSAIN
ISSMGE Australia Representative

Dr Muhammad Shazzad Hossain is a Professor in Geotechnical Engineering at UWA and a former ARC Future Fellow. He was named as the Woodside Early Career Scientist of the Year 2013 by the Government of WA. He actively leads international collaborations between UWA and industries and academic institutions in South Korea and Indonesia.

Dr Hossain's research focuses on jack-up vessels for offshore renewable energy and anchoring solutions for mooring floating wind turbines, wave energy devices, solar panels, oil and gas platforms, and aquaculture facilities. He is also championing repurposing of Australia's decommissioned subsea infrastructure and contributing engineering measures to protect Australia's ocean territories from plastic pollution.

Dr Hossain has been (i) serving AGS, WA Chapter, as a Committee Member since 2013; (ii) representing Australia on ISSMGE TC209 and TC104 since 2018; (iii) leading ME-092-1 Committee (Australian Mirror of ISO TC67/SC7) for ISO 19905-1 and ISO 19905-4 since 2019; and (iv) serving ISO TC67/SC7/WG7/P4 (Jack-ups) as a Core Member since 2011.

ROBERT BERTUZZI
ISRM Australia Representative

Robert graduated from the University of Sydney in 1985 with a bachelor's degree in mining engineering and the University Medal. He completed a masters in rock mechanics (subsidence) at the University of Sydney in 1989 while working in underground and open pit coal mining (Coal & Allied, ACIRL, Mae Moh (Thailand)). He then lost his way and became a tunnelling engineer on the English Channel Tunnel. Having joined PSM in January 1994 where he is now the Chair of its Board, he splits his work between mining and tunnelling.

Robert completed his PhD in 2017 at University of New South Wales with the thesis "Rock mass properties for tunnelling". He is fortunate in having worked on many mining and tunnelling projects in Australia with some outstanding people within the consulting, mining and civil contracting professions.

MEGAN PACKER
IAEG Australia Representative

Megan is a Principal Engineering Geologist with PSM in Brisbane, bringing extensive international and Australian experience to complex civil infrastructure projects. After completing her postgraduate Honours at the University of Queensland she undertook a MSc at Imperial College London, receiving the Lapworth Medal. Megan spent a decade working in the UK before returning home to Australia in 2017, joining PSM and strengthening her commitment to building meaningful connections between Australian practitioners and the global engineering geology community.

Her professional expertise spans dams, tunnels, bulk excavations, pumped hydro schemes, rail and road projects, deep piled foundations, and major earthworks, contributing to large-scale infrastructure across diverse environments. Megan recently served as Organising Committee Co Chair for ACEG2025, the inaugural Australian Conference on Engineering Geology held in Brisbane — a highly rewarding opportunity that deepened her engagement with the broader professional community and reinforced her passion for advancing the discipline.

AUSTRALIAN GEOMECHANICS JOURNAL

HUGO ACOSTA-MARTINEZ
Editor, *Australian Geomechanics*

Hugo is a Technical Director – Geotechnical at WSP Australia. He has more than 28 years of consulting experience, mainly in transport, near shore, resources and renewable energy infrastructure.

In his current role, Hugo provides technical leadership and independent verification on projects across the country. As a passionate advocate for inspiring the next generation of geotechnical engineers, Hugo is involved in mentoring young and emerging professionals and has previously served as the National Chair of the AGS (2016-17). With strong links to academia, Hugo is also a regular peer reviewer of leading geotechnical engineering journals and actively participates in forums that promote industry-academia collaboration.

INVITED MEMBERS

NATALIE QUINLISK
Chair of WIAGS Sub-Committee

Natalie is an Associate Geotechnical Engineer at Jacobs, currently serving as the Section Leader for the Tunnels and Ground Engineering Team across QLD, SA and WA. She has a degree in Civil Engineering from QUT, Brisbane and obtained her Master's Degree in Soil Mechanics and Engineering Seismology at Imperial College, London.

Natalie has been an active member of the AGS QLD Chapter since 2016, holding various executive roles over the past 10 years. In 2026, she will continue to lead the national Women in AGS sub-committee in our mission to increase women's engagement in the AGS community, celebrate their successes and foster an inclusive culture that attracts and retains women!

GENERAL MANAGER

JON GIBBS
AGS General Manager

Jon joined the AGS in July 2022 for a 3-month handover process with Peter Robinson, who officially retired at our Annual General Meeting in October 2022. Jon holds a Bachelor degree in Human Movement Studies through UTS Sydney. He has over 35 years' experience working in retail & international banking, local government leisure services and sports management. He has helped establish and incorporate eight volleyball clubs in NSW and Queensland. As General Manager of Queensland Volleyball Association 2008-19, Jon rebuilt the organisation from financial and operational collapse in 2008 to transform it into the national benchmark on and off the court.

ADMIN SUPPORT

SARA LANESMAN
Advertisement *Australian Geomechanics*

Sara has been the Australian Geomechanics advertising liaison since 2003 and has been corresponding with some of the same advertisers since taking on the role. When not responding to email enquiries or sending out reminders about forthcoming editions and artwork deadlines, Sara works as the Office Manager for a Family Office.

PhD Thesis abstracts for publication in *Australian Geomechanics*

AUSTRALIAN GEOMECHANICS SOCIETY

The Australian Geomechanics Society invites PhD students to submit an abstract of their thesis completed in 2026 to *Australian Geomechanics*.

This invitation is restricted to PhD theses submitted to Australian universities and accepted as partial fulfilment of the requirements for the degree of Doctor of Philosophy and to PhD theses by Australian students submitted at overseas institutions.

The thesis should have been completed and accepted within one year of the abstract being published in *Australian Geomechanics*.

The invitation is open to all theses related to geomechanics topics. AGS requests promotion of this initiative among PhD students and academic networks.

The abstracts will be published in the March 2027 issue of *Australian Geomechanics*.

The following information is required for publication:

- Author's name (with current affiliation and contact information)
- Thesis title
- Date submitted/approved
- Sponsoring Professor / Academic Supervisor and University (contact address, telephone and e-mail address)
- A brief abstract (strictly max 250 words)
- Scanned page of Title Page of thesis.
- Information should be submitted to the *Australian Geomechanics* Editor, via email: editor@geomechanics.org.au Please attach as a MS Word document.

Deadline: Friday 5th February 2027

REVIEWERS

AUSTRALIAN GEOMECHANICS REVIEWERS

The following is a list of volunteer referees that have reviewed papers considered for publication in *Australian Geomechanics* in 2025. The Australian Geomechanics Society is very grateful for their assistance. The Editor would like to offer a special recognition to Andy Fourie, David Reid and Daniel King for contributing as associated editors of themed editions of the journal published in 2025.

Mahmoud Ahmed
Giovanny Alvarado-Gutierrez
Andrew de Ambrosis
Nelson Amoah
Harry Asche
Cameron Bik
Eduardo Bittar
Tierney Boulter
Chris Bridges
Kim Chan
Luis Fernando Contreras
Michael Davies
Davide Donati
Matthey Duthy
Ricardo Fanni
David Field
Andy Fourie
Chaminda Gallage
Camilla Gibbons
Alexandre Gomes
Sean Goodall
Scott Gover
Jason Hellmuth
Paul Hewitt
Yuxia Hu
Robert Kamuhangire
Mark Jaksa
Graeme Jardine
Ian Johnston
John Kemeny
Daniel King
David Lacey
Allan Lee Goh
Barry Lehane
Roger Lim
Arcesio Lizcano
Marcelo Llano-Serna
Dennis Loffell
Logan Loganathan
Burt Look
Mario Martinelli
Gordon McPhail
Desmond Mossop
Hamish Nelson
David Oliveira
Kaiwen Ouyang
Ali Parsa-Pajouh
Rick Piovesan
Harry Poulos
Hongyu Qin
Joe Quinn
David Reid
Joe Rola
Hao Shen
Shuilong Shen
Mandeep Singh
Kyle Smith
Sri Srithar
Jun Sugawara
Ying Tay
Ian Thompson
Yinghui Tian
Zack Tuckey
Philip Wade
Justin Walls
Dong Wang
Pabasara Wanniarachchige
Douglas Warne
Bo Xu
Eddy Yong
David Zhang

AWARDS

AUSTRALIAN GEOMECHANICS AWARD (2025)

The paper "Bayesian calibration of NorSand model parameters using triaxial test data" by Luis-Fernando Contreras, Humberto Rojas-Huaroto, Alexandra Halliday and Marcelo Llano-Serna, has been selected as the winner of the Australian Geomechanics Award for 2025. This award recognises the authors of the best paper published in Australian Geomechanics in each calendar year.

The paper was published in Vol 60(4), pp. 21-37.

DOI: https://doi.org/10.56295/AGJ6041

In relation to the papers the authors said:

The motivation for this paper stemmed from a shared recognition that calibrating critical state models like NorSand often relies on subjective and labour-intensive visual fitting. To address this, the authors collaborated to develop a rational, objective framework that integrates experimental triaxial data with Bayesian statistics. By utilising Markov Chain Monte Carlo (MCMC) methods, the study not only streamlines parameter estimation but also quantifies uncertainty and parameter correlations—crucial factors often overlooked in conventional analysis. This work bridges the gap between theoretical soil mechanics and practical application, providing an open-source Python tool designed to enhance the reliability of tailings management and geotechnical risk assessments.

Dr Luis-Fernando Contreras has contributed to the geotechnical engineering field for over 45 years. His areas of expertise encompass risk evaluation for mining project optimisation, open pit design, tunnel engineering, and geotechnical assessment of underground excavations for civil engineering projects. He has worked in diverse geotechnical studies including site investigations, rock-fill and earth-fill dam design, instrumentation design and rock mechanics analysis of geotechnical structures. His experience covers different stages of project development from conceptual and feasibility studies through to detailed design and specialised advisory during construction. Throughout his career, Luis-Fernando has served as Principal Consultant at SRK in Chile, South Africa, and Australia, focusing on quantitative risk evaluation for mining projects. He holds a PhD in geotechnical engineering from the University of Queensland and is both a Chartered Professional Engineer and a Fellow of the Institution of Engineers Australia. He is currently promoting the application of the Bayesian approach to improve the treatment of uncertainty in geotechnical analysis.

Humberto Rojas-Huaroto, a Civil Engineer specialising in Geotechnics from the National University of Engineering (Peru), began his career as an intern at Anddes Asociados S.A.C. between 2023 and 2024, where he contributed to geotechnical analysis and numerical modelling projects in the mining sector. Since August 2024, he has served as a Geotechnical Staff Consultant at SRK Consulting Peru. His expertise includes analysing and designing mining-geotechnical structures such as tailings dams, leach pads, and waste rock dumps, emphasising physical stability assessments and stress-strain analysis using FLAC, Plaxis, and Anura3D software. Additionally, Humberto leverages Python programming to streamline processes and enhance data-driven decisions. He is keen on integrating his geotechnical expertise with programming abilities to deliver advanced, comprehensive solutions.

Alexandra Halliday is a Chartered Principal Tailings and Dams Engineer with over a decade of experience across consulting and owner–operator environments in the global geotechnical and mining sector. She specialises in tailings and water storage facility governance, risk management and technical assurance for complex operations. Her experience spans the design, construction and surveillance of tailings and water retaining structures across diverse jurisdictions, with particular expertise in soil mechanics and embankment behaviour. She is actively involved in international industry initiatives aimed at strengthening governance frameworks, technical standards and transparency in tailings management.

Dr Marcelo Llano-Serna is a geotechnical engineer specialising in tailings engineering and dam safety, with interests in statistics, large-deformation analysis of geomaterials, and risk-informed design. His work focuses on high-consequence mining assets, integrating advanced soil mechanics into practical design, performance assessment, and failure investigation. He has contributed to more than 50 projects internationally across the lifecycle of tailings facilities, including design management, Engineer of Record services, third-party reviews, and forensic studies. Marcelo holds a PhD in geomechanics and is a Registered Professional Engineer of Queensland (RPEQ). He continues to promote research-informed approaches to improve dam safety practice.

OBITUARY

It is with great sadness that we share news of the 12 November 2025 passing of inaugural AGS Life Member, Dr William (Bill) Bamford following a decline in his health.

Born in 1936 in Tahiti, Bill spent his childhood in New Zealand and Norfolk Island before moving to Sydney in 1950 where he attended high school. He commenced his civil engineering studies part time at Sydney Technical College in 1953 while working as a cadet engineer at Woollahra Council. He progressed to fulltime study at UNSW in 1955 with National Service in the RAAF at Laverton Base in 1956-57. He obtained his Bachelor of Engineering in Applied Geology from the University of NSW in 1958. He spent a summer at the Snowy Mountains Hydroelectric Authority as a vacation student in 1957 and started fulltime as a graduate in 1958 under the direction of David Stapledon. He worked on the Tumut 1 underground power station and its tailrace tunnel, the Geehi Dam and Murray 1 Underground Power Station investigations, and was resident geologist on the Murrumbidgee-Eucumbene Tunnel. It was whist drilling deep exploratory diamond drill holes on Broken Back Spur that he became involved in heat-flow investigations being carried out by Professor John Jaeger, a relationship that would later influence the (future) Australian Geomechanics Society award bearing Professor Jaeger's name.

In 1960 Bill accepted a job offer from John Neilson to work at the Geological Survey of Victoria and remained there until 1964. During this time he was involved in many projects around the state including proving the brown coal resource at Anglesea which fuelled the Alcoa power station that supplied Point Henry smelter. Importantly, he commenced geotechnical investigations for the Melbourne Underground Rail Loop, subsequently transferring to the Victorian Railways Construction Board 1965-67, where he led the geotechnical investigations for the project that would change public transport through the city.

In 1967 he was appointed to the position of Lecturer in Rock Mechanics in the Mining Department at the University of Melbourne. This was the first Lecturer in Rock Mechanics to be appointed in Australia, recognition of the advances in tunnelling being made in Australia over that period. His inaugural student cohort included Jim Enever, Jim Askew and Leigh Clifford. He continued to supervise post-graduates until his final PhD student, Frank Lai, in 2011. While developing the course structure, Professor Jaeger invited Bill to spend some time with him at the Australian National University to discuss teaching and research in the field of rock mechanics. During this visit, Bill witnessed high pressure triaxial testing of Wombeyan Marble shearing along a distinctive 30-degree failure plane. Twelve years later Bill would immortalise Professor Jaegar's tests, when he was asked to prepare an award recognising contributions of the highest order over a lifetime commitment to the geotechnical profession in Australia. Mounted on white marble, the AGS Jaegar Award adopts the shape of the triaxial samples Bill had observed in the ANU laboratory; interestingly, he was unable to reliably replicate the 30-degree surface because the chamfered point tended to break off under slight pressure; as a result the award contains a plane cut at 45 degrees instead. Bill also arranged production of mementos, cut from granite drill core, for presenters at Victorian AGS meetings, affectionately known as 'Bamfords'.

Bill was the AusIMM representative on the National Committee of the AGS from the time it was formed in 1971 until he became National Chair of the AGS in 1975. In 1970 Bill had organised a symposium on tunnelling as an adjunct event to the AusIMM conference in Melbourne; this was the precursor to the Australian Underground Construction and Tunnelling Association (AUCTA), formed in 1972 and subsequently the Australian Tunnelling Society (ATS). At that time AUCTA remained under the auspices of the AGS and so Bill assumed the role of AUCTA Chair as well. He continued to be a member of the National Committee of the AGS from 1971 until 1987 and was a member of the Victoria Chapter committee from 1968 until 2012. During this time he served as Victoria chairman for 3 terms; initially in the mid-70s, again in the mid-80s, and once more in the mid-90s. He also served on the Australian Tunnelling Society National Committee from 1975 until 2002, and on the Victorian Chapter Committee from 2011 until 2015. He was also involved in the International Tunnelling Association (ITA), which included being on the organising committee for the 1987 World Tunnel Congress in Melbourne.

At the completion of his term as AGS National Chairman in 1979, Bill was nominated to be the ISRM Australasian regional Vice-President 1979 to 1987. He contributed to the Commission on Testing Methods, the

Commission on the Teaching of Rock Mechanics, and was the President of the Commission on Swelling Rocks and the Commission on Rock Boreability Cuttability & Drillability. Under his tenure Australia hosted the 1983 ISRM Congress, for which he was the organising chairman.

Bill was awarded his PhD for his thesis on 'Geotechnical Studies for Machine Tunnelling' at the University of Melbourne in 1983. In 1987 he accepted the position of Director of First-Year Engineering Studies. He was subsequently appointed Associate Dean – Academic for the School of Engineering, a role he maintained alongside a full undergraduate teaching load and postgraduate supervision. He was also generating significant income for the School of Engineering by consulting externally through his rock mechanics laboratory.

By 1996 his commitments to the university started to reduce. As a Principal Fellow and Associate Professor, Bill continued with a partial teaching load, and importantly maintained operation of the rock mechanics laboratory for external consulting.

In 1997 the AGS proposed a joint ISRM, IAEG, and ISSMFE event; GeoEng 2000 - an International Conference on Geotechnical and Geological Engineering, to be held in Melbourne Australia in November 2000. Bill was part of the organizing committee who successfully pitched the event to the 3 international societies, after which he assumed responsibility for organizing the "Underground Works" stream.

Bill was appointed a Senior Principal at Coffey in 2011, moving the lab from the University of Melbourne 44 years after he set it up on campus. Bamford Rock Testing Services (BRTS) was established in 2014, and continues to provide specialist rock testing to clients from around Australia and the world. Bill remained active in overseeing and reviewing test results to the end.

As a final accolade, Bill was awarded the Allen Neyland Tunnelling Achievement Award for 2025, something that pleased him greatly although he regretted not being able to receive it in person.

Over the years Bill has taught many students, supported innumerable societies and committees, established many dedicated clients, and earned many friends. Among other activities, he was also a talented dancer and performed with a number of groups at Hamer Hall as well as the Lygon St Festa. With access to his consulting funds, he arranged for a sprung floor and full length mirrors to be installed in the Frank Tate Building in the University where dance rehearsals could take place.

Bill is survived by his partner Jenny, son David and daughter Barbara.

It has been a privilege to have known Bill as a lecturer, colleague and friend; our careers wouldn't have been the same without him.

Chris Coulson & Andrew Campbell

UPDATE OF THE AGS (2007) GUIDELINES FOR LANDSLIDE RISK MANAGEMENT - PROJECT PROGRESS REPORT

PROJECT PROGRESS REPORT: UPDATE OF THE AGS (2007) GUIDELINES FOR LANDSLIDE RISK MANAGEMENT

The joint AGS and NZGS project to update the AGS (2007) Guidelines for Landslide Risk Management is progressing towards the latter stages of the project, and our four Working Groups (WG), comprised of experts from across Australia and New Zealand, have achieved some important milestones. We have previously provided progress updates at the 1st Australian Engineering Geology Conference (AEGC) in Brisbane (July 2025), at the NZGS Symposium in Auckland (October 2025), and a more recent summary of the project progress in the NZGS Geomechanics newsletter (October 2025). A current project update to January 2026 is provided below.

DOCUMENT STRUCTURE

The revised guidelines will be comprise three main documents: (i) Principles of Landslide Risk Management, (ii) Landslide Mapping, and (iii) Landslide Risk Assessment with a fourth complimentary report on the state of international practice in landslide management. Each of these documents has a specific target audience and aims, but with interrelated content. The revised guidelines are intended to complement other existing documents, including the NSWPWS Guidelines for Quantitative Risk to Life Calculations for Landslides, the NZGS Slope Stability Guidance documents and the NSW RMS Guide to Slope Risk Analysis, which is used by some roading authorities in Australia and New Zealand.

WORKSHOPS

The Landslide Mapping and Risk Assessment working groups each initially held workshops in Melbourne in May 2025, and the Principles of landslide risk management working group held a workshop in Sydney in September 2025. These workshops have supported content drafting and refinement, as well as coordination among authors. In addition, the Steering Committee and WG Chairs held a workshop in July 2025 in Brisbane, coinciding with the 1st AEGC, where participants reviewed progress and draft content, and discussed next steps. These workshops have proven incredibly valuable in progressing the guideline development and further workshops are proposed to incorporate review comments and finalise the guidelines.

Further specific updates for each of the four working group preparing the guidelines are presented below.

INTERNATIONAL PRACTICE

Reports have been received from 12 international experts which summarise landslide risk management practice in their countries. These reports have been assigned to the WGs for review, feedback, and to support their updates. A separate publication is planned that summarise these international reports. It was noted through the process of engaging experts from around the globe that AGS (2007) is still very well recognised internationally and is looked to by others to provide guidance on landslide risk management.

PRINCIPLES OF LANDSLIDE RISK MANAGEMENT

This WG is developing general guidance on landslide risk management which is primarily intended for a broad range of non-geotechnical stakeholders, including regulators, landowners and land managers. A final draft of the document is now complete and is currently in review. This document will be further reviewed and aligned once the other guidelines are complete and will provide a more general overview to the risk management process written in plain English as well as an important connection to the other more technical documents.

LANDSLIDE MAPPING

The Landslide Mapping WG is developing guidance for geotechnical practitioners on preparing landslide inventories, susceptibility, hazard, and risk maps, along with advice on how to use them for planning and landslide risk management. Some of the key updates to the guideline, compared to the existing AGS (2007) guidelines, will include the consideration of uncertainty in mapping, a new flow chart to set out the methodology and a more data driven approach to developing the maps. The guideline is in the final stages of development and is entering the review stage. It is intended to seek broader AGS/NZGS membership comment before seeking international peer review around mid-2026.

LANDSLIDE RISK ASSESSMENT

The working groups is preparing updated guidelines for geotechnical practitioners setting out best practice for landslide risk assessment. While the current AGS 2007c guideline provides the foundation for the draft, several new topics and guidance on different risk scenarios have been identified for inclusion in this revision. This includes further guidance on the use of engineering geological models in landslide risk assessment and a shift from the previous residential focus to a wider range of applications, as well as additional guidance on uncertainty and probability in landslide risk assessments. The landslide risk management flow chart is being updated to incorporate these updates, and worked examples will be included to support the reader's understanding and application of the guidelines. This guideline is near complete and entering the peer review and editing stage.

NEXT STEPS

The guidelines are reaching the final phase of development where the technical content has been, or will be soon complete. The next stage of the process will include detailed internal review by the project steering committee and working group members to ensure consistency and alignment between the three documents, then industry feedback from within Australia and New Zealand and international peer review. This process is expected to be complete by mid-2026.

We will also take the opportunity to present progress and seek further feedback at the upcoming joint JTC1/JTC3 international workshop on Landslide Risk and Geo-Education (LaRGE2026) in Queenstown, NZ in April 2026.

Technical editing and graphics design is proposed in Q3 and Q4, 2026, with the view to publishing what will become the newly revised ANZ Landslide Risk Management Guidelines by the end of 2026.

Once again, we want to thank all those who have contributed to the project so far. Contributions, queries, comments and discussion is welcome at any time through our queries page on the AGS website: www.australiangeomechanics.org/2024/03/05/ags-technical-committee-for-landslide-risk-management.

DIGITAL TRANSFORMATION WORKING PARTY

Chair: Dr. Ali Parsa-Pajouh

Overview

The Australian Geomechanics Society (AGS) established the Digital Transformation Working Party (DTWP) in early 2025 to coordinate digital initiatives relevant to geomechanical engineering. The formation of the Working Party reflects the increasing role of digital data management, collaborative platforms, and emerging tools in ground engineering practice. As the projects increase in scale and complexity, the profession faces a critical need to enhance data accessibility, improve cross-disciplinary integration, and enable more effective use of historical and real-time geoscientific information.

The DTWP includes representatives from all AGS chapters to support national alignment and information sharing. Its scope focuses on practical aspects of digital practice, including the development and organisation of geotechnical and geological data resources, promotion of standardised digital data formats, and examination of the application of artificial intelligence (AI) and related computational tools in professional workflows. These activities aim to support more efficient knowledge exchange and contribute to the gradual improvement of digital capability across the profession.

To address these areas, the Working Party operates through three dedicated subcommittees focusing on:

- **Nationalisation of the Queensland Geotechnical Database**, contributing toward a broader Australian geotechnical and geological data resource;
- **AGS Data Format Advocacy,** encouraging wider understanding and use of structured digital data exchange approaches; and
- **Application of Artificial Intelligence / Generative AI in Geomechanics,** reviewing and demonstrating practical uses of emerging tools.

During 2025, the DTWP has undertaken a series of activities related to digital collaboration environments, data organisation, and professional engagement. These efforts represent an initial step in supporting more consistent digital practices within the AGS community.

Key Achievements

- **Digital Environment Integration.** Migration to the AGS Microsoft 365 environment has been completed, with SharePoint and Teams channels established to support collaboration and data management. A consistent structure has been implemented across the three subcommittees to facilitate communication and knowledge sharing.
- **Nationalisation of Queensland Geotechnical Database** AG Journal papers (1971–2025) and selected ANZ conference papers (1971 and 1975) have been integrated with spatial geolocation, supported by an interactive mapping interface. The scope has been extended to include ANZ, YGPC, ACEG and AGS Symposium records. This work represents an initial step toward development of the Australian Geotechnical Database (AGD). A draft flyer is being prepared to describe the database structure, purpose, and intended use.
- **Application of AI / Generative AI in Geomechanics** A technical event titled Practical Applications of Generative AI in Geotechnical Engineering was held in Sydney on 10 September 2025, jointly hosted by Engineers Australia, AGS, and ISSMGE, with more than 350 attendees. The session presented practical examples of AI applications in ground engineering and generated interest in further related activities. A recording of the event and a reflection report are available through EA On-Demand and the AGS website.
- **AGS Data Format Advocacy Group**. Activities include promoting wider adoption of the AGS data format and digital ground engineering practices. A Community of Practice framework has been initiated, together with engagement with asset owners through chapter-led meetings. An industry survey is being prepared to assess AGS data usage, and collaboration with Geoscience Australia, as well as development of a digital geotechnics and AI training course, is under consideration.
- **Knowledge Sharing & Promotion**. Chapters are being encouraged to upload recordings of technical presentations to the AGS website to support broader knowledge sharing.

Next Steps (2026)

Planned activities for 2026 include the launch and promotion of a pilot interface for the Australian Geotechnical Database (AGD), organisation of geo-data–focused events, development of a national training program in digital geotechnics and AI, and continued integration of digital tools and AI workflows into chapter activities and member resources.

AGS Sydney Session on Generative AI in Geotechnical Engineering, 10 September 2025.

AUSTRALIAN PHD THESIS ABSTRACTS 2025

The purpose of this compilation is to bring to the notice of readers of *Australian Geomechanics* some topics in geotechnical engineering which are currently, or have recently been, subjects of research at universities in Australia.

The abstracts are arranged in alphabetical order; firstly by university and then by surname.

BIKASH DEVKOTA
ADELAIDE UNIVERSITY

Reactive soil movement under current and future climate, and their influence on geotechnical structures

Expansive soils are widespread globally and undergo significant volume changes with moisture content variations, causing effective stress changes and substantial ground movement. Lightweight structures such as residential footings built on such soils are highly vulnerable in certain climate zones. Structures built today may experience additional stresses in the future due to climate change.

The effect of climate change on expansive soil behaviour was investigated using two distinct approaches to account for climate variables in numerical investigation. Data from a monitored research site were used to validate the reliability of the numerical model. A research site was established in the southern suburbs of Adelaide, Australia, where extensive instrumentation was employed. Field investigation continued over five years and included sub-soil exploration, near-surface movement measurement (at 64 locations), monitoring of soil moisture (8 locations, up to 6 m depth at 0.5 m interval), and observation on the development and propagation of cracks. A weather station was also installed near the site to capture meteorological variables. In addition, two soakage trenches were installed at the research site to evaluate how the installation of a soakage trench influences the moisture dynamics around it and the resulting ground movement. Interactions at the soil-vegetation-atmosphere (SVA) boundary and other physical and hydraulic boundary conditions were analysed to evaluate moisture movement, related suction changes, and vertical ground movement.

Climate change and cracked conditions are likely to negatively affect the moisture dynamics and, thus, vertical ground movement. Such conditions need to integrate into geotechnical design to develop climate-resilient structures.

Supervisors: A/Prof Md Rajibul Karim, Prof Md Mizanur Rahman and Dr Hoang Bao Khoi Nguyen

SAGUN SHRESTHA
ADELAIDE UNIVERSITY

Evaluation of geosynthetic stabilised pavements (GSP) for mitigating pavement damage on expansive soil

Expansive soil is a clayey material that undergoes substantial volume change with variation in moisture content and is termed reactive soil in Australia due to this moisture sensitivity. These soils occupy extensive areas worldwide and a significant proportion of Australian surface soils, leading to widespread infrastructure distress. Seasonal wetting and drying induce differential ground movements that particularly affect lightly loaded, shallow-founded structures such as residential buildings, footpaths and pavements. In pavements, exposed edges experience cyclic heave and settlement, longitudinal cracking and reduced service life, imposing a considerable maintenance and rehabilitation burden.

This research evaluates the performance of geosynthetic-stabilised pavements (GSP) constructed over expansive subgrades using complementary field and laboratory programs. Three full-scale trial roads were established across Metropolitan Adelaide, each comprising two GSP sections with different geosynthetics and one unstabilised control section. Biannual condition surveys following Austroads procedures, together with International Roughness Index (IRI) measurements from a smartphone-based inertial profiler, were used to characterise in-service performance. Undisturbed samples enabled assessment of subgrade reactivity, while performance metrics such as the Longitudinal Crack Index (LCI) and Crack Mitigation Ratio (CMR) were developed to link cracking with reactivity and roughness.

Laboratory tests (shrink-swell, Atterberg limits, suction, CBR, DSS) showed strong correlations between soil reactivity and pavement performance. Large-scale box tests confirmed that geosynthetics reduced surface deformation and swelling pressures, with higher longitudinal strains in the machine direction. Overall, field and laboratory results demonstrated that GSPs exhibit superior resistance to moisture-induced damage compared with untreated sections.

Supervisors: Prof Md Mizanur Rahman, A/Prof Md Rajibul Karim and Dr Khoi Nguyen

XILIN CHEN
MONASH UNIVERSITY

Sustainability of underground infrastructure: digitalisation-based embodied carbon assessment and design optimisation

Decarbonising underground infrastructure is essential for achieving Net Zero targets, yet embodied carbon in tunnelling remains poorly quantified due to inconsistent system boundaries, fragmented data, and the complex interaction between excavation methods, structural design, and material usage. This study develops an integrated, digitalisation-based framework for embodied carbon assessment and low-carbon design in mechanised tunnelling and underground stations.

A unified methodology is proposed that combines Building Information Modelling (BIM), life cycle assessment (LCA), geotechnical analysis, and multi-objective optimisation. Generalised construction components and tunnel-specific lifecycle boundaries are established to enable consistent accounting across projects. Automated BIM-embedded workflows are developed to calculate embodied carbon in lifecycle modules A1–A5 and to visualise emissions by material, construction activity, and design parameter.

Case studies of rail and road tunnels demonstrate how key variables, such as lining thickness, concrete strength, reinforcement ratio, and TBM operational parameters, affect embodied carbon performance. Through convergence–confinement modelling and parametric studies, the thesis quantifies the trade-offs between structural safety and carbon reduction, generating Pareto-optimal design solutions under varying geotechnical conditions.

A digital decision-support toolbox, TunCO□, is introduced to integrate carbon accounting with structural evaluation and optimisation analytics, enabling practitioners to explore and compare low-carbon design strategies.

The proposed framework improves the transparency, consistency, and applicability of embodied carbon assessments for underground works. It provides a scalable foundation for future benchmarking efforts and supports early-stage, data-driven decisions for sustainable and resilient underground infrastructure.

Supervisors: A/Prof Qianbing Zhang and Prof Yu Bai

PENGXUAN JI
MONASH UNIVERSITY

Fracturing characteristics in geomaterials with circular hole and flaws under various loading conditions

Different types of discontinuities significantly affect the stability of rock during underground excavation. Crack growth from flaws can lead to engineering failures. Therefore, a deep understanding of the initiation, propagation, and coalescence of cracks in rock masses with natural discontinuities or artificial fractures is important. Seismic activities are widely used to evaluate infrastructure stability. Micro-seismic (MS) monitoring and laboratory-based acoustic emission (AE) techniques provide effective means to investigate fracture characteristics at different scales.

This study explores the fracturing behaviours of defected geomaterials. The event automatic classification is applied to an MS dataset. To overcome the limitations of in-situ MS monitoring, a series of quasi-static biaxial compression tests is conducted in the laboratory on geomaterials with pre-existing defects. Coupled static and dynamic loading tests are also performed. Measurement techniques used in the tests include digital image correlation (DIC), AE monitoring, and X-ray computed tomography (CT). The laboratory tests demonstrate the feasibility of the integrated measurement framework, and indicate the effects of defect geometry, flaw–hole interactions, loading conditions and impact velocity on the fracturing characteristics of defected samples. Furthermore, AE characteristics are explored using deep learning to enable automatic event processing. Multi-scale numerical modelling is employed to extend laboratory tests to field-scale simulations. This approach validates experimental findings and facilitates the prediction of critical zones in engineering applications.

Supervisors: A/Prof Qianbing Zhang, Prof Jian Zhao and Dr Gisela Viegas

YUXI LIU
MONASH UNIVERSITY

Underground structure stability compatibility analysis and support optimisation

As global population growth and urbanisation accelerate, demand for underground space continues to rise, highlighting the importance of structural stability and resource efficiency. Complex structures, mixed ground conditions, and weathered or bedded rock increase uncertainties and may lead to deformation or instability. Tunnel projects along Australia's East Coast illustrate these complexities and emphasise the need for quantified support design and stability assessment to optimise

processes and manage uncertainty effectively.

This thesis reviews underground support design and stability assessment methods and identifies certain limitations, including insufficient quantitative compatibility measures, the lack of a unified stability framework for complex geological conditions, and constraints in high dimensional optimisation. For simple geological conditions, analytical methods were applied to establish compatibility indexes for support strength and stiffness, while sensitivity and reliability analyses were used to assess their applicability. The results indicate that the compatibility index helps identify key parameters governing support performance and reduces the likelihood of over-design or under-design. For mixed-ground complex geological conditions, numerical modelling was employed to develop a stability index for three dimensional underground structures. Excavation depth, soil layer depth, and the angle between bedding orientation and the structural axis were identified as the governing factors, demonstrating multi-parameter interaction effects. Two high-dimensional optimisation methods, surface fitting combined with chaotic search and an MLP-BP neural network, were applied to identify influential parameters, improve design efficiency, and determine optimized parameter combinations through stability visualisation and weight analysis.

Supervisors: Prof Jian Zhao and A/Prof Qianbing Zhang

YAOLAN TANG
MONASH UNIVERSITY

Gradation-dependent constitutive modelling of crushable granular materials

Particle breakage, together with the resulting evolution of grain size distribution (GSD), fundamentally modifies the stiffness, strength, and dilatancy of granular materials such as calcareous sand and rockfill when subjected to high stress. To address these coupled mechanisms, this thesis establishes a unified gradation-dependent constitutive modelling framework that explicitly incorporates GSD evolution into stress-strain formulations. The study begins by deriving a breakage-based yield criterion from elastic potential energy contours and formulating a hardening parameter that links yield surface expansion to the crushing degree and void ratio, thereby producing a constitutive model capable of reproducing the essential behavior of crushable materials. Building on this foundation, a gradation-state-dependent elastoplastic model is developed by integrating a GSD evolution law with state-dependent dilatancy and strength, supported by a family of critical state lines and modified compliance matrices to capture stiffness degradation and dilation-contraction responses observed in laboratory tests and DEM simulations. To overcome the complexity and parameter richness of the elastoplastic formulation, the final stage introduces a gradation-dependent hypoplastic model that retains the core mechanisms of GSD evolution and critical state modification while substantially reducing the number of calibration parameters. Enhanced density functions and correction terms further enable accurate simulation of undrained and hydrostatic responses. The resulting framework, evolving coherently from elastoplastic to hypoplastic formulations, provides a practical and robust tool for modelling particle crushing in geotechnical applications

Supervisor: Prof Jian Zhao

FENG XIAO
MONASH UNIVERSITY

Subsurface fluid injection and induced fault reactivation with hydro-mechanical coupling simulation

Scientific research is crucial for addressing societal challenges like the transition to renewable energy and climate change mitigation. Subsurface systems are central to these efforts, making the prediction and control of fluid processes in fractured geological environments a critical research area. This work investigates three key applications: pressurised tunnel design, hydropower tunnel stability, and hydraulic fracturing.

For pressurised tunnels, a design and CO assessment framework is proposed, using multi-level BIM to integrate parametric modelling with numerical analysis. 3DEC simulations analyse the mechanical response of segmental linings under high water pressure, optimising design and waterproofing in complex geology.

A hydro-mechanical coupling framework, integrating TOUGH and FLAC3D, assesses the long-term stability of hydropower tunnels. Applied to fault reactivation scenarios, it demonstrates that impermeable linings reduce pore pressure diffusion, mitigating the risk of fault slip and structural instability.

In hydraulic fracturing, numerical simulations examine how pressure- and temperature-dependent CO properties influence fracture propagation. Using the Span-Wagner and Fenghour equations of state, results show supercritical CO provides the most efficient fracturing, enabling rapid pressurisation and complex fracture network development.

Overall, this research advances the understanding of subsurface hydro-mechanical processes, offering valuable insights for optimising underground infrastructure and promoting sustainable engineering.

Supervisors: A/Prof Qianbing Zhang, Prof Jian Zhao and Dr Saeed Salimzadeh

YIMO ZHU
MONASH UNIVERSITY

Assessing lifetime resilience of underground infrastructure to multi-hazard based on unified modelling and sustainable optimisation

Underground infrastructure plays a pivotal role in modern society, supporting critical functions in transportation, utilities, energy, and storage. Its lifecycle, spanning design, construction, operation, and maintenance, necessitates a robust framework for effective management and risk mitigation. The increasing complexity of multi-hazard scenarios, driven by interdependencies between natural and anthropogenic hazards, underscores the need for a unified approach to resilience and sustainability assessment. This thesis addresses these gaps by proposing a comprehensive framework for resilience assessment and optimisation of underground infrastructure under multi-hazard conditions, grounded in unified modelling and lifecycle performance evaluation. The research begins with a statistical analysis of risk sources, focusing on construction-phase accidents and operational-phase hazards. Subsequently, a dynamic cumulative damage model is developed to capture the behaviour of geomaterials under static, dynamic, and creep conditions, enabling simulation of damage progression under complex multi-hazard conditions. A unified approach is then applied for quantified resilience assessment, integrating abrupt hazards with long-term deterioration in circular tunnels and embedding hazard impacts and restoration strategies. Finally, a framework combining resilience and sustainability is developed, where lifecycle cost-analysis helps select optimal strategies that align resilience outcomes with economic and environmental objectives. This research demonstrates the critical role of resilience quantification in the lifecycle assessment of underground infrastructure. The findings provide a comprehensive framework for evaluating risks, quantifying recovery, and optimising infrastructure performance under complex multi-hazard conditions. By addressing the interdependence between resilience and sustainability, the thesis contributes to the advancement of adaptive and durable underground infrastructure systems.

Supervisors: A/Prof Qianbing Zhang and Prof Jian Zhao

AYESH DUSHMANTHA GUNATHILAKA PEELLWATHTHA GAMARALALAGE
QUEENSLAND UNIVERSITY OF TECHNOLOGY

Use of real-time measured pavement moisture to assess the pavement's suitability to allow traffic after a flood event

Flooding poses a critical threat to road infrastructure, particularly for unbound granular pavements that are highly sensitive to moisture ingress. In flood-prone regions such as Queensland, Australia, elevated moisture levels within pavement layers significantly reduce resilient modulus, accelerate permanent deformation, and compromise structural integrity, often necessitating prolonged road closures. These closures, while essential for asset protection, result in substantial socio-economic disruption. This study presents a scientifically grounded, moisture-based decision-making framework to support timely and safe post-flood road reopening. The research integrates real-time field monitoring, predictive modelling, laboratory testing, and performance-based decision analysis. A flood-prone road section was instrumented with embedded moisture sensors, thermocouples, and a weather station, generating over two and a half years of continuous data. Pavement moisture variation was modelled using three complementary approaches: (i) an analytical climate-informed model, (ii) traditional machine learning algorithms, and (iii) numerical seepage modelling using SEEP/W. Laboratory testing, including soil-water characteristic curves, permeability, and repeated load triaxial experiments, quantified the influence of Degree of Saturation (DoS) on resilient modulus and plastic strain. A novel Pavement Suitability Index (PSI), combining elastic stiffness and deformation accumulation, was developed to link moisture state with pavement performance. Critical and ultimate DoS thresholds were identified, enabling classification of traffic operation into safe, cautionary, and critical zones. The resulting PSI–DoS–ESA framework provides a practical tool for estimating allowable traffic under varying moisture conditions. Field validation demonstrated strong agreement between predicted recovery trends and observed pavement behaviour, highlighting the framework's effectiveness for real-time, evidence-based flood recovery decision-making.

Supervisor: A/Prof. Chaminda Gallage

CLARENCE JOHN BUTCHER
UNIVERSITY OF NEWCASTLE

Application of StADSS to large in-situ rock discontinuities: practical challenges and theoretical developments

Predicting the shear strength of large in situ rock discontinuities remains a

longstanding challenge in rock mechanics, primarily due to scale effects. This thesis advances the Stochastic Approach for Discontinuity Shear Strength (StADSS), an emerging methodology that bypasses the effects of scale by making predictions of shear strength at full scale. Addressing the gap between laboratory validation and field implementation, the research undertakes three major investigations to enable the practical application of StADSS to natural discontinuities. First, a field ready digitisation workflow was developed to extract discontinuity seed traces from photographic imagery. The study quantified the influence of camera orientation, resolution, and post processing on trace accuracy, demonstrating that errors can be constrained within $\pm$10% when using a ground sampling distance below 1.4 mm/pixel and maintaining a near perpendicular imaging angle. Secondly, rock strength variability was investigated through an extensive testing program on various rock materials to find economic methods for determining strength variability. A Monte Carlo algorithm was presented to capture the influence of material strength variability in predictions of shear strength by StADSS. Finally, StADSS was applied to a large limestone discontinuity, predicting peak and residual shear strengths of 442.9 kPa and 16.0 kPa respectively. For comparison, an experimental full-scale pull test resulted in an in situ measured shear strength of 27.1 kPa. While peak predictions could not be validated due to prior displacement, residual predictions aligned closely with observed stability, confirming the feasibility of applying StADSS at field scale. The thesis identifies key avenues for refining roughness digitisation and expanding in situ validation of StADSS.

Supervisors: Prof Olivier Buzzi, Prof Anna Giacomini, Dr Robert Bertuzzi and Prof Vaughan Griffiths

XIN LI
UNIVERSITY OF NEWCASTLE

Discrete element modelling of soil-buried pipe interaction problems

Accurate modelling of soil-pipe interaction is essential for the stress analysis of buried pipelines exposed to differential ground movements. In practice, this is done using beam-on-nonlinear Winkler spring models. However, methods in current piping guidelines for calculating spring parameters rely on simplifications, such as shallow embedment depths, specific ground movement directions (vertical, axial and lateral), and neglect of scale effects. While previous studies have attempted to address these gaps by physical and continuum-based numerical modelling, large-scale experiments are costly and continuum-based methods face challenges in simulating large deformations of granular backfill.

This thesis presents a Discrete Element Method (DEM)-based numerical methodology for analysing sand-pipe interactions. DEM contact parameters are calibrated using a Bayesian framework based on the simultaneous integration of independent triaxial and one-dimensional compression tests, resulting a unique parameter set that accurately reproduce the macroscopic behaviour of granular material across varying densities, stress paths, and stress levels. The methodology is validated against independent element tests and published 1-g physical model tests for pipe uplift, vertical penetration and lateral dragging. Computational techniques are also developed to efficiently simulate deeply buried and/or large-diameter pipes.

Predictions from the rigorously calibrated DEM models provide insights into: i) The mechanics underlying the critical embedment depth for pipe uplift, beyond which the normalised reaction does not futher increase with pipe embedment; ii) Scale effects on the peak lateral soil reaction; iii) The variation of the peak reaction on the pipe with the direction of imposed ground movement. Outcomes are further analysed to refine current state-of-practice methods for calculating Winkler spring parameters.

Supervisor: A/Prof. George Kouretzis

ADAM DAVID LINES
UNIVERSITY OF NEWCASTLE

Transversely isotropic brittle enhanced representation (TIBER) for better capturing the impact of discontinuity stiffness and damage initiation on extent of failure

Accurately simulating brittle failure in sedimentary rocks requires improved characterisation of damage thresholds and stiffness properties. Although numerical models have advanced significantly, their predictive capability remains limited by assumptions applied to key input parameters, particularly crack initiation thresholds and shear stiffness. This thesis addresses these limitations through experimental testing, constitutive criterion development, and numerical modelling.

The research first investigates crack initiation thresholds in sedimentary rocks by examining their relationship with unconfined compressive strength (UCS). A database of more than 500 UCS tests on sandstone, siltstone, and coal was compiled, with crack initiation identified using the Volumetric Strain Response Method and analysed through lognormal correlation and regression. The results show that crack initiation is strongly lithology-dependent, however maintains a consistent ratio to UCS within narrow ranges. These findings provide a robust statistical basis for estimating crack initiation in coal measure rocks.

The second component examines shear stiffness as a function of applied effective normal stress using direct shear tests on bedding-parallel fractures. Traditional assumptions were evaluated against experimental data that explicitly accounted for seating displacement and intact rock response. Results demonstrate that shear stiffness increases non-

linearly with effective normal stress and is best represented by a stress-dependent function.

These findings were implemented in FLAC2D models to assess their influence on failure extent. Models incorporating stress-dependent shear stiffness produced failure extents that matched observed field behaviour, validating the approach. Overall, this research links laboratory-derived parameters directly to numerical modelling inputs, improving the failure predictions for roof support design and stability analysis.

Supervisors: A/Prof Klaus Thoeni, Prof Olivier Buzzi and Prof Anna Giacomini

MAHNOUSH GHAREHDAGHI
UNIVERSITY OF NEW SOUTH WALES

Analytical and numerical modelling of consolidation and strain localisation in unsaturated soils

Unsaturated soils are commonly encountered in geotechnical applications, such as roads, embankments, dams, and retaining walls. Their behaviour is governed by the coexistence of air and water phases, and the interactions between the pore fluids and the soil matrix strongly influence their hydro mechanical response. Understanding phenomena such as consolidation and strain localisation in unsaturated soils is therefore essential for evaluating the performance and stability of geo structures.

This research presents analytical solutions to determine the pore air and pore water pressure parameters of unsaturated soils under undrained conditions, formulated within the effective stress framework. The solutions consider the effect of hydraulic hysteresis on the effective stress parameter and the soil water characteristic curve. Validation against experimental data and discussions on the effects of the initial degree of saturation, hydraulic hysteresis, and soil compressibility on the pore pressure parameters are provided. An analytical consolidation framework is further established, yielding two simplified diffusion type equations analogous to Terzaghi's formulation, enabling prediction of pore pressures evolution and settlement in unsaturated soils.

Additionally, a fully coupled numerical model is introduced for analysing strain localisation in unsaturated soils, based on the concept of effective stress and incorporating a novel viscoplastic constitutive formulation based on the consistency condition. Implemented in COMSOL Multiphysics, the model captures rate dependent behaviour in geomaterials and regularises strain localisation problem, effectively mitigating mesh sensitivity. Through a series of simulations, the effects of permeability, strain rate, confining pressure, drainage conditions, and initial suction are studied on the strain localisation in saturated and unsaturated porous media.

Supervisors: Prof. Nasser Khalili and Dr. Babak Shahbodagh

ARTURO JIMENEZ HUAMANLAZO
UNIVERSITY OF NEW SOUTH WALES

CPT results and liquefaction of variably saturated tailings

This research investigates the saturated and unsaturated behaviour of one silty Platinum and one sandy Copper tailings to assess their susceptibility to static and dynamic liquefaction. The cone penetration test (CPT) is employed to characterise their properties under saturated and unsaturated conditions, focusing on loose, contractive states with high degrees of saturation.

Water retention properties were determined using filter paper and pressure plate tests. A novel empirical method is proposed for rapid estimation of the Water Retention Curve (WRC), incorporating void ratio dependency. This method links fractal and other Particle Size Distribution (PSD) characteristics to the WRC parameters, demonstrating good agreement with experimental data for both soils and tailings.

The stress-strain behaviour was established via saturated triaxial, closed-system triaxial, and oedometer tests. The closed-system condition, relevant for rapid post-failure deformations where pore air and water become trapped, was modelled using a bounding surface plasticity framework. This constitutive model integrates Boyle's Law and hydraulic hysteresis to simulate the coupled variations in pore pressures, suction, and volume change, achieving validated simulations against triaxial results.

CPTs conducted in calibration chambers and shear stacks utilized cavity expansion analysis, incorporating the closed-system behaviour via the bounding surface model (for air volume fractions below ~15%). This analysis yielded charts correlating normalised cone resistance to the initial state parameter across a range of air volume fractions, enhancing CPT interpretation.

Shaking table tests enabled the development of Critical State-based correlations between Cyclic Stress Ratio (CSR) and Arias Intensity with cone tip resistance to assess liquefaction triggering and settlement under seismic loading.

Supervisor: Prof Adrian Russell

SANA SHAHOVEISI
UNIVERSITY OF NEW SOUTH WALES

A fully coupled hydro-mechanical model for the analysis of fractured porous media

This thesis presents a comprehensive study of hydraulic fracture propagation in poroelastic media using advanced numerical techniques. This work proposes two numerical frameworks: (i) a hydromechanical fully coupled, dynamic phase-field model, and (ii) a Physics-Informed Neural Network (PINN) framework for elastic fracture analysis.

First, a novel phase-field formulation is developed to simulate fluid-driven fracture propagation. The model introduces a new strain-based crack width formulation, offering improved numerical stability, ease of implementation and enhanced estimation of fracture aperture and permeability. Implemented in COMSOL Multiphysics, the formulation captures the dynamic response of fractured porous media by incorporating inertial effects and a fully coupled treatment of fluid pressure and solid deformation. The phase-field model is first verified against the classical KGD solution. Additionally, dynamic fracture propagation in a concrete gravity dam is modelled. The model is extended to simulate multizone hydraulic fracturing and multi-layered porous media with varying mechanical and hydraulic properties. The model is further applied to simulate hydraulic fracturing in multi-layered media containing pre-existing (natural) fractures enabling the simulation of branching, coalescence, and asymmetric growth paths.

Next, a PINN framework based on NVIDIA Modulus is developed as a mesh-free and flexible alternative for elastic fracture modelling. The framework is extended by employing adaptive loss weights to improve training efficiency and accuracy, particularly in regions with sharp stress gradients near crack tips. Extensive verification studies, including two-dimensional inclined single cracks, heavily fractured domains, and three-dimensional single and multiple penny-shaped fractures, demonstrate strong agreement between the PINN predictions and high-fidelity finite element results.

Supervisors: Prof. Nasser Khalili, Dr. Babak Shahbodagh and Dr. Mohammad Vahab

PENGHAO ZHANG
UNIVERSITY OF NEW SOUTH WALES

Efficient simulation of quasi-brittle cracking in concrete and rock using the phase field method and scaling theory

Engineering structures made of rock and concrete may fracture, often due to extreme external loads arising while in service. Understanding and simulating accurately the fracturing processes assists with the optimization of structural design and enhances reliability. Numerical models based on continuum and fracture mechanics are employed extensively to simulate and interpret these fracturing processes. However, many mesh-based continuum methods have mesh-dependent limitations. This study presents a new and enhanced phase-field fracture mechanics model, and novel scaling laws that are implemented within it, to address these critical issues. First a new dimensionless framework of basic phase-field models is proposed. New scaling laws for the fracture toughness and characteristic length are proposed that enable the non-dimensionalized model outputs to be rescaled and made applicable to any size as long as the structure and load configuration similarities are maintained. An enhanced phase-field fracture model that incorporates the damage constitutive law is also proposed. This model is capable of simulating the quasi-brittle fracturing process, size effects and compressive-shear cracking phenomenon in concrete samples and rocks at laboratory and field scales. Finally, the proposed fracture mechanics model is used to simulate failures caused by tunnel excavations in rock masses. The crack initiation and ultimate macroscopic failure features at the tunnel scale are reproduced. The proposed scaling theory for characteristic length and mesh size minimizes computational resource consumption when applied to tunnel excavation case studies. Accurate and efficient simulations of the failure patterns and depths, and corresponding deformations induced by excavation, are attained.

Supervisors: Prof Adrian Russell and A/Prof Kurt Douglas

AAYUSH KUMAR
UNIVERSITY OF QUEENSLAND

Thermo-mechanics of asphalt mixes with crushed waste glass aggregates

The growing focus on sustainable pavement construction has encouraged the use of synthetic alternative aggregates such as crushed waste glass (CWG) in hot mix asphalt (HMA). As the topmost and most expensive layer, asphalt must withstand traffic loads, temperature variations, and rainfall. Therefore, understanding its fracture and thermo-mechanical behaviour under combined stresses is crucial, especially when new materials like CWG are used. This study investigates the fracture behaviour and thermo-mechanics of dense-graded HMA mixes with varying CWG contents (2.5–42.5%) replacing natural fine aggregates. Standard and advanced testing methods were employed to evaluate stiffness, cracking resistance, and deformation under simple and complex stress states. Aggregate morphology—including sphericity, roundness, angularity, and surface roughness—was characterized using image analysis, 3D profilometry, and fractal analysis. Specimens designed using the Marshall method were tested using IDEAL-CT and Brazilian tests, coupled with stereo high-speed photography at –20°C, 0°C, and 60°C to capture crack initiation, propagation, and speed. Thermal properties (conductivity, diffusivity, and specific heat) were measured using the Transient Plane Source method; while rutting and moisture susceptibility were evaluated via Hamburg Wheel-Tracking tests. Further, ultrasonic pulse velocity (UPV) tests identified crack thresholds during uniaxial and biaxial loading. True triaxial test results, fitted to Mogi-linear, Mogi-power, and Drucker–Prager criteria, showed CWG's influence on

stiffness and failure characteristics. Overall, the study demonstrates that CWG enhances rutting resistance and mix stiffness yet offers a sustainable and mechanically distinct alternative aggregate for asphalt mixtures.

Supervisors: Dr Mehdi Serati, Ian van Wijk, A/Prof Prashanth Vangla and Prof G V Ramana

KEITH MANDISODZA
UNIVERSITY OF QUEENSLAND

Tailings dam design process, parameters, and risk assessment

The engineering of modern Tailings Storage Facilities (TSFs) is struggling to keep pace with increased mineral waste production, relying on static, deterministic procedures inherited from water dam design. TSFs are complex, dynamic systems, yet current design specifications critically fail to account for the inherent knowledge uncertainty in key design parameters (e.g., material properties, site conditions) and operational changes. This reliance on simplified methodologies (like static Fault Tree Analysis, FTA) often leads to suboptimal, costly designs or, critically, catastrophic failures like Mount Polley and Brumadinho.

This thesis comprehensively critiques the current TSF design process, risk tolerability standards, and traditional risk assessment methods. It introduces Bayesian Networks (BNs) as a dynamic, probabilistic framework to improve the treatment of these uncertainties. The methodology involves mapping the FTA models from historical failure expert panel reports (Mount Polley, Fundão, Cadia, Brumadinho) into BNs.

This process enables quantitative dependency analysis, allows for the inference updating of prior probabilities upon receiving new monitoring data, and facilitates predictive accident analysis. The findings lead to the proposal of a streamlined, risk-informed design method that integrates uncertainty analysis. This optimisation approach minimises uncertainty in input parameters, thereby ensuring that TSF designs are neither over-designed nor under-designed, significantly improving dam safety and economic efficiency.

Supervisors: Emeritus Prof David Williams

ZHONGYU XU
UNIVERSITY OF QUEENSLAND

Large ring test for restrained shrinkage cracking in concrete and shotcrete

The Restrained shrinkage is a common cause of early-age cracking in shotcrete tunnel linings. This thesis develops and evaluates an upscaled concentric ring test to investigate restrained shrinkage at practical scales.

The study commenced with parametric analyses to inform specimen geometry and drying conditions. A large concentric apparatus was procured and comprehensively instrumented. The experimental programme evolved from half to full Wheatstone bridge configurations, incorporating calibration procedures and temperature cancellation. These measures enabled stable, multi-week measurements and reliable crack detection.

Experimental and numerical studies demonstrated that interface friction governs both the magnitude and angular distribution of restraint. Four series of large-ring tests examined the effects of instrumentation, drying mode, sealing, and interface preparation. Numerical models reproduced these effects and showed that peak stresses localise within high-friction or bonded sectors, while subdivision and symmetry of stick–slip regions mitigate stress concentrations.

An energy-based interpretation was developed by distinguishing between the reference elastic energy associated with free shrinkage and the elastic energy inferred from steel-ring strain measurements. Application to large-ring data indicates that early-age behaviour is dominated by relaxation loss, while stored elastic energy increases as concrete stiffness develops and shrinkage rates decline.

The thesis concludes with practical recommendations on test geometry, instrumentation, boundary control, interface preparation, and data interpretation, and outlines future work on thick-ring calibration and field correlation. Together, these contributions establish an upscaled ring methodology that enhances the reproducibility and diagnostic value of restrained-shrinkage testing for tunnel linings.

Supervisors: Dr Jurij Karlovšek, Dr Harry Asche and Dr Lucija Hanžič

SHIMA ENTEZAM
UNIVERSITY OF SOUTHERN QUEENSLAND

Load transfer mechanisms of composite rock bolts for strata reinforcements

Fully grouted rock bolts are central to strata reinforcement in underground mining and civil excavations. Still, their reliability depends on how the load is transferred through the rock bolt-grout-rock system as bonding degrades. Due to limited research on axial load transfer in fibreglass reinforcement, this thesis examines composite rock bolts. It develops practical pathways and advanced manufacturing technologies to improve the performance of fully grouted rock bolts. A systematic review consolidates research on the axial and shear loading mechanisms of fully grouted rock bolts and identifies gaps in test standardisation, the interpretation of bond-slip response, and the integration of data-driven modelling. Laboratory pull-out tests on fully grouted fibreglass rock bolts then quantify the effects of embedment length, confinement diameter,

rock bolt diameter, grout strength, water-to-grout ratio and curing time on peak load capacity and post-peak load-displacement behaviour. Using the experimental database, machine-learning models are developed to predict the axial load-bearing capacity of fibreglass and steel rock bolts and the grout uniaxial compressive strength. An ensemble framework with SHAP-based interpretation shows that curing time, grout strength and water content dominate capacity, providing transparent, physically consistent guidance for grout optimisation and rock bolt selection. Then, a new generation fibreglass rock bolt is manufactured using a hybrid pultrusion-braiding process with nano graphene-modified epoxy. Large-scale mechanical testing, including single- and double-shear, pull-out, tensile, and torsional tests, demonstrates improved shear capacity, ductility, and stability compared with conventional fibreglass rock bolts. Thesis outcomes deliver an integrated mechanistic, predictive and manufacturing pathway for corrosion-resistant composite rock bolts.

Supervisors: Prof Ali Mirzaghorbanali, Prof Kevin McDougall, Prof Warna Karunasena and Prof Naj Aziz

BEHSHAD JODEIRI SHOKRI
UNIVERSITY OF SOUTHERN QUEENSLAND

A step toward better understanding rock bolt technology

This thesis advances rock bolt technology through a coordinated program of systematic review, laboratory testing, three-dimensional numerical simulation, machine-learning-based prediction, and the development of fibreglass rock bolts. A systematic review of axial load-transfer research identified persistent gaps related to grout-controlled behaviour, realistic installation deviations, and the absence of reliable predictive frameworks for assessing rock-bolt performance under practical design conditions. Controlled laboratory pull-out testing generated datasets for axial capacity, beginning with 34 tests in which curing time (CT) and water-to-grout ratio (W/G) were varied, and predictive performance was evaluated using multiple linear regression, multilayer perceptron neural networks, Bayesian-regularised neural networks, generalised feed-forward neural networks, and extreme gradient boosting. The modelling framework was subsequently expanded to incorporate grout type, grout uniaxial compressive strength (UCS), fly ash content, and confinement diameter, and to couple gradient-boosting ensembles with metaheuristic optimisation algorithms to improve robustness and generalisation. To investigate the mechanical behaviour of grout, 253 UCS tests were conducted on Australian commercial grouts across a range of CT and W/G values, enabling the development of ANN- and CatBoost-based predictive models. Installation realism was addressed through pull-out testing of fully resin-encapsulated systems with varying levels of eccentricity and inclination, together with validated three-dimensional ABAQUS finite-element modelling to examine stress redistribution and the development of interface damage; peak load reductions of up to 69.6% were observed at the highest eccentricity. Also, a new prototype of fibreglass rock bolt was manufactured and assessed through single-shear testing, demonstrating a 26% increase in shear capacity compared with conventional ones.

Supervisors: Prof Ali Mirzaghorbanali, Prof Kevin McDougall, Prof Warna Karunasena and Prof Naj Aziz

REEM OMAR ALQAISI
UNIVERSITY OF TECHNOLOGY SYDNEY

Engineering characteristics of expansive soils stabilised with eggshell powder and lime/cement: a sustainable approach

Expansive soils, characterised by low bearing capacity and significant volume changes due to moisture fluctuations, pose major challenges for construction projects such as pavements, highways, foundations, and canal linings. These soils are widespread in regions including South Africa, Australia, India, and the United States, where shrink–swell behaviour can cause serious structural damage. With increasing global construction activity, effective stabilisation is essential to improve their engineering performance. Chemical stabilisation using lime or cement is commonly applied to enhance strength and reduce swelling. This study investigates eggshell powder (ESP), a calcium oxide–rich bio-waste, as a supplementary additive to hydrated lime or cement for expansive soil stabilisation. ESP was produced by rinsing, crushing, and sieving discarded eggshells, offering a sustainable and cost-effective alternative. While ESP has been used in bricks, concrete, and alkali-activated binders, limited research has examined its combined use with lime or cement in expansive soils.

An experimental program evaluated electrical, physical, mechanical, and microstructural properties of stabilised soils, supported by numerical modelling of embankment performance on treated soft soils in Australia. Artificial expansive soil composed of kaolinite, bentonite, and fine Sydney sand was tested. Electrical conductivity results identified optimal ESP–lime or ESP–cement ratios. Mixtures of 5% lime with 5% ESP and 6% cement with 6% ESP significantly improved CBR, UCS, and Gmax compared with lime or cement alone. Numerical modelling in Ballina, NSW, confirmed reduced settlement and lateral displacement, demonstrating ESP as an effective sustainable stabilisation additive.

Supervisors: Prof Hadi Khabbaz and Prof Behzad Fatahi

MARLISIO OLIVEIRA CECILIO JUNIOR
UNIVERSITY OF TECHNOLOGY SYDNEY

Shear behaviour of saturated infilled rock joints under cyclic loading in the hollow cylinder apparatus

The proper estimation of stresses generated by train passage is of fundamental importance for the serviceability and longevity of railways; however, limited knowledge is available where the track substructure is built on a jointed rock mass. The present study introduces an analytical solution for estimating the three-dimensional ground stresses arising from moving wheel loads, applied to a jointed rock subgrade to determine the normal and shear stresses acting along a specific discontinuity plane. A discussion is presented on the experimental investigation of the shear behaviour of saturated, undrained, infilled rock joints, with particular emphasis on realistic laboratory simulation of cyclic loads induced by train passage. The Hollow Cylinder Apparatus is identified as the most suitable device for this purpose, following key adaptations including the installation of mini pore pressure transducers directly at the joint and the fabrication of a bottom platen extension, together with other minor innovations. Numerical models based on the Distinct Element Method are developed to simulate jointed samples, aiming to anticipate laboratory behaviour and support pre-established hypotheses. A series of static tests is first conducted on clean joints with planar, saw-tooth, and natural profiles, as well as on saturated infilled joints, to validate the applicability of the HCA for rock joint testing, particularly with respect to pore water pressure application, maintenance, and measurement within the infill soil. Finally, dynamic cyclic tests are performed on saturated, undrained, infilled rock joints using loading histories derived from the proposed analytical solution, simulating realistic Australian railway traffic patterns and assessing the influence of joint orientation on the experimental response.

Supervisors: Prof Buddhima Indraratna and Prof Cholachat Rujikiatkamjorn

RAMESH GEDELA
UNIVERSITY OF TECHNOLOGY SYDNEY

Bioremediation of soft subgrade for enhanced performance of rail infrastructure

The demand for faster and heavier railway transportation has increased axle loads and train speeds, intensifying subgrade instability problems in soft coastal soils in Australia. These soils frequently experience mud pumping and excessive deformation under unfavourable cyclic loading and drainage conditions, resulting in high maintenance requirements. Although conventional ground improvement methods exist, a sustainable solution for mitigating subgrade instability remains limited. This study investigates the potential of the biopolymer Xanthan Gum (XG) as an eco-friendly stabilisation method for low-plasticity subgrade soils under railway loading. The soil was obtained from an active railway site with a history of mud pumping. A series of laboratory tests were conducted to evaluate the influence of fines content and XG dosage on soil strength, stiffness, critical state behaviour, and undrained cyclic response. The effects of loading parameters, including cyclic stress ratio and loading frequency, on treated soils were also examined. The results indicate that an optimum XG content of approximately 1.5–2.0% by dry soil weight significantly enhances stiffness, strength, and residual resistance, while reducing strain softening. Increasing fines content further improved soil performance. Under cyclic loading, XG-treated soils exhibited reduced excess pore water pressure generation and plastic strain accumulation compared with untreated soils. The treatment effectively limited internal moisture migration and suppressed upward fines movement, thereby mitigating subgrade fluidisation. Overall, XG treatment provides apparent cohesion through interparticle bonding, substantially improving resistance to cyclic loading and offering a promising sustainable solution for railway subgrade stabilisation.

Supervisors: Prof Buddhima Indraratna, Dr Subhani Medawela, Dr Thanh Nguyen and Prof Behzad Fatahi

LAKSHMI NAIR
UNIVERSITY OF TECHNOLOGY SYDNEY

Subgrade soil behaviour under a three-dimensional stress state, including principal stress rotation

The increasing demand for sustainable railway transportation has highlighted the vulnerability of soft subgrade soils with low to medium plasticity when subjected to high cyclic stresses and inadequate drainage. Such conditions often lead to instability phenomena such as mud pumping, driven by the rapid accumulation of excess pore water pressure (EPWP), particularly under heavier and faster train operations where principal stress rotation (PSR) becomes significant. This study investigates the combined effects of cyclic vertical stress and torsional shear stress on the load–deformation behaviour of low-plasticity subgrade soil using a hollow cylinder apparatus. Soil specimens were retrieved from a coastal railway site affected by mud pumping. Continuous and multi-stage intermittent cyclic loading tests, incorporating drained and undrained rest periods, were conducted to examine EPWP evolution and multidirectional strain responses. The results demonstrate that strain accumulation is strongly influenced by the interaction between vertical and torsional stresses, with increasing torsional stress significantly accelerating instability. A critical torsional-to-vertical stress ratio was identified, beyond which soil instability is triggered. To characterise this behaviour, a stiffness degradation index (δ_0) accounting for PSR effects

is proposed as an early indicator of instability. In addition, a normalised torsional stress ratio (NTSR) is introduced to quantify the influence of torsional loading, with higher NTSR values leading to premature failure. The findings further highlight the crucial role of drainage and loading history in controlling subgrade stability. Finally, a constitutive model based on the multilaminate framework with bounding surface plasticity is proposed to predict cyclic soil behaviour under PSR.

Supervisors: Prof Cholachat Rujikiatkamjorn, Prof Buddhima Indraratna and Dr Thanh Nguyen

ABU SADAT MOHAMMAD RIYAD
UNIVERSITY OF TECHNOLOGY SYDNEY

Geotechnical characteristics of a rubber-mixed granular medium under monotonic and cyclic loading

Improving the safety and resilience of transport substructures is crucial for ensuring long-term durability. As transportation infrastructure grows to meet the demands of developing communities, the need for raw materials, often sourced from natural quarries, continues to increase. Traditional railway substructure materials, however, are prone to breakage and require more maintenance compared to recycled alternatives. In response, environmental agencies are promoting eco-friendly practices, advocating for the use of repurposed waste materials as a sustainable alternative. Previous studies have explored the potential of combining rubber crumbs and mining waste as a replacement for conventional substructure materials, particularly for railway capping layers. This study focuses on coal wash and rubber crumb (CWRC) mixtures as a sustainable alternative for railway infrastructure, specifically targeting the capping layer. The monotonic behaviour of CWRC mixtures was analysed under single-stage and multi-stage triaxial loading conditions. The results reveal that a 10% rubber crumb (RC) content provides optimal deformation, strength, and energy dissipation, consistent with previous studies. A semi-empirical model was also introduced to describe the single-stage monotonic triaxial behaviour of CWRC mixtures, considering the compressibility of RC. Additionally, the study examines the influence of single-stage cyclic triaxial loading on CWRC mixtures, investigating shear performance, fatigue behaviour, disturbance, and modulus degradation. The research also explores the shakedown behaviour of CWRC mixtures with 10% RC content under multi-stage cyclic triaxial loading, reflecting the varying stress levels that railway substructure materials are subjected to over time. The findings will support more accurate material evaluations, enhancing long-term performance predictions for railway substructures.

Supervisors: Prof B Buddhima Indraratna, Prof Hadi Khabbaz, Dr Yujie Qi, Dr Chathuri Madhusanka Kulappu Arachchige

JUNSIK BAE
UNIVERSITY OF WESTERN AUSTRALIA

A new frontier in dynamically installed anchors

Dynamically installed anchors offer a cost-effective alternative to conventional anchoring systems, as they are installed by freefall penetration without the need for external energy, making them suitable for deep-water applications. This thesis presents an integrated investigation into the development, optimisation, and validation of a novel dynamically installed anchor (DIA), referred to as the maverick anchor, for mooring offshore floating facilities.

The anchor geometry was systematically developed using large-deformation finite element (LDFE) analyses in clay and computational fluid dynamics (CFD) simulations in water. Key design features include a narrow tip angle, sloped shaft, optimally positioned trapezoidal main fins, and trailing fins to enhance stability, embedment depth, and diving potential. A novel frictional algorithm was also developed to more accurately capture velocity-dependent anchor–soil interface behaviour during installation.

Water tank tests and CFD simulations demonstrated that the maverick anchor achieves higher freefall velocities and a lower drag coefficient than existing dynamically installed anchors. LDFE analyses indicated significantly deeper penetration, and an improved analytical framework based on cavity expansion theory was proposed to better predict embedment depth. Loading analyses further revealed enhanced diving and keying behaviour, leading to higher holding capacity with reduced loss of embedment.

Finally, centrifuge model tests conducted in Gulf of Mexico clay and North-West Shelf calcareous silt were used to validate the numerical results. The maverick anchor achieved deeper embedment and higher capacity than the reference anchors tested under the same conditions, indicating its improved performance across the examined soil types and loading scenarios.

Supervisors: Prof Muhammad Shazzad Hossain and Dr Youngho Kim

PUORYA KAZEMI ESFEH
UNIVERSITY OF WESTERN AUSTRALIA

Numerical modelling of vibratory pile installation in sand

Vibro-driving has emerged as a promising alternative to conventional impact hammering for pile installation, particularly in sand, offering faster and quieter installation. However, despite its growing adoption, key uncertainties persist regarding the vibro-driveability of open-ended piles and their post-installation behaviour. This PhD research aims to address

these uncertainties by numerically investigating the soil mechanisms governing pile vibro-driving in saturated sand. The findings underscore the significant influence of vibratory parameters, such as the dynamic-to-static force ratio and frequency, and soil permeability on total soil resistance, penetration rates, soil state evolution, and excess pore pressure generation during installation.

Supervisors: Prof. Britta Bienen and Prof. Fraser Bransby

BINGCHANG ZHANG
UNIVERSITY OF WESTERN AUSTRALIA

Scour-induced span elongation and associated hydrodynamics

Scour-induced span development and elongation beneath subsea pipelines and power cables can significantly affect their on-bottom stability and structural integrity. Although several predictive models for free-span development exist, they are all derived from small-scale laboratory tests, and the associated scaling effects remain insufficiently understood. In addition, the spatiotemporal evolution of scour and the governing hydrodynamics remains insufficiently understood.

Motivated by these knowledge gaps, this PhD thesis documents a series of laboratory experiments undertaken to investigate scaling effects on span development and elongation beneath a model pipeline. The results revealed that bed ripple formation under live-bed conditions is an important scale effect, offering a clear explanation for the variability in span elongation rate commonly observed in previous studies. This scaling effect was further examined through experiments conducted across a wide range of model scales in one of the world's largest flume facilities. The outcomes confirmed the influence of bed ripples and enabled the development of a new predictive model for span elongation that explicitly accounts for scaling effects.

The study also provided systematic characterisation of the spatiotemporal evolution of three-dimensional scour features near the span shoulder. Complementary numerical simulations, incorporating realistic scour-hole geometries, were performed to investigate the underlying mechanisms of span elongation and the hydrodynamic processes acting on the free span.

Overall, this research delivers a comprehensive understanding of scour evolution and span development across scales ranging from laboratory models to field conditions. This understanding improves our ability to extrapolate laboratory observations to full-scale subsea pipelines and power cables, better informing pipeline and cable design and the adoption of more robust span mitigation strategies.

Supervisors: Dr Hongwei An and Prof Scott Draper

ABDULLAH MUHAMAD ALI AL-RAWABDEH
UNIVERSITY OF WOLLONGONG

Experimental and numerical modelling of helical pile foundation

Helical (screw) piles are an advanced foundation system that uses a steel foundation with a helical bearing plate attached to be driven into the ground. Helical piles use has grown rapidly due to advantages such as quick installation; cost effectiveness; high tensile and compression bearing capacities; and carrying loads immediately after installation. Despite these advantages, conventional design approaches idealise the helix as a flat disc, disregarding its actual 3D geometry and its influence on performance. The impact of helix shape on key parameters such as torque, capacity, and soil–structure interaction remains insufficiently understood. Furthermore, helical pile finite element models have largely neglected the complex deformations induced during installation and often overlook the role of helix geometry in altering the load-transfer mechanism. This study aims to fill these critical gaps by investigating the effects of helix geometry and shape on the installation process and axial-bearing performance of helical piles. A large-scale apparatus was developed to conduct laboratory experiments incorporating a variety of novel and conventional helix shapes to examine their influence. A robust 3D FE model, leveraging the Coupled Eulerian Lagrangian approach developed to analyse Key factors such as installation torque, soil disturbance, and load transfer mechanisms. The experimental and numerical simulations provide a comprehensive understanding of the influence of helix shape on the behaviour of helical piles and help to develop equations to enhance the predictive accuracy of installation torque–capacity relationships and refine empirical and numerical methods of predicting the helix shape effect on helical pile ultimate capacity.

Supervisors: A/Prof Jayan S. Vinod, Prof Timothy McCarthy and Dr Martin D. Liu

CHAPTER NEWS

NEW SOUTH WALES

2025 NSW Research Award Night
Event Mentors: Stefano Pirrello (Deep Foundation Solutions), Dr Pan Hu (Western Sydney University), and A/Prof Jianfeng Xue (University of New South Wales)

The 2025 NSW Research Award Night on 13 August, hosted by the Sydney NSW and Newcastle Chapters of the Australian Geomechanics Society (AGS), was a resounding success, showcasing the cutting-edge research of emerging geotechnical professionals from across New South Wales. Held in Sydney and Newcastle, the event provided a vibrant platform for postgraduate students to present their work to a broad audience of industry experts, academics, and fellow engineers.

This prestigious annual event reflects AGS's ongoing commitment to supporting academic institutions and fostering the next generation of geotechnical leaders. The award aims to highlight outstanding research in Geotechnical Engineering and Engineering Geology, encouraging knowledge exchange between universities and the professional community.

The evening was expertly coordinated by Stefano Pirrello, Pan Hu, and Jianfeng Xue, whose efforts ensured a seamless and engaging experience for all attendees. Their dedication to promoting academic excellence and industry collaboration was evident throughout the event.

AGS extends its sincere thanks to Arcadis, and in particular Dr Jim Yang and his team, for generously hosting the event. Their support provided a welcoming and professional environment that helped make the evening both enjoyable and impactful.

Five exceptional finalists were selected to present their research, each offering unique insights into the challenges and innovations shaping the future of geotechnical engineering:

Winner: Guilherme Barros (University of Newcastle) presented his PhD research on dynamic coupling of boundary and discrete element methods for large-scale geotechnical simulations. His work in computational mechanics advances the accuracy and efficiency of numerical modelling in geomechanics.

Isabella Novais Silva (University of Technology Sydney) shared her work on enhancing railway infrastructure resilience, focusing on soft soil behaviour, soil stabilisation, and sustainable ground improvement using recycled materials. Her research has already earned international recognition, including the ISSMGE Bright Spark Lecture Award in 2024.

Maria Julieta Rottemberg (University of New South Wales) presented her research on energy tunnels and the thermo-hydro-mechanical behaviour of energy geostructures. Her advanced numerical modelling offers a practical framework for integrating geothermal energy into underground infrastructure, contributing to climate-adaptive urban planning.

Farshad Bahootoroody (University of Newcastle) discussed his work on geotechnical risk management of scenic rock cliffs. With a strong publication record and international research collaborations, Farshad's research addresses safety and sustainability in natural hazard-prone environments.

Sajjad Vaseghi (University of Technology Sydney) showcased his expertise in unsaturated soils and soil dynamics, with applications in transportation geotechnics and underground infrastructure. His research bridges academic theory and engineering practice, contributing to safer and more efficient geo-infrastructure design.

Each finalist delivered a compelling presentation tailored to an audience of practicing geotechnical engineers, demonstrating not only technical excellence but also the relevance of their work to real-world challenges.

Winner: Guilherme Barros, Finalists: Farshad Bahootoroody, Sajjad Vaseghi, Maria Julieta Rottemberg, Isabella Novais Silva, Event host: Stefano Pirrello (From left to right)

2025 AGS GOLD50+ Presentation
Event Coordinator: Dong Wang (PSM)

On Wednesday, 8 October 2025, the AGS Sydney Chapter proudly hosted the Gold 50+ Membership Talk at Engineers Australia, featuring Mr. Tim Sullivan presenting on "Complex Systems in Slope Engineering." Drawing over 750 registrations, it was one of the year's most attended AGS Sydney events.

Tim shared insights from his five decades of geotechnical experience, combining technical expertise with a reflective perspective on slope behaviour. He explored how applying complex systems thinking can deepen understanding of natural slopes, drawing lessons from fatal landslides, mine river diversions, and large open-pit slopes. Tim emphasised that many failures arise not from incompetence but from underestimating the dynamic, interconnected, and evolving nature of slopes.

Through vivid case studies, he illustrated key principles of complexity science. Natural slopes are open systems, constantly exchanging energy and matter, never in true equilibrium, and subject to gradual entropy. Minor instabilities can quietly develop over years, ultimately triggering

catastrophic failures under conditions unforeseen by traditional analysis.

Tim also highlighted the nested and interlinked nature of slope systems, where small changes in one subsystem can trigger abrupt shifts in stability elsewhere. He encouraged engineers to embrace uncertainty and adopt a systems perspective, explicitly considering entropy, system boundaries, coupling, self-organisation, and emergent behaviour. While risk can never be entirely eliminated, engaging with complexity enhances understanding, informs design, and reduces the likelihood of catastrophic failures.

Attendees responded enthusiastically, appreciating Tim's approach to blend rigorous technical insights with real-world lessons and reflective thinking. His presentation reminded engineers of the limits of prediction in geotechnical practice, while inspiring a broader, systems-focused approach to slope engineering.

The AGS Sydney Chapter thanks Mr. Tim Sullivan for sharing his wisdom and experience and expresses gratitude to the committee and volunteers whose efforts made this landmark event a success.

2025 AGS Gold 50+ event, from left to right: Ali Aref Nia, Cholachat Rujikiatkamjorn, Louise Sullivan, Tim Sullivan, Dong Wang

AGS Sydney Reactive Soils and Site Classification Course 2025
Event Mentors: Manuel Neves (Fortify Geotech)

Building on the continued demand for high-quality professional development across the industry, the AGS Sydney Chapter hosted the first edition of the Reactive Soils and Site Classification Course on 22 October 2025. Delivered by renowned educator Dr Stephen Fityus, the course provided attendees with a clear and practical understanding of reactive clay behaviour and the application of AS 2870 – Residential Slabs and Footings for site classification.

The one-day program blended theory with practical examples, giving participants valuable insights into the origins of soil reactivity, the key properties and behaviours of reactive clays, and how these factors influence foundation design. The course also explored the primary drivers of soil movement, common causes of residential foundation distress, and the principles of effective site investigation—including appropriate methods for testing soil reactivity.

Dr Fityus's clear explanations, real-world case studies, and engaging teaching style were standout features for many participants.

The session attracted a strong mix of early-career professionals and experienced practitioners seeking to refresh their understanding of reactive soil behaviour—highlighting the ongoing importance of robust site classification within the Australian geotechnical industry.

The AGS Sydney Chapter extends its appreciation to Dr Fityus, the event volunteer Manuel Neves, and all participants for contributing to another successful professional development event. We look forward to continuing to offer valuable training opportunities throughout the coming year.

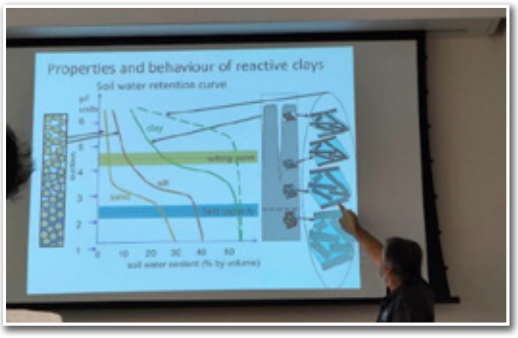

Dr. Stephen Fityus explaining the impact of soil moisture variation in the volumetric expansion of different soil types

2025 AGS Sydney Symposium
Event Coordinator: Alice Clark (Aurecon), Ali Parsa (JK Geotechnics), Hadi Khabbaz (UTS), Cholachat Rujikiat-kamjorn (UTS), Saman Zargarbashi (WSP), Sam Mirlatifi (Arcadis), AHM Kamruzzaman (TfNSW), Mehdi Tamadon (GHD), Mehrnaz Alibeikloo (WSP), Hamid Mortazavi Bak (Beca), Ali Aref Nia (Intrax), Pan Hu (Western Sydney University).

On Friday, 14 November 2025, the AGS Sydney Chapter proudly hosted the 29th Annual AGS Sydney Symposium at the Australian National Maritime Museum. With over 150 attendees, this flagship event focused on the theme "Climate-Responsive Ground Engineering" and brought together practitioners, researchers, and industry leaders to explore how geotechnics is both adapting to and driving solutions for a changing climate.

The program featured four themed sessions, two keynote presentations, and two invited speakers. International guest speaker Professor Slobodan Mickovski (Glasgow Caledonian University) delivered a compelling keynote on the use of vegetation and nature-based solutions for slope stability and resilience. Later in the day, Jim Yang (Arcadis) presented case studies highlighting how climate change is reshaping assumptions in design and construction across major infrastructure projects.

Across the event, speakers presented on a wide spectrum of climate-

relevant challenges. Topics included post-flood site reclassification, the coastal-geotechnical interface, rockfall risk simulation, and the reuse of landfill waste for infrastructure. Additional presentations explored the performance of temporary anchors beyond design life, reclassification and integration of uncontrolled fill, and the use of monitoring tools to optimise design. Afternoon sessions introduced attendees to interesting infrastructure case studies and emerging technologies in energy geo-structures.

The event reinforced the value of systems thinking, adaptive engineering, cross-disciplinary integration, and the need for climate-aware design frameworks. Throughout the day, Q&A discussions, networking breaks, and the post-event balcony drinks helped spark meaningful dialogue between professionals across sectors.

The Symposium concluded with a preview of next year's theme:

"Geotechnical Forensics: Lessons learnt from projects, courtrooms, and expert witnesses."

The AGS Sydney Chapter extends its thanks to all speakers, attendees, volunteers, and to Platinum Sponsor MM Geomechanics for their generous support. Special thanks also go to the organising committee for delivering a timely and energising event.

AGS Sydney Symposium registration desk

AGS Sydney Symposium speakers' trophies

AGS Sydney Debate Night
"Modern Codes for Modern Problems: Is Eurocode 7 the Solution to Australia's Geotechnical Design Challenges?"
Event Coordinator: Mehdi Hajian (GDA)

The AGS Debate Night on 10 December brought together four experienced geotechnical professionals to critically examine whether Eurocode 7 (EC7) offers a suitable framework for addressing Australia's evolving geotechnical design challenges. Rather than a simple "yes or no" outcome, the discussion highlighted that EC7 provides valuable lessons but is not a direct plug-and-play solution for Australian practice.

Each panellist provided their view as follows:

Eurocode 7: Ambition, Strengths, and Practical Challenges

Jamie focused on the structure and evolution of Eurocode 7, noting its ambition, breadth, and strong emphasis on harmonisation across Europe. He also noted recent EC7 updates were recognised for improvements in ground modelling, parameter selection, and design value assessment

However, concerns were raised about the complexity and length of the code, extensive cross-referencing, and the separation of design from construction execution. It was argued that, in some areas, valuable practical knowledge embedded in older standards may have been diluted or lost. The discussion also highlighted limitations in EC7 regarding performance monitoring, particularly the difficulty of directly monitoring ultimate limit state performance in geotechnical systems.

Reliability- and Risk-Based Design as the Real Gap

Ramtin argued that the core issue is not the absence of codes, but the lack of explicit reliability calibration in many Australian geotechnical standards. Geotechnical design was framed as an uncertainty-dominated discipline, where traditional ASD and LRFD approaches are reaching their limits for complex problems.

He noted that risk-based and reliability-based design were presented as essential tools for modern practice, enabling engineers to quantify uncertainty, consequences, and cost-of-risk more transparently. It was suggested that second-generation Eurocodes demonstrate a clear shift in this direction and offer a useful reference for the future evolution of Australian standards.

Ondrej emphasised that Australia already has a successful example of a reliability-based geotechnical standard in AS2159 (Piling). AS2159 was highlighted as a code that has been implemented very effectively and has performed well over many years, providing a practical balance between reliability, constructability, and industry usability. This was cited as evidence that reliability-based frameworks can work well in Australian practice when they are well calibrated, clearly written, and aligned with construction realities.

Lessons for Australian Codes — Not Direct Adoption

Sam's contribution emphasised that Eurocode 7 is not necessarily "the solution", but it does provide important insights. Australian geotechnical codes were seen as needing to evolve over the next decade in a way that is evidence-based, locally calibrated, and mindful of constructability and cost-effectiveness

The panel reviewed current Australian standards (including AS2159, AS4678, AS5100.3, AS2870, and AS1726), identifying gaps in reliability calibration, inconsistencies between load and resistance factors, and limited guidance for complex problems such as embedded walls and slopes.

Then debate started and panellists answered questions from their own viewpoints.

Overall Conclusion

Rather than reaching a single conclusion, the debate deliberately highlighted the complexity of modern geotechnical design and code development. The discussion reinforced that questions around Eurocode 7, reliability-based design, and Australian standards do not have simple answers.

The debate underscored that Australia already has examples of effective, reliability-informed practice, while also facing clear challenges around consistency, calibration, and guidance for complex problems. Eurocode 7 was viewed neither as a solution nor as something to dismiss outright, but as a reference point to provoke discussion, comparison, and critical thinking.

Ultimately, the session achieved its aim of stimulating informed debate, encouraging the profession to reflect on how geotechnical codes should evolve to address uncertainty, risk, constructability, and future demands — with the understanding that this conversation is ongoing and far from settled.

QUEENSLAND

This report includes the Queensland Chapter news from November 2025 to February 2026. The activities included multiple evening technical presentations and our annual Brisbane Symposium. Please visit the AGS Queensland Chapter webpage for future events.

New Diaphragm Wall Construction Method for Micro Sites and Underground Applications
Thursday 6 November 2025

Over 40 members gathered at the WSP Brisbane office to hear James Morris reveal insightful details, construction methodologies, and recent advancements in diaphragm wall construction on highly constrained sites and further showcasing international examples.

James Morris delivering his presentation on diaphragm walls at the WSP Brisbane office.

Speaker dinner, Left to Right: Burt Look, Jaime Wilson, Mark Chapman, James Morris, Vincent Blanchet, Arsh Kaur.

Brisbane Symposium - From Setbacks to Success: Geotechnical Lessons Learned
Tuesday 25 November 2025

The AGS Brisbane Symposium was successfully held for the very first time at The Star ballroom, in the recently completed Queens Wharf precinct. The theme was opened by keynote speaker and local legend John Wagstaff and further supported by eminent industry speakers from various organisations including consultancies, infrastructure agencies, principal contractors and specialist contractors.

The AGS Brisbane Symposium prides itself as an annual platform for knowledge sharing and promoting technical excellence as well as a great networking opportunity.

The event was a huge success and broke all previous records with 280 attendees, making it the largest AGS annual symposium event ever. This success was possible by the unwavering dedication and hard work of the organising committee, comprising, Dr Arsh Kaur (Symposium Chair), Natalie Murphy, Dr Bindu Aery, Dr Amir Shahkolahi, Vincent Blanchet, Any Doe, Jared Priddle, Dr Chris Bridges, and Jaime Wilson Moya.

AGS Brisbane Symposium 2025 at The Star

The program started with a brief QLD Chapter AGM by Vincent Blanchet (QLD Chair), supported by Dr Arsh Kaur, sharing both national and chapter updates, which was followed by technical presentations including:

- Whispers from the Earth: Six Decades Navigating the Complexities of Soil and Rock. Keynote Lecture by John Wagstaff from Wagstaff Piling.
- Ground risk due to underground anomalies – A case study of failure and remediation of a water tank by Dr Sujatha Manoj from Tetra Tech Coffey.
- Lessons from ongoing tailings dam failures by Em. Prof. David Williams from The University of Queensland.
- Building failures caused by adjacent construction activities by Prof. Harry Poulos from Tetra Tech Coffey.
- Site-specific seismic hazard assessment and its implications in design by Dr Narges Khajavi from GHD.
- Lessons learnt from failure of MSE retaining walls by Dr Amir Shahkolahi from Global Synthetics.
- When soil-structure interaction goes wrong – lessons learned from a Structural Engineer by Evelyn Storey from Aurecon.
- Geo-calamities – three short stories of projects gone badly wrong by Allan McConnell from Insitu Geotech Services.
- The Best-Laid Plans…Often Go Awry – Tales From a Mega-Project by Jaime Wilson Moya from FSG.
- Results of the 2025 TMR Geotechnical Working Group and the way forward by Dr Jun Sugawara from Transport and Main Roads.
- The perils of the GIR by Ian Shipway & Sally Roberts-Kelly from EDG Consulting.
- Case studies on the ABCs of design compared with the DEFG …. WXYZ of construction by Dr Burt Look OAM from AGTRE.

We were also joined by AGS Director Joanna Sylvester from Newcastle who provided an update on National-level AGS initiatives and what the volunteer committees are doing in the background to make a difference within the industry. Joanna also presented Honorary Life Membership awards to John Wagstaff and Allan McConnell who have been strong pillars within the geotechnical industry both nationally and internationally, but especially in Queensland over the past 60 years.

The Symposium was once again very well supported by a wide range of sponsors including Diamond (Wagstaff Piling Pty Ltd), Platinum (Ischebeck Titan, Black Insitu), Gold (IGS, Macquarie Geotech, Geomotion, Menard), Silver (Insitutek, BGC Engineering, Kurloo, Infinity Studio, Geofabrics, Global Synthetics, O'Sullivan) and Bronze (Tensar, Engeo, Tablogs, Rockwell Drilling, Chadwicks and Conetec).

Speakers, Organising Committee and Sponsors of the AGS Brisbane Symposium 2025.

Honorary Life Members, John Wagstaff and Allan McConnell with AGS Director Joanna Sylvester.

The Brisbane Symposium crowd.

Significant recent advances in insitu testing of very soft soils and other gooey stuff
Tuesday 10 February 2025

Over 80 members and non-members gathered at Rydges Fortitude Valley to hear Allan McConnell share significant advances in insitu testing of soft and very soft soils, with a focus on CPT, DMT, and vane shear testing. Allan is a respected figure both locally and internationally with nearly six decades of geotechnical experience and over 20 years specialising in insitu testing. Allan highlighted multiple recent paradigm-shifting developments that challenge long-held assumptions in industry standards and practice with a particular focus on calibration requirements and design improvements in commercially available equipment to accurately test soft and very soft soils.

Allan McConnell delivering his presentation on significant recent advances in insitu testing.

Dinner with Allan McConnell, Left to Right: Jaime Wilson, Jared Priddle, Allan McConnell, Vincent Blanchet.

SOUTH AUSTRALIA AND NORTHERN TERRITORY

Chapter Events

In October 2025, we hosted our biannual symposium at the National Wine Centre, themed "Geotechnical Challenges and Lessons Learnt." The event featured 17 speakers and welcomed 70 attendees, offering a series of insightful presentations on topics such as the implementation of generative AI, strategies for managing unexpected issues and various project case studies.

Dr Jack Pappin delivered a compelling keynote exploring legal considerations in geotechnical projects that have gone wrong. His presentation unpacked real-world cases, emphasising how early decision-making, documentation, and professional responsibility can shape outcomes when challenges arise. Delegates appreciated the practical relevance of Jack's insights, reinforcing the importance of proactive risk management and clear communication across project teams.

Allan McConnell, Founder of Insitu Geotech Services, followed with an engaging keynote on recent advances in in-situ testing, with a particular focus on CPT technologies. Allan challenged long-held assumptions around test accuracy and reliability, illustrating how evolving methodologies, improved calibration, and critical review of results are redefining modern site investigation practices. His reflections highlighted how proper site characterisation remains fundamental to successful geotechnical design.

The event highlighted for us to anticipate new challenges, learn from setbacks, and share experiences with our peers, because theory alone can only take us so far. It was a strong reminder to find smarter and more sustainable ways of working, and encourage others to join and grow within this field. The day was a wonderful opportunity to come together and strengthen our local and interstate connections within the AGS and the broader ground engineering community.

A big thank you to our presenters, sponsors and organising committee, who's contributions and support make this prestigious event possible.

Adelaide 2025 Symposium – Group Shot

Adelaide 2025 Symposium – National Wine Centre

Adelaide 2025 Symposium – Q&A

To round out an already exceptional event season, the Chapter also hosted its 2025 Rooftop Social and Congress on 4 December, held at the WGA office rooftop with sweeping views over the Adelaide CBD. The evening brought together members for a relaxed celebration of the year, combining open networking, and a warm atmosphere that encouraged reflection on the collective achievements of 2025. The Congress meeting provided an opportunity for Lauren Amato, Chapter Chair, to share annual highlights and updates from the committee, and an opportunity to acknowledge contributions, and look ahead to the next year of Chapter initiatives.

Congress Chair's Report – Lauren Amato

In true SA/NT spirit, we stepped into 2026 with a warm committee lunch to reconnect, welcome new and continuing members, and set the tone for another exciting year ahead. Looking forward to seeing what 2026 holds for the SA/NT Chapter.

Lauren Amato; SA/NT Chapter Chair

VICTORIA

As we move into the first quarter of 2026, the Victoria Chapter continues to plan and deliver events and initiatives across our key focus areas: technical CPD content, digital engineering, Women in AGS, and industry–academic engagement.

Before recapping the final events of 2025, we would like to thank the outgoing committee members, and in particular our previous chapter chair, Clare Bridgeman (Douglas Partners), for her contributions.

The new committee, led by chapter chair Yuqi Tan (ATC Williams), has now taken the reins. Shiaohuey Chow (University of Melbourne) joins as Deputy Chair, with Mike Shackelton (CGC) serving as Secretary.

We are delighted to welcome our brand-new committee members: Andrew McIntyre (Douglas Partners), Glenn Daniel (EDG), Susan Sam (Arup), Wai Leung Ng (Coffey TetraTech), and Wendy Greatbatch (Tonkin and Taylor).

Returning members include Jay Lee (GS E&C), Kathryn Jones (Coffey TetraTech), Liuxin Chen (James Cook University), Marvin Bedary (GHD), Mohammad Saberian (RMIT), Negin Yousefpour (University of Melbourne), Stuart Pennington (Intrax), and Yunlong Tang (Tonkin and Taylor).

Last Victoria Chapter committee meeting of 2025 at UoM

Jack Morgan Young Geotechnical Practitioners Award 2025

On Wednesday, 13 August 2025, the AGS Victoria Chapter hosted the Jack Morgan Young Geotechnical Practitioners Award 2025, bringing together members to celebrate emerging talent within the Victorian geotechnical community. First presented in 2009, the biennial award recognises an outstanding Victorian geotechnical practitioner under the age of 35. Following a call for abstracts issued to members in May, four finalists—Shashika Gajanayake, Paddy Beasley, Reza Asadi, and Yunlong Tang—were selected to present on their chosen technical topics. Presentations were assessed based on the applicants' contributions to geotechnics and their understanding of key geotechnical issues, with Jack Morgan in attendance to select the winning presentation. The event showcased the high calibre of young practitioners within the profession and provided an excellent forum for technical discussion and professional development.

Reza Asadi receiving the Jack Morgan Young Geotechnical Practitioners Award 2025.

AGS 2025 Victoria Chapter Symposium Retention Solutions: Innovations, Challenges, and Future Directions

On Thursday, 25 September 2025, the AGS Victoria Chapter successfully hosted the AGS Victoria Symposium 2025 at the State Library of Victoria. The sold-out event brought together industry professionals, academics, and students for a full day of technical presentations, discussion, and collaboration. The Chapter extends its sincere appreciation to all keynote speakers, presenters, sponsors, volunteers, and attendees whose contributions made the symposium a resounding success.

The Symposium featured keynote presentations by James Martin (Spark Consortium), Professor Samanthika Liyanapathirana (Western Sydney University), and Rob Day (Arup Australia).

Special thanks are extended to Symposium Co-Chairs Mohammad Saberian and Marvin Bedary, and to the Symposium Sub-Committee: Yunlong Tang, Mike Shackleton, and Liuxin (Lucy) Chen, for their leadership, dedication and extensive efforts in planning and delivering the event.

The Chapter also acknowledges the invaluable support of its volunteers, whose behind-the-scenes assistance ensured the symposium ran smoothly, and thanks AGS Victoria Chair Clare Bridgeman for her guidance and continued support throughout the symposium's development and delivery. Thanks to our sponsors: Chadwick Geotechnics (Platinum), Insitu Geotech Services Pty Ltd (Gold) and Global Synthetics Pty Ltd(Gold), and Intrax Consulting Group (Silver), Menard Oceania(Silver), and Black Insitu Testing(Silver).

AGS Victoria Symposium 2025, State Library of Victoria

61st Rankine Lecture Constitutive Modelling in Computational Geomechanics

On Wednesday, 15 October 2025, the AGS Victoria Chapter hosted a viewing of the 61st Rankine Lecture, Constitutive Modelling in Computational Geomechanics, presented by Emeritus Professor John Carter. The event attracted strong attendance and provided members with an insightful overview of the development of constitutive models in computational geomechanics, highlighting the fundamental role of soil and rock behaviour in supporting reliable geotechnical analysis and design. The Chapter thanks all attendees for their participation and for the valuable technical discussions that followed the lecture.

Emeritus Professor John Carter presenting at University of Melbourne on 15 October 2025

2025 AGS Victoria AGM & Annual Dinner

On Tuesday, 25 November 2025, the AGS Victoria Chapter hosted 2025 AGS Victoria Annual General Meeting and Annual Dinner. The event was a resounding success, bringing together members for an evening of professional engagement, reflection, and celebration. The AGM formally concluded with the successful election of the AGS Victoria Committee and Executive Committee for 2026, with the Chapter extending its thanks to all members who participated in the nomination and voting process, reinforcing the strength and vitality of the Victorian Chapter. The Annual Dinner was fully subscribed, reflecting strong member support and providing an excellent opportunity for networking among both long-standing and new members. The evening included a comprehensive overview of the Chapter's activities and achievements throughout 2025, presented by Chair Clare Bridgeman. Attendees were also treated to an engaging keynote presentation by Rob Wilson, formerly Senior Principal Engineering Geologist at Coffey / Tetra Tech, who shared insights from his distinguished career spanning more than 35 years across Australia and internationally. The Chapter sincerely thanks all attendees and contributors for making the event a memorable success and looks forward to another productive year under the newly appointed 2026 Committee.

Rob Wilson presenting at the AGM dinner on 25 November 2025

Women in AGS Victoria – Walk & Talk Series

As a way to connect with members and broader The AGS Victoria Chapter launched the Walk & Talk series, a relaxed and energising way to connect with peers across the geotechnical community. The inaugural event was held on Thursday, 21 August, with a follow-up on Thursday, 4 December 2025.

Participants enjoyed a scenic walk along the Yarra River and through the Royal Botanic Gardens, with complimentary morning coffee provided by AGS Victoria. The series offered an informal environment for conversation, networking, and professional connection.

The Chapter thanks the local organising group of Women in AGS, including Subcommittee Chair Negin Yousefpour and event organiser Kathryn Jones (Coffey TetraTech), for their efforts in delivering these events.

Rob Wilson presenting at the AGM dinner on 25 November 2025

Upcoming AGS Victoria events in 2026 include: -

- Monday 23 March - EH Davis Memorial Lecture Professor Anna Giacomini (University of Newcastle)
- Tuesday 21 July– Course on Implementation of Deformation-based Support Design in Geo-engineering and Rockburst Hazard Assessment at Mining Operations
- Tuesday 21 until Friday 24 July– Australian Conference on Rock Mechanics
- Wednesday 19 August - Victoria PhD Research Award

Special thanks to Marvin Bedary, Clare Bridgeman, Yuqi Tan and Negin Yousefpour, for their assistance in preparing this article.

WESTERN AUSTRALIA

It is already 3 months into 2026 and reflecting on the latter part of 2025, the AGS WA Chapter hosted multiple technical seminars and its annual symposium.

Technical seminars

A technical seminar in August 2025 by Tristan Menzies from WSP showcased how engineering geological models were important in supporting decision making. The seminar titled 'The Value of Software Driven Engineering Geological Models' provided examples of ground models and their applications in evaluation of geological, geomorphological and hydrogeological conditions that could impact projects and engineering characteristics.

Tristan Menzies explaining the importance of engineering geological models.

In September 2025, Joe Rola from SRK presented a case study spanning nearly 7 years, from concept through to design on a tailings dam embankment lift. Firsthand account of the challenges and solutions for the case study were shared in the seminar titled 'Case study: Tailings Dam Stabilisation (ground improvement) Project – from options to implementation'. The talk raised discussion on the role of engineers on tailings storage facility stabilisation given recent catastrophic tailings dam failures.

Joe Rola sharing lessons from a case study of a tailings storage facility.

Later in October 2025, Jess Dalton and Ken Chen (both) from WSP delivered a presentation on the Yanchep Rail Extension, highlighting its numerous geotechnical and geological complexities. The seminar titled 'Strain Softening and Navigating Karstic Risks in the Design and Construction of Large Retaining Walls' explored key considerations in both the design and the construction phases of such structures. Ken Chen discussed how strain softening was implemented in modelling for retaining wall design, while Jess Dalton provided a pragmatic approach during project construction when encountering karstic conditions in Tamala limestone.

Ken Chen (left) and Jessica Dalton (right) presenting on retaining walls in Yanchep Rail Extension.

AGS WA Symposium 2025

The AGS WA Symposium 2025 was held in October with the theme "Managing Geotechnical Risk and Complex Ground Conditions – Challenges, Solutions and Lessons Learned". The symposium brought together the WA and interstate geomechanics community to explore geotechnical risk. The symposium highlighted the identification and management of geotechnical risks, presenting challenges, solutions and key lessons from across the industry.

WA Symposium 2025 held on 24 October 2025

Keynote speakers provided great insights including David Kinlan from Inframara on contracts in 'Foundations of Trust: Ground Condition Issues in Construction Contracts', Richard Kelly from SMEC Australia on 'Balanced Decision Making in the Face of Uncertainty' and Kim le Roux from Rio Tinto Iron Ore on whole of life mine decisions in 'Today's Design Decisions Impact Long Term Operational and Closure Options'.

The symposium also showcased a further 10 speakers, covering a range of topics, including:

- Hudson Moore from CMW Geosciences on 'Managing Geotechnical Risk for the Fitzroy Crossing Bridge Replacement'
- Terry Waters from Local Geotechnics on 'Managing Geotechnical Challenges in the Western Australian Residential Environment'
- Simon Burgmans from in2Dredging on 'Site Investigation for Dredging: Informing Destructive and Reconstitutive Soil Mechanics'
- Vince Gingoyon from CMW Geosciences on 'Optimized Temporary Crane Platform Designs and use of Observational Approach over Very Soft Complex Soils for the Boorloo Pedestrian & Cyclist Bridge, Perth, Western Australia'
- Babak Hamidi from Menard Oceania on 'The Application of Cut-off Walls for Contaminated Sites in Australia'
- Alex Petty from PTG Consulting on 'Development of a Semi Quantitative Risk Management Framework for Rockfalls'
- Ryan Singh from HATS Consulting on 'Performance Envelopes – Risk-informed Approach to Tailings Dams Safety'
- Ian Gray from Sigra Pty Ltd on 'Air lifted wick drains – a novel technology for tailings dams consolidation'
- Sudheer Prabhu from Red Earth Engineering on 'Geotechnical Risk and MPM: A New Standard in Tailings Assessment'
- Wensong Zhang from Rio Tinto Iron Ore on 'A Case Study of Open Pit Slope Design Optimisation in Complex Ground Conditions'

The success of the event was supported by nine sponsors across various categories, including Probedrill as the platinum sponsor, and gold sponsors with Monitel, Geomotion Australia and Sovereign Hydroseal, along with silver sponsors from CMW Geosciences, Menard, Rockfield, WML Consulting Engineers and in2Dredging.

Australian Geomechanics Society Prize, University of Western Australia

AGS continues to support the AGS Prize at the University of Western Australia, awarded to the engineering student who presents the best combination of thesis (or technical report) and a seminar on a geotechnical topic for the degree of Bachelor of Engineering, or the Bachelor of Engineering component of a combined course. This year the prize went to Rachel Lim.

Vince Gingoyon (right) on behalf of the AGS presenting the AGS Prize, UWA, accepted on Rachel Lim's behalf.

33rd GFWA Prize in Geomechanics and WA Chapter Annual General Meeting

The GFWA Prize in Geomechanics sponsored by GFWA Pty Ltd, is awarded by the AGS to the author of the best finalyear student paper in Geomechanics at universities in Western Australia. The 2025 event was held in November and featured presentations from two students from Curtin University and two students from the University of Western Australia (UWA), each showcasing their research to a wider audience.

The finalists this year included Ronin Maximus O'Connor and Cameron Birkholz from Curtin University and Tara Smith and Jordan Moscarda from UWA. Their topics demonstrated applicability of the university research in current geomechanics issues including shaft friction in clays, microbially induced carbonate precipitation to prevent coastal erosion, mine slip failures and microbially induced magnesium carbonate precipitation in rammed earth.

Tim Palmer from GFWA (far right) with the finalists in the 33rd GFWA Prize in Geomechanics, from left to right, Tara Smith, Jordan Moscarda, Cameron Birkholz, Ronin Maximus O'Connor

The winner for this award was Ronin Maximus O'Connor from Curtin University who presented outcomes from varying calcium-to-magnesium ratios in microbially induced carbonate precipitation for resisting wave erosion and its potential future applicability. In addition, he was voted by the audience as the as the recipient of the "Best Presentation" award.

For the WA Chapter Annual General Meeting, Andrew Lim, (now) immediate past WA Chapter Chair, signed off on 2025 and his term as the WA Chapter Chair with thanks to the 2025 WA committee members, in particular, Amy Tsagopoulos (now former WA Chapter Secretary). Andrew provided positive reflections on the range of interesting technical seminars, workshops and symposiums that the AGS has provided the geomechanics community. Andrew and Amy will continue on the WA Committee in 2026.

Eddy Yong, AGS WA Chapter Chair

CONFERENCE CALENDAR

APRIL 2026	
16-17	8th International Conference on Geotechnics, Civil Engineering and Structures (CIGOS), Ho Chi Minh City, Vietnam *https://cigos2026.sciencesconf.org/*
27-3 May	Landslide Risk & Geo-Education (LaRGE) - First International Joint Workshop of JTC1 and JTC3, Queenstown, New Zealand *https://landsliderisk.nz/* **AGS SUPPORTED EVENT**
MAY 2026	
11-13	8th Asia Pacific Meeting on Near Surface Geoscience & Engineering (NSGE), Bandung, Indonesia *https://eage.eventsair.com/8th-asia-pacific-meeting-on-near-surface-geoscience-engineering*
15-21	World Tunnel Congress (WTC2026) - Connecting Communities through Underground Infrastructure, Montréal, Canada *https://www.tunnelcanada.ca/wtc2026.php*
24-27	16th International Conference "Under *https://www.ucprague.com/*
26-27	2026 ICOLD International Symposium - Water, Energy, and Society: The Evolving Role of Dams in a Changing World, Guadalajara, Mexico *https://www.icoldmexico2026.com/*
JUNE 2026	
1-3	Geohazards 9 - 9th Canadian Conference on Geotechnique and Natural Hazards, Edmonton, Alberta, Canada *https://www.geohazards9.ca/*
11-14	8th International Young Geotechnical Engineers Conference (8iYGEC), Graz, Austria *https://www.tugraz.at/institute/ibg/events/8iygec*
14-19	21st International Conference on Soil Mechanics and Geotechnical Engineering, Vienna, Austria *https://www.icsmge2026.org/en/*
21-24	60th US Rock Mechanics / Geomechanics Symposium, Tucson, Arizona, USA *https://armarocks.org/tucson-2026-symposium/*
22-24	12th International Conference on Bearing Capacity of Roads, Railways, and Airfields (12 BCRRA 2026), Ljubljana, Slovenia *https://bcrra.si/*
JULY 2026	
13-17	13th U.S. National Conference on Earthquake Engineering (13NCEE), Portland, Oregon, USA *https://13ncee.eeri.org/*
21-24	Australian Conference on Rock Mechanics (ACRM), Melbourne, Australia *https://australiangeomechanics.org/meetings/acrm2026/* **AGS EVENT**
AUGUST 2026	
6-10	12th International Symposium on Field Monitoring in Geomechanics 2026, Indore, India *https://isfmg2026.com/*
11-13	Caving 2026, Ulaanbaatar, Mongolia *https://www.acgcaving.com/*
14-16	10th International Conference on Geoscience Education (GeoSciEd X), Adelaide, Australia *https://eventstudio.eventsair.com/geoscoed-conference-2026/*
24-25	4th International Conference on Geotechnical Engineering - Resilient Geotechnics for a Sustainable Future, Colombo, Sri Lanka *https://icgecolombo2026.org/*
24-26	International Conference on Advances and Innovations in Soft Soil Engineering, Delft, Netherlands *https://www.issmge.org/events/international-conference-on-advances-and-innovations-in-soft-soil-engineering-2026*
26-28	X Latin American Congress on Rock Mechanics - an ISRM Regional Symposium, Brasilia, Brazil *https://isrm.net/conference/show/6388*
SEPTEMBER 2026	
7-8	3rd International Conference on Construction Resources for Environmentally Sustainable Technologies (CREST 2026), Cambridge, UK *https://engage-events.ifm.eng.cam.ac.uk/IC-CREST2026#/*
12-16	GeoQuébec 2026 - 79th Canadian Geotechnical Conference, Québec, Canada *https://geoquebec2026.ca/en/*
13-17	13 ICG – 13th International Conference on Geosynthetics - "Legacy, Evolution & Revolution in Geosynthetics", Montreal, Canada *https://www.13icg-montreal.org/*
15-19	Eurock 2026 - Risk Management in Rock Engineering - an ISRM Regional Symposium, Skopje, North Macedonia *https://isrm.net/conference/show/6376*
16-18	Fourth International Symposium on Geotechnical Engineering for the Preservation of Monuments and Historic Sites, Athens, Greece *https://tc301-athens.com/*
20-23	The 5th International Conference on Coupled Processes in Fractured Geological Media: Observation, Modeling, and Application, Uppsala, Sweden *https://www.coufrac2026.com/*

CONFERENCE CALENDAR

OCTOBER 2026	
13-16	6th International Conference on Information Technology in Geo-Engineering, Graz, Austria *https://www.icitg2026.com/*
22-25	7th International Conference on Environmental Geotechnology, Recycled Waste Materials, and Sustainable Engineering (EGRWSE-2026), Surat, India *www.egrwse2026.com*
26-29	Slope Stability 2026 - Slope for Safety Performance, Lima, Peru *https://www.slopestability2026.com/en*
30-6 Nov	XV IAEG World Congress, Delft, The Netherlands *https://iaeg.info/event/xv-iaeg-world-congress/*
NOVEMBER 2026	
4-6	International Conference on Performance-Based Design in Earthquake Geotechnical Engineering (PBD), Puerto Varas, Chile *https://www.pbd-v-chile.com/*
22-27	14th Asian Rock Mechanics Symposium - Rock Mechanics for the Next Generation – Innovations, Sustainability, and Resilience, Fukuoka, Japan *https://www.ec-convention.com/ARMS14/*
26-27	6th International Conference on Geotechnics for Sustainable Infrastructure Development, Hanoi, Vietnam *https://geotechn.vn/*
MARCH 2027	
17-19	7th International Conference on Grouting and Deep Mixing, Florence, Italy *https://dfi.org/events/upcoming-events/*
17-19	Geotechnics for Mountrain Infrastructure, GeoMandu 2027, Kathmandu, Nepal *https://geomandu.ngeotechs.org/*
APRIL 2027	
12-14	International Symposium on Ground Improvement (IS-GI Lyon 2027,TC-211 Symposium), Lyon, France *https://www.menard-group.com/isgi-lyon2027/*
23-29	World Tunnel Congress (WTC 2027), Antwerp, Belgium *https://about.ita-aites.org/future-events*
MAY 2027	
11-13	5th International Conference on Shaft Design and Construction (SDC2027), London, UK *https://www.iom3.org/events-awards/5th-international-shaft-design-construction.html*
11-14	IFCEE 2027 International Foundations Congress and Equipment Expo, Grapevine, Texas, USA *https://www.geoinstitute.org/events/ifcee-2027-international-foundations-congress-and-equipment-expo*
12-14	International Symposium Cone Penetration Testing CPT '27, Vancouver, British Columbia, Canada *https://www.cpt27.org/*
SEPTEMBER 2027	
21-24	11th European Conference on Numerical Methods in Geotechnical Engineering (NUMGE 2027), Graz, Austria *https://www.tugraz.at/events/numge2027/*
OCTOBER 2027	
17-23	16th ISRM International Congress on Rock Mechanics, Seoul, Korea *http://isrm2027.website.or.kr*
JANUARY 2028	
9-12	12th International Symposium on Geotechnical Aspects of Underground Construction in Soft Ground (IS-Doha 2028), Doha, Qatar *https://www.issmge.org/news/is-doha-2028-early-announcement*
MARCH 2028	
26-29	18th Panamerican Conference on Soil Mechanics and Geotechnical Engineering and Geo-Congress 2028, Chicago, Illinois, USA *https://www.geocongress.org/*
JUNE 2028	
25-30	Eurock2028 - Advances in rock mechanics and rock engineering to cope with increasingly extreme conditions, Aix-en-Provence, France *https://isrm.net/conference/show/6396*
AUGUST 2028	
21-25	19th European Conference on Soil Mechanics and Geotechnical Engineering (ECSMGE 2028), Istanbul, Türkiye *https://zmgm.org.tr/tr*
SEPTEMBER 2029	
1-5	6th International Conference on Transportation Geotechnics, Southampton, United Kingdom *https://inconference.eventsair.com/cmspreview/ictg-2029*

AGS advises that the status of events at any time should be checked using the links to the event websites.

CORPORATE MEMBERS

The Australian Geomechanics Society gratefully acknowledges the contribution made by its Corporate Members.

FIRM	ADDRESS				PHONE
A. S. James Pty Ltd	15 Libbett Avenue	CLAYTON SOUTH	VIC	3169	(03) 9547 4811
AECOM Australia Pty Ltd	PO Box 1307	FORTITUDE VALLEY	QLD	4007	(07) 3553 3276
Arup Australia Services Pty Ltd	Level 26, 123 Albert St	BRISBANE CITY	QLD	4000	0482 420 152
Aitken Rowe Testing Laboratories Pty Ltd	PO Box 5158	WAGGA WAGGA	NSW	2650	(02) 6939 5555
Alliance Geotechnical Pty Ltd	10 Welder Road	SEVEN HILLS	NSW	2147	0427 197 575
Anora Foundations Pty Ltd	PO Box 3282	DARRA	QLD	4076	(07) 3279 7966
Aurecon Australasia Pty Ltd	Level 2, 116 Military Rd	NEUTRAL BAY	NSW	2089	(02) 9465 5386
BGC Engineering Pty Ltd	Level 3, 31 Merivale St	SOUTH BRISBANE	QLD	4101	(07) 3709 7034
Barrason's Engineers	Level 2, 66 Victor Cres	NARRE WARREN	VIC	3805	(03) 5940 2638
Butler Partners Pty Ltd	79 Doggett St	NEWSTEAD	QLD	4006	(07) 3852 3800
CMW Geosciences Pty Ltd	60 Kingsford Smith Drive	ALBION	QLD	4010	(07) 3320 8503
Chadwick Geotechnics Pty Ltd	25 Metcalf St	DANDENONG SOUTH	VIC	3175	(03) 8796 7900
Civiltest Pty Ltd	PO Box 537	MORNINGTON	VIC	3931	(03) 5975 6644
CONETEC Pty Ltd	6 Chapman Place	EAGLE FARM	QLD	4009	0473 923 084
Douglas Partners Pty Ltd	96 Hermitage Rd	WEST RYDE	NSW	2114	(02) 9809 0666
Durham Geo Slope Indicator	c/- Rockfield Technologies Australia, 51 Colin St	WEST PERTH	WA	6014	1300 015 580
EDG Consulting Pty Ltd	Level 1, 18 Wandoo St	FORTITUDE VALLEY	QLD	4006	0435 743 775
EI Australia Pty Ltd	Unit 01, 55 Miller St	PYRMONT	NSW	2009	(02) 9516 0722
EcoFine Material Pty Ltd	27 Rogers Way	LANDSDALE	WA	6065	(08) 9303 9297
Fortify Geotech Pty Ltd	39 Sydenham Road	ALEXANDRIA	NSW	2204	(02) 9188 4033
Fugro Australia Pty Ltd	Level 1, 1060 Hay Street	WEST PERTH	WA	6005	(07) 8942 3335
GB Geotechnics Pty Ltd	Unit 28, 7 Salisbury Rd	CASTLE HILL	NSW	2154	0447 022 755
Geofabrics Australia Pty Ltd	83-93 Canterbury Road	BRAESIDE	VIC	3195	(03) 8586 9100
GEOFIRST Pty Ltd	Unit 2, 7 Luso Drive	UNANDERRA	NSW	2526	0433 184 319
GHD Pty Ltd	Locked Bag 2727	ST LEONARDS	NSW	1590	(02) 9462 4859
Geobrugg Australia Pty Ltd	PO Box 2468	MALAGA	WA	6944	(08) 9249 9939
Geomotion (Australia) Pty Ltd	9/31-33 Chaplin Drive	LANE COVE	NSW	2066	0438 700 356
Geotechnique Pty Ltd	PO Box 880	PENRITH	NSW	2751	(02) 4722 2700
Geotesta Pty Ltd	Unit 6, 31-37 Howleys Rd	NOTTING HILL	VIC	3168	(03) 9562 8808
Global Synthetics Pty Ltd	41 Sammut St	SMITHFIELD	NSW	2164	(02) 9725 4321
Ground Recruitment	Level 28 - AMP Tower, 140 St Georges Tce	PERTH	WA	6000	0499 988 011
HAWK GEO Pty Ltd	42 Douglas Farm Road	KURRAJONG HILLS	NSW	2758	0448 086 608
Intrax Consulting Engineers Pty Ltd	35 Banks St	MELBOURNE	VIC	3205	(03) 8371 0100
Ischebeck Titan (Australia) Pty Ltd	197 Queens Road	KINGSTON	QLD	4114	0414 838 891
JC Geotechnics Pty Ltd	Suite 3A, Level 3, 1C Grand Ave	ROSEHILL	NSW	2142	(02) 8066 0665
JK Geotechnics Pty Ltd	115 Wicks Road	MACQUARIE PARK	NSW	2113	(02) 9888 5000
Jacobs Group (Australia) Pty Ltd	452 Flinders St	MELBOURNE	VIC	3000	0424 446 277
KCB Australia Pty Ltd	Level 3, 150 Mary St	BRISBANE CITY	QLD	4000	(07) 3518 0907
MM Geomechanics Pty Ltd	Unit 2, 19 Chaplin Drive	LANE COVE WEST	NSW	2066	0400 393 008
Mott MacDonald Australia Pty Ltd	Level 17, Tower One, Collins Square, 727 Collins St	MELBOURNE	VIC	3008	(03) 9037 7575
Norwegian Geotechnical Institute Pty Ltd	Level 7, 40 St Georges Tce	PERTH	WA	6000	(08) 6559 6491
PSM Holdings Aust Pty Ltd	G3, 56 Delhi Rd	NORTH RYDE	NSW	2113	(02) 9812 5000
Piling and Concreting Australia	PO Box 1605	RUNAWAY BAY	QLD	4216	(07) 5500 5898

FIRM	ADDRESS				PHONE
Precision Geotechnical Services	10 Hungerford St	NORTHGATE	QLD	4013	(07) 3444 6600
Probedrill Pty Ltd	9 Baling St	COCKBURN CENTRAL	WA	6164	(08) 9417 9933
SCT Operations Pty Ltd	131a Kembla St	WOLLONGONG	NSW	2500	(02) 4222 2777
SIXENSE OCEANIA	92 Thistlethwaite Street	SOUTH MELBOURNE	VIC	3205	(03) 9510 0582
SLR Consulting Australia Pty Ltd	202 Submarine School, Sub Base Platypus	LANE COVE	NSW	2060	0402 142 942
SMEC Australia Pty. Ltd	Level 5 20 Berry St	NORTH SYDNEY	NSW	2060	(02) 9925 5555
Scherzic Ground Investigations	PO Box 555	HOBART NORTH	TAS	7002	(03) 6273 6565
Site Geotechnical Pty Ltd	Factory 3, 8 Cannery Court	TYABB	VIC	3913	1300 557 260
Statewide Geotechnical Pty Ltd	17-20 Summer Lane	RINGWOOD	VIC	3134	(03) 9879 2999
Sunwater	Unit 9, 515 St Pauls Terrace	BRISBANE	QLD	4006	(07) 3120 0327
Terrascan Pty Ltd	81 Egerton St	SILVERWATER	NSW	2128	0408 723 340
Tetra Tech Coffey Pty Ltd	Level 19 - Tower B, Citadel Tower, 799 Pacific Hwy	CHATSWOOD	NSW	2067	(02) 9406 1192
Tonkin & Taylor Pty Ltd	Level 3, 99 Coventry St	SOUTHBANK	VIC	3006	(03) 8796 7900
Transport for NSW	Level 4 - Octagon Building, 101 George St	PARRAMATTA	NSW	2150	(02) 8837 0246
Trilab Pty Ltd	346A Bilsen Rd	GEEBUNG	QLD	4034	(07) 3265 5656
WSP Australia Pty Ltd	Level 4 - Northbank Plaza, 69 Ann St	BRISBANE CITY	QLD	4001	(07) 3854 6044
Wagstaff Piling Pty Ltd	PO Box 117	ASHGROVE	QLD	4060	(07) 3366 2555

ADVERTISERS

The Australian Geomechanics Society gratefully acknowledges the support from firms that advertise in *Australian Geomechanics.*

AUSTRALIAN GEOMECHANICS SOCIETY

We need YOU!

Australian Geomechanics was established to meet the needs of the practicing geotechnical professional. As such we are keen on publishing practical papers that are of use to local consultants and researchers.

We are always pleased to receive content in the form of review articles, technical papers, letters to the Editor, original research papers, case studies, and methodologies or methods.

Submissions are required at least 4 months prior to publication and can vary in length from 1-page to 20-pages.

More details on our Editorial Policy can be found at the AGS website (geomechanics.org.au)

BROONS
IMPACT ROLLERS

IMPACT ROLLERS FOR MAXIMUM COMPACTION

We add value by minimising compaction cost and risk.

The value in any project lies above the ground, but the high-risk cost can be out of sight. Broons Impact Rollers minimise the risk below ground level so you can maximise the visible return. Manufactured and tested in Australia, our square rolling dynamic compaction equipment works in every corner of the globe on some of the Earth's largest projects. Get tangible results in real time with accurate surface monitoring that paints a true picture of what's underground.

Call our engineering staff now to see how we can add value to your next project and manage the geotechnical risks.

Get in touch

1300 002 764

sales@broonsimpactrollers.com

broonsimpactrollers.com

SIMULATING TIME-DEPENDENT ROCKFALL INITIATION BY PROGRESSIVE SUBCRITICAL CRACK GROWTH

Zack Tuckey
Jacobs Group (Australia) Pty Ltd

https://doi.org/10.56295/AGJ6111

ABSTRACT

Progressive brittle fracture plays an important role in rockfall initiation. Although the magnitude of in situ stress near the surface of a slope may be low relative to the strength of intact rock, gravitational stresses become concentrated near the tips of pre-existing discontinuities, promoting the slow process of subcritical crack growth. Over time, subcritical crack propagation reduces the size of intact rock bridges that interrupt an incipient failure surface, increasing the stress intensity at the advancing crack front. Eventually the stress intensity reaches a critical threshold where the fracture toughness of intact rock is exceeded, causing a rapid acceleration of crack growth and sudden failure.

This paper demonstrates a modified fracture mechanics model for time-dependent subcritical crack growth, applied using the bonded block discrete element method. A series of conceptual numerical models are developed based on the geological environment of Blue Mountains National Park in New South Wales, where the Triassic sandstone formations of the Narrabeen Group outcrop in cliffs up to 200 m high. The landscape of the Blue Mountains has been shaped by stream incision and escarpment retreat processes that now are dominated by gravity-driven slope failures, including rockfalls that vary in magnitude from discrete minor block falls up to rock mass scale cliff collapse events. This investigation first explores a simplified model for progressive failure of an overhanging sandstone slab, driven by time-dependent propagation of a vertical rear release joint. The methodology is then extended to consider collapse of a sandstone cliff by undermining failure of a weaker underlying shale layer. The models demonstrate how the time required for rockfall initiation varies depending on the geometry and persistence of pre-existing discontinuities and the intact rock bridges that must fail for an incipient rockfall block to detach. When combined with empirical methods for estimating rockfall magnitude-frequency relationships, the proposed methodology can help to improve the temporal estimates of rockfall probability that form a critical input to rockfall risk assessment.

1 INTRODUCTION

Slope risk assessment requires geotechnical practitioners to develop a temporal estimate for the probability of failure. For discontinuity-controlled rockfalls, failure is frequently triggered by the sudden brittle fracture of intact rock bridges that interrupt the incipient failure surface, providing the cohesion and tensile strength that supports the rock block *in situ*. The timing of brittle failures is difficult to predict: the rockfall detachment surface may develop through a stepwise process of damage accumulation, characterised by instantaneous crack growth events followed by long periods of apparent quiescence (Donati et al., 2023). Collapse may occur suddenly, involving a rapid acceleration of crack growth once the area of the incipient release surface reaches a critical threshold. Figure 1 shows a conceptual illustration of time-dependent rock slope failure, with progressive damage accumulation and reduction in factor of safety by (1) episodic processes that cause a nearly instantaneous reduction in shear or tensile strength; and (2) slow, continuous processes that reduce rock strength through cyclical changes in stress that produce hysteretic deformation.

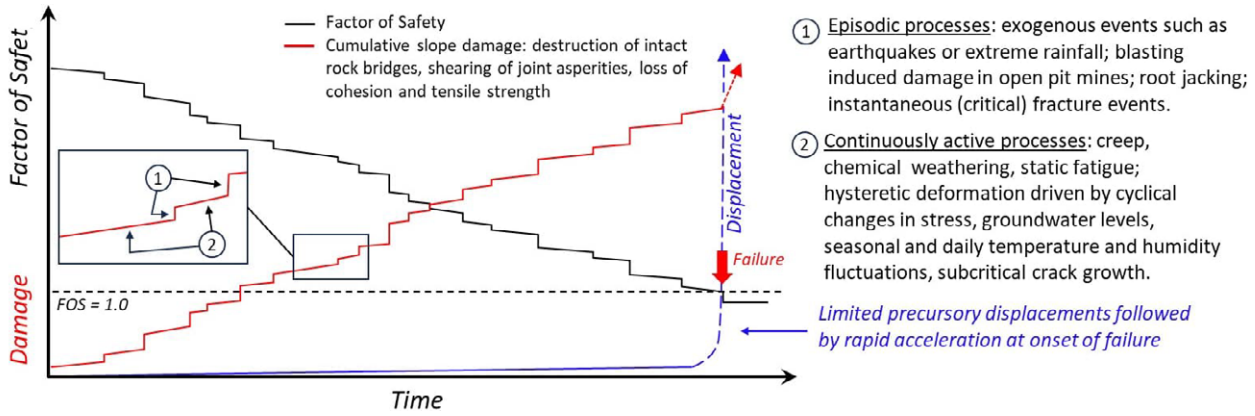

Figure 1: Conceptual illustration of time-dependent brittle slope failure (modified after Donati et al., 2023)

This investigation presents a study of time-dependent rockfall initiation based on the geological environment of Blue Mountains National Park, where the NSW National Parks and Wildlife Service (NPWS) manages an extensive trail network encompassing hundreds of kilometres of walking tracks and bushfire management trails. Some of the most popular trails are visited by hundreds of thousands of walkers each year, and many of them pass below sandstone cliffs over 200 m high. Over the last decade, landslides and rockfalls have infrequently caused serious injuries and fatalities, and more frequently caused major damage to walking tracks and fire trails. In response, NPWS has developed and published a set of landslide risk management procedures based on the quantitative risk assessment (QRA) framework of the Australian Geomechanics Society (2007).

Estimating the annualised probability of rockfall remains a key source of QRA uncertainty. This investigation demonstrates how the discrete element method can be used to simulate the time-dependent brittle failure processes that precede rockfall initiation, thereby helping to improve temporal estimates of rockfall probability. First, a series of conceptual models are developed in *UDEC* using the bonded block methodology, with a fracture mechanics model adapted from Kemeny (2005) to simulate time-dependent subcritical crack growth. The conceptual models investigate the release of a discrete overhanging sandstone slab bounded by a non-persistent vertical rear release joint. The modelling methodology is then extended to consider collapse of a sandstone cliff by undermining failure of a weaker underlying shale layer. The results demonstrate how the time required for rockfall initiation varies depending on cliff geometry, the persistence of pre-existing discontinuities and intact rock bridges, and *in situ* stress.

2 THE ROLE OF INTACT ROCK BRIDGES IN SLOPE STABILITY

For over sixty years geotechnical researchers have recognised that intact rock bridges play a crucial role in the stability of rock slopes. Terzaghi (1962) introduced the concept of coplanar or "in plane" rock bridges represented as patches of intact rock along non-persistent discontinuities. Jennings (1970) extended this concept to a limit equilibrium approach to estimate factor of safety against planar sliding, with equivalent Mohr-Coulomb cohesion and friction angle calculated based on the proportions of intact rock bridges and pre-existing discontinuity surfaces along a composite failure plane. Although Jennings' original method ignored tensile failure, Figure 2 shows how the concept of a continuity coefficient K can be adapted to the problem of an overhanging rock wedge bounded by pre-existing joints (J1 and J2) and bedding (B), where the tensile strength of intact rock bridges $\sigma_{t(eq)}$ may be expected to govern stability.

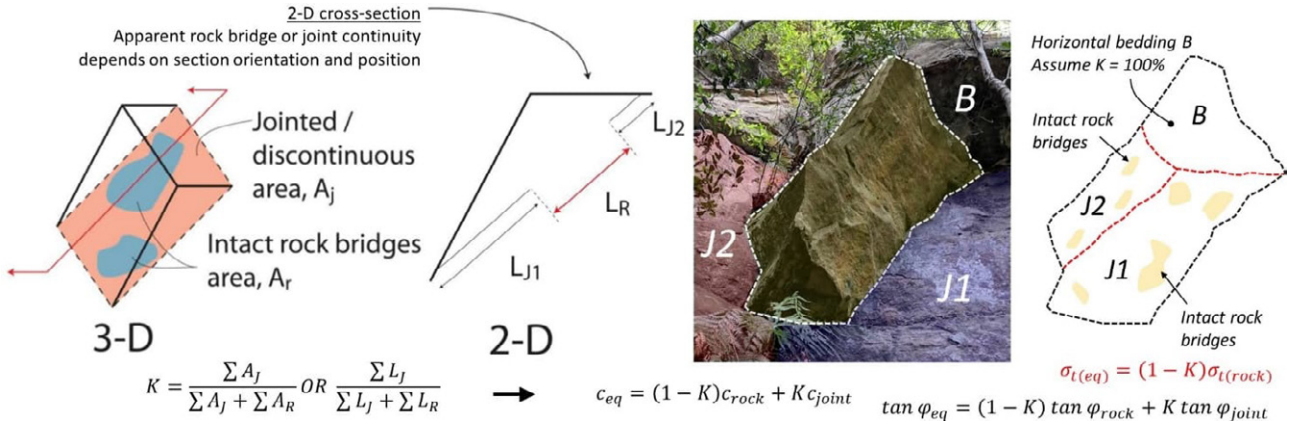

Figure 2: Conceptual illustration of coplanar intact rock bridges and example of an overhanging wedge

Early investigations into the role of rock bridges in slope stability focused on the problem of step-path failure in large open pit slopes, where an inter-ramp or overall slope scale failure surface could comprise segments of pre-existing discontinuities separated by intact rock or larger *rock mass* bridges (Baczynski, 2000). Researchers extended the Jennings-limit equilibrium approach by using statistical techniques to estimate the shear strength of many potential step-paths generated using geometry statistics for discontinuities and intact rock bridges derived from field mapping data (Call and Nicholas, 1978; McMahon, 1979; Einstein et al. 1983). Step-path shear strength statistics could then be used for probabilistic or deterministic limit equilibrium slope stability analysis. Computing advancements over the last few decades have enabled increasingly complex approaches to simulate the fracture of intact rock bridges in slopes: discrete fracture networks (DFN) can explicitly represent a rock mass fracture network (Dershowitz et al., 1998), and these DFN models can be incorporated into synthetic rock mass (SRM) numerical analyses that simulate brittle fracture using bonded particle methods (Mas Ivars et al, 2011), hybrid finite-discrete element techniques (Stead et al., 2006), finite difference and boundary element methods (Scavia, 1990), or lattice-spring models (Havaej and Stead, 2016).

Despite the development of increasingly sophisticated modelling tools, two main sources of uncertainty continue to challenge the prediction of brittle rock slope failures. First, reliable measurement of intact rock bridges may not be

possible until after failure has occurred (Elmo et al., 2018). Even for small rockfalls with simple geometry, it is not practical to directly measure intact rock bridges in the field, because they are occluded inside the rock mass. Empirical studies have measured intact rock bridge content *a posteriori* by examination of rockfall detachment scars (e.g. Paronuzzi and Serafini, 2009; Fraysinnes and Hantz, 2006). Shang et al. (2017) introduced a "forensic excavation" technique where expansive grout is injected into rock blocks along incipient discontinuities; the split discontinuity surfaces can then be inspected to measure failed rock bridges. Although these methods provide insight into rock bridge content of failed blocks, they cannot be directly extended to a predictive estimate of *in situ* rock bridge content of a stable slope. Emerging research shows that geophysical techniques including ground penetrating radar (Deparis et al., 2007) and infrared thermography (Guerin et al., 2018) may be able to provide indirect measurement of intact rock bridges under certain conditions, but these techniques have not been advanced into to accepted engineering practice.

The second challenge relates to the temporal dimension of brittle rock slope failure, which is the primary subject of this paper. Limit equilibrium methods consider that all rock bridges fail simultaneously and instantaneously. In contrast, field studies have shown that brittle rockfalls are time-dependent and progressive. For example, Collins and Stock (2016) used terrestrial LiDAR combined with crack meters, temperature, and light sensors to monitor deformation of exfoliation slabs on granite cliffs in Yosemite National Park in California, USA; they showed that daily, seasonal, and annual temperature fluctuations cause cyclic opening, closure, and propagation of incipient exfoliation joints. The daily temperature-deformation response forms hysteretic loops that result in long-term permanent deformation, which the authors propose is due to subcritical crack growth. Although numerical methods may be used to simulate progressive fracture processes, the mechanical timestep used in the solution process does not represent real time. To overcome this limitation, this investigation expands on a fracture mechanics model for subcritical crack growth first proposed by Kemeny (2003, 2005). The model is implemented with the discrete element method to simulate the time-dependent loss of cohesion and tensile strength from the progressive destruction of intact rock bridges.

3 ROCKFALL IN BLUE MOUNTAINS NATIONAL PARK

3.1 GEOLOGICAL SETTING

Blue Mountains National Park is part of a world heritage-listed conservation area spanning over one million hectares of protected wilderness on the western outskirts of Sydney. The park encompasses an uplifted tableland of Triassic sandstone that has been incised by rivers and streams, forming deep valleys surrounded by cliffs. The upper cliffs are comprised of the massive, quartzose Banks Wall Sandstone of the Narrabeen Group. The Banks Wall Sandstone is underlain by the Mount York Claystone, a marker unit of low strength, red-brown kaolinitic claystone that that forms a continuous bench in the middle of the cliffs that can be traced for kilometres across the escarpment. The lower cliffs are formed by the Burra-Moko Head Sandstone, an early Triassic quartzose to quartz-lithic sandstone that is up to 110 m thick, underlain by interbedded claystone, shales, and quartz-lithic sandstones of the Caley Formation, which forms the basal unit of the Narrabeen Group and the Permian-Triassic boundary. The late Permian Illawarra Coal Measures outcrop at the base of the cliffs, comprising coal seams, torbanite (oil shale), siltstone, and minor sandstone layers. Figure 3 shows an interpreted cross section and annotated photogrammetry image highlighting the main geological units and walking tracks that traverse across the cliffs and colluvial slopes near Wentworth Falls. Zones of geologically frequent rockfall are inferred from the presence of overhangs and pale, fresh sandstone.

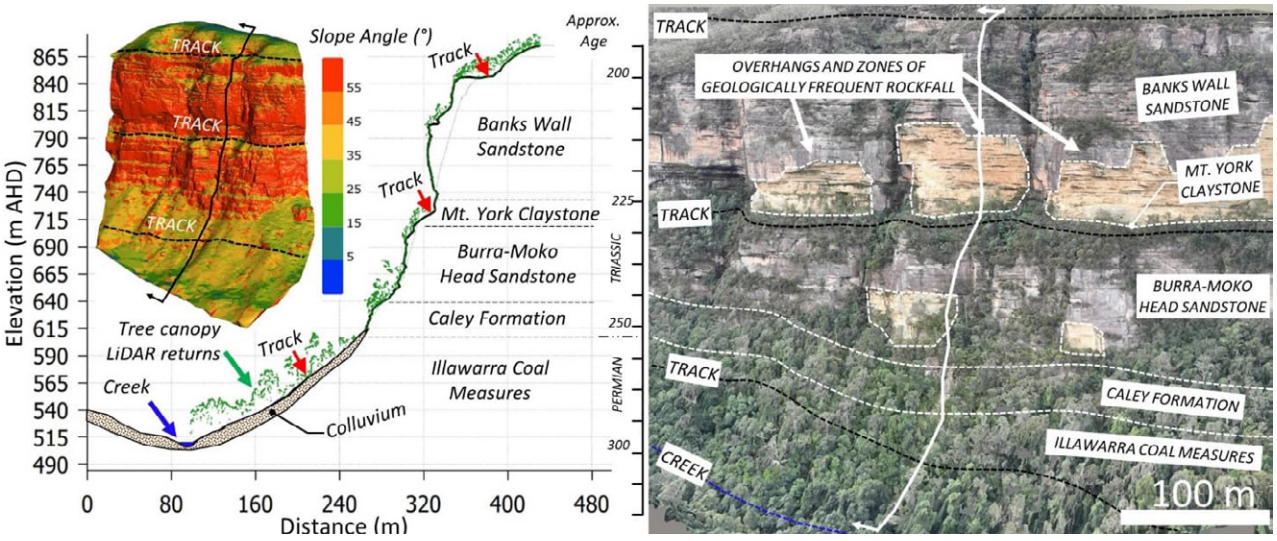

Figure 3: Interpreted LiDAR cross section and photogrammetry imagery of the cliffs near Wentworth Falls

Two orthogonal sets of high persistence vertical joints developed during the process of lithification and uplift, typically trending roughly east-west and north-south. Combined with horizontal bedding discontinuities, these joint sets provide kinematic release for rockfalls, with preferential erosion of underlying claystone producing sandstone overhangs that eventually topple or slide from the cliffs and onto the colluvial talus slopes below.

3.2 COMMON ROCKFALL FAILURE MECHANISMS

Initial uplift of the Blue Mountains occurred during the Cretaceous and this was followed by further episodes of uplift during the Cenozoic (Fergusson and Hatherly, 2023). Since approximately the late Miocene (~10 Ma) the geomorphic processes shaping the landscape have been dominated by erosion from stream incision and gravity-driven slope failures (Hatherly, 2019). Rockfalls are ubiquitous along the escarpment cliffs, being products of the long-term processes of valley incision and escarpment retreat that have produced the modern landscape. Typically, a new rockfall or landslide is reported somewhere in the park about once per month, frequently impacting popular walking tracks that connect the top of the escarpment to the valleys below by descending steep switchbacks, fabricated metal and carved stone stairways that pass directly under cliffs and overhangs.

Rockfalls in the Narrabeen Group rocks often involve failure of overhanging or undermined blocks of sandstone, with cubic to tabular blocks formed by the two main subvertical joint sets and subhorizontal bedding. Where walking tracks pass directly under natural or excavated overhangs, blocks may freefall just a few metres directly onto the track; other recorded rockfalls have involved long runout of blocks onto tracks that traverse the valley slopes below the cliffs. Figure 4 shows selected examples of overhanging sandstone blocks where stability is inferred to be influenced by the presence of intact rock bridges. Rockfall initiation may be promoted by tree root jacking, elevated pore pressures from intense rainfall events, or may occur with no obvious external trigger, as the culmination of slow, long-term subcritical crack growth driven by gravitational loading under self-weight.

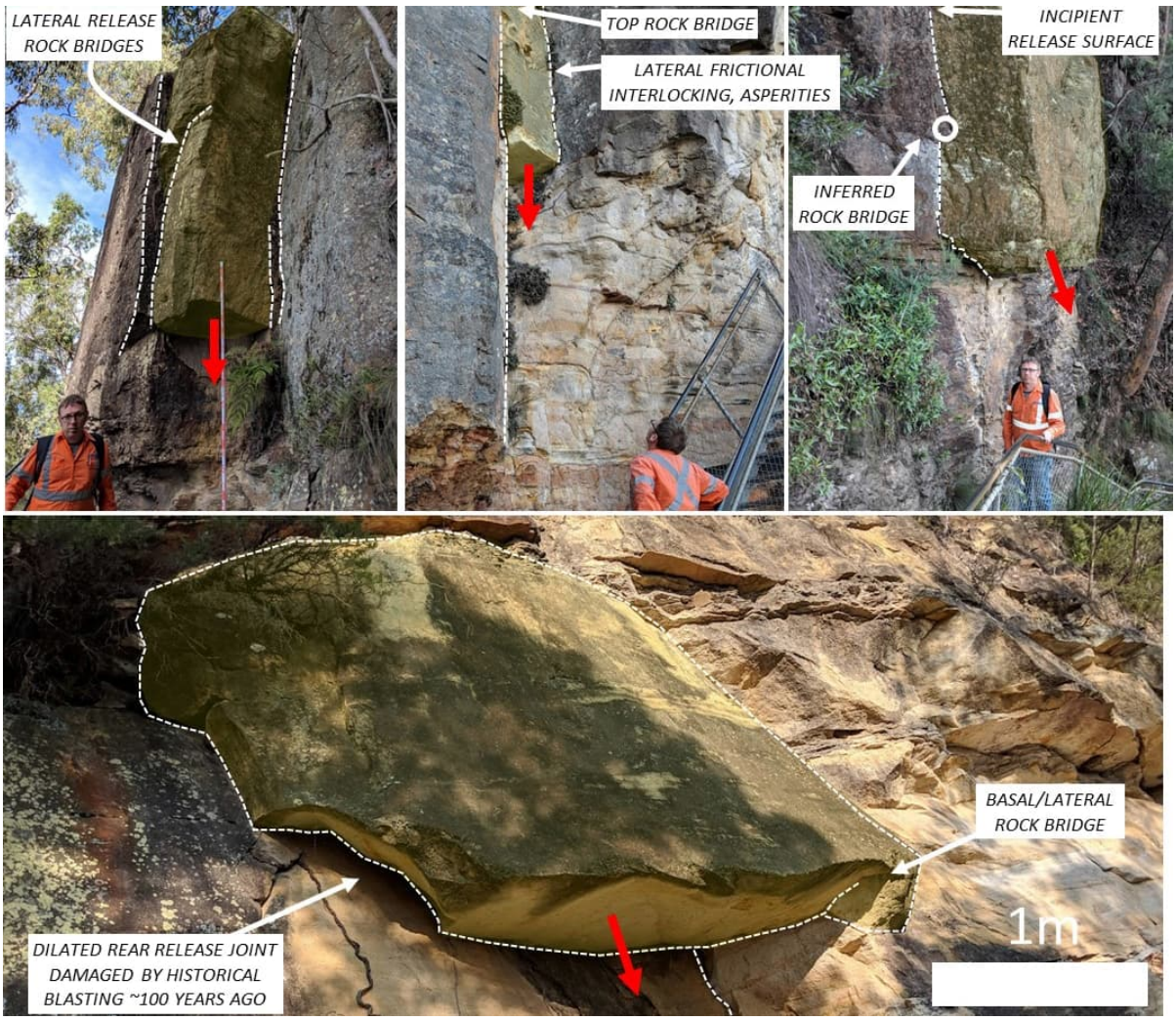

Figure 4: Examples of potential rockfall blocks involving propagation of vertical joints

The development of sandstone overhangs is promoted by the preferential erosion of weak shale and claystone layers that degrade with cyclical changes in moisture content. As the weaker horizon is eroded, the overhang depth increases, promoting extensile strains in the rock mass above, causing subvertical joints to dilate and tilting the overlying sandstone rock mass towards the valley below. In some cases, this preferential erosion has been accelerated by deliberate excavation of shale or claystone layers during the construction of walking tracks in the early 1900s. After the rear release joints have fully propagated, the eventual collapse may involve rotational toppling, or time-dependent bearing capacity failure of the eroding shale or claystone layer (Figure 5).

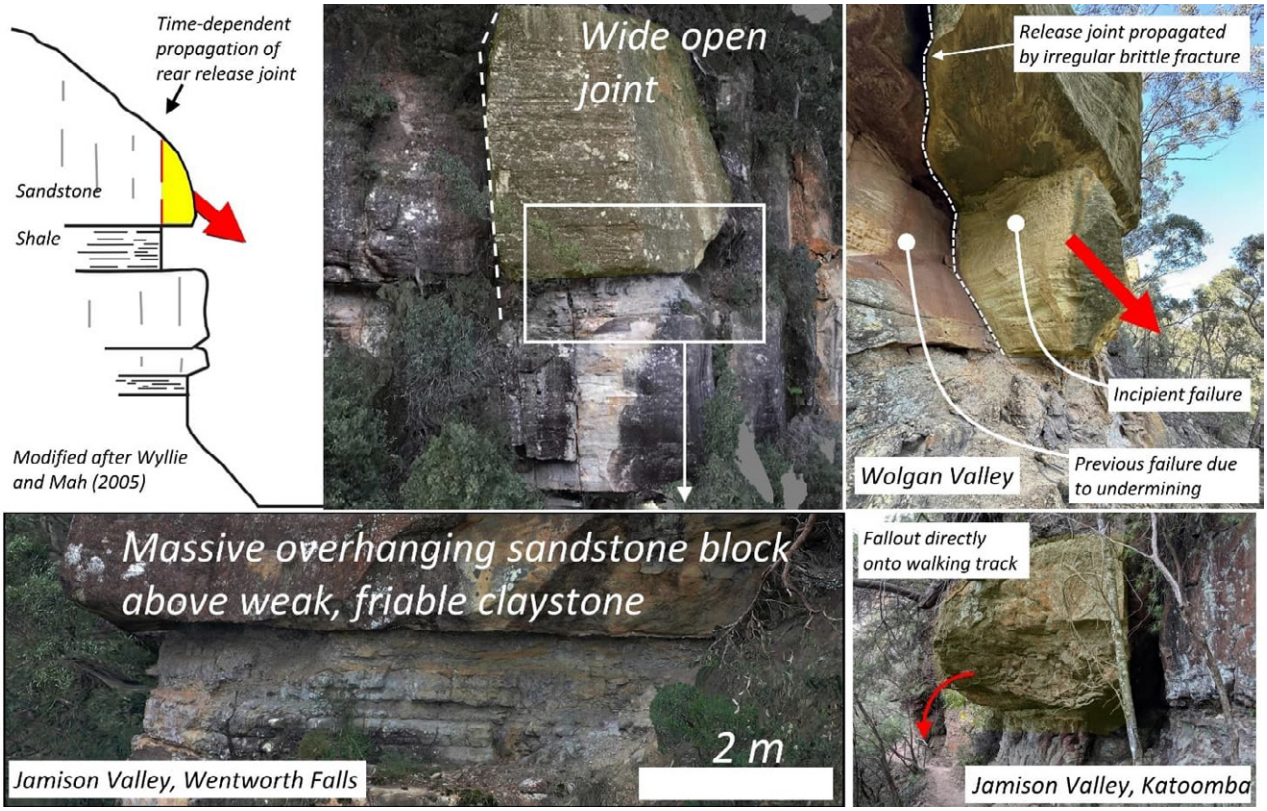

Figure 5: Examples of undermining by erosion of weak shale or claystone

Although the two processes of joint propagation and shale undermining may occur simultaneously, field evidence suggests that vertical rear release joints are often fully developed and significantly dilated many years before failure occurs in the underlying shale. However, if no basal shale layer is present, then failure of a "freestanding" overhang should be controlled by the propagation of rear and lateral release joints. The next section introduces a numerical modelling technique to model the time-dependence of these two failure mechanisms.

4 DISCRETE ELEMENT METHOD METHODOLOGY

4.1 THE BONDED BLOCK METHOD

The bonded block method (BBM) is a subset of the discrete element method where intact material is represented by an assembly of 2D polygons or 3D polyhedra with strong, stiff contacts; breakage of the bonded contacts simulates the process of brittle fracture. Previous BBM research has investigated the use of polygonal Voronoi tessellations to represent brittle failure of strong intact rock and jointed rock masses (Christianson et al., 2006; Alzo'ubi, 2009). Voronoi tessellations produce an assembly of random interlocking polygons that tends to produce a stiff macroscopic response predisposed to localised tensile contact failure with rough, irregular failure surfaces. This study applies the trigon discretisation methodology in *UDEC*, first introduced by Gao (2013), where Voronoi polygons are further subdivided into triangular blocks. In contrast with Voronoi models, trigon discretisation allows a greater degree of kinematic freedom in the bonded block assembly. Whereas the macroscopic response of Voronoi models is strongly influenced by particle interlocking effects, trigon models can be more directly controlled by the strength and stiffness of bonded contacts. Previous research has demonstrated the ability of trigon models to simulate laboratory scale failure of coal measures rocks and field scale failure of underground coal mine roadways (Gao and Stead, 2014). The BBM

trigon technique has also been applied to large rock slope failures mechanisms including flexural toppling (Zheng et al., 2018) and mining-induced collapse of sandstone cliffs in the Blue Mountains (Tuckey, 2023).

A significant advantage of the BBM method is the ability to model non-persistent discontinuities that terminate in intact rock, with the breakage of bonded block contacts simulating fracture propagation. Figure 6 illustrates a conceptual example of a fractured rock slope containing multiple scales of pre-existing discontinuities varying from microcracks through to high persistence joints and faults. A non-daylighting sliding surface is included near the toe of the slope. Conventional discrete element models require convex blocks with complete perimeters; to accommodate computing limitations the model will exclude discontinuities below a lower bound persistence limit, while retaining the key high persistence discontinuities that are expected to control slope kinematics. Bandis (2004) described this in terms of the "effective block" concept, with block properties adopting scaled stiffness and shear strength parameters to account for low persistence and incipient discontinuities that are not explicitly included in the model.

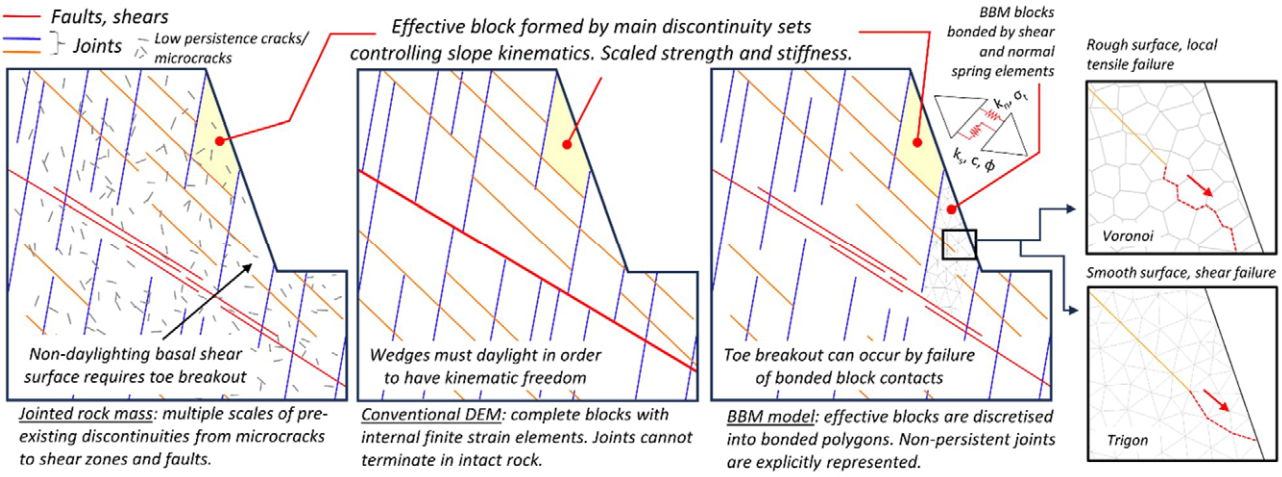

Figure 6: Conceptual illustration of the effective block concept and BBM discretisation

While the conventional discrete element model cannot explicitly include a non-daylighting wedge, the BBM approach can simulate toe breakout along a rough, irregular failure surface that develops by localised contact tensile failure in the case of Voronoi discretisation, or a smooth failure surface dominated by contact shear failure for a trigon model. The next section describes the implementation of a fracture mechanics model in *UDEC* for modelling time-dependent degradation of bonded block contact cohesion and tensile strength, driven by subcritical crack growth.

4.2 A FRACTURE MECHANICS MODEL FOR SUBCRITICAL CRACK GROWTH

Kemeny (2003) introduced a fracture mechanics model to simulate the effect of intact rock bridges along a planar sliding surface subject to constant normal stress. Time-dependent reduction in cohesion was calculated using a closed-form solution for subcritical crack growth assuming a mode II (shear) failure mechanism. Kemeny (2005) extended the approach using the discrete element method software *UDEC* to simulate time-dependent cohesion loss in pre-existing joints surrounding an underground excavation, accounting for changing stress conditions as the zone of damage (i.e. excavation-induced fractures) develops around the tunnel profile. Sampaleanu (2017) further developed the model, incorporating mode I (tensile) failure of bonded Voronoi blocks into analysis of rockfall in an open pit mine slope.

The subcritical crack growth model is based on an idealised coplanar or "in plane" rock bridge of width $2a$ separating the tips of two pre-existing discontinuities in a rock block of width of $2w$. Failure can occur in mode I (tension) or mode II (shear). It is assumed that failure will occur when the mode I stress intensity K_I or mode II stress intensity K_{II} exceeds the fracture toughness parameters K_{IC} or K_{IIC} which are material properties of intact rock with units of $MPa\sqrt{m}$. By considering the limit state where $K_{II} = K_{IIC}$ the equation for mode II stress intensity can be re-arranged to estimate the initial cohesion of a bonded contact c_0 as a function of rock bridge geometry and fracture toughness:

$$Rock\ bridge\ cohesion = c_0 = \frac{K_{IIC}\sqrt{\pi a}}{2w} \quad (1)$$

Equation 2 shows the corresponding equation for initial rock bridge tensile strength σ_{t0} as proposed by Sampaleanu (2017), considering mode I (tensile) failure occurring when $K_I = K_{IC}$.

$$Rock\ bridge\ tensile\ strength = \sigma_{t0} = \frac{K_{IC}\sqrt{\pi a}}{2w} \quad (2)$$

Figure 7 illustrates the conceptual rock bridge model under mode I (tensile) and mode II (shear) loading conditions. The stress intensity factors depend on the specimen width *2w*, the rock bridge half width *a*, and the imposed loads. Mode I stress intensity K_I is calculated using the normal stress σ_n and mode II stress intensity K_{II} is calculated using mobilised cohesion ($\tau - \sigma_n \tan \varphi$) where τ is shear stress and φ is the friction angle of the two pre-existing discontinuity segments. At the limit state these equations can be rearranged to estimate the initial cohesion and tensile strength provided by the intact rock bridge. Conversely, if the initial joint cohesion, tensile strength and fracture toughness is known, then the same equations can be re-arranged to calculate the initial rock bridge width *2a*.

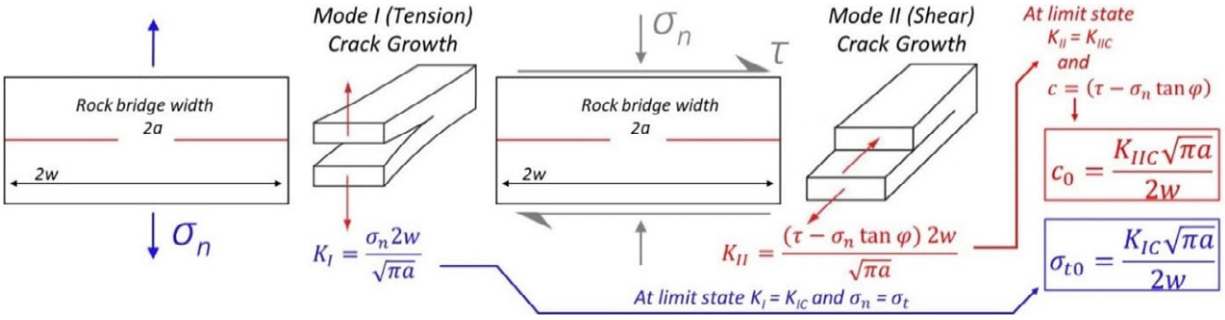

Figure 7: Rock bridge model with formulae for stress intensity used to estimate cohesion and tensile strength

After the initial BBM tensile strength and cohesion are defined, a strength degradation algorithm is applied at each numerical timestep. Over time, subcritical crack growth causes the rock bridge width *2a* to decrease, reducing the cohesion and tensile strength provided by the rock bridge. Kemeny (2005) proposed that the rate of subcritical crack growth could be estimated using a version of the Charles power law adapted for mode II loading, where crack growth velocity is calculated using the ratio of mode II stress intensity K_{II} to the critical mode II fracture toughness parameter K_{IIC} and material constants *A* and *n* which are properties of intact rock that can be measured in the laboratory:

$$Subcritical\ shear\ crack\ growth\ velocity = a'(t) = A\left(\frac{K_{II}}{K_{IIC}}\right)^n \tag{3}$$

For this investigation, the Charles law equation is modified to consider the combined effects of mode I and mode II crack growth. The local magnitudes of K_I and K_{II} for each bonded contact are used to resolve an effective stress intensity K_{EFF} which is compared against a weighted fracture toughness parameter that accounts for the relative proportions of mode I and mode II loading. After calculating the subcritical crack growth velocity for each contact, it is necessary to estimate a suitable timestep Δt so that the change in rock bridge width can be calculated as follows:

$$Change\ in\ rock\ bridge\ width = \Delta a = a'(t) \times \Delta t \tag{4}$$

UDEC applies an explicit finite difference solution scheme to solve the equations of force and motion for block contacts and internal finite strain elements within deformable blocks, based on a mechanical timestep that is not directly relatable to real time. This study therefore assigns a "subcritical timestep" Δt at each calculation cycle, such that an upper bound subcritical timestep in the order of 10^7 seconds is adopted for low stress conditions; this limit has been demonstrated to produce stable results for modelling of long-term strength reduction over hundreds to tens of thousands of years (Kemeny, 2005). The subcritical timestep decreases exponentially to a minimum of 10 seconds as stress intensity approaches the limiting fracture toughness. After calculating the reduction in rock bridge width, equation 1 is used to calculate the updated (reduced) contact cohesion; the reduction in contact tensile strength is assumed to be proportional to the reduction in contact cohesion. Cycling is then continued until failure is observed.

In summary, the strength degradation algorithm applies the following steps, looping through all bonded block contacts at every mechanical timestep:

- **Step 1:** Read current values for cohesion *c*, friction angle φ, current tensile strength σ_t. Calculate the current rock bridge length a_0 for each contact, based on the current contact cohesion, by re-arranging the equation for mode II stress intensity as shown below:

$$Current\ rock\ bridge\ length\ = a_0 = \left(\frac{c\ 2w}{K_{IIC}\sqrt{\pi}}\right)^2 \tag{5}$$

- **Step 2:** Read contact shear force, normal force, and contact length. Shear and normal stresses are derived by dividing forces by contact length. Calculate stress intensity parameters K_I and K_{II} for each bonded contact.
    - Calculate the effective stress intensity for each contact, accounting for mode I and mode II loading:

$$K_{EFF} = \sqrt{K_I^2 + K_{II}^2} \tag{6}$$

- Find the maximum stress intensity $K_{EFF(MAX)}$ occurring in the model and calculate an appropriate subcritical timestep Δt such that the maximum timestep is in the order of 10^7 seconds. For the given model conditions, the following equation was adopted:

$$\Delta t = (1.33 \times 10^8) \times e^{(-3.28\times10^{-5})\times K_{EFF(MAX)}} \quad (7)$$

- Crack growth rate $a'(t)$ is calculated for each bonded contact, using a modified version of Equation 3 that incorporates both mode I and mode II stress intensity:

$$Subcritical\ crack\ growth\ velocity = a'(t) = A\left(\frac{K_{EFF}}{\frac{2\theta}{\pi}K_{IC}+(1-\frac{2\theta}{\pi})K_{IIC}}\right)^n = A\left(\frac{K_{EFF}}{K_{C(EFF)}}\right)^n \quad (8)$$

$$\text{Where } \theta = tan^{-1}\frac{K_I}{K_{II}}$$

- Use the crack growth rate $a'(t)$ and subcritical timestep Δt to calculate the new rock bridge width:

$$a_1 = a_0 + (a'(t) \times \Delta t) \quad (9)$$

- **Step 3**: Use the new rock bridge width a_1 to calculate the updated value of cohesion according to equation 1. The reduction in contact tensile strength is assumed to be proportional to the reduction in contact cohesion. New cohesion and tensile strength values are assigned to the bonded contact. Cycling is continued until failure is observed. The rate of tensile and shear contact failure versus accumulated subcritical time is recorded.

Figure 8 shows a graphical representation of the strength degradation algorithm; note that the edges of each bonded trigon element are each discretised into two bonded half-lengths of dimension $2w$.

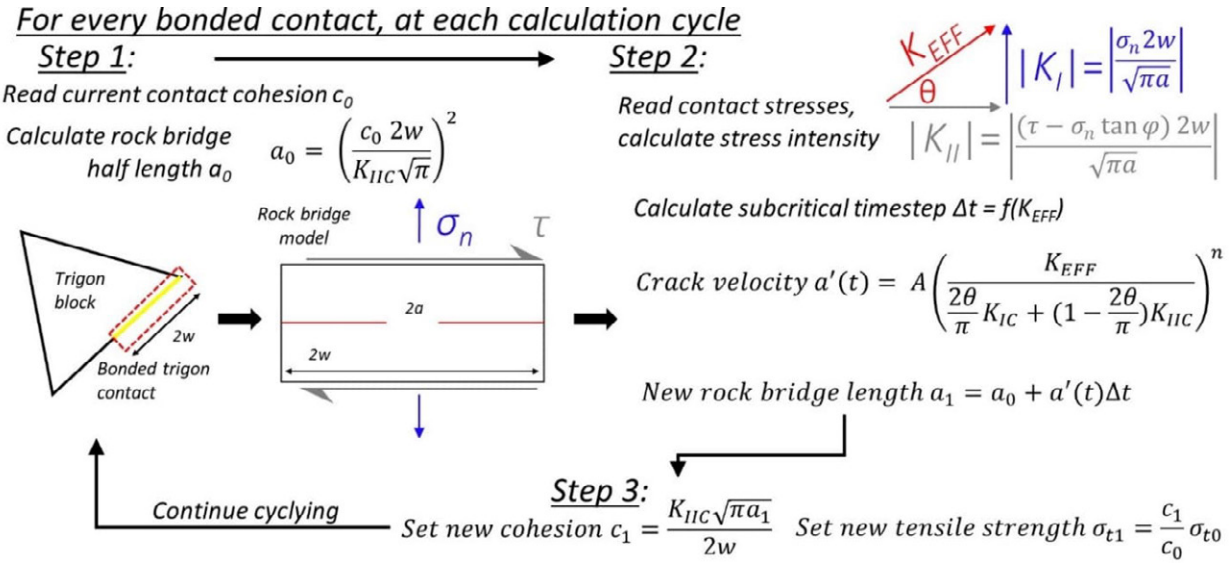

Figure 8: Strength degradation algorithm carried out at each mechanical timestep for every BBM contact

Section 5 presents a conceptual numerical modelling study of an overhanging sandstone slab, where the BBM strength degradation algorithm is used to simulate time-dependent loss of bonded contact cohesion and tensile strength, leading to failure by propagation of a non-persistent vertical release joint. Section 6 extends the modelling technique to consider time-dependent rockfall initiation by preferential undermining failure of a weak shale or claystone layer.

5 TIME-DEPENDENT FAILURE OF AN OUTCROP-SCALE OVERHANG

5.1 MODEL SETUP

A simplified outcrop-scale model was constructed to consider an overhanging slab of massive sandstone. Failure occurs by propagation of a non-persistent vertical rear release joint. The overhanging slab is 5 m high and 1 m wide. Various intact rock bridge geometries were modelled, with the bridge placed at the top, middle, or bottom of the slab, and a further scenario with intact rock bridges distributed across the joint. The distributed rock bridge scenario represents the pre-existing joint as fully persistent contact interrupted by strong rock bridge segments of 0.25 m length; the other scenarios model the joint as a non-persistent discontinuity with explicit terminations in intact rock. Figure 9 shows the model geometry, with a region of 0.2 m edge length trigon blocks bonded to a far field elastic continuum.

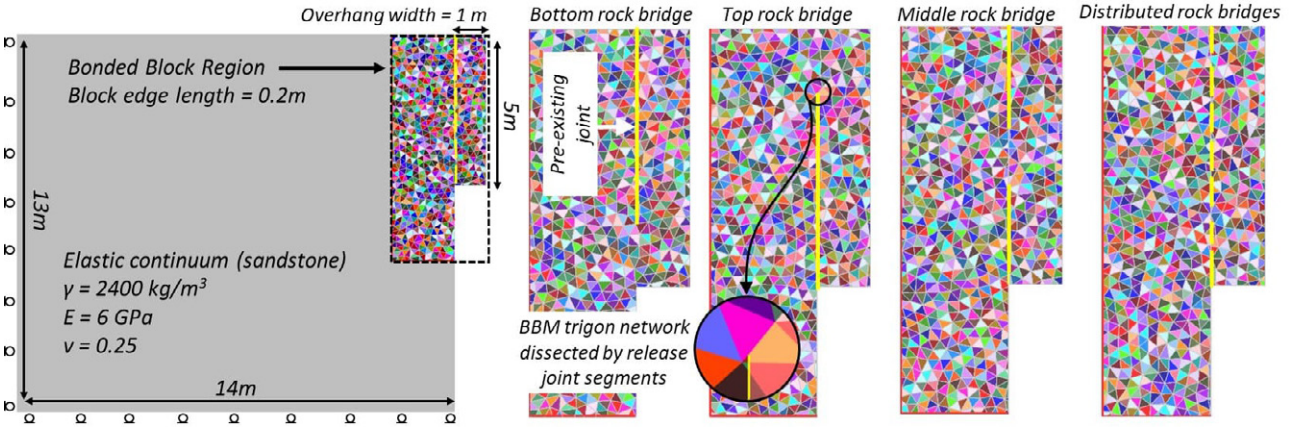

Figure 9: Geometry of simple overhang stability model with variable rock bridge geometry

The pre-existing vertical joint is modelled as a frictional surface with zero cohesion and tensile strength. In situ stresses are initialised according to gravitational self-weight and displacement versus time is recorded at the crest of the cliff. Intact rock bridge content is varied from 5% to 30% representing a total intact rock bridge length of 0.25 m to 1.5 m measured vertically from the non-persistent joint tips. BBM contact parameters are derived from laboratory-scale trigon simulations by Tuckey (2023) to represent good quality Class I/II sandstone under the Sydney Rock Mass Classification System as described by Bertuzzi and Pells (2002) and Oliveira (2014). Table 1 summarises material parameters used to define the strength and stiffness of bonded blocks and the pre-existing joint. Stiffness parameters for BBM contacts are scaled according to the recommendations of Itasca and Christianson et al. (2006) as a function of BBM contact length. The initial BBM cohesion and tensile strength consider a bonded trigon contact half-length $2w$ of 0.1 m comprised of 50% initial rock bridge ($2a$ = 0.05 m). Fracture toughness parameters K_{IC} and K_{IIC} are estimated from intact rock brittleness indices that depend on UCS and tensile strength σ_t after Nejati and Moosavi (2017).

Table 1: Summary of key input parameters to simple overhang model

Application	Parameter	Sandstone	Pre-existing joint
Intact Rock	Density ρ (kg/m^3)	2400	n/a
	Reference UCS σ_c (MPa)	25	
	Reference Tensile Strength σ_t (MPa)	2.5	
	Young's Modulus E (GPa)	6	
Bonded trigon block contacts	Mode I Fracture Toughness K_{IC} (MPa $\sqrt{\text{m}}$)	0.4	
	Mode II Fracture Toughness K_{IIC} (MPa $\sqrt{\text{m}}$)	0.8	
	Initial contact cohesion c_0 (MPa)	2.2	0
	Initial contact tensile strength σ_{t0} (MPa)	1.1	0
	Contact Friction angle φ	35°	36°
	Contact normal stiffness j_{kn} (GPa/m)	360	10
	Contact shear stiffness j_{ks} (GPa/m)	144	1
	Subcritical parameter A (m/s)	0.2	n/a
	Subcritical parameter n	16	

Subcritical crack growth parameters A and n are based values published by Lee (2007) who modelled time-dependent failure of slopes in Coconino sandstone, and Ko and Kemeny (2011) who undertook laboratory investigations of subcritical crack growth in Coconino sandstone from Arizona, USA, using a variety of test techniques including the double torsion test, wedge splitting test, double cantilevered beam test, and modified punch-through shear test.

At laboratory scale the crack velocity parameter A can vary across several orders of magnitude from 10^{-4} to 10^{-1} m/s. The parameters adopted for this investigation are upper bound estimates, which are considered suitable for these field-scale simulations. The upper bound crack growth velocity estimates implicitly account for exogenous environmental factors that may accelerate crack growth, but are not directly included in the model, such as: root jacking from trees growing into pre-existing discontinuities; thermally induced strains based on daily and seasonal temperature fluctuations; and water infiltration into joints from surface water runoff and groundwater seepage.

5.2 RESULTS

The results demonstrate that the brittle failure mechanism and subcritical time required for failure to develop vary significantly depending on the geometry and proportion of intact rock bridges. When the intact rock bridge is positioned at the base of the slab, failure involves progressive development of an irregular tensile fracture surface that propagates downward from the bottom tip of the pre-existing joint, initially curving back from the free face. Figure 10 shows the contours of block displacement, failed contact states, and stress intensity for BBM contacts at timesteps from 916 years up to failure (kinematic release) after 2640 years of simulated "subcritical time".

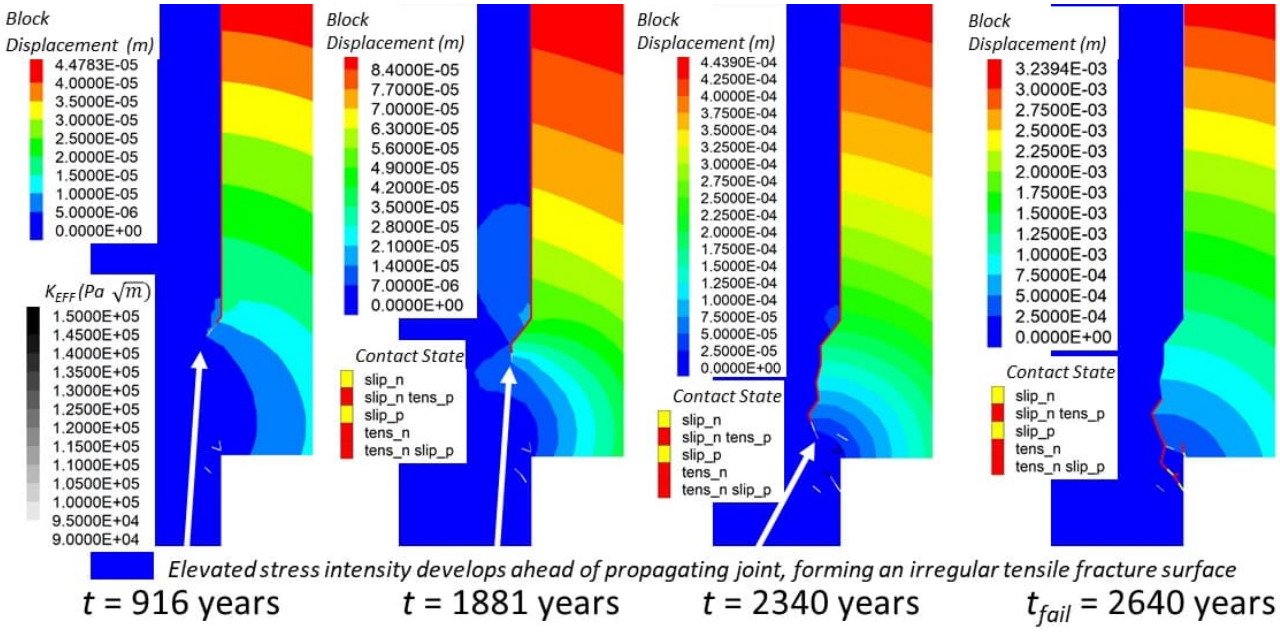

Figure 10: Examples results for a 1.5m (30%) bottom rock bridge failing after 2640 years

The history plots of maximum stress intensity $K_{EFF(MAX)}$ and subcritical timestep Δt shows how the crack growth simulation "slows down" as stress intensity increases ahead of the advancing crack front (Figure 11). The right-hand plot shows the history of crack length (BBM contact length failed in tension and shear), and cliff crest displacement.

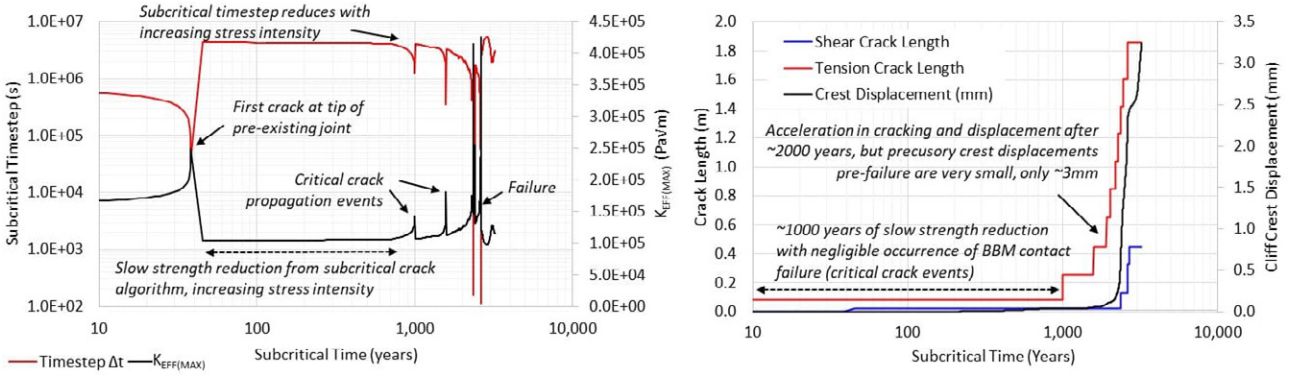

Figure 11: Histories of $K_{EFF(MAX)}$, subcritical timestep, displacement, and crack length (1.5m bottom rock bridge)

Subcritical crack growth is modelled as a continuously active process, simulated by the progressive reduction in BBM cohesion and tensile strength. In contrast, the failure of BBM contacts in shear or tension represent episodic processes involving critical crack growth events with rapid failure of bonded contacts. For the model incorporating a "bottom rock bridge" at the base of the rockfall slab, subcritical crack growth dominates during the first 1000 years of simulation time, with episodic critical crack growth events occurring between 1000 and 2600 years, leading up to failure. Precursory displacements at the crest of the slab are limited to about 3 mm. Tensile cracks dominate the failure process.

The failure mechanism and "subcritical time" required for failure to develop vary depending on the rock bridge content and geometry. Figure 12 illustrates the failure mechanisms that develop for the maximum rock bridge scenario, with approximately 30% of the rear release surface comprising intact rock bridges placed either at the top of the slab, in the

middle of the rear release joint, or distributed across the rear release surface. The plots of total BBM crack length versus subcritical time shows how the subcritical time required for failure to develop may vary from hundreds of years for the "top rock bridge" geometry, to tens of thousands of years for the "distributed rock bridge" geometry. For the top, middle, and distributed rock bridge scenarios, failure develops in a "bottom-up" process, with release of a lower "sub-slab" by propagation of subhorizontal tensile fractures. The time to failure appears to depend on the height of this critical "sub-slab" which is determined by rock bridge geometry. The "top rock bridge" scenario imposes the highest tensile loading because this geometry produces the greatest effective "sub-slab" slab height.

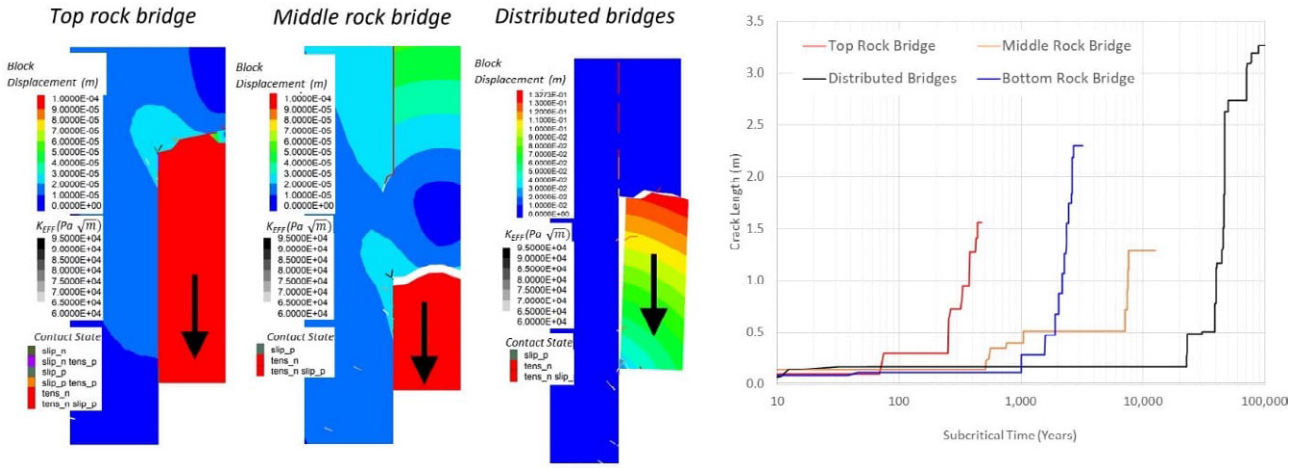

Figure 12: Comparison of failure mechanisms for top, middle, and distributed rock bridges (30% length)

Figure 13 shows the corresponding results for the 10% rock bridge scenario. The time to failure is reduced by roughly two orders of magnitude when compared with the 30% rock bridge case. Failure develops fastest for the bottom rock bridge scenario, after approximately 10 years, with two discrete shear cracking events in the basal rock bridge. Tensile failure occurs after approximately 100 years for the "top rock bridge" scenario. The "middle rock bridge" failure involves release of a basal slab after 330 years, and release of the remaining upper slab after about 800 years.

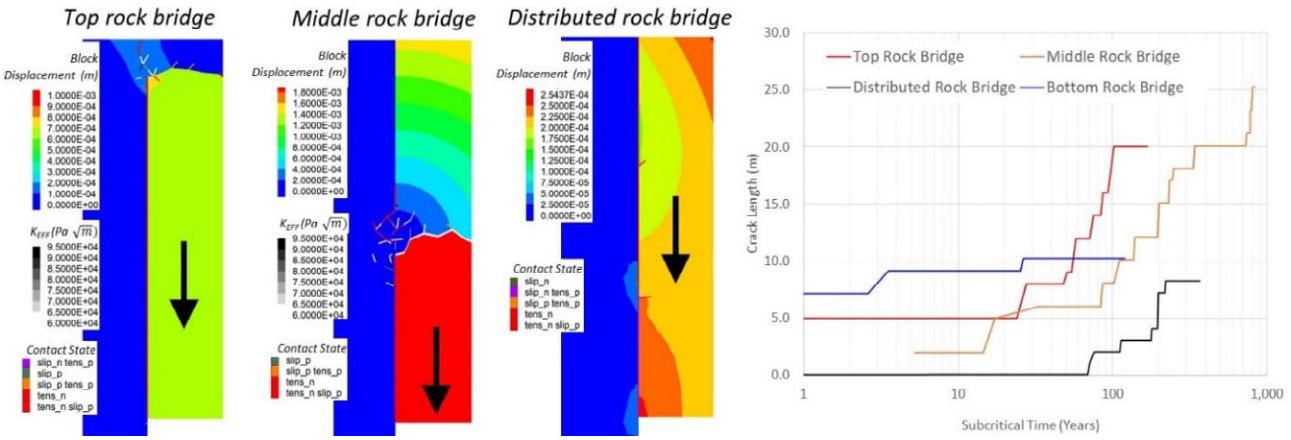

Figure 13: Comparison of failure mechanisms for top, middle, and distributed rock bridges (10% length)

The results demonstrate how the rock bridge geometry influences the brittle failure mechanism and timespan required for failure. Larger intact rock bridges require more time for interaction to develop between the tips of pre-existing joints, and the brittle release surface tends to propagate sub-horizontally. As the rock bridge length is decreased, incipient brittle fractures interact earlier, forming a composite release surface sub-parallel to the rear release joint.

Figure 14 presents a semi-logarithmic plot of time to failure t_f versus rock bridge content for each case. A secondary horizontal axis indicates the corresponding persistence of the rear release joint, with an inferred "zero" point included where time to failure t_f is assumed to be less than 0.1 years for 0% rock bridges, representing effectively instantaneous failure in the case of a fully persistent rear release joint. The 25% and 30% "distributed rock bridge" scenarios apply an accelerated subcritical timestep to achieve manageable computation times, due to the reduced stress intensity that occurs when the weight of the overhanging slab is distributed across a greater number of intact rock bridges.

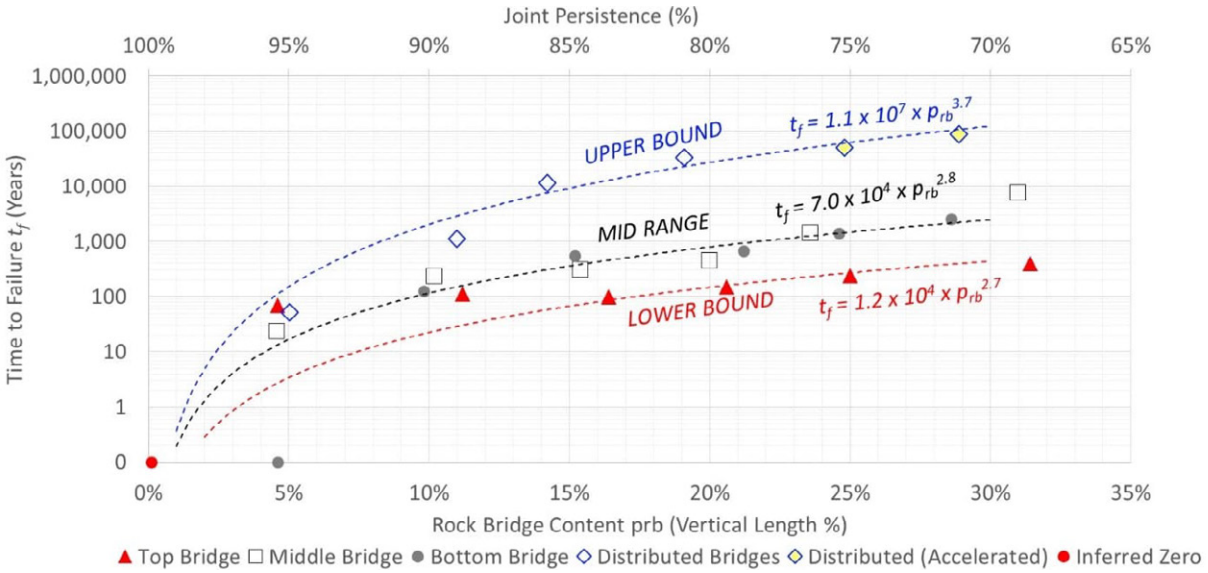

Figure 14: Time to failure versus rock bridge content for various rock bridge geometry scenarios

Power law curves appear to give a reasonable conceptual fit to upper bound and lower bound trends for time to failure t_f versus rock bridge content. Key observations include:

- The distributed rock bridge geometry scenarios produce the longest time to failure t_f because subcritical crack growth rate is proportional to stress intensity, and when the weight of the slab is distributed among a greater number of rock bridges, the stress intensity at any one rock bridge is reduced.
- The top rock bridge geometry produces the most rapid failures; this is interpreted to occur because these scenarios subject the rock bridge to direct tension loading and the greatest effective "sub-slab" height.
- When rock bridge content is reduced below 5% to 10% there is a marked decrease in stability, with time to failure decreasing by roughly an order of magnitude for every 3% decrease in rock bridge content.

The results reflect the dependence of the subcritical crack growth rate on localised stress concentrations at the tips of pre-existing joints. The next section extends the time-dependent strength degradation model to consider failure of a sandstone cliff by progressive undermining of a weaker underlying shale layer.

6 PROGRESSIVE CLIFF-SCALE COLLAPSE PROMOTED BY UNDERMINING

6.1 MODEL SETUP

The subcritical crack growth model introduced in the previous section was extended to consider time-dependent brittle failure of an overhanging sandstone cliff undermined by a layer of weaker shale or claystone, representing a common landform in Blue Mountains National Park. Figure 15 shows the model geometry, incorporating a 50 m high cliff, with the upper 20 m forming an overhanging sandstone face underlain by a 4 m thick layer of weaker shale. The shale and upper sandstone rock masses are discretised into trigon elements of 0.6 m length, bonded to a far-field elastic continuum. The lower half of the cliff is represented by jointed elastic sandstone blocks. The trigon discretisation is overprinted by pre-existing joints and bedding discontinuities with negligible cohesion and tensile strength.

Discontinuity geometry and rock block shapes reflect observations from geotechnical mapping of sandstone cliffs in the Blue Mountains (e.g. Tuckey, 2023). Discontinuity spacing is "upscaled" and bonded trigon block edge lengths are limited to 0.6 m to manage computational requirements, while retaining key structural controls slope failure kinematics. The reference properties for sandstone are unchanged from the previous outcrop-scale models.

The shale layer is based on a Class II shale with intact rock UCS of 15 MPa, with calibrated BBM contact parameters derived from Tuckey (2023). The reference fracture toughness values are K_{IC} = 0.25 MPa $\sqrt{m}$ in tension and K_{IIC} = 0.6 MPa $\sqrt{m}$ in shear, based on relationships with UCS and σ_t as proposed by Nejati and Moosavi (2017). Initial BBM cohesion and tensile strength are calculated using the same initial rock bridge geometry as the outcrop-scale model, where $2w$ = 0.1 m and $2a$ = 50 mm. The subcritical timestep Δt is calculated from the maximum stress intensity ratio $K_{EFF}/K_{C(EFF)}$ such that the maximum subcritical timestep is in the order of 10^7 seconds or less, reducing exponentially as stress intensity increases to maintain numerical stability.

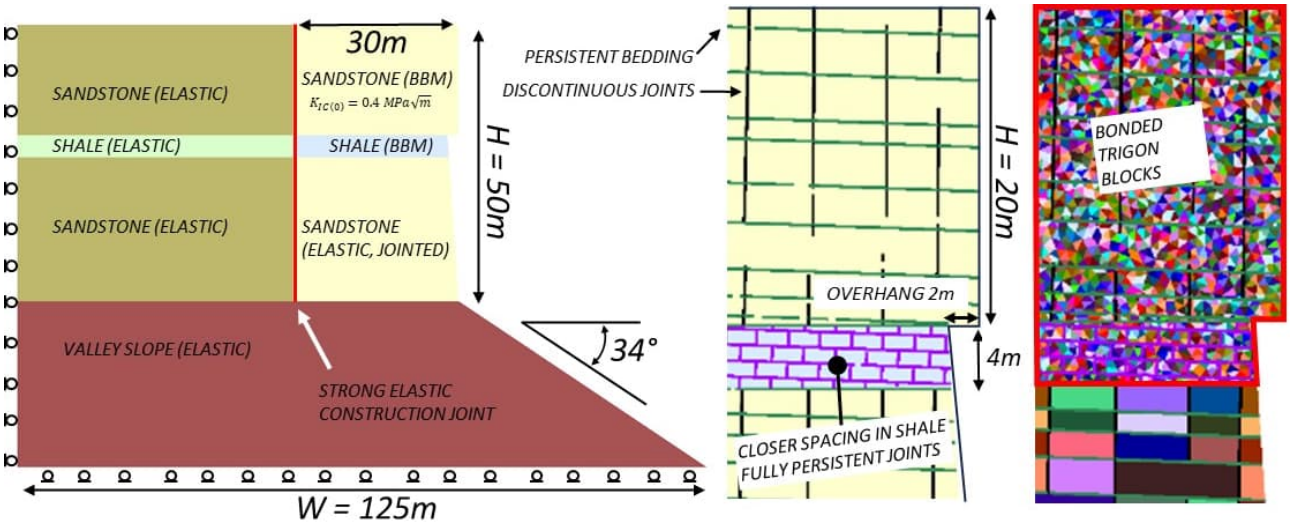

Figure 15: Geometry of cliff scale model with bonded block region surrounding a sandstone overhang

While the outcrop-scale model in the previous situation adopted uniform values for bonded contact strength and subcritical crack growth parameters A and n, the cliff scale model incorporates additional calculations to account for the influence of confining stress in suppressing subcritical crack growth. Laboratory experiments have measured how confining stress suppresses crack growth and increases the critical fracture toughness parameters K_{IC} and K_{IIC} while also reducing subcritical crack growth velocity. Changes to fracture toughness and the subcritical crack growth parameter n can be simplified as a linear, whereas the subcritical A parameter decreases exponentially with increasing confinement. Figure 16 shows the relationships adopted for the cliff-scale model, based on published values for sandstone from Backers (2004), Lee (2007), and Ko and Kemeny (2011). The confinement-dependent parameters yield lower fracture toughness and increased crack velocity where confining stress is low: consequently, the model should demonstrate how brittle failure fist develops in the unconfined near-surface rock mass at the cliff face.

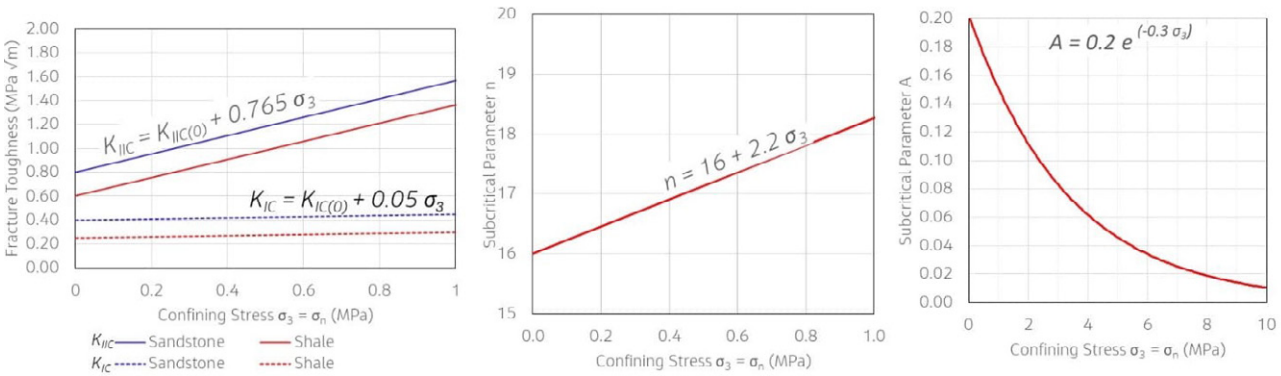

Figure 16: Fracture toughness and subcritical crack parameters versus confining stress

Two different *in situ* stress scenarios were investigated: the first scenario considers a lithostatic stress regime, assuming that high horizontal tectonic stresses have been relieved by slow, long-term escarpment retreat and erosion. The second scenario applies a high horizontal major principal stress ($\sigma_1 = \sigma_x = \sigma_H$) based on the relationships proposed by Oliveira and Parker (2014), who demonstrated the dependence of *in situ* stress on rock mass stiffness in the layered sedimentary formations of the Sydney Basin, where the sandstone units are stiffer and thus attract higher horizontal stresses than the softer shale units. Both scenarios adopt the following modelling sequence:

- **Step 1:** Initialise *in situ* stresses for a rectangular model domain representing the subsurface profile before any valley incision has occurred. Vertical stress $\sigma_y = \sigma_v$ is calculated using an average unit weight for the rock mass of 23.5 kN/m^3. The lithostatic scenario then sets horizontal stress $\sigma_x = \sigma_H$ equal to vertical stress. The high horizontal stress scenario adopts horizontal stresses as summarised below:

$$\textbf{\textit{Sandstone}}\ \sigma_x = \sigma_H = 3\ \sigma_V + 1\ \text{MPa} \tag{10}$$

$$\textbf{\textit{Shale}}\ \sigma_x = \sigma_H = 1.4\ \sigma_V + 0.4\ \text{MPa} \tag{11}$$

- **Step 2:** Excavate the valley. Cycle the model until equilibrium is reached, using artificially strong BBM contact properties to prevent failure due to rapid stress changes associated with the instantaneous removal of confinement. Stresses redistribute to accommodate the escarpment morphology and geological structure.
- **Step 3**: Calculate stress-dependent fracture toughness and subcritical crack growth parameters. Use the fracture toughness parameters to derive initial values for BBM cohesion c_0 and tensile strength σ_{t0} considering an initial rock bridge geometry where $2w$ = 0.1 m and $2a$ = 50 mm as per the outcrop-scale simulations.
- **Step 4:** Activate the shear strength degradation algorithm and cycle the model until failure is observed. The crack growth rate is recorded in terms of the length of BBM contacts failed in tension and shear versus subcritical time. When rock blocks are kinematically freed from cliff face by new brittle fractures, the strength degradation algorithm is temporarily paused, and mechanical cycling is continued to allow the newly detached blocks to fall away from the cliff. Detached blocks are then deleted from the model, and strength degradation algorithm is re-activated to continue modelling long-term subcritical crack growth.

Figure 17 illustrates the influence of *in situ* stress on the confinement-dependent BBM contact strength in terms of the initial cohesion c_0. The lowest BBM cohesion tends to occur on subvertical contacts near the face of the cliff, where confining stress is lowest. With increasing depth behind the cliff face, confining stress and initial BBM cohesion (and tensile strength) increase. The high stress scenario imposes greater confining stress that produces a corresponding increase in the initial BBM cohesion and tensile strength for deeper zones of rock mass, further from the cliff face.

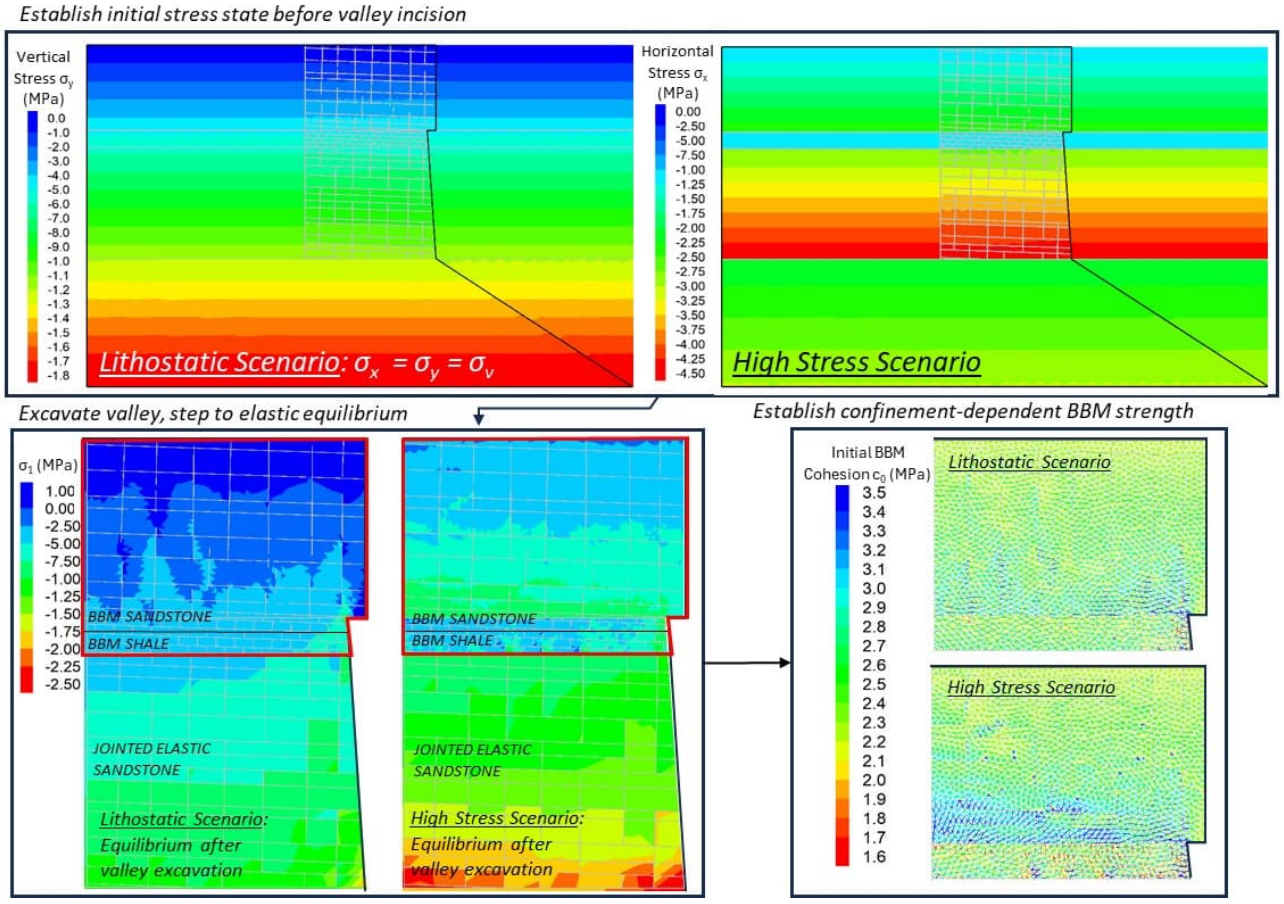

Figure 17: Comparison of stress initialisation and initial BBM strength for lithostatic and high stress scenarios

Although the high stress scenario provides greater confinement and initial BBM strength, it also produces zones of locally elevated normal and shear stress which may act as preferred zones for fracture initiation.

Figure 18 shows the relative change imposed by the high stress scenario, with BBM contacts coloured by the difference in shear stress as fraction of BBM cohesion (ratio τ / c_0) and the difference in tensile normal stresses as fraction of tensile strength (ratio σ_n / σ_{t0}). The accompanying histograms illustrate how the high stress scenario produces a marked increase in shear loading of the BBM shale relative to initial cohesion c_0; increases in tensile loading also occur but are limited to a small number of localised BBM contacts.

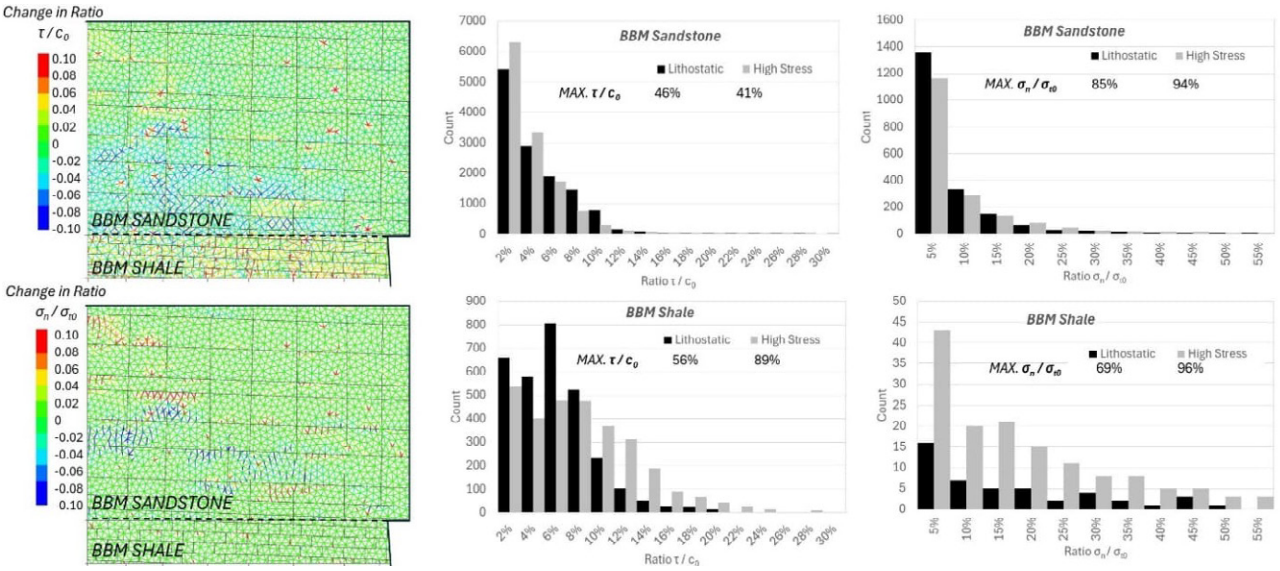

Figure 18: Change in initial stress ratios τ/c_0 and σ_n/σ_{t0} produced by the high stress scenario

The next section shows key results from both *in situ* stress scenarios, focussing on how the initial stress regime influences the rate of subcritical crack growth and the development of time-dependent brittle slope failure.

6.2 RESULTS

Figure 19 shows results from the lithostatic stress model at selected subcritical timesteps from 7.9 years up to 2410 years, focused on BBM discretisation region. Blocks are shaded by rotation in radians to highlight the progressive release of overhanging blocks by new brittle fractures.

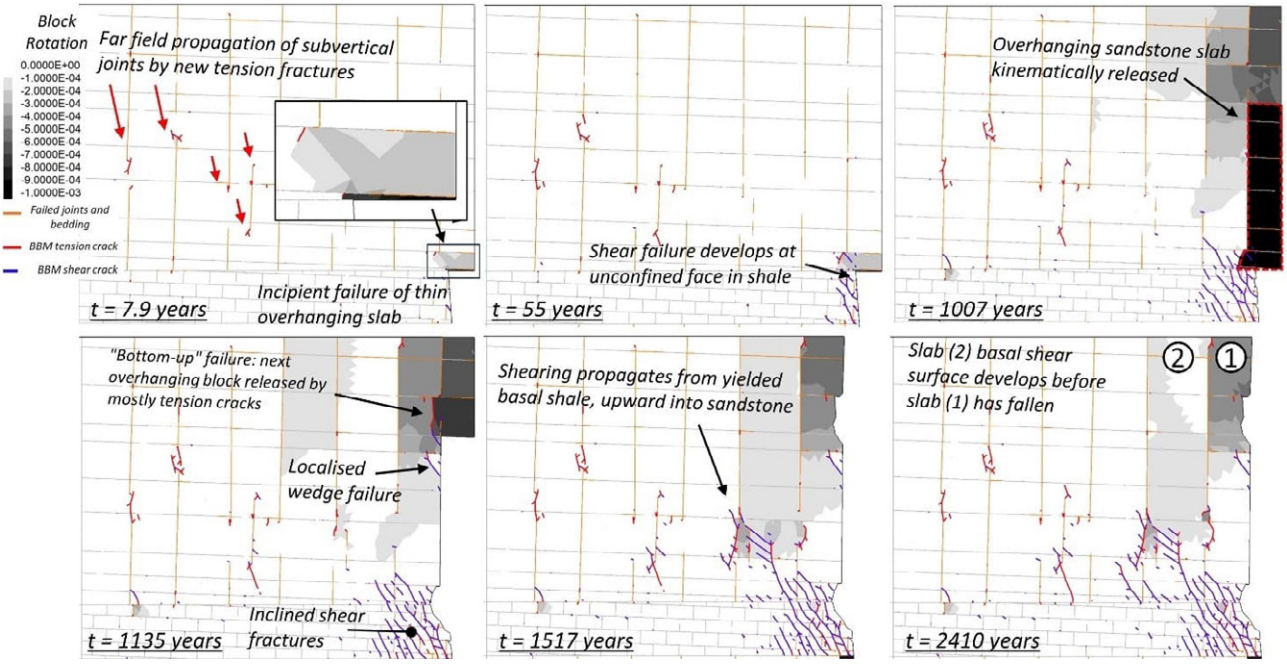

Figure 19: Progressive cliff failure for lithostatic stress scenario

The earliest BBM contact failures involve far-field tension cracking initiating from the tips of non-persistent subvertical joints; this effect demonstrates how the stress field associated with the escarpment landform promotes the propagation of very high persistence vertical joints; this is consistent with field observations of the two regionally ubiquitous, very high persistence orthogonal joint sets that play a critical role in the escarpment retreat processes that produced the modern landscape of the Blue Mountains (Hatherly and Brown, 2022). Figure 20 shows corresponding plots of the high stress scenario for subcritical timesteps up to 1803 years.

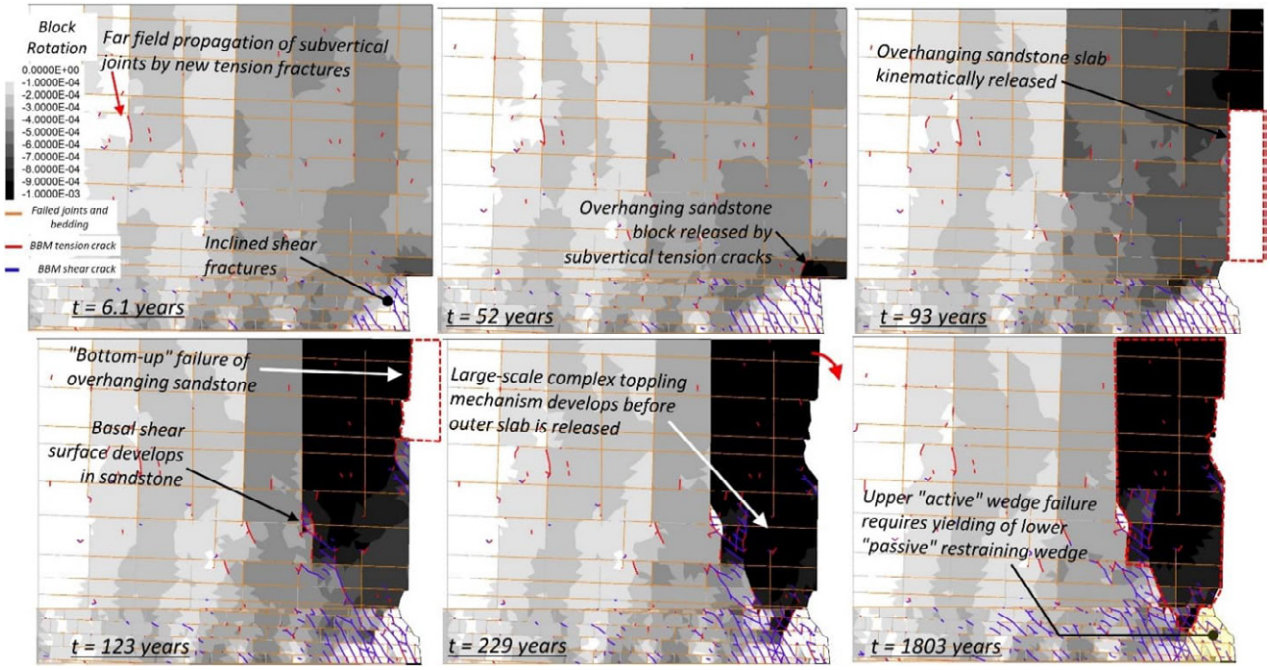

Figure 20: Progressive cliff failure for high *in situ* stress scenario

Figure 21 presents history plots for both stress scenarios, showing (1) subcritical timestep Δt and the maximum stress intensity ratio versus subcritical time; and (2) the rate of brittle failure in terms of the total length of BBM contacts failed in tension and in shear. The crack length histories highlight the main difference between the two scenarios: the lithostatic model records a slow rate of crack growth for the first ~1000 years of subcritical time, followed by a rapid phase of accelerated brittle failure between 1000 and 1200 years. The high stress scenario records rapid shear crack growth from the start of cycling up to approximately 200 years of subcritical time.

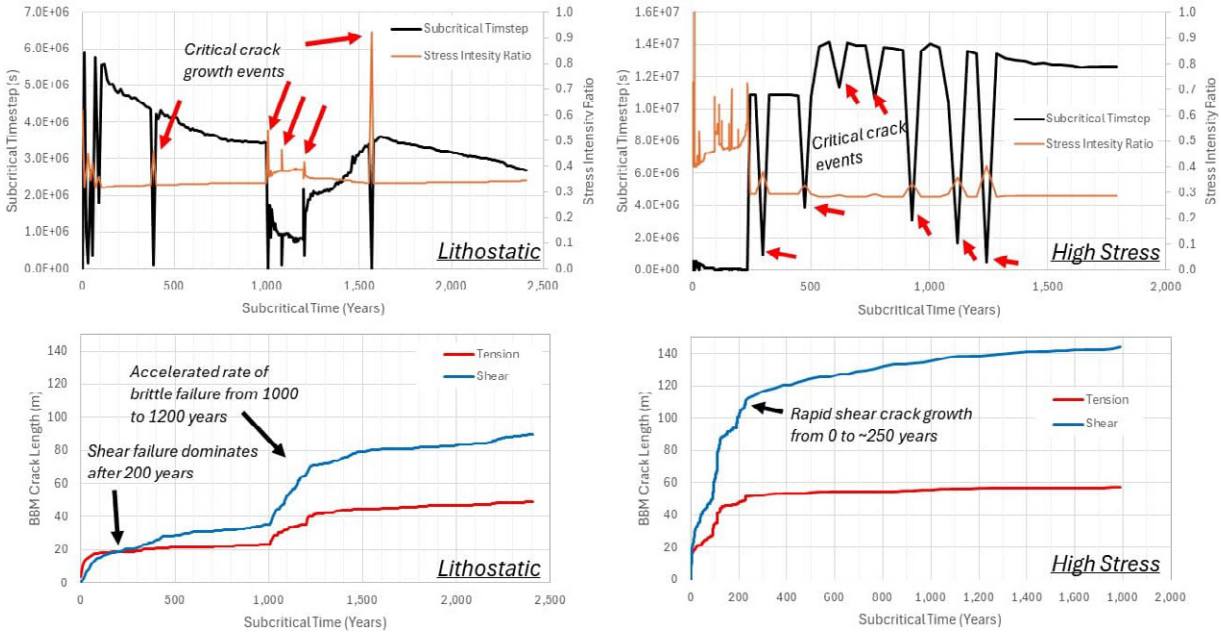

Figure 21: Comparison of subcritical crack data histories for lithostatic and high stress scenarios

The lithostatic scenario is dominated by tensile failure for the first 200 years of subcritical time; this is followed by 800 years of slow progressive failure dominated by subcritical crack growth, until a marked acceleration in BBM contact failure occurs between 1000 and 1200 years, leading to the development of a large scale basal shearing surface that connects through the sandstone rock mass and into the weaker underlying shale. In contrast, the high stress scenario produces an accelerated rate of crack growth, with most damage developing during the first 200 years.

The high stress scenario produces a greater magnitude of displacement at any given timestep. Both simulations suggest that the first block to fail is a thin overhanging slab bounded above by bedding on the immediate "roof" of the overhanging sandstone cliff, with incipient failure developing within the first 10 years of subcritical time. Failure progresses in a "bottom up" process as brittle tension fractures propagate upward, subparallel to the cliff face, releasing newly exposed overhanging sandstone blocks. Large-scale cliff failure involves the development of inclined shear fractures that interact with subvertical joints to allow slabs to detach from the cliff. BBM tensile failure dominates where cracks propagate from the tips of subvertical joints, and shear failure dominates in the basal shale layer.

7 DISCUSSION

The outcrop-scale simulations presented in Section 5 show how intact rock bridges play a critical role in rockfall initiation when failure is controlled by discontinuity propagation. The location of intact rock bridges on the incipient release surface determines their prevailing loading conditions. If rock bridges are subject to tensile loading, failure is controlled by the tensile strength of intact rock and the mode I fracture toughness K_{IC}. In most brittle materials (including rock) K_{IC} is less than the mode II (shear) fracture toughness K_{IIC} and consequently, rock bridges loaded in tension are associated with higher rates of subcritical crack growth. Given two rock bridges of equal size subject to loading in shear and tension respectively, the rock bridge loaded in tension is expected fail first.

For a conceptual 5 m high sandstone slab with a fixed rock bridge content, the time to failure t_f may vary over three orders of magnitude depending on rock bridge geometry. The time to failure versus rock bridge content can be conceptually approximated with power law relationships, such that a marked acceleration in subcritical crack growth occurs when rock bridge content is reduced below 5% to 10% of the slab height. The results demonstrate that relatively small changes in intact rock bridge content have a significant impact on the timescale required for rockfall to initiate. Although it may be impossible to precisely measure the 3D geometry of intact rock bridges occluded inside an outcrop, geotechnical field mapping may be improved with careful attention to the geometry of the specific discontinuities that are expected to control failure kinematics. Measuring the geometry of discontinuity tips that terminate in intact rock may provide a useful indication of apparent intact rock bridge geometry. Classifying the degree of "incipiency" of critical joint sets in terms of their persistence, aperture, and connectivity may provide a useful starting point for estimating the potential cohesion and tensile strength provided by intact rock bridges (Shang et al., 2018).

The cliff-scale simulations presented in Section 6 showed how a subcritical crack growth algorithm can be used to model multi-scale progressive brittle failure driven by undermining. Stress-dependent subcritical crack growth parameters account for the effect of confinement in suppressing crack growth behind the cliff face: the sequence of progressive failure begins with localised brittle fracture near the unconfined cliff face, with progressive release of overhanging blocks in a "bottom up" process as new brittle fractures propagate subparallel to the cliff face.

When the *in situ* stress field is assumed to be lithostatic, brittle crack growth is slow for the first 1000 years of simulated subcritical time. During this phase, localised critical crack growth events involve propagation of subvertical tension cracks in the sandstone unit, and the development of inclined shear cracks in the weaker underlying shale layer. When an anisotropic high horizonal stress field is adopted, crack growth is markedly accelerated, with most of the slope damage (indicated by failed BBM contacts) developing during the first 200 years of subcritical time. In either case, the first rockfalls to release from the cliff are localised metre-scale blocks of sandstone where failure kinematics involve free-fall of wedges or slabs formed by overhanging sandstone beds. Larger overall slope-scale failure requires hundreds to thousands of years of time for the development of a global basal rupture surface.

The cliff-scale modelling suggests that careful consideration must be given to the initial stress conditions and the subcritical timestep Δt. Empirical observations from the Blue Mountains suggest that naturally occurring, large-scale cliff collapse events repeat on a timescale of hundreds to thousands of years. These results suggest that the lithostatic stress model produces a reasonable temporal progression of cliff-scale failure, supporting the hypothesis that the escarpment cliffs have become "de-stressed" over geological time, by the slow removal of horizontal confinement.

8 CONCLUSIONS

This paper has demonstrated how an idealised model for the stress intensity around a coplanar intact rock bridge can be used to simulate time-dependent rockfall initiation controlled by subcritical crack growth. Bonded block discrete element models can represent outcrop-scale or rock mass scale brittle failure processes, using a stress-dependent subcritical timestep and a modified version of the Charles power law that accounts for crack growth under mode I (tensile) and mode II (shear) loading.

The numerical models from this investigation are not calibrated to site-specific slope monitoring data. However, the results demonstrate how the time required for failure to develop can vary depending on *in situ* stress conditions and the geometry of intact rock bridges and pre-existing discontinuities. The order-of-magnitude estimates of time to failure can provide preliminary guidance on the annualised probability of failure used for rockfall risk assessment.

When rock bridge content is less than 5% to 10% of the failure surface, rockfall initiation under gravitational self-weight may occur over tens to hundreds of years, depending on rock bridge geometry. Larger rock mass scale cliff collapse events involve complex interactions between pre-existing discontinuities and brittle fractures that develop in tension and shear, requiring hundreds to thousands of years to propagate and coalesce into a global rupture surface. Future trials of this technique may help to constrain temporal estimates for probability of failure across a broad range of scales and in different geological environments.

CRediT authorship contribution statement

Zack Tuckey: Conceptualisation, Investigation, Writing - original draft.

9 REFERENCES

Alzo'ubi, A.M. (2009). The effect of tensile strength on the stability of rock slopes. PhD thesis, University of Alberta.

Australian Geomechanics Society (AGS) (2007). Practice note guidelines for landslide risk management. *Australian Geomechanics Journal*, 42(1), 63-114.

Backers, T. (2004). Fracture toughness determination and micromechanics of rock under mode I and mode II loading. Doctoral dissertation, University of Potsdam.

Baczynski, N.R.P. (2000). STEPSIM4 "Step-path" method for slope risks. In: *GeoEng 2000*, *Proceedings of the International Conference on Geotechnical and Geological Engineering*, Melbourne.

Bandis, S.C. (2004). Numerical modelling of discrete materials in rock mechanics: developments and engineering applications. In: *Proceedings of the 1st International UDEC/3DEC Symposium*. Bochum, Germany

Bertuzzi, R. and Pells, P.J. (2002). Geotechnical parameters of Sydney sandstone and shale. *Australian Geomechanics: Journal*, 37(5), 41-54.

Call, R.D., and Nicholas, D.E. (1978). Prediction of step path failure geometry for slope stability analysis. In: Proceedings of the 19th US Symposium on Rock Mechanics, Stateline, Nevada; *International Journal of Rock Mechanics and Mining Sciences & Geomechanics Abstracts*, 16(1).

Christianson, M., Board, M. and Rigby, D. (2006). UDEC simulation of triaxial testing of lithophysal tuff. In *ARMA US Rock Mechanics/Geomechanics Symposium*.

Collins, B.D. and Stock, G.M. (2016). Rockfall triggering by cyclic thermal stressing of exfoliation fractures. *Nature Geoscience*, 9(5), 395-400.

Deparis, J., Garambois, S. and Hantz, D. (2007). On the potential of Ground Penetrating Radar to help rock fall hazard assessment: A case study of a limestone slab, Gorges de la Bourne (French Alps). *Engineering Geology*, 94(1-2), 89-102.

Dershowitz, W.S., Lee, G., Geier, J., and LaPointe, P.R. (1998). *FracMan: interactive discrete fracture data analysis, geometric modelling and exploration simulation.* User documentation, Golder Associates Inc., Seattle.

Donati, D., Stead, D. and Borgatti, L. (2023). The influence of slope damage on the kinematics of landslides. *Italian Journal of Engineering Geology and Environment*, 39-47.

Einstein, H.H., Veneziano, D., Baecher, G.B. and O'Reilly, K.J., (1983). The effect of discontinuity persistence on rock slope stability. *International journal of rock mechanics and mining sciences & geomechanics abstracts*, 20(5), 227-236.

Elmo, D., Donati, D. and Stead, D. (2018). Challenges in the characterisation of intact rock bridges in rock slopes. *Engineering Geology*, 245, 81-96.

Fergusson, C. and Hatherly, P. (2023). Segmentation and fault–monocline relationships in the Lapstone Structural Complex, Sydney Basin, New South Wales. *Australian Journal of Earth Sciences*, 70(3), 375–392

Frayssines, M. and Hantz, D. (2006). Failure mechanisms and triggering factors in calcareous cliffs of the Subalpine Ranges (French Alps). *Engineering Geology*, 86(4), 256-270.

Gao, F.Q. and Stead, D. (2014). The application of a modified Voronoi logic to brittle fracture modelling at the laboratory and field scale. *International Journal of Rock Mechanics and Mining Sciences*, 68, 1-14.

Gao, F. (2013). Simulation of failure mechanisms around underground coal mine openings using discrete element modelling. Doctoral dissertation, Simon Fraser University, Department of Earth Sciences.

Guerin, A., Jaboyedoff, M., Collins, B.D., Derron, M.H., Stock, G.M., Matasci, B., Boesiger, M., Lefeuvre, C. and Podladchikov, Y.Y. (2019). Detection of rock bridges by infrared thermal imaging and modeling. *Scientific Reports*, 9(1).

Hatherly, P. (2019). Landscape evolution of the Blue Mountains revealed by longitudinal river profiles and Cenozoic basalts and gravels. *Australian Journal of Earth Sciences*, 67(2), 243-263.

Hatherly, P. and Brown, I. (2022). *The Blue Mountains: Exploring landscapes shaped by the underlying rocks, uplift and erosion*. Windy Cliff Press.

Havaej, M. and Stead, D. (2016). Investigating the role of kinematics and damage in the failure of rock slopes. *Computers and Geotechnics*, 78, 181-193.

Jennings, J.E. (1970). A mathematical theory for the calculation of the stability of slopes in open cast mines. In: *Proceedings of Planning Open Pit Mines*. A.A. Balkema, Cape Town, 87-102.

Kemeny, J. (2003). The time-dependent reduction of sliding cohesion due to rock bridges along discontinuities: a fracture mechanics approach. *Rock Mechanics and Rock Engineering*, 36, 27-38.

Kemeny, J. (2005). Time-dependent drift degradation due to the progressive failure of rock bridges along discontinuities. *International Journal of Rock Mechanics and Mining Sciences*, 42(1), 35-46.

Ko, T.Y. and Kemeny, J. (2011). Subcritical crack growth in rocks under shear loading. *Journal of Geophysical Research: Solid Earth*, 116(B1).

Lee, J.S. (2007). Time-dependent crack growth in brittle rocks and field applications to geologic hazards. PhD Dissertation, University of Arizona.

Mas Ivars, D., Pierce, M.E., Darcel, C., Reyes-Montes, J., Potyondy, D.O., Young, R.P. and Cundall, P.A. (2011). The synthetic rock mass approach for jointed rock mass modelling. *International Journal of Rock Mechanics and Mining Sciences*, 48(2), 219-244.

McMahon, B.K. (1979). *Report to Bougainville Copper Limited on Slope Design Studies*, Pan Hill. McMahon, Burgess and Yeates, Sydney.

Nejati, H.R. and Moosavi, S.A. (2017). A new brittleness index for estimation of rock fracture toughness. *Journal of Mining and Environment*, 8(1), 83-91.

Oliveira, D. (2014). An alternative view on geotechnical parameters for tunnel design in Sydney. *Australian Geomechanics Journal*, 49(3), 95-108.

Oliveira, D., and Parker, C. (2014). An alternative approach for assessing in situ stresses in Sydney. In: *Proceedings of the 15th Australasian Tunnelling Conference*, 189-194. Sydney, NSW, 17-19 September.

Paronuzzi, P. and Serafini, W. (2009). Stress state analysis of a collapsed overhanging rock slab: a case study. *Engineering Geology*, 108(1-2), 65-75.

Sampaleanu, C. (2017). The role of intact rock fracture in rockfall initiation. MSc Thesis, Simon Fraser University.

Scavia, C. (1990). Fracture mechanics approach to stability analysis of rock slopes. *Engineering Fracture Mechanics*, 35(4-5), 899-910.

Shang, J., West, L.J., Hencher, S.R. and Zhao, Z. (2018). Geological discontinuity persistence: Implications and quantification. *Engineering Geology*, 241, 41-54.

Shang, J., Hencher, S.R., West, L.J. and Handley, K. (2017). Forensic excavation of rock masses: a technique to investigate discontinuity persistence. *Rock Mechanics and Rock Engineering*, 50, 2911-2928.

Stead, D., Eberhardt, E. and Coggan, J.S. (2006). Developments in the characterization of complex rock slope deformation and failure using numerical modelling techniques. *Engineering Geology*, 83(1-3), 217-235.

Terzaghi, K. (1962). Stability of steep slopes on hard unweathered rock. *Geotechnique*, 12(4), 251-270.

Tuckey, Z. (2023). The role of progressive brittle fracture in the 1931 landslide at Dogface Rock, Katoomba. *Australian Geomechanics Journal*, 58(3), 77-93.

Wyllie, D.C. and Mah, C. (2005). *Rock slope engineering*, 4th Edition. Taylor & Francis.

Zheng, Y., Chen, C., Liu, T., Zhang, H., Xia, K. and Liu, F. (2018). Study on the mechanisms of flexural toppling failure in anti-inclined rock slopes using numerical and limit equilibrium models. *Engineering Geology*, 237, 116-128.

IMAT™

The Power of FLAC3D
designed for mining.

Get geomechanical insights faster with mining-native workflows and a modern, click-driven interface.

Mining decisions demand speed, accuracy, and workflows that match how your operation runs. Built on FLAC3D's engine, IMAT simplifies setup with mining-native tools. Staged excavations, block-model integration, and seismic analysis happen in a point-and-click interface that removes scripting barriers.

From production engineers to rock mechanics specialists, IMAT expands who can build and trust geomechanical models without sacrificing depth experts expect.

Your next study doesn't need overhead; it needs IMAT.

Ready to see how IMAT can accelerate your geomechanical insights?

Learn more at **itascasoftware.com**

ITASCA Software

WAGSTAFF GROUND IMPROVEMENT

Wagstaff Ground Improvement is Australasia's leading specialist contractor, since 1981.

BUILDING WORLD-CLASS SOLUTIONS WITH YOU

Images from TSF7 Causeway, Telfer, WA. Wagstaff Piling undertook stabilistation of tailings pond using casing grouting and jet grouting to 35m.

FULL GEOTECHNICAL SERVICE

WORLD-LEADING EXPERTISE

INSTALLATION AND CONSTRUCTION

FROM DESIGN TO INSTALLATION, WE'LL BUILD WORLD-CLASS FOUNDATIONS FOR ALL YOUR GROUND IMPROVEMENT NEEDS.

PILING AND FOUNDATION SPECIALISTS FEDERATION · DFI · CONCRETE INSTITUTE of AUSTRALIA

BSI · ISO 45001 Occupational Health and Safety Management CERTIFIED · ISO 9001 Quality Management Systems CERTIFIED · ISO 14001 Environmental Management CERTIFIED

WAGSTAFF GROUND IMPROVEMENT

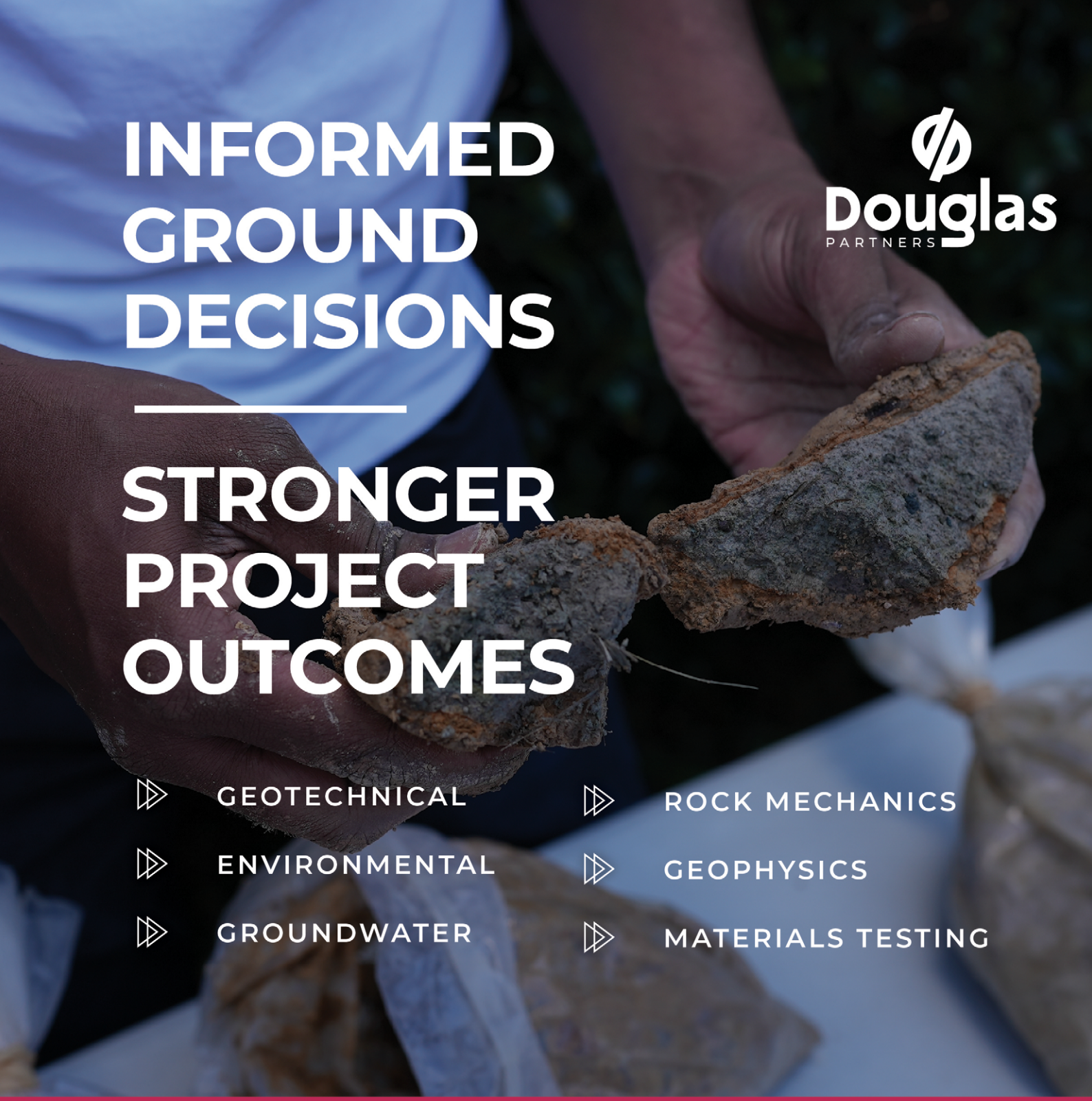

INFORMED GROUND DECISIONS

Douglas PARTNERS

STRONGER PROJECT OUTCOMES

- GEOTECHNICAL
- ENVIRONMENTAL
- GROUNDWATER
- ROCK MECHANICS
- GEOPHYSICS
- MATERIALS TESTING

AUSTRALIA'S CHOICE FOR GROUND EXPERTISE

Douglas Partners is an Australian employee-owned engineering consulting firm, trusted for over 60 years to deliver practical, cost-effective solutions. With 19 offices and 14 labs nationwide, we provide grounded solutions in various fields.

- 22 Client Choice Awards awards won since 2008.
- Data driven insights.
- 60 years of retained industry knowledge.

WWW.DOUGLASPARTNERS.COM.AU

MACHINE LEARNING APPROACH FOR APPROXIMATING DESIGN PARAMETERS FROM ENGINEERING CHARTS

WaiLeung Ng
Tetra Tech Coffey, Melbourne, Australia

https://doi.org/10.56295/AG6112

ABSTRACT

Geotechnical engineers have traditionally relied on engineering charts for the analysis and design of specific geotechnical problems. However, interpolating target design parameters, particularly on logarithmic scale charts, can be time consuming and susceptible to human error. Recent advancements in machine learning enable engineers to efficiently approximate design parameters by training models on extensive datasets, thereby minimizing both time and manual intervention. Furthermore, coefficients for closed-form equations can be derived from these models in some cases, streamlining computational analysis and enhancing design workflows. This paper presents two case studies: one focused on shallow footing settlement assessment and the other on single pile settlement assessment. It illustrates the application of non-linear regression, high-degree polynomial regression, Gaussian process regression and fully connected neural networks in developing effective machine learning models for graphical approximation.

1 INTRODUCTION

For many years, engineers have depended on engineering charts for assessments and designs related to geotechnical problems. These practices often originate from academic research or field observations, leading to the development of specialized charts that provide valuable guidelines for practitioners, significantly simplifying engineering processes. Even with the development of powerful numerical methods such as the finite element method, chart-based methods remain important for checking the results of complex numerical analyses.

Nowadays, it remains common for engineers to extract data points from charts in prominent publications and convert them into tabular formats, facilitating linear interpolation of intermediate target parameters. However, this method is time-consuming and prone to inaccuracies due to human error, particularly with data presented on logarithmic scales.

As artificial intelligence (AI) gains popularity, its application in geotechnical engineering is becoming increasingly prevalent. A fundamental application involves fitting regression models to obtain optimal lines or surfaces from engineering charts. This regression can be performed using machine learning (ML) techniques where data is input into an ML algorithm, and the model is trained to minimize a defined loss function, thereby enhancing predictive accuracy.

Once trained, ML models can be reformulated into simplified closed-form equations or visual representations, improving interpretability and facilitating their integration into engineering workflows. This paper presents a practical approach to digitising and approximating geotechnical design charts using ML algorithms. Two case studies are provided to demonstrate the improved efficiency and scalability of this method in routine geotechnical analysis.

2 LITERATURE REVIEW

The integration of ML methods into geotechnical engineering has evolved significantly, progressing from early theoretical studies to practical and field-ready applications. Initial efforts in the 1990s were largely confined to basic regression models, limited by both sparse datasets and restricted computational capabilities. However, with the rapid expansion of data availability and advances in computing power, the application of ML techniques in geotechnical engineering has grown substantially (Shahin, 2025). Over the past three decades, a range of sophisticated ML models including artificial neural networks (ANN), support vector machine (SVM), Gaussian process regression (GPR) and decision trees (DT) have been employed to address a wide variety of geotechnical problems.

Shao et al. (2023) assessed the performance of various ML algorithms in tasks such as soil classification, landslide susceptibility mapping, rock type classification, rock deformation forecasting and compressive strength prediction. Similarly, Zhao et al. (2024) provided a comparative review of ML methods for optimising the prediction of key geotechnical properties such as compressibility parameters, permeability coefficients and uniaxial compressive strength. In an earlier study, Shahin (2014) utilised data from load tests on piles to train ANN models for estimating the ultimate bearing capacity of piles. More recently, Shen and She (2023) applied a hybrid approach combining Independent Component Analysis and Multivariate Adaptive Regression Splines (ICA–MARS) to model the load–displacement behaviour of pre-stressed ground anchors.

While much of the existing literature emphasises the use of complex ML models to capture intricate and non-linear relationships within large datasets, this paper instead focuses on the development of simple and scalable ML applications customised to everyday geotechnical engineering practice. In particular, it addresses the automation and enhancement of Category 2 design and analysis workflows, which are widely used in geotechnical design due to their balance of theoretical rigour and practical simplicity (Poulos, 1989).

Category 2 methods typically rely on semi-empirical procedures involving engineering design charts derived from analytical or experimental studies. Although these charts are conceptually straightforward, they often require manual interpretation, interpolation between curves or repetitive calculations when applied to multiple design cases or parametric studies. Such processes are not only time-consuming but also prone to user interpretation error, especially when dealing with low-resolution charts or large-scale design tasks.

This paper proposes a structured approach to digitising these traditional design charts, transforming them into machine-readable datasets through coordinate extraction, curve fitting and numerical interpolation techniques. Once digitised, the charts can be integrated into lightweight ML models that allow for real-time querying, automated chart reading and bulk design evaluations. This not only enhances computational efficiency but also preserves the interpretability and traceability in Category 2 designs, thereby facilitating a practical step toward modernising geotechnical workflows.

3 DIGITISATION AND MACHINE LEARNING WORKFLOW

A workflow diagram summarising the machine learning process is presented in Figure 1. It illustrates the key stages from data acquisition to model deployment. The process begins with the collection and digitisation of engineering data from design charts, followed by data preprocessing which may include cleaning, normalisation and log transformation. Model development involves selecting suitable algorithms and tuning their hyperparameters. After training and validation, the model is tested across various design scenarios to assess its robustness. Finally, the model is deployed to support Category 2 geotechnical design tasks with outputs translated into design parameters and integrated into practical engineering workflows.

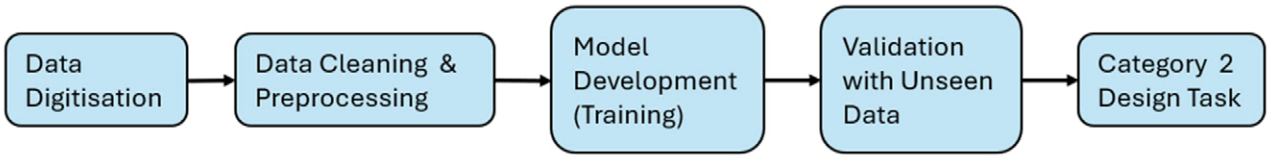

Figure 1: Workflow diagram of machine learning process

Data acquisition is carried out using WebPlotDigitizer which is an open-source tool that applies machine learning and computer vision to extract data from images. Being widely used across disciplines including astrophysics (Marin et al., 2017), it enables efficient and accurate digitisation of graphical plots. This makes it particularly suitable for converting engineering design charts into structured and machine-readable formats, streamlining the data preparation process.

Data cleaning is a critical step to remove noise, inconsistencies and outliers that may adversely affect model performance. The choice of preprocessing strategy depends on the nature and distribution of the extracted data. In some cases, models perform adequately using raw and unprocessed values, particularly when the data is well-structured and uniformly distributed. However, for datasets exhibiting skewness or large magnitude variations, normalisation can improve learning efficiency and convergence. In scenarios where relationships span several orders of magnitude, log transformation has proven effective in enhancing model performance by linearising trends.

Selecting appropriate ML algorithms is essential to model development and depends on the complexity and characteristics of the dataset. In this study, models such as Gaussian process regression (GPR) and artificial neural networks (ANN) were considered for their ability to capture nonlinear relationships common in geotechnical design problems. Once selected, each model's performance is optimised through hyperparameter tuning, which involves adjusting settings such as kernel functions in GPR or the number of layers and neurons in ANN. This process aims to enhance model accuracy and generalisation across different design scenarios.

Following model selection, the dataset is divided into training and validation subsets to assess the model's ability to generalise beyond the data it was trained on. The training phase involves fitting the model to a portion of the data, allowing it to learn patterns and relationships between input features and target outputs. The validation phase then evaluates the model's performance on unseen data to detect overfitting. Key performance metrics include the coefficient of determination (R^2 score) which measures how well the predicted values align with actual observations, and the mean squared error (MSE) which quantifies the average squared difference between predicted and true values. A high R^2 value (closer to 1) and a low MSE indicate strong predictive performance and robustness, both of which are essential for reliable application in engineering design tasks

4 MACHINE LEARNING ALGORITHMS

Three ML algorithms were used across the two case studies presented in this paper: non-linear regression, GPR and fully connected neural networks (FCNN). Each was selected based on its suitability for the structure and complexity of the underlying data, as well as the characteristics of the design charts being digitised. Further details on these algorithms can be found in Nield (2022) and on the scikit-learn website at https://scikit-learn.org.

The non-linear regression approach used in Case 1 is well-suited to problems where the functional form of the relationship can be inferred from engineering principles or visual chart interpretation. In this case, a modified logistic function was used to represent the displacement influence factor I_G which varies with the dimensionless variable β and footing geometry. Polynomial regression was applied to fit the constants in the function to known data, resulting in a generalised closed-form expression. This approach provides a transparent and interpretable model which is desirable in many engineering applications.

GPR was applied in Case 2 to approximate the complex relationships associated with the bearing stratum correction factor R_b for end-bearing piles. GPR is a probabilistic modelling technique that is particularly effective for small to medium-sized datasets with non-linear patterns. It provides not only point predictions but also associated uncertainty estimates. In this study, several kernel functions were evaluated and optimised through a grid search procedure, with the best-performing kernel selected to produce the final model predictions.

The third algorithm, FCNN was also implemented in Case 2 to model complex and multi-dimensional relationships. Unlike GPR, FCNN does not rely on predefined functional forms or kernel structures. Instead, they learn underlying patterns through iterative adjustments of connection weights across multiple layers of neurons. In this study, a five-layer architecture was adopted, demonstrating strong predictive performance and robustness across unseen data.

The ML models developed in this study were implemented using widely adopted open-source Python libraries: scikit-learn, scipy and keras. Scikit-learn provides a robust framework for supervised learning including tools for regression, classification, model validation and hyperparameter tuning. Scipy complements this with advanced numerical optimisation capabilities which are particularly useful for non-linear curve fitting. Keras, built on top of TensorFlow, offers a high-level interface for designing and training neural networks, making it suitable for constructing and experimenting with deep learning models such as FCNN. These libraries are well-documented, actively maintained and widely used in both academic research and industry, ensuring transparency, reproducibility and efficient model deployment.

5 CASE 1: SETTLEMENT OF A SHALLOW FOOTING

This case study addresses the assessment of surface settlement beneath the centre of a shallow footing. A simplified non-linear regression approach was employed to approximate one of the key parameters in the current analytical formulation.

5.1 CURRENT EQUATIONS FOR A CIRCULAR FOOTING

To assess the settlement of a flexible circular footing, Mayne and Poulos (1999) recommend the following equation, which accounts for homogeneous to Gibson soil modulus profiles, finite layer thickness, foundation flexibility, undrained and drained loading conditions, and embedment:

$$\rho_{center} = \frac{q \cdot d \cdot I_G \cdot I_F \cdot I_E \cdot (1 - \nu^2)}{E_o} \tag{1}$$

where q is the average applied loading, d the equivalent footing diameter, I_G the displacement influence factor, I_F the foundation flexibility correction factor, I_E the foundation embedment correction factor, v the soil Poisson's ratio and E_o is the soil Young's modulus at the surface.

The foundation flexibility correction factor I_F is approximately given by:

$$I_F = \frac{\pi}{4} + \frac{1}{4.6 + 10 \cdot K_F} \tag{2}$$

where $K_F = \frac{E_f}{E_{sav}}(\frac{2t}{d})^3$, E_f is the footing Young's modulus, E_{sav} the average soil Young's modulus and t is the footing thickness.

The foundation embedment correction factor I_E is approximately given by:

$$I_E = 1 - \frac{1}{3.5 \cdot exp(1.22\nu - 0.4) \cdot \left(\frac{d}{z_e} + 1.6\right)} \tag{3}$$

where z_e is the depth of embedment of footing base below surface.

The chart for the displacement influence factor I_G is extracted from Mayne and Poulos (1999) and is illustrated in Figure 2.

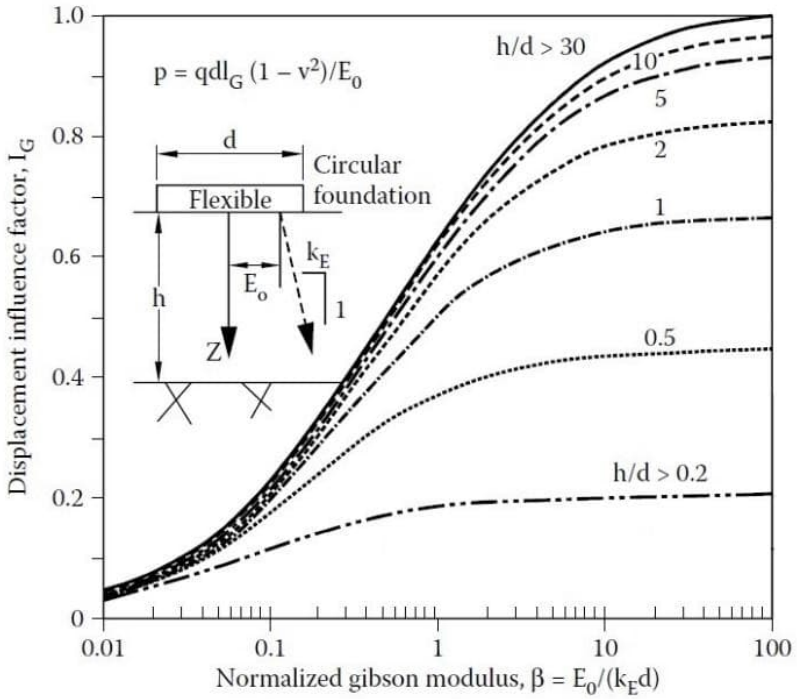

Figure 2: Displacement influence factor I_G (Adapted from Mayne and Poulos 1999)

To enable automation of the settlement calculation, a closed-form expression for I_G is required that approximates the family of S-shaped curves shown in Figure 2. These curves can be represented using a modified logistic function. The parameter β is plotted on a base-10 logarithmic scale, and the proposed form of the equation is:

$$I_{G,x} = f(\beta) = \frac{1}{m_x + n_x \cdot 10^{-k_x(log\beta)}} \tag{4}$$

which is simplified as:

$$I_{G,x} = f(\beta) = \frac{1}{m_x + n_x \cdot \beta^{-k_x}} \tag{5}$$

where $x = ln\left(\frac{h}{d}\right)$

5.2 MODEL DEVELOPMENT USING NON-LINEAR REGRESSION

For a specific value of x, there exists a corresponding modified logistic function characterized by the constants m_x, n_x, and k_x. To determine these constants, data points from each curve were extracted using WebPlotDigitizer. These data points were then analysed using a selected non-linear regression algorithm implemented in the open-source Python modules 'sklearn' and 'scipy'. The resulting values of m_x, n_x, and k_x are summarized in Table 1.

Table 1: Values of h/d with the associated constants

h/d	x = ln (h/d)	m_x	n_x	k_x
30	3.401	0.980	0.604	0.753
10	2.303	1.018	0.601	0.779
5	1.609	1.059	0.595	0.787
2	0.693	1.201	0.541	0.831
1	0.000	1.493	0.490	0.869
0.5	-0.693	2.240	0.446	0.892
0.2	-1.609	4.898	0.405	0.945

The next step involves formulating the values presented in Table 1 into a generalized function. To achieve this, each constant (m_x, n_x, and k_x) is treated as a dependent variable correlated with the independent variable x through a closed-form equation. The rationale for associating m, n and k with ln (h/d) instead of h/d is based on improved fitting performance.

Several trials of polynomial regression from first degree to third degree have been performed to search for the best fit functions based on R^2 scores and MSE. The results of the regression exercise are expressed in the following polynomials.

$$m(x) = (-0.0059x^3 + 0.0411x^2 - 0.0978x + 1.0855)^5 \quad (6)$$

$$n(x) = -0.0032x^3 + 0.0011x^2 + 0.0655x + 0.4927 \quad (7)$$

$$k(x) = 0.0043x^2 - 0.0465x + 0.8603 \quad (8)$$

Consequently, the displacement influence factor I_G can be expressed in a generalized form as follows:

$$I_G = f(\beta, x) = \frac{1}{m(x) + n(x) \times \beta^{-k(x)}} \quad (9)$$

Finally, all data points are input into Equation (9) to assess the overall accuracy. The resulting R^2 score of 0.9996 and MSE of 3.08e-5 indicate an excellent fit of the input data to the constructed equation. This is also corroborated by Figure 3, where the input data points (represented as green dots) align perfectly with the curved surface generated by Equation (9). Moreover, the smooth transitions observed between the known data points suggest that the equation is capable of delivering reliable and continuous predictions for unseen inputs.

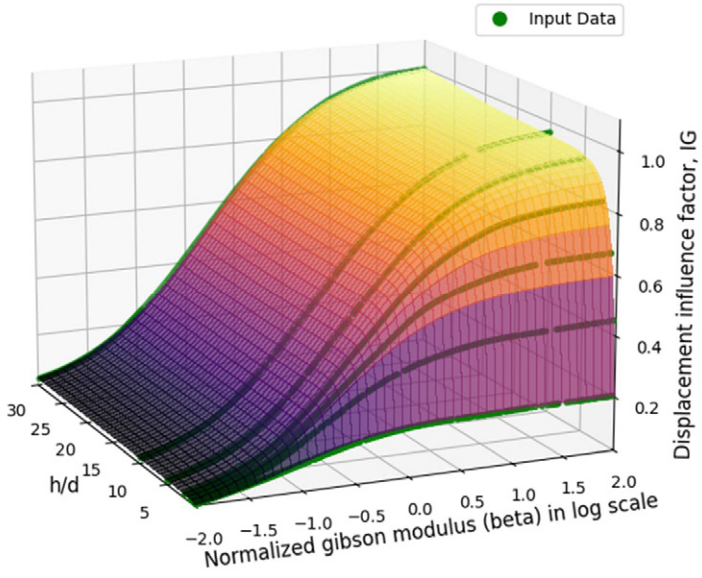

Figure 3: Three-Dimensional Illustration of I_G Value

5.3 MODEL VALIDATION AGAINST COMMERCIAL SOFTWARE – PLAXIS 3D

The reliability of Equation (9) is further verified using Plaxis 3D, a commercial finite element analysis (FEA) software developed by Bentley, specifically designed for advanced geotechnical engineering applications. As the derivation of Figure 2 is based on elastic theory, a linear elastic soil model was adopted in Plaxis 3D to ensure a consistent basis for comparison. To isolate the influence of the displacement factor I_G, the effects of embedment and footing flexibility were eliminated by positioning the footing at the ground surface and neglecting its thickness, thereby setting both I_E and I_F equal to 1.

Four scenarios with varying geometries and parameter combinations, none of which lie directly on the eight predefined design curves in Figure 2, were selected to test the generalisation capability of the model. Settlements calculated using Equations (1) and (9) are compared with those obtained from Plaxis 3D, as summarised in Table 2. Despite minor differences at the decimal level, the results from both methods are in close agreement. This comparison justifies the ability of the proposed non-linear regression model to produce reliable predictions, even for unseen combinations of geometric and material parameters.

Table 2: Comparison of settlements predicted by the non-linear regression model and Plaxis 3D

Scenario	Load, q (kPa)	Influence depth, h (m)	Footing diameter, d (m)	h/d	E_o (MPa)	k_E (MPa/m)	β	I_G	Assessed settlement (mm)	
									Non-linear regression	Plaxis 3D
1	150	15	2	7.5	25	0.2	62.5	0.94	10	10
2	300	10	4	2.5	25	1	6.3	0.79	35	35
3	300	5	4	1.25	35	0.5	17.5	0.70	22	22
4	200	5	3	1.67	35	1.5	7.8	0.74	12	12

6 CASE 2: SETTLEMENT OF A SINGLE END-BEARING PILE

The approach used in Case 1 requires a certain level of mathematical insight, which enables one to make an initial guess regarding the form of the equation. However, this ability is often a privilege of mathematicians and can sometimes rely on luck. In contrast, Case 2 illustrates an approximation exercise where a closed-form equation is not strictly required.

6.1 CURRENT CHART-BASED APPROACH FOR AN END-BEARING PILE

To assess the settlement of a single end-bearing pile, Poulos and Davis (1980) recommend the following equation:

$$S = \frac{P}{dE_s} I_1 R_K R_b R_v \tag{10}$$

where P is the applied load, d the pile diameter, E_s the average soil modulus along the pile shaft, I_1 the influence factor for a rigid pile in a semi-infinite mass and R_k, R_b, R_v are the correction factors for the effect of pile compressibility, bearing stratum stiffness and Poisson's ratio respectively.

While this assessment involves four factors, only the factor R_b will be utilised to demonstrate the approximation exercise. The charts for R_b are extracted from Poulos and Davis (1980) and are presented in Figure 4. The value of R_b depends on three independent variables: the ratio of E_b/E_s, the ratio of L/d and the K value. Here, E_b represents the Young's modulus of the founding stratum and L is the pile length. The variable K is defined as:

$$K = \frac{E_p R_A}{E_s} \tag{11}$$

where E_p is the Young's modulus of pile and R_A is the area ratio of pile.

Identifying the complex relationship between the target R_b and the other three variables through a closed-form equation appears impractical. An alternative approach is to employ supervised machine learning algorithms directly, without the necessity of fully understanding the underlying data patterns. Two common methods, GPR and FCNN implemented in the open-source Python modules 'sklearn' and 'keras' are utilised to train ML models in this case.

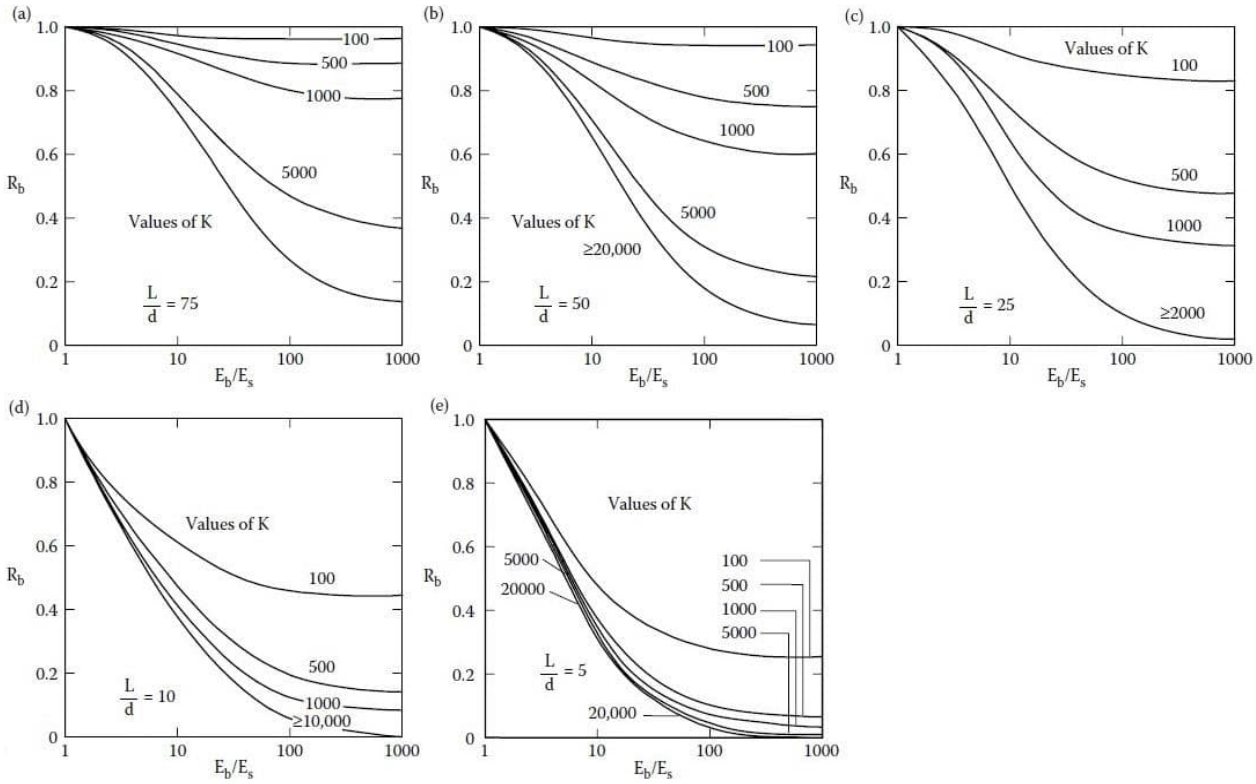

Figure 4: Bearing stratum correction factor R_b for values of L/d of 75, 50, 25, 10 and 5 (Adapted from Poulos and Davis, 1980)

To initiate this process, data points were extracted from Figure 4 using WebPlotDigitizer. The extracted data was then used to train the two selected ML algorithms, resulting in the development of two digital models that can recognize the underlying relationships among all input variables. Rather than producing a simple equation, the digital models encapsulate these relationships within specific internal mathematical structures, which will be discussed further in the following paragraphs. Once constructed, these digital models can be saved for future predictions.

6.2 PERFORMANCE OF GAUSSIAN PROCESS REGRESSION

The performance of GPR is sensitive to the absence of some data in Figures 4(c) and 4(d), where no data is available for K values beyond 2,000 and 10,000 respectively. This lack of data complicates predictions beyond these bounds and may lead to overfitting of the model to the input data. To mitigate this issue, supplementary data points were added by extending the original dataset from the original maximum bounds, as illustrated in Figures 5(c) and 5(d). Furthermore, for the case where L/d equals 25, cross lines were generated using polynomial regression at K-R_b planes for log (E_b/E_s) values of 1, 1.5, 2, 2.5 and 3 as shown in Figure 5(c).

Another important factor influencing regression performance is the choice of kernel (covariance function) and its hyperparameters. Selecting an appropriate kernel requires knowledge of data science, which is beyond the scope of this paper. In this study, a grid search approach was employed to identify the best-performing kernel among the Radial Basis Function (RBF), Matern and Rational Quadratic kernels. The combination of hyperparameters for each kernel that yielded the lowest MSE was selected as the optimal estimator.

Before analysing the four-dimensional relationship, three-dimensional trials were conducted for each value of the L/d ratio separately, allowing for a review of preliminary results with the optimal kernel. The settings for the optimal kernel are as follows:

- Kernel: Rational Quadratic
- Scale mixture parameter α: 1
- Length scale parameter: 1

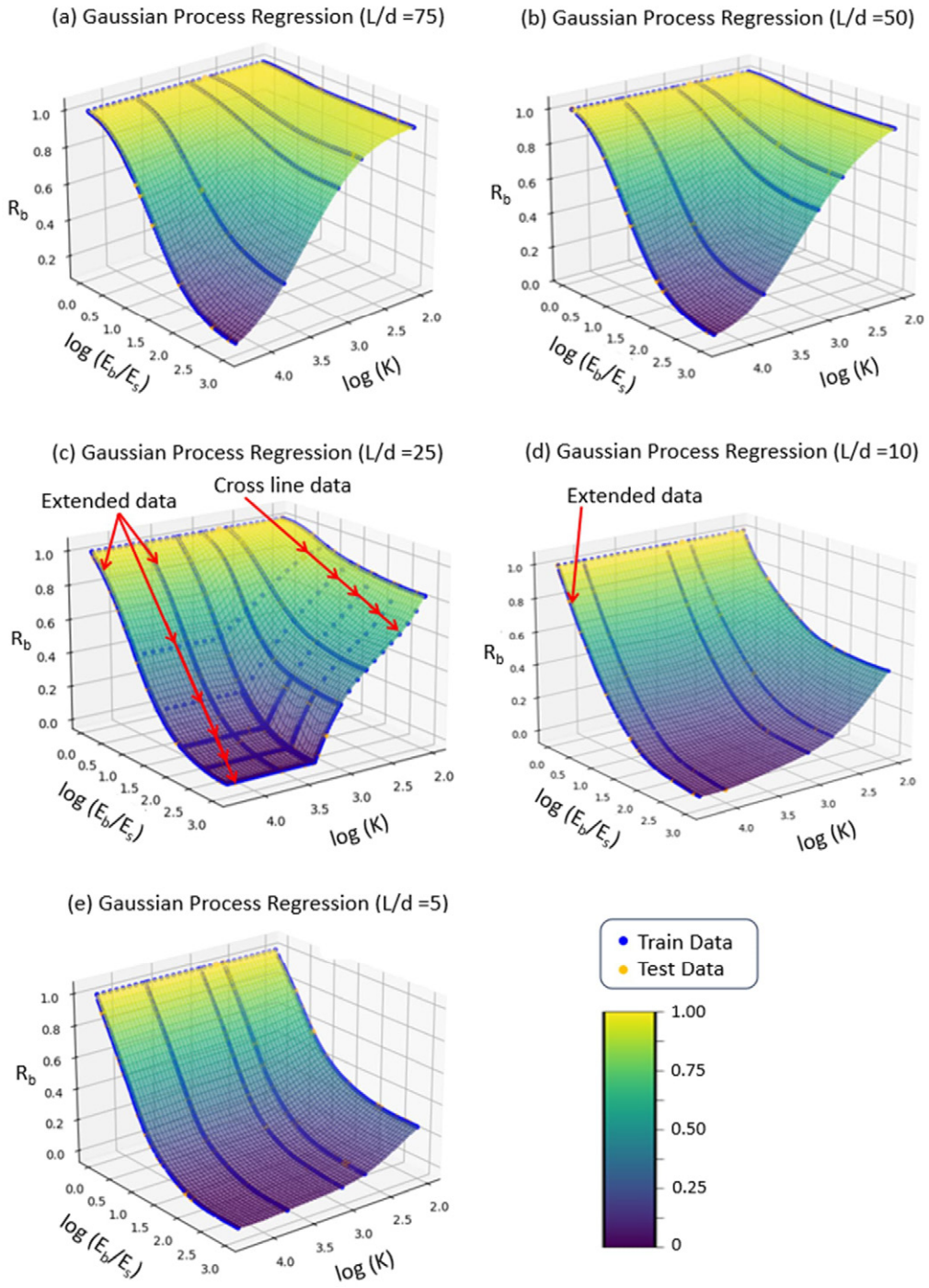

Figure 5: Approximation of R_b for various L/d values using GPR

Three-dimensional plots illustrating the data relationships for five different L/d ratios are presented in Figure 5. Each L/d layer represents predictions for 200 x 200 grid points along two axes, i.e. log (K) and log (E_b/E_s). The maximum MSE of these trials is 1.25e-6, indicating that the GPR model fits the training data well.

The subsequent stage involves the construction of a comprehensive four-dimensional model that simultaneously incorporates all four input variables, utilising the optimal kernel hyperparameters determined from prior three-dimensional trials. The resulting model achieves a MSE of 1.54e-6 on the 10% testing dataset.

As the model depends on three independent input variables, it represents a four-dimensional function that cannot be directly visualised using standard graphical methods. To facilitate interpretation, eight discrete values of the L/D ratio are selected, while the remaining variables log (K), log (E_b/E_s) and R_b are varied continuously along the orthogonal axes.

A series of simplified three-dimensional plots corresponding to each selected L/D value is presented in Figure 6. Although only eight values or layers are depicted, it should be noted that L/D is treated as a continuous variable within the model framework. Importantly, three of the selected L/D values (60, 35, and 20) correspond to data points entirely excluded from the training set. The smooth transitions observed across the plotted layers indicate the model's robustness and its ability to generalise effectively to previously unseen data.

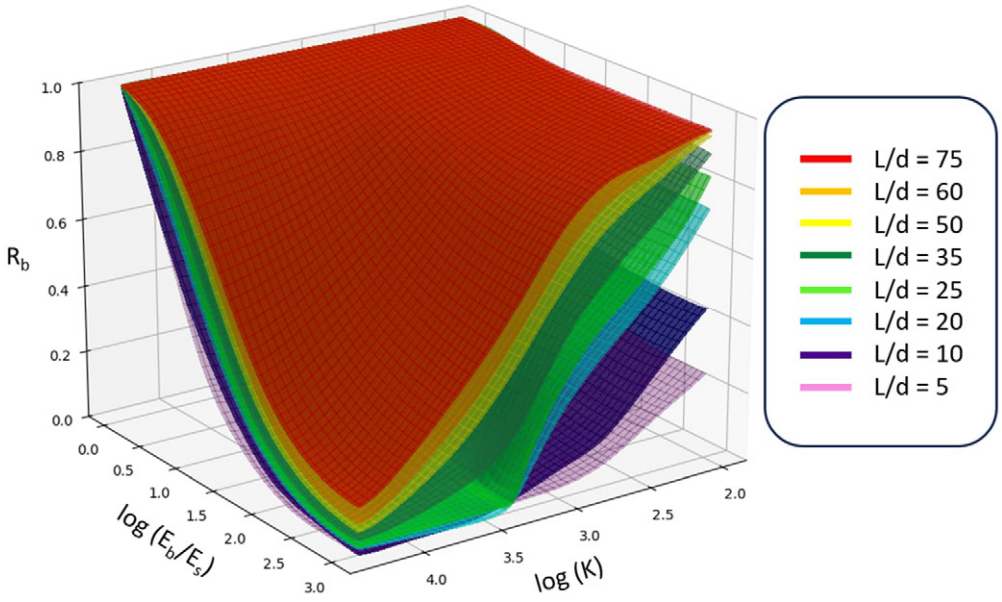

Figure 6: Combined three-dimensional plot of R_b for various L/d values using GPR

A key advantage of GPR is its ability to provide not only a mean prediction but also an associated variance estimate, enabling the construction of prediction intervals. For the 10% test dataset, the average predictive standard deviation was approximately 0.0009, resulting in a 95% confidence interval of around ±0.0018. This narrow interval indicates a high level of model confidence within the prediction domain.

6.3 PERFORMANCE OF FULLY CONNECTED NEURAL NETWORK

A fully connected neural network (FCNN) is a type of artificial neural networks in which each neuron in one layer is connected to every neuron in the subsequent layer. According to the Universal Approximation Theorem, a feedforward neural network with at least one hidden layer containing a finite number of neurons can approximate any continuous function on a compact subset of R^n to any desired degree of accuracy, provided that a suitable non-linear activation function is employed. Here, R^n denotes an n-dimensional Euclidean space and the function in question pertains to a bounded and continuous subset of four-dimensional space.

In this study, five hidden layers were configured with the following number of neurons: 128, 64, 64, 32 and 8 respectively. The Rectified Linear Unit (ReLU) was selected as the activation function for each hidden layer, while a linear activation function was assigned to the final output layer which consists of a single neuron. The other parameters for the training configuration are as follows:

- Optimizer: Adam
- Epochs: 100
- Batch size: 32
- Validation split: 0.1

The MSE for 10% testing data is 1.81e-5, indicating strong predictive performance. Similarly, a series of simplified three-dimensional plots corresponding to eight selected L/D value is presented in Figure 7, providing a visual representation of the trained FCNN model. Notably, unlike GPR, cross line data is not required for the FCNN, as overfitting is not a concern with this model.

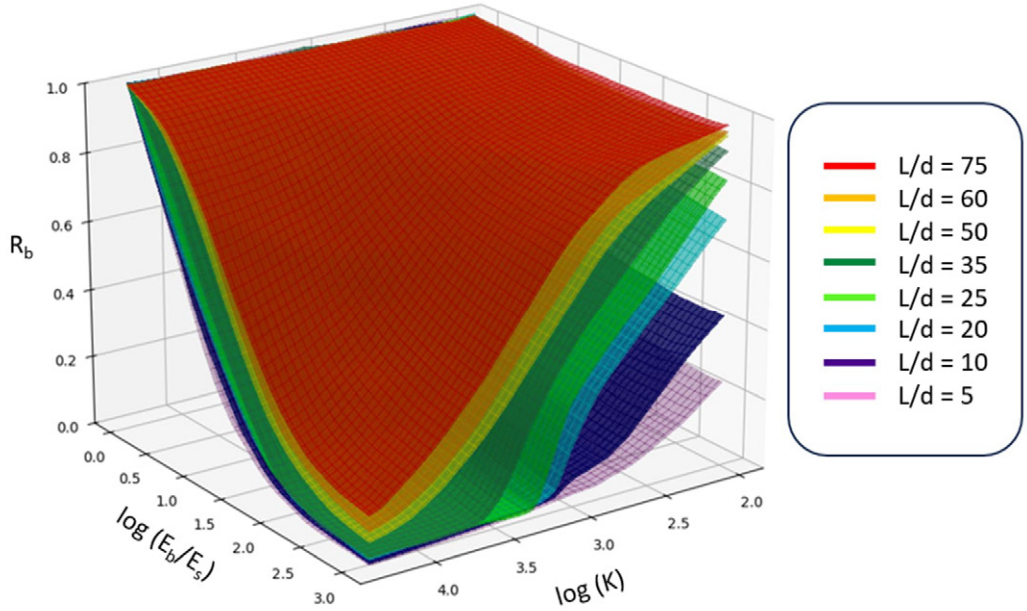

Figure 7: Combined three-dimensional plot of R_b for various L/d values using FCNN

To assess predictive uncertainty, a Monte Carlo (MC) dropout version of the deterministic FCNN model was developed. The dropout model applied a dropout rate of 0.1 at each neural layer and performed 100 stochastic forward passes for each prediction. The average standard deviation across the test dataset is approximately 0.06, indicating a low level of uncertainty relative to the target range of 0 to 1. While this standard deviation is higher than that of the GPR model, the variation remains negligible in the context of pile settlement assessment, where a reasonable degree of tolerance is generally acceptable under Category 2 design methods.

6.4 COMPARISON OF MODEL OUTPUTS

To compare the outputs of the two constructed digital models, ten points from different clusters are randomly selected for assessment. The predictions generated by these models using a Python interpreter are compared with those obtained through a manual interpolation method performed by the author using visual estimation and a ruler. The comparison results are presented in Table 3.

While there are slight deviations in the predictions, particularly for intermediate values of L/d ratios and K values, the order of magnitude for each R_b value remains generally consistent across the different methods.

Table 3: Comparison of R_b using different methods

L/d	K	E_b/E_s	log (E_b/E_s)	R_b			Max. Difference
				GPR	FCNN	Manual	
75	2000	100	2.0	0.65	0.68	0.65	0.03
60	800	80	1.9	0.77	0.78	0.78	0.01
60	2000	50	1.7	0.62	0.62	0.63	0.01
50	300	500	2.7	0.83	0.82	0.85	0.03
50	2000	50	1.7	0.54	0.54	0.55	0.01
40	300	10	1.0	0.90	0.90	0.86	0.04
25	300	10	1.0	0.83	0.81	0.80	0.03
25	800	500	2.7	0.39	0.38	0.36	0.03
15	300	30	1.5	0.52	0.49	0.50	0.03
10	300	30	1.5	0.37	0.35	0.38	0.03

6.5 DIGITISATION OF OTHER FACTORS

The other three factors can be determined in the same way as I_G in Case 1 using non-linear regression model or R_b in this case using GPR or FCNN. After non-linear regression approximation, I_1 and R_v can be expressed by Equations (12) and (13) respectively. The plots of I_1 and R_v computed from these equations are shown in Figures 8(a) and 8(b) respectively. The excellent agreement with the original charts in Poulos and Davis (1980) validates the precision of the regression-based approximations.

$$I_1 = f\left(\frac{d_b}{d}, \frac{L}{d}\right) = A \cdot x^2 + B \cdot x + C \tag{12}$$

$$R_v = f(K, v_s) = m \cdot v_s + c \tag{13}$$

where d_b is the diameter of pile base and v_s is the Poisson's ratio

$$A = 0.005\left(\frac{d_b}{d}\right)^2 - 0.0493\left(\frac{d_b}{d}\right) + 0.139$$

$$B = -0.0107\left(\frac{d_b}{d}\right)^2 + 0.1445\left(\frac{d_b}{d}\right) - 0.5312$$

$$C = 0.0036\left(\frac{d_b}{d}\right)^2 - 0.1029\left(\frac{d_b}{d}\right) + 0.5433$$

$$x = log\left(\frac{L}{d}\right)$$

$$m = 0.046(logK)^3 - 0.4199(logK)^2 + 1.3189(logK) - 1.0762$$

$$c = -0.023(logK)^3 + 0.2105(logK)^2 - 0.6615(logK) + 1.5405$$

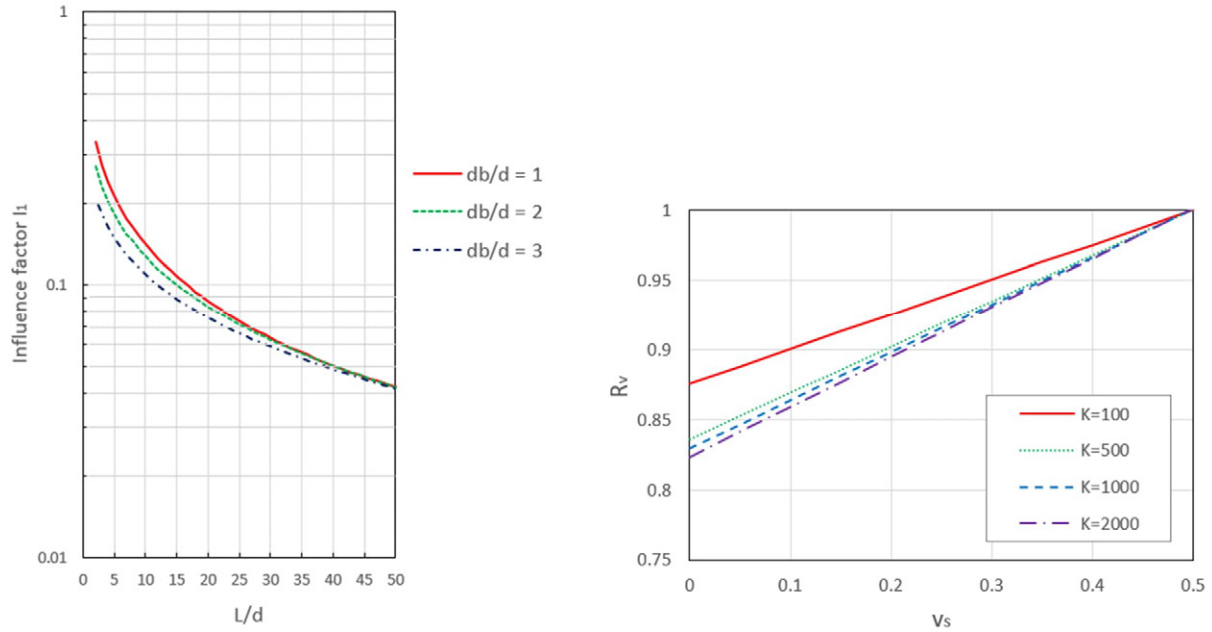

(a) Influence factor I_1 **(b) Correction factor R_v**

Figure 8: Plots of I_1 and R_v using approximate equations

The remaining correction factor R_k are defined by the following function:

$$R_K = f\left(K, \frac{L}{d}\right) \tag{14}$$

Similar to R_b factor, a FCNN was trained and validated to approximate this function with engineering accuracy so that the R^2 score is close to 1. Figure 9 plots the corresponding regression surface of this trained model.

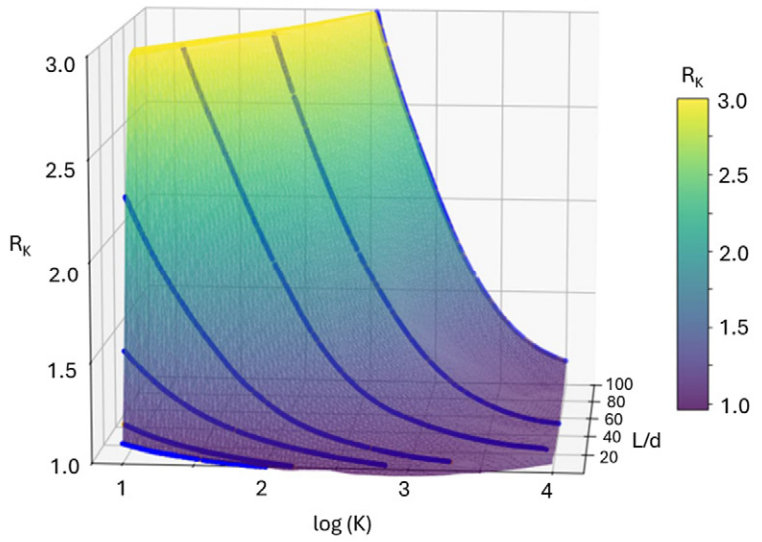

Figure 9: Graphical representation of R_K using FCNN

6.6 MODEL VALIDATION AGAINST COMMERCIAL SOFTWARE – PLAXIS 3D

The reliability of Equations (12) and (13) along with the two trained ML models was validated using Plaxis 3D. Since all four factors in Equation (10) were derived based on elastic theory originally, a linear elastic soil model was adopted in Plaxis 3D to ensure a consistent basis for comparison. The pile was modelled as a circular concrete pile with a modulus of elasticity (E_p) of 33,000 MPa and simulated as a volume element with rigid interface conditions. The Young's modulus of the shaft soils (E_s) ranges from 30 MPa to 60 MPa, while that of the bearing stratum (E_b) at the pile base varies between 360 MPa and 5,000 MPa. A uniform Poisson's ratio of 0.3 was applied across all materials.

To assess the generalisation capability of the models, geometric configurations were intentionally selected such that the resulting data points did not coincide with the predefined chart lines. The corresponding input parameters are summarised in Table 4.

Predicted settlements obtained from the ML models are compared against those computed using Plaxis 3D, as presented in Table 5. The close alignment between the two sets of results affirms the predictive reliability of the proposed ML approach, even when applied to previously unseen combinations of geometric and material parameters across all four scenarios.

Table 4: Geometric and material properties used in model validation

Scenario	Load, P (kN)	L (m)	d (m)	d_b (m)	d_b/d	L/d	E_s (MPa)	E_b (MPa)	E_b/E_s	K
1	4000	10	0.6	0.6	1	16.7	40	5000	125	825
2	6000	15	0.75	0.75	1	20	35	1000	29	943
3	4500	25	0.6	0.6	1	41.7	30	3000	100	1100
4	20,000	35	2	2.5	1.25	17.5	60	360	6	550

Table 5: Comparison of settlements predicted by ML models and Plaxis 3D

Scenario	Computed values of influence factor and correction factors				Assessed settlement (mm)	
	I_I	R_K	R_b	R_v	ML models	Plaxis 3D
1	0.093	1.074	0.221	0.933	4	5
2	0.082	1.089	0.392	0.933	8	9
3	0.053	1.272	0.549	0.932	9	10
4	0.091	1.132	0.697	0.935	11	10

7 DISCUSSION

Case 1 illustrates the procedures for applying basic machine learning techniques, specifically non-linear regression and polynomial regression in graphical approximation. It is important to note that integral solutions for the influence factor I_G are indeed available, as detailed in the works of Davis & Poulos (1968) and Mayne & Poulos (1999). While it remains a good practice to perform numerical integration to evaluate settlements precisely using the elastic displacement theory upon which Figure 2 is based, this paper does not aim to replace the original integration method. Instead, it offers an alternative to both the integration method and the traditional chart reading method, establishing a closed-form solution that simplifies computation while preserving accuracy.

Case 2 illustrates the application of GPR and FCNN to explore the relationships among multiple variables. While the data reveals certain patterns, deriving a simple closed-form equation that associates all variables seems impractical. Therefore, GPR and FCNN were utilised to directly predict the dependent variable R_b, eliminating the need to determine the equation's form. The outcome of these regression analyses consists of two ML models available as digital files for download from GitHub at https://github.com/OpenGTi/ML_graph_approximation. The online folder also contains the raw data and simple instructions for using the digital models. Readers are encouraged to clone the entire repository and load the ML models directly for predictions using the Python code provided in the repository.

7.1 RECOMMENDATION ON MODEL SELECTION

A key feature of the GPR model that facilitates prediction is the covariance matrix, which is computed using the specified kernel settings and the training data prepared by the author. This covariance matrix encapsulates the mathematical relationships between the trained data points. If readers apply the same kernel settings with different data points, the resulting covariance matrix will differ significantly. In essence, each GPR model is unique to its original training data, even if the output predictions may be similar.

In contrast, the hidden mathematical relationships within the FCNN model are defined by the weights and bias of each neuron in the network. The behaviour of each neuron is influenced by the activation function applied to the weighted sum of its inputs. This combination of weights, biases and activation functions enables a neural network to learn complex mappings from inputs to outputs. However, it is important to note that the author's model may not be the optimal one. The number of hidden layers in the neural network can significantly affect the smoothness of the curvature of each L/d layer. Readers intending to develop their own models should consider the trade-off between computational time and model accuracy.

There is no simple rule for selecting the most appropriate ML model, as performance depends heavily on the underlying data patterns. In most cases, a trial-and-error approach is necessary. From a complexity perspective, the GPR model is generally more intricate due to the non-intuitive nature of kernel functions, particularly for those without a background in data science. In terms of training time, the GPR model used in Case 2 required approximately 30 minutes to train, whereas the FCNN model completed training in just 5 minutes for 100 epochs. These durations are based on a laptop equipped with an AMD Ryzen 7 series CPU. Considering its relative simplicity and reduced training time, the FCNN model is recommended for similar applications involving the digitisation and prediction of engineering chart data.

7.2 INTERPRETABILITY OF NEURAL NETWORKS

Artificial neural networks are often perceived as "black-box" models due to their limited interpretability. To enhance interpretability of the FCNN model in Case 2, a permutation feature importance analysis was conducted. This technique evaluates the contribution of each input variable by measuring the increase in MSE when the values of a given feature are randomly shuffled. The results indicate that the model is most sensitive to log (E_b/E_s) with an associated increase in

MSE of approximately 0.12, followed by L/d value (0.07) and log (K) (0.04), which exhibits comparatively lower influence. Although log (E_b/E_s) contributes the most, the overall magnitudes are of the same order. This suggests that all three features have a similar meaningful impact on the model's predictions.

7.3 MACHINE LEARNING MODEL LIMITATIONS

There are several limitations associated with the adopted ML approaches. Both the GPR and FCNN models may suffer from overfitting, particularly when trained on limited or non-representative datasets which can reduce their ability to generalise to unseen scenarios. The performance of these models is highly dependent on the density and distribution of the training data. Sparse or unevenly spaced points can compromise prediction accuracy. Furthermore, the models are only reliable within the parameter range captured during training. Therefore, extrapolation beyond this range should be approached with caution. Another critical limitation lies in the quality of the digitised input data. Inaccuracies during the digitisation process such as resolution issues or coordinate misinterpretation may introduce systematic errors. These challenges underline the importance of robust validation procedures, careful data preparation and transparency in model development to ensure practical applicability and reproducibility.

7.4 FUTURE POTENTIALS

While digitising design charts may initially appear more complex than using traditional tools such as spreadsheets or commercial software like PIGLET or RSPile, the additional effort is well justified once the process is embedded within an automated workflow. This transformation converts hard-copy figures or image-based charts into structured, machine-readable data that can be processed programmatically.

More importantly, digitised design charts become compatible with modern generative AI tools, including large language models (LLMs). This opens new possibilities for intelligent design automation, real-time decision support and integration with advanced geotechnical analysis systems.

Since the introduction of ChatGPT, there has been a noticeable shift, with more geotechnical engineers beginning to explore programming languages such as Python. Free platforms like Google Colab and Anaconda have further lowered the barrier to entry by offering accessible environments and extensive support for coding and data analysis. As a result, basic programming, machine learning, generative AI and prompt engineering are emerging as foundational skills for the next generation of geotechnical engineers. With chart-based knowledge in a digital format, engineers are increasingly empowered to develop custom tools and applications that enhance productivity in practice.

8 CONCLUSION

The case studies presented herein demonstrate accessible approaches to developing ML models for digitising graphical data, solving non-linear regression problems and uncovering relationships among multiple variables. Compared to traditional graphical interpolation, ML offers a practical and efficient alternative for geotechnical engineers, streamlining routine design workflows. In particular, the FCNN employed in Case 2 illustrates a simple yet effective method for capturing complex data relationships with minimal manual data handling.

In recent years, generative AI has gained significant attention. However, its integration into geotechnical engineering remains constrained by the limitations of traditional chart-based methods. The digitisation of design charts serves as a crucial step in bridging the gap between established engineering practices and emerging AI technologies. The methodology demonstrated in this study is scalable well beyond the scope of the presented cases. For instance, if the equations and charts from an entire textbook are converted into structured and machine-readable datasets, they can be integrated into large language models (LLMs). A customised AI agent can then provide informed responses to queries across a wide range of geotechnical topics including retaining walls, tunnelling and slope stability. This approach represents more than the digitisation of individual charts. It signifies the transformation of geotechnical knowledge into an interactive and AI-driven tool.

The rapid advancement of AI provides opportunities to replace laborious manual processes with efficient and automated solutions. This shift is increasingly evident within the engineering sector, where digital transformation is no longer exclusive to large software developers but is becoming embedded in the everyday practices of individual engineers. It is anticipated that this evolution will continue, advancing from traditional analytical solutions toward numerical methodologies.

The author is committed to making the findings of this study publicly accessible. Readers are encouraged to explore the accompanying online resources available on GitHub, including raw datasets, Python codes and two trained machine learning models, in accordance with the specified licensing terms. As the profession moves into the era of the fourth industrial revolution, the role of AI in geotechnical engineering is expected to expand significantly, shaping the future of design, analysis and decision-making in the field.

9 ACKNOWLEDGEMENT

The author sincerely appreciates Professor Harry Poulos for his invaluable suggestions, which have significantly enhanced the quality and clarity of this paper.

CRediT authorship contribution statement

WaiLeung Ng: Conceptualization, Writing - original draft, Writing – review & editing.

10 REFERENCES

Davis, E.H. and Poulos, H.G. (1968). The use of elastic theory for settlement prediction under three-dimensional conditions. *Géotechnique 18, Issue 1,* 67-91.

Marin, F., Rohatgi, A. and Charlot, S. (2017). Webplotdigitizer, a polyvalent and free software to extract spectra from old astronomical publications: application to ultraviolet spectropolarimetry. *Société Française d'Astronomie et d'Astrophysique (SF2A) 2017,* 237-241.

Mayne, P.W. and Poulos, H.G. (1999). Approximate displacement influence factors for elastic shallow foundations. *Journal of Geotechnical and Geoenvironmental Engineering, ASCE 125,* 453-460.

Nield, T. (2022). *Essential math for data science*. Sebastopol: O'Reilly.

Poulos, H.G. and Davis, E.H. (1980). *Pile foundation analysis and design*. New York: John Wiley.

Shahin, M. A. (2014). State-of-the-art review of some artificial intelligence applications in pile foundations, *Geoscience Frontiers (2014)*, 1-12

Shahin, M. A. (2025). Progression of artificial intelligence / machine learning in geotechnical engineering. *Machine Learning and Data Science in Geotechnics*, *Volume 1, Issue 1 (2025),* 1-5

Shao, W., Yue, W., Zhang, Y., Zhou, T., Zhang, Y., Dang, Y., Wang, H., Feng, X. and Chao, Z. (2023). The application of machine learning techniques in geotechnical engineering: a review and comparison. *Mathematics 2023, 11, 3976*, 1-16

Shen, H. and She, W. (2023). Load-displacement prediction of pre-stressed ground anchors: a hybrid machine learning approach. *Proceedings of the 14th Australia and New Zealand Conference on Geomechanics, Cairns 2023 (ANZ2023)*

Zhao, T., Shen, F. and Xu, L. (2024). Review and comparison of machine learning methods in developing optimal models for predicting geotechnical properties with consideration of feature selection. *Soils and Foundations, 64 (2024) 101523*, 1-28

1998 EST.
PREMIER PROVIDER OF ENGINEERING TRAINING WORKSHOPS

ENGINEERING TRAINING INSTITUTE AUSTRALIA

ETIA GEOTECHNICAL WORKSHOPS 2026

Over 40 Design & Construction Workshops

PROFESSIONAL DEVELOPMENT | SMALL GROUPS | LIVE STREAM | FACE-TO-FACE

GEOTECHNICAL WORKSHOPS	DATES	CPD
Pile Foundations Design Geotechnical Workshop	24 + 25 February 2026	16 HOURS
Residential Slabs and Footings Design Workshop	4 + 5 March 2026	16 HOURS
Shallow Foundations Design Workshop	17 March 2026	8 HOURS
Retaining Walls Design Workshop	21 April 2026	8 HOURS
Slope Stability Design Workshop	22 April 2026	8 HOURS

★★★★★
15% DISCOUNT ON NEW FINE GEO5 SOFTWARE PURCHASES FOR 2026 WORKSHOP ATTENDEES
★★★★★

Paul Uno

ETIA Director & FINE GEO5 Agent

BE MBdgSc MIE(Aust) CPEng NER RPEQ APEC Engineer IntPE(Aus)

VIEW OUR COURSES

FINE GEO5 SOFTWARE AGENTS FOR AUSTRALIA & NEW ZEALAND

Contact us: **(02) 9899 7447** | **registrations@etia.net.au** | **www.etia.net.au** *Connect with us:*

Platinum Sponsors

BarChip Inc. The Synthetic Fibre Experts

DANLEY

KATANA FOUNDATIONS

THE INFLUENCE OF TUNNEL DEFORMATION PATTERNS ON SURFACE SETTLEMENT: A CASE STUDY

Gang Niu[1], Shaoheng Dai[1], Yunhan Wang[2], Haoding Xu[3] and Xuzhen He[1]

[1]University of Technology Sydney, Australia; [2]Shandong Jiaotong University, China;
[3] Xi'an University of Technology, China

https://doi.org/10.56295/AG6113

ABSTRACT

Tunnelling-induced ground surface settlement (GSS) poses potential risks to buildings and underground utilities in urban areas. Commonly used approaches for GSS assessment, including three-dimensional (3D) numerical simulations and artificial intelligence techniques, are often limited by high computational costs or poor generalizability. To overcome these limitations, this study proposes a simplified and efficient two-dimensional (2D) numerical method for rapid estimation of GSS at different tunnel cross-sections. The approach replaces the detailed 3D step-by-step excavation processes by employing 2D plane strain conditions, while incorporating convergence patterns characterized by the gap parameter (g) and volume loss (V_L). Several typical tunnel deformation models are numerically analysed to evaluate their influence on the resulting settlement troughs. The results demonstrate that the proposed method can effectively capture key GSS characteristics while improving computational efficiency. In addition, this method enables probabilistic analysis in the absence of comprehensive field data, supporting early design decisions. Future research can further refine this approach by incorporating more advanced soil constitutive models and considering tunnel–soil interaction effects to improve the accuracy of GSS evaluation.

1. INTRODUCTION

Urbanization in recent years has increased the need for underground space utilization. Tunnel construction offers an effective solution to alleviate traffic congestion (Song et al., 2023, Yan et al., 2023). However, the settlement of ground surface induced by tunnelling is a crucial concern in urban area, as it can impact the structural integrity of surface buildings and infrastructure (Franza et al., 2019; Huang et al., 2022; Chen et al., 2024).

There are many methods that have been proposed for tunnelling-induced GSS analysis, including empirical, analytical, numerical and artificial intelligence methods. Empirical methods, which can provide a brief estimation of GSS, are based on field observations and engineering experience (Islam and Iskander, 2021; Tang and Na, 2021). Analytical solutions, including Loganathan and Poulos (1998), Verruijt and Booker (1996), Park (2005), Zhang et al. (2011), Zhang and Huang (2012), Zareifard (2019), Zhu et al. (2023), Cao et al., (2024) and so on, offer a preliminary evaluation of GSS. These analytical methods either rely on the elasticity theory or provide complex formulas. Some important soil parameters such as cohesion and friction angle are overlooked, and the nonlinear elastic behavior of soil is neglected. Consequently, both empirical and analytical methods fail to precisely represent tunnelling-induced GSS across diverse geotechnical conditions and tunnel projects (Hussaine and Mu, 2022; Kim et al., 2022; Tang and Na, 2021; Zhang et al., 2020; Zhou et al., 2024). Many machine learning approaches, such as artificial neutral network (Boubou et al., 2010; Chen et al., 2019; Moghaddasi and Noorian-Bidgoli, 2018; Pourtaghi and Lotfollahi-Yaghin, 2012; Zhang et al., 2020), recurrent neutral network (Mahmoodzadeh et al., 2020; Zhang et al., 2020) and random forest (Huang et al., 2023; Ling et al., 2022; Liu et al., 2022), have been proposed to predict GSS caused by tunnelling using soil properties and tunnel boring machine (TBM) operation parameters as inputs. However, the generalization ability of machine learning models is often restricted, which means the trained machine learning models are only applicable to individual tunnel projects due to limitation of training data.

Numerical simulation is another effective tool capable of assessing GSS across a diverse range of geotechnical conditions. Finite Element Method (FEM) and Finite Difference Method (FDM) have been widely adopted to analyse tunnelling activities and the resulting GSS. In numerical simulations, step-by-step simulation of tunnel excavation is the most popular approach (Niu et al., 2023; Santos and Celestino, 2008). These simulations generally show good agreement with field measurements. However, step-by-step simulation of tunnelling activities is time-costing and resource-intensive. Establishing 3D numerical model and simulating tunnelling process by multiple steps repeatedly are relatively complicated. For different tunnelling methods, such as sequential excavation, drilling and blasting, tunnelling under the

protection of shield and TBM methods, it is difficult to employ a numerical simulation model to deal with all situations. Furthermore, in the 3D approach, GSS is affected by many factors, such as face pressure, grouting pressure, grouting consolidation, excavation speed, stoppage etc., where these parameters are not well known before tunnelling, as TBM operation parameters depend on geotechnical conditions and need to be adjusted dynamically (Dias and Kastner, 2013). As a result, 3D simulation of tunnelling process generally concentrates on back-analysis (Miro et al., 2015; Russo et al., 2015). In addition, tunnels do not always maintain a horizontal trajectory but may curve or move up and down (Shen et al., 2022; Hu, et al., 2024). However, 3D numerical simulations usually focus on a specific distance of tunnel excavation, assuming constant tunnel depth and uniform distribution of soil layers along this distance. Geotechnical variability (e.g. soil layers distribution, ground properties), tunnelling parameter fluctuations (e.g. advancement speed, grouting pressure), and tunnel geometry complexity (e.g. tunnel depth, tunnelling direction) also challenge full length 3D tunnelling simulations.

Because of simplicity, 2D simulation of tunnelling activities has been widely adopted, with many methods proposed such as gap method (Rowe et al., 1983), convergence confinement method (Paraskevopoulou and Diederichs, 2018), stress reduction method (Möller and Vermeer, 2008), displacement-controlled method (Cheng et al., 2007; Do et al., 2014; Hejazi et al., 2008; Ma et al., 2018), volume loss control method (Shiau and Sams, 2019) and so on. These approaches aim to study GSS by analysing tunnel profile deformation along tunnel cross-sections. However, the simulation result is significantly sensitive to some specific parameters that are difficult to determine, such as the stress relaxation coefficient. In addition, the proposed tunnel convergence patterns are not comprehensive and need further exploration.

To solve these problems, this study employs 2D numerical model for analysis of tunnelling-induced GSS, by simplifying the complex tunnel excavation processes into different tunnel convergence models using the displacement-controlled method (DCM). The significance and practical value of this study is that GSS trough can be estimated at the early stages of a tunnel project using limited data such as geotechnical properties, tunnel geometry, and tunnel convergence parameters (g or V_L). On the other hand, for back-analysis, this approach also enables the probabilistic assessment of transverse GSS troughs at different tunnel cross-sections.

As shown in Figure 1, the structure of this paper is organized as follows. Section 2 explains GSS principle and indicates commonly used parameters for the assessment of the GSS problem. Section 3 reviews DCM and proposes some tunnel convergence models based on the g or V_L, respectively. The corresponding tunnel convergence functions for each model are derived and presented. Section 4 uses case studies to verify the effectiveness of the introduced method by comparing the simulation results with field data. The parametric study is conducted in Section 5, clarifying the relationships of the maximum GSS (S_{max}) with tunnel depth (H), tunnel diameter (D), gap parameter (g) and volume loss (V_L). In Section 6, the advantages and limitations of this study are discussed, with future improvements suggested.

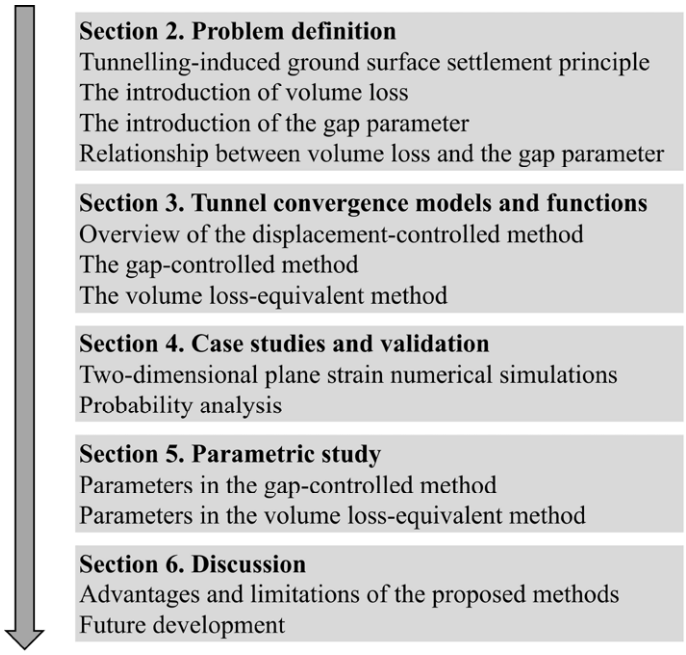

Figure 1: The workflow diagram of this study.

2. PROBLEM DEFINITION

As shown in Figure 2, the tunnelling activity disturbs the geostatic balance, causing the surrounding soil to move inward toward the tunnel, which results in the finished area being smaller than the excavated area. This phenomenon is known as volume loss, which describes the difference between the excavated tunnel area and the planned tunnel area. It is calculated by taking the difference between the actual excavated volume and the planned volume, and dividing this by the planned tunnel volume. Factors such as geotechnical properties, tunnelling method, and tunnel geometry can significantly influence the magnitude of volume loss (Golpasand et al., 2016; Niu et al., 2023; Vu et al., 2016).

Generally, the space created between the tunnel boundary and the lining is filled by collapsing soil from above the tunnel. This soil displacement leads to localized ground movement and GSS (see Figure 2). The void, particularly at the tunnel crown, represents the physical distance between the excavated tunnel boundary and the lining, playing a critical role in determining the magnitude of GSS. Larger voids cause more significant GSS due to increased soil collapse. The gap parameter indicates the size of this void, reflecting the potential extent of soil collapse and displacement, and indirectly represents the magnitude of volume loss.

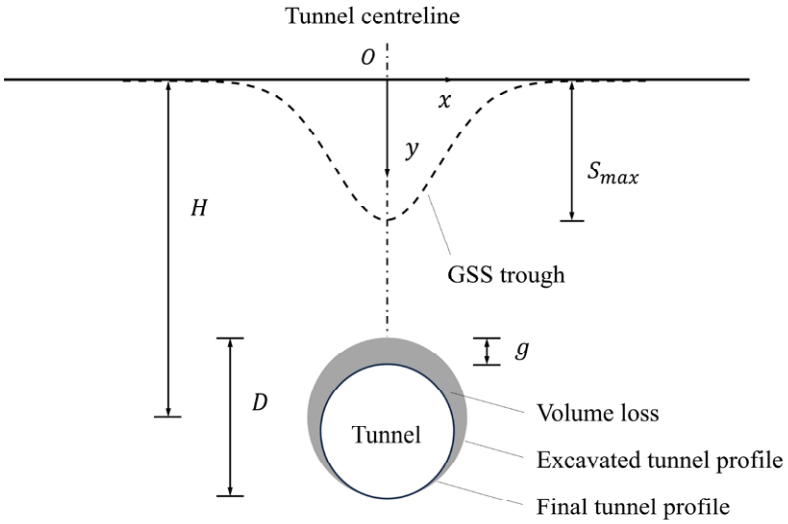

Figure 2: An illustration of tunnelling-induced ground movement and surface settlement.

The g and V_L are two important indicators for assessing the stability and safety of the liner as well as evaluating tunnelling-induced GSS (Jallow et al., 2019; Lin et al., 2021; Zakhem and El Naggar, 2019). They can be determined through back-analysis utilizing monitoring data and appropriate modelling techniques. To obtain g, one method is to measure the settlement of the tunnel crown at construction site directly. This is relatively different for TBM constructed tunnel (Xie et al., 2021). Lee et al. (1992) proposed that g depends on TBM tail void and the quality of workmanship. Zhu and Li (2017) conducted a more detailed investigation into this parameter and identified six key contributing factors. Another approach involves fitting the measured GSS data with a Gaussian curve to estimate g. By analysing the width and depth of GSS trough and correlating it with H and D, g can be inferred. The same condition applies to V_L. The fitted Gaussian curve can be used to evaluate the value of V_L. On the other hand, numerical methods can also assist in back-calculating V_L by adjusting model parameters until the simulated GSS trough closely matches field observations.

Loganathan and Poulos (1998) simplified the correlation between g and V_L (see Equation 1) and provided analytical solutions under the assumption that the converged tunnel maintains an ideal shape with its excavated profile. The g is defined as the maximum settlement of the tunnel crown during tunnelling (Cao et al., 2020).

$$g = 2R(\sqrt{V_L + 1} - 1) \quad (1)$$

3. DISPLACEMENT-CONTROLLED METHOD AND TUNNEL CONVERGENCE PATTERNS

GSS is primarily influenced by ground properties, tunnel geometry as well as excavation and support method (Niu et al., 2023; Santos and Celestino, 2008). These factors are reflected through tunnel convergence and ground loss, which is the main contributors to GSS in the short term (Feng et al., 2022). Other factors such as creep and consolidation of soil and thermal effect have limited contributions, as a result, they are often neglected in short-term GSS analysis (Le et al., 2023).

DCM is a method of implementing confinement forces or specified displacements to the tunnel wall (Do et al., 2014). It is widely used to simulate ground response due to tunnelling. For example, tunnelling process can be simply simulated through a uniform radial contraction of the excavated tunnel profile (Hejazi et al., 2008). This means tunnel contracts radially until the predefined ground loss is reached. In some conditions, the tail void grouting and subsequent consolidation phases can also be simulated by accounting for the variations in the excavation boundary to better represent real construction procedures. For example, grouting injection phase can be depicted by an increase in tunnel diameter, while the consolidation phase can be characterized by a subsequent reduction in tunnel diameter (Dias and Kastner, 2013). The simulation of grouting injection phase captures the immediate expansion of tunnel boundary due to grouting, while the consolidation phase reflects the long-term ground response that occurs after the grout hardens and excess pore pressures dissipates. However, in practise, tunnel convergence exhibits highly nonuniformity, with more crown settlement and less invert heave (Cheng et al., 2007; Zhang and Huang, 2012). It is reported that the nonuniform convergence patterns of tunnel can provide more realistic and accurate predictions of GSS (Park, 2005; Zhang and Huang, 2012).

Based on g and V_L, this study presents multiple typical tunnel convergence models to describe tunnel convergence characteristics and uses DCM to analyse the resultant GSS. Specifically, tunnel convergence functions are derived based on the assumed tunnel convergence patterns. These functions are then implemented in the finite element software ABAQUS to simulate the targeted deformation at the tunnel periphery. For these scenarios, the corresponding GSS troughs are obtained, and the area covered by these various GSS troughs represents the probabilistic GSS outcome.

3.1 GAP-CONTROLLED METHOD

The potential ground movement at the tunnel crown, referred as ‘gap’, is an important parameter for assessing tunnel convergence and resultant GSS. For tunnel constructed using TBM, the diameter excavated by cutterhead is always larger than the outer diameter of lining. The void between the excavated tunnel boundary and the lining outer skin is commonly filled with grouting injection, effectively minimizing the gap and reducing the GSS. The effectiveness of grouting depends on many factors, such as grouting pressure, grouting volume, soil permeability and the types of grouting materials used. Higher grouting pressure can enhance the filling of the void, thereby reducing GSS. However, excessive pressure can lead to grout overflow and destabilize the surrounding soil, potentially exacerbating deformations. In addition, the grouting volume should be adequate to fill the void, while soil permeability influences the ability of grouting material to spread and bond effectively with the surrounding soils. The selection of grout type is also crucial, as it should be suited to the specific soil conditions. For example, high-flow grouts are ideal for permeable soils to ensure proper filling of voids, while fast-setting grouts are used in areas with high water inflow to provide rapid stabilization.

There are multiple methods for the evaluation of g. For example, Lee et al. (1992) proposed the following equation for calculating g.

$$g = G_P + U_{3D}^* + \omega \tag{2}$$

Where G_P is the physical gap which is the distance between the excavated tunnel boundary and outer skin of the lining, U_{3D}^* is the 3D elastoplastic deformation at the tunnel face, ω is the workman factor. The determination of these parameters can refer to Loganathan and Poulos (1998), Chakeri et al. (2013), Chi et al. (2001), Yang et al. (2021) and Yang et al. (2022).

Zhu and Li (2017) further studied this parameter, identifying six primary contributing factors. These include the face pressure at tunnel face, the grouting effect, the supporting pressure between surrounding soil and liner, yawing and pitching of TBM, and the long-term volume loss of disturbed soil. The estimation of these factors (gap induced by inadequate shield support pressure, gap due to grouting, gap due to intermittent shield alignment, gap due to shield yawing, gap due to shield pitching and gap due to long term volume loss) can be found in Zhu and Li (2017) accordingly.

In the proposed gap-controlled method, while g at the tunnel crown remains constant, the effect of different tunnel ovalization degrees on the GSS is investigated. As presented in Figure 3, pattern one represents a uniform radial

contraction. Remaining patterns indicate more complex scenarios, taking into account the impacts of vertical movement and ovalization of the liner. The dashed lines represent the original shape of tunnel periphery after excavation, whereas the solid lines represent converged tunnel periphery. It should be noted that the gap configurations shown in Figure 3 are not unique and can vary under different ground conditions. Parameters such as the lateral earth pressure coefficient (K_0) and ground stiffness have a significant influence on the deformation mode of the tunnel periphery. For example, under a high K_0 condition, tunnel deformation is dominated by horizontal convergence due to the relatively larger in-situ horizontal stress. As a result, inward displacement is concentrated at the sidewalls, while vertical deformation at the crown and invert is comparatively restrained. The tunnel cross-section therefore tends to evolve toward a horizontally compressed and vertically elongated shape.

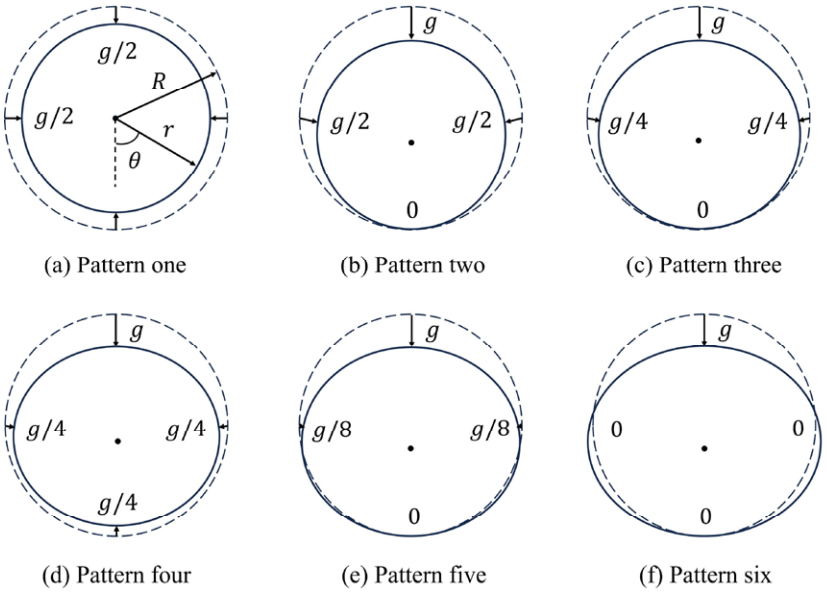

Figure 3: Illustration of gap-controlled method.

The boundary conditions corresponding to each pattern are listed as follows.

$$u_r(r = R) = -\frac{1}{2}g \tag{3}$$

$$u_r(r = R) = -\frac{1}{\pi}g\theta \tag{4}$$

$$u_r(r = R) = -\frac{1}{\pi^2}g\theta^2 \tag{5}$$

$$u_r(r = R) = -g(\frac{1.5}{\pi^2}\theta^2 - \frac{0.75}{\pi}\theta + \frac{1}{4}) \tag{6}$$

$$u_r(r = R) = -g(\frac{1.5}{\pi^2}\theta^2 - \frac{0.5}{\pi}\theta) \tag{7}$$

$$u_r(r = R) = -g(\frac{2}{\pi^2}\theta^2 - \frac{1}{\pi}\theta) \tag{8}$$

Where u_r is the boundary condition that represents the displacement magnitude along the tunnel periphery, R is non-deformed tunnel radius after excavation, g is gap parameter, r is radial coordinate in the cylindrical coordinate system and θ is angular coordinate (the angle counterclockwise from tunnel invert), ranging from 0 to π, as shown in Figure 3 (a).

3.2 VOLUME LOSS-EQUIVALENT METHOD

When quantifiable volume loss is calculated, an alternative approach named volume loss-equivalent method can be adopted, which focuses on the equivalent volume loss. It assumes that the tunnel liner maintains a similar shape after deformation. This method involves progressively lowering the converged tunnel periphery, step by step, to assess the resulting GSS (see Figure 4). Figure 4 (a) is the case of uniform radial contraction, while Figure 4 (f) represents the case that the invert of converged tunnel is tangent to its non-deformed shape. For other cases, a normalized parameter $g^{'}$ is used (presented in Equation 9), indicating the intermediate state of tunnel periphery convergence from the uniform contraction to the tangent case.

$$g^{'} = g_{new}/g \tag{9}$$

Where $g^{'}$ is normalized gap parameter, g_{new} represents the displacement of tunnel crown, g is gap parameter.

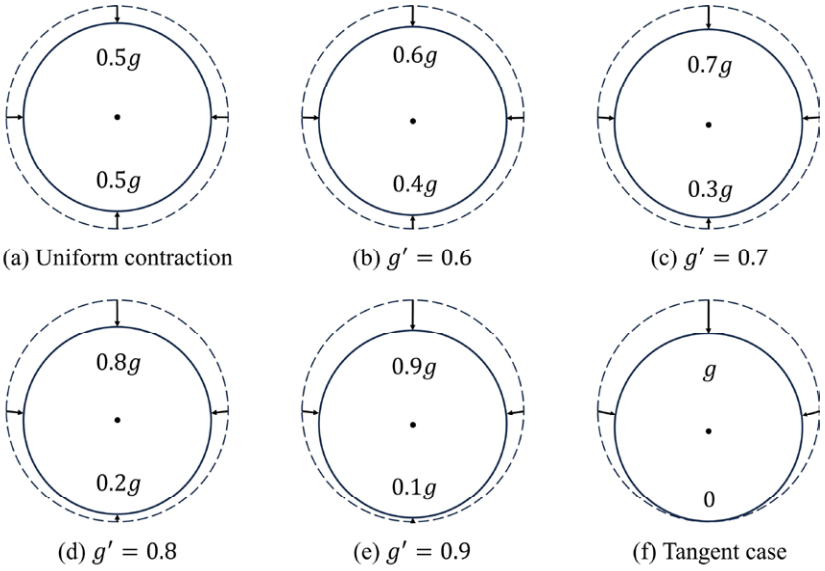

Figure 4: Illustration of volume loss-equivalent method.

The corresponding equations for each case are detailed as follows:

$$u_r(r = R) = -\frac{1}{2}g \tag{10}$$

$$u_r(r = R) = -g(\frac{0.2}{\pi}\theta + 0.4) \tag{11}$$

$$u_r(r = R) = -g(\frac{0.4}{\pi}\theta + 0.3) \tag{12}$$

$$u_r(r = R) = -g(\frac{0.6}{\pi}\theta + 0.2) \tag{13}$$

$$u_r(r = R) = -g(\frac{0.8}{\pi}\theta + 0.1) \tag{14}$$

$$u_r(r = R) = \frac{g}{\pi}\theta \tag{15}$$

4. CASE STUDIES

The effectiveness of the proposed methods is verified through case studies. In each case study, a 2D finite field is established, with its size determined based on literature (Jin et al., 2022; Shen et al., 2014). For example, it is suggested that the distance between tunnel invert and field bottom should be larger than one tunnel diameter to eliminate the potential influence of boundary conditions (Chen et al., 2013; Noubissi et al., 2024; Shahin et al., 2011; Shahin et al., 2019). Moreover, Mohr- Coulomb (MC) constitutive model is used to describe soil behaviors in all 2D plane strain simulations in this study.

The numerical simulation procedure mainly includes two steps:

(1) Applying gravity to all soil elements to achieve geostatic balance. The predefined stress field is established based on soil density and gravity acceleration (taking $g_0 = 10m/s^2$), with lateral earth pressure coefficient (K_0) assigned for each soil layer respectively.

(2) Deactivating soil elements within the tunnel periphery while applying displacement boundary conditions (as presented in Figure 3 and 4) to the tunnel periphery.

4.1. XI'AN METRO LINE 2

4.1.1 Background

Xi'an Metro Line 2 is located in Shanxi, China, constructed using Earth Pressure Balance Shield Machine (EPBSM). The excavation diameter of this tunnel is 6.16m, and the diameter of liner outer skin is 6.0m. It passes through silty clay deposits and old loess, with a buried depth varies from 12.6m to 22.4m. As the tunnel excavation proceeds, variations in soil properties, tunnel depth and volume loss are monitored, leading to variations in GSS at different sections. According to back-analysis from Zhu and Li (2017), Section 13+290, where the tunnel has a 14.2m axis depth with a 31.4mm gap parameter, is selected for detailed analysis in this study.

4.1.2 Geotechnical conditions

The soil composition surrounding the upper part of the tunnel consists of a mixture of fill, soft saturated loess, and new loess (Ma et al., 2016; Peng et al., 2017). Meanwhile, the soil around the lower part of the tunnel is mainly sandy soil (Lai et al., 2020). Physical and mechanical parameters of soil are mainly determined from laboratory triaxial compressibility tests. Based on laboratory experiments and engineering experience, Zhu and Li (2017) proposed the weighted average of physical and mechanical parameters for the soils around the tunnel (shown in Table 1).

Table 1: Soil parameters at Section 13+290 (Zhu and Li, 2017).

Parameter, symbols and unit	Value
Unit weight γ, kN/m^3	19.0
Cohesion c, kPa	27.6
Friction angle φ, °	26.4
Young's modulus E, MPa	31.5
Poisson's ratio v	0.383
Earth pressure at rest K_0	0.62

4.1.3 Model establishment

The numerical simulation model is shown in Figure 5, where the field size is 28.4m in height and 100m in width. Centre of tunnel is located at approximately 14.2m depth with an equivalent 6.16m excavation diameter. For boundary conditions, the base of the field is fixed, ensuring no vertical or horizontal displacement occurs at the bottom boundary. Both lateral sides are treated as rollers, allowing vertical movement but restraining horizontal displacement. The size of square element (CPE4R) is 0.5m, which is densified in the region surrounding the tunnel. In this case, a total of 11560 elements with 11817 nodes is generated in ABAQUS.

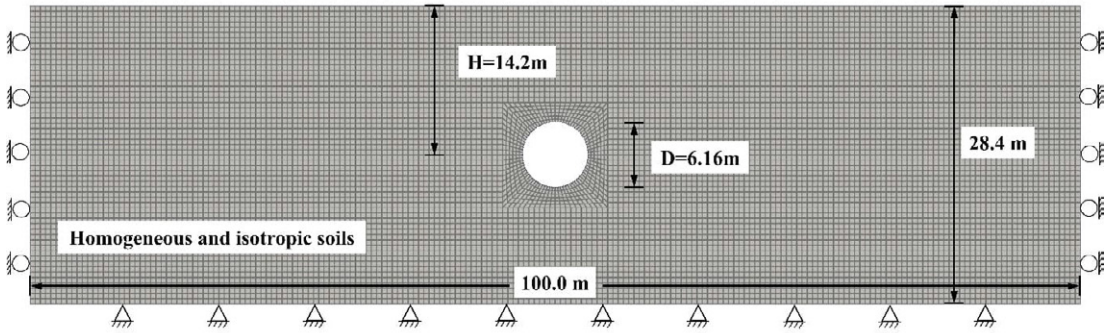

Figure 5: Setup of 2D numerical simulation model of Xi'an Metro Line 2.

4.1.4 Results

Keeping g at the tunnel crown constant, different tunnel convergence patterns due to ovalization are studied. Based on Equation 3 to 8 and Figure 3, the gained numerical simulation results are compared with field measurements (see Figure 6). As can be illustrated, GSS trough obtained from FEM is in good agreement with in-situ observations, both in shape and magnitude. Results also indicate that the uniform radial contraction pattern (pattern 1 in Figure 3) cannot reflect GSS trough accurately. Since tunnel geometry is symmetrical while the loading acting on tunnel periphery is not, the assumption of uniform contraction around tunnel periphery is over-ideal. As a result, it cannot accurately represent the actual tunnel convergence behaviors in reality. On the other hand, pattern 2, which is characterized by the invert of converged tunnel aligning tangentially with that of the excavated tunnel, tends to over-estimate GSS trough. This is consistent with field observations that the invert of excavated tunnel commonly experience heave. Since tunnel excavation releases the stresses in the surrounding soil, the redistribution of stress can lead to a reduction in compressive stress within the stratum, leading to the convergence of tunnel periphery such as settlement of the crown and heave of the invert.

In addition, Figure 6 also indicates that the non-uniform tunnel convergence patterns (pattern 3, 4, 5 and 6) can provide more precise GSS trough estimation. The g value has significant influence on the maximum GSS. As this parameter is ensured, the variation of the maximum GSS is limited. The dark grey region depicts the state of GSS trough resulted from no tunnel springline displacement (pattern 6) to large springline movement (pattern 2), representing the area of higher probability of GSS occurrence. For the light grey region, it corresponds to area where GSS results from uniform convergence of tunnel periphery (pattern 1) to no movement of tunnel springline (pattern 6), indicating a lower probability of GSS occurrence.

The shapes and slopes of GSS trough are also crucial in assessing the impact of tunnelling on adjacent structures. While the maximum GSS indicates the extent of ground movement, the slopes of the trough reveal the pattern of settlement distribution across the affected area. Steeper slopes can create sharper gradients of ground deformation, increasing the risk of structural damage to nearby buildings, utilities, and infrastructure due to differential settlement. In contrast, broader and gentler slopes indicate a more gradual transition in ground deformation, typically resulting in less severe structural impacts.

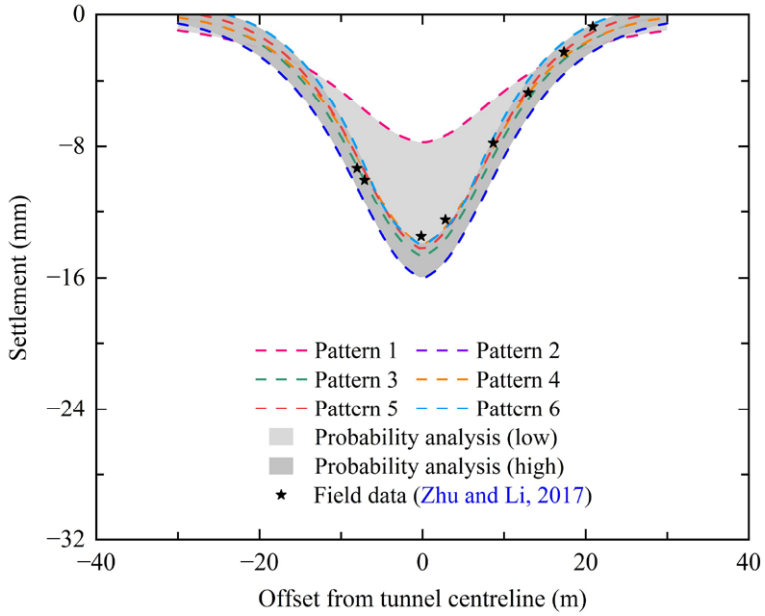

Figure 6: Transverse ground surface settlement of Xi'an Metro Line 2 Section 13+290.

4.2 MILAN METRO LINE 1

4.2.1 Background

The Milan underground Line 1 is constructed in alluvial sandy area of Padana Plain, using EPBSM. Tunnel depth varies between 8 and 19 meters beneath ground surface. Featuring a cutter head diameter of approximately 6.54m, the tunnel is lined with segments having an outer diameter of 6.3m and a thickness of 0.3m. The space between the excavated wall and outer skin diameter of the lining is filled with grout injection. During tunnelling process, variation of H, V_L and S_{max} are monitored at different cross-sections along tunnel length (Migliazza et al., 2009). Based on field measurements from Migliazza et al. (2009), a cross-section with 13.5m depth and 0.36% volume loss is employed for analysis in this study.

4.2.2 Geotechnical conditions

Geotechnical investigations, including in situ and laboratory tests, have revealed that the soil materials at the site predominantly consist of sandy ground (Migliazza et al., 2009). The upper layer is identified as sandy-gravel, while the layer beneath is characterized as silty-sandy. The geometry and geology of Milan Metro Line 1 are presented in Figure 7. Soil parameters employed in numerical simulation are shown in Table 2. More information of soil properties at Milan region can refer to Boldini et al. (2018), Fargnoli et al. (2013) and Fargnoli et al. (2015).

Table 2: Soil parameters in Milan Metro Line 1 (Migliazza et al., 2009).

Parameter, symbols and unit	Layer 1	Layer 2
Thickness t, m	<15	>15
Unit weight γ, kN/m^3	22	18
Cohesion c, kPa	0	0
Friction angle φ	30°	30°
Young's modulus E, MPa	100	75
Poisson's ratio v	0.3	0.3
Earth pressure at rest K_0	0.46	0.46

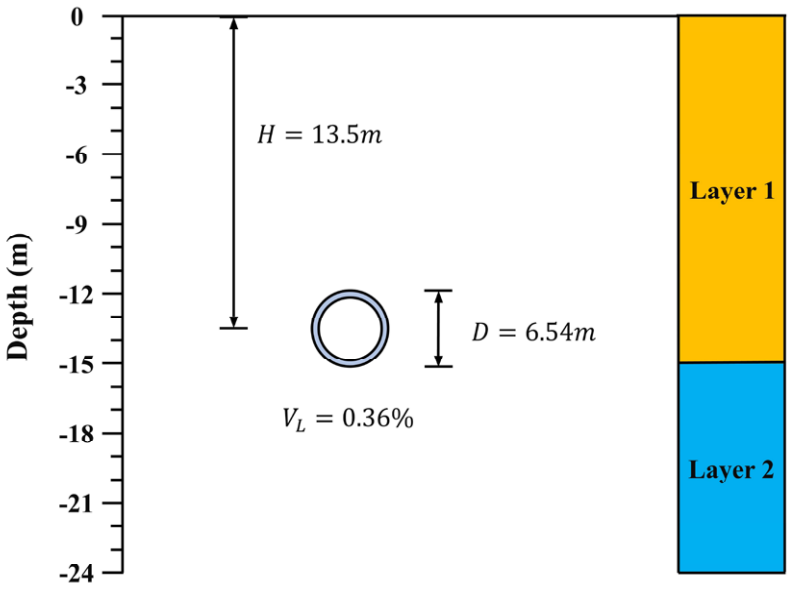

Figure 7: Geometry and geotechnical conditions of Milan Metro Line 1.

4.2.3 Results

The gap parameter was not recorded in this project. Instead, emphasis was placed on recording the volume loss of each tunnel cross-section. Numerical simulation results based on the proposed tunnel convergence patterns are compared with field data, as displayed in Figure 8. It reveals that the GSS troughs predicted by FEM are wider than that of field observations, which is consistent with the conclusions of many researchers such as Addenbrooke et al. (1997), Franzius et al. (2005), Grammatikopoulou et al. (2008) as well as Hejazi et al. (2008). Reasons can be contributed by the simplification of simulation procedure and soil constitutive models. Tunnel could experience ovalization in reality, but this was ignored in the simulation due to data limitation. With data of volume loss only, the actual tunnel convergence patterns cannot be accurately deduced, therefore, the tunnel periphery is assumed to maintain its original shape after convergence. This results in the discrepancy between the GSS trough predicted by the FEM and the one observed at the field. Furthermore, simplified 2D plane strain analysis does not consider the 3D effects of tunnelling and MC model cannot describe the non-linear response of soil behaviors.

However, despite the simplification of tunnelling simulation steps and 3D condition, the volume loss-equivalent method still provides a valuable probability analysis of GSS trough. Especially, under the tangent case, the simulated maximum GSS shows the closest agreement with field measurements. In this condition, the invert of the converged tunnel is tangent to its non-deformed profile, which indicates that deformation is primarily concentrated in the upper portion of the tunnel, while the invert experiences limited inward displacement.

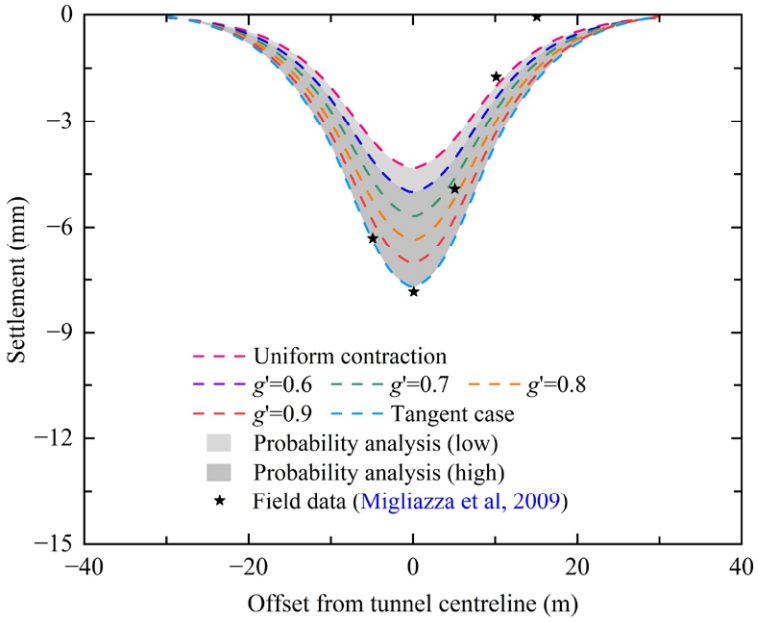

Figure 8: Transverse ground surface settlement of Milan Metro Line 1 Section 5-29.

4.3 ROME METRO LINE C

4.3.1 Background

Located in Rome, Italy, Rome Metro Line C extends from Monte Compatri-Pantano to San Giovanni, comprising two single-track tunnels (tunnel A and tunnel B). These two tunnels are constructed using EPBSM with an excavation diameter of 6.7m approximately. The external diameter of the liner is 6.4m. A cross-section near Carducci school is used for validation. This section (Section 11) has an axis depth of 25.4m. According to back-analysis, a volume loss of 0.48% can provide an accurate description of the monitored GSS trough (Miliziano and de Lillis, 2019).

4.3.2 Geotechnical conditions

Geotechnical investigations reveal that soil materials mainly consist of hard pyroclastic layers (Losacco and Viggiani, 2019). From ground surface, the encountered soil strata include: (1) 16m thickness man-made fill, characterized by medium dense to loss coarse-grained soil; (2) fluvial-alluvial deposit composed of clayey silt and sandy silt, with a maximum thickness of 18m; (3) pre-volcanic fluvial deposit, which is comprised of very dense silty sand, clayey silt, sandy gravel, and other materials. The physical and mechanical parameters of these materials are summarized in Table 3 and represented in Figure 9.

Table 3: Soil parameters in Rome Metro Line C Section 11 (Miliziano and de Lillis, 2019).

Layer	Description	$\gamma\ (kN/m^3)$	$c\ (kPa)$	$\varphi\ (°)$	$E\ (MPa)$	v	K_0
1	Coarse-grained soil	17.5	10	32	40	0.3	0.47
2	Clayey silt and sandy silt	17.5	15	32	22.5	0.3	0.68
3	Silty sand and clayey silt	20.0	10	35	52.5	0.3	0.64

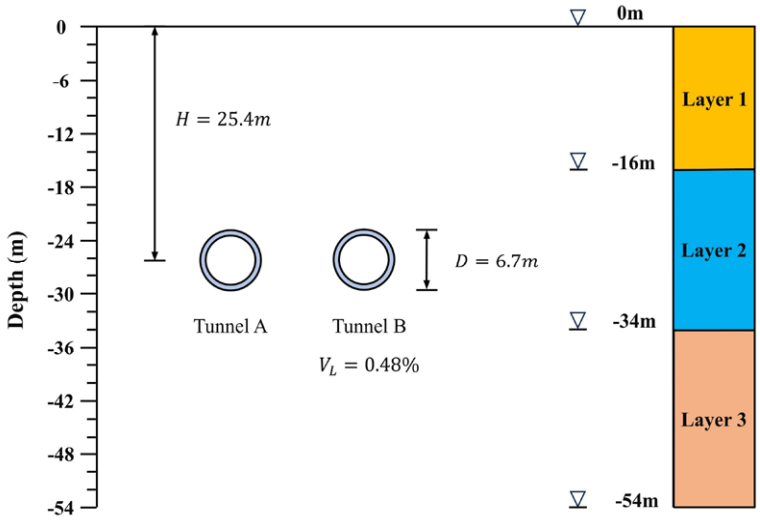

Figure 9: Geometry and geotechnical conditions of Rome Metro Line C.

4.3.3 Results

Following the same simulation procedure and using the equivalent volume loss, different tunnel convergence patterns are analyzed according to Equation 10 to 15 and Figure 4. GSS troughs predicted by DCM due to these tunnel convergence models are compared with field measurements in Figure 10. As can be seen, the obtained GSS troughs align well with field observations. The difference between field measurement and numerical results can primarily be attributed to the assumption that tunnel remains an ideal shape after convergence. As mentioned, for predicting GSS before tunnel excavation, the actual tunnel convergence pattern cannot be accurately deduced only from the volume loss data obtained from previous tunnel projects or back-analysis. In this condition, various typical tunnel convergence models are proposed based on field observations and centrifuge experiments, providing a probability analysis of GSS trough. The light grey region, which represents the phase from uniform convergence to slightly vertical displacement of liner ($g' = 0.6$), means a low probability of GSS occurrence since these conditions are idealistic. The dark grey area, which represents the intermediate states between slightly vertical displacement of liner ($g' = 0.6$) and the tangent situation ($g' = 1$), more aligns with the actual tunnel convergence situations and thus has higher GSS occurrence probability. More tunnel convergence measurement data can enhance the precision of fitting tunnel convergence functions and better characterize tunnel convergence, thereby improving the accuracy of GSS prediction.

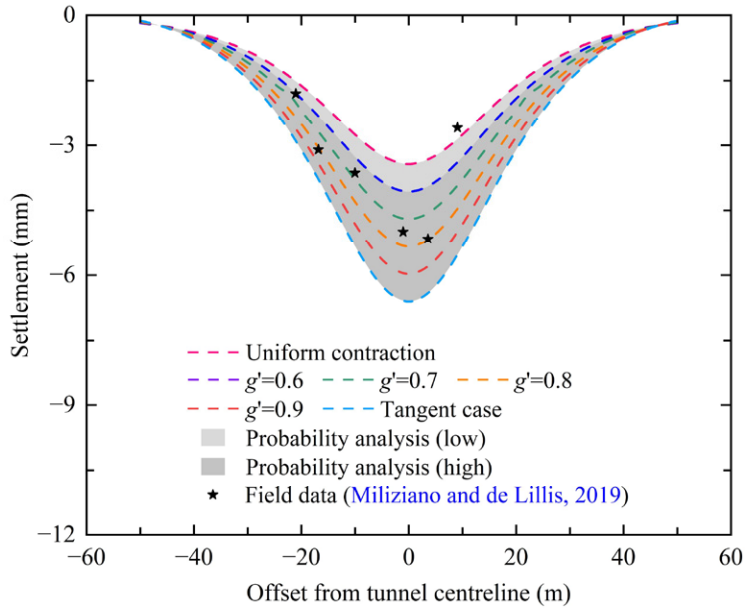

Figure 10: Transverse ground surface settlement of Rome Metro Line C Section 11.

5. PARAMETRIC STUDY

The parametric study is conducted based on Section 13+290 of Xi'an Metro Line 2, as previously studied. With the numerical model and soil parameters remain unchanged, variations are introduced in tunnel geometry and the extent of tunnel convergence. In other words, to isolate the effects of geotechnical variations, the soil parameters, including cohesion, friction angle, elastic modulus and Poisson's ratio, are kept constant. This ensures that the differences in the results are due to the alterations in tunnel geometry and convergence magnitude. The variations of tunnel geometry include changes in D and H. By changing these geometric parameters, the parametric study aims to understand their impacts on the maximum GSS. In addition, the numerical simulation results are also compared against empirical and analytical solutions.

5.1 EMPIRICAL AND ANALYTICAL METHODS

For the empirical method, Peck (1969) proposed that Gaussian curve can effectively fit the GSS trough. Based on field observations and engineering experience, he developed empirical formulas for tunnelling-induced GSS assessment shown as follows.

$$S_v = S_{max}\exp\left(\frac{-X^2}{2i^2}\right) \tag{16}$$

$$S_{max} = \frac{V_s}{2.5i} \tag{17}$$

$$V_s = \frac{V_L \pi D^2}{4} \tag{18}$$

Where S_v is the vertical surface settlement at the X distance from tunnel centreline, S_{max} is the maximum ground surface settlement that usually occurs above tunnel centreline, i is the point of inflexion of the settlement trough, V_s is the settlement volume per unit advancement, V_L is volume loss, D is tunnel diameter.

The position of inflexion point *i* has been modified by many researchers based on field observations or experimental findings. For instance, Knothe (1957) introduced Equation 19, indicating that *i* is associated with tunnel depth and soil friction angle. Herzog (1985) suggested Equation 20, drawing from observations in Germany. Equation 21 was introduced by Arioglu, (1992). Chakeri et al. (2013) proposed Equation 22 by averaging multiple empirical solutions for standard deviation consideration.

$$i = \frac{H}{\sqrt{2\pi}\tan\left(\frac{\pi}{4} - \frac{\varphi}{2}\right)} \tag{19}$$

$$i = 0.4H + 1.92 \tag{20}$$

$$i = 0.9\left(\frac{D}{2}\right)\left(\frac{H}{D}\right)^{0.88} \tag{21}$$

$$i = \frac{1}{7}\left[2.116H + R\left(0.9\left(\frac{H}{D}\right)^{0.88} + \left(\frac{H}{D}\right)^{0.8}\right) + 6.46\right] \tag{22}$$

In terms of analytical method, Loganathan and Poulos (1998) introduced elasticity-based analytical solutions. The validation of proposed formulas was verified in multiple tunnel projects ranging from very stiff to soft clay. Detailed representations are shown as follows.

$$S_v = 4(1-\nu)R^2\frac{H}{H^2+X^2}\frac{4gR+g^2}{4R^2}\exp\left[-\frac{1.38X^2}{(H+R)^2}\right] \tag{23}$$

Where g is the gap parameter, H is tunnel depth, R is tunnel radius, ν is Poisson's ratio of soil.

5.2 PARAMETERS IN GAP-CONTROLLED METHOD

According to tunnel convergence models presented in Figure 3, which adopt a constant gap parameter, Figure 11 shows the variation of S_{max} in response to changes in H, D, and g. As can be seen, the overall trend of numerical simulation results aligns well with empirical and analytical solutions. However, the uniform radial contraction of tunnel periphery (pattern 1) fails to accurately reflect tunnel deformations in real-world conditions due to its oversimplification. Among the empirical solutions, Arioglu (1992) predicts significantly higher S_{max} values than others, while Knothe (1957) provides comparatively lower values. The empirical solution 2 and 4 provide similar S_{max} estimations with the analytical solution. All three tend to overestimate S_{max} under loess conditions, where Xi'an Metro Line 2 is located. Compared to the analytical solution, numerical simulation results are more consistent with field measurements.

Figure 11 (a) illustrates that S_{max} nonlinearly reduces with the increasing of H, as deeper tunnels have smaller influence on the ground surface. The reduction rates in empirical and analytical solutions are faster than that calculated in numerical simulations. Figure 11 (b) shows that S_{max} increases as D increases. Similarly, the rate of increase in empirical and analytical solutions is faster compared to numerical simulations. This can be attributed to the relatively more comprehensive consideration of various influencing factors in numerical simulations, including soil properties and various tunnel convergence models. The relationship of g and S_{max} is depicted in Figure 11 (c). It shows that S_{max} increases with an increase in g, indicating that greater tunnel convergence can lead to more surface settlement. The increasing trend in numerical simulation results is in good agreement with empirical and analytical solutions, which both exhibit a nearly linear relationship.

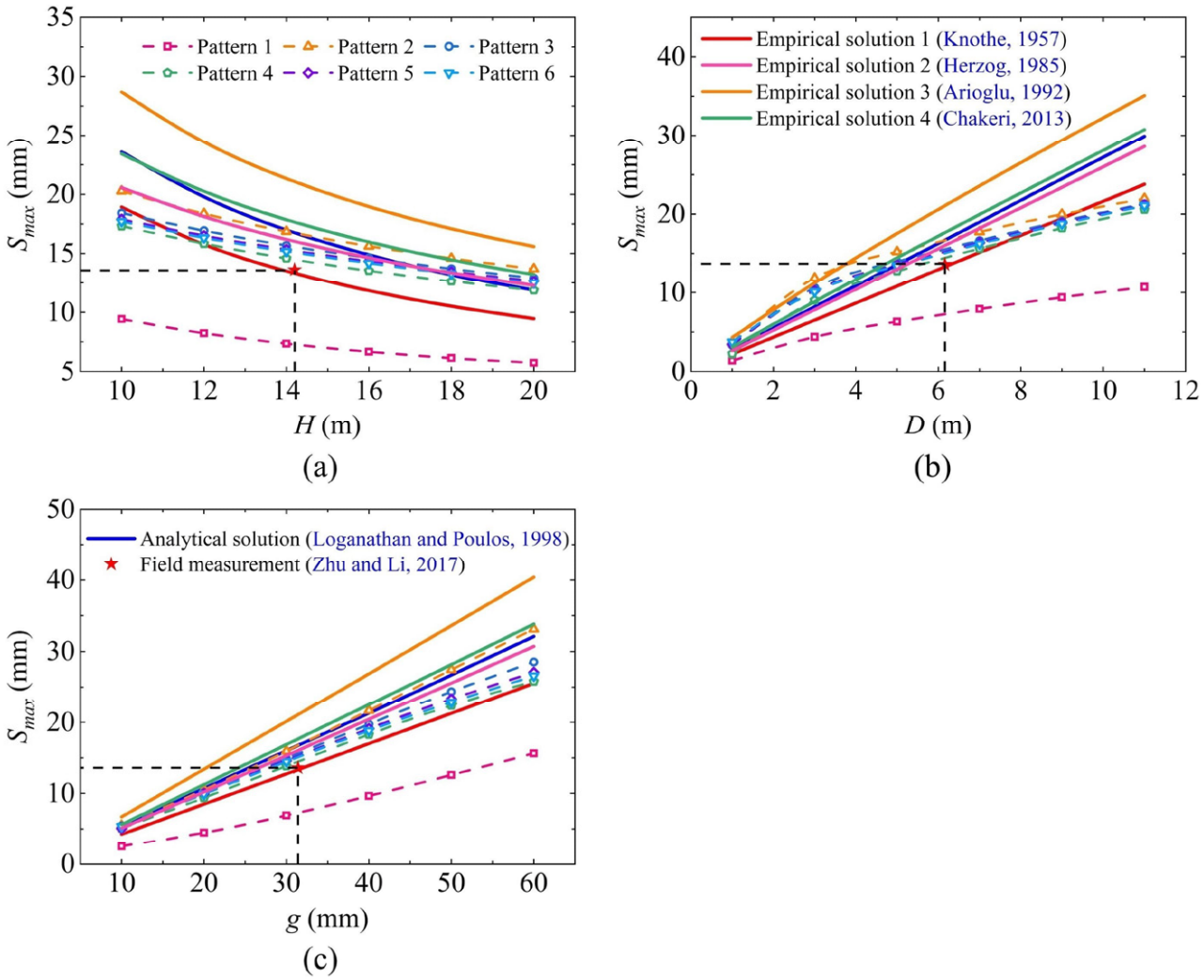

Figure 11: Variation of the maximum ground surface settlement with changing of (a) tunnel depth, (b) tunnel diameter and (c) gap parameter in the gap-controlled method.

5.3 PARAMETERS IN VOLUME LOSS-EQUIVALENT METHOD

Incorporating field observations and an analysis of the gap parameter at Section 13+290 of Xi'an Metro Line 2, a volume loss value of 1.02% is suggested (Zhu and Li, 2017). Follow the same procedure conducting the parametric analysis for tunnel convergence patterns based on the equivalent volume loss. Figure 12 displays the dependency of S_{max} on the variation of H, D and V_L, comparing various empirical solutions and convergence patterns. Overall, the numerical simulation results exhibit good agreement with empirical and analytical solutions. While the numerical results based on different convergence patterns align closely with the field measurement, the analytical and empirical solutions tend to overestimate S_{max} under the same V_L value.

Figure 12 (a) illustrates a reduction in S_{max} as H increases, with numerical simulations showing a slower rate of decrease compared to empirical and analytical solutions. Figure 12 (b) displays that S_{max} increases nonlinearly with increasing D, where empirical and analytical solutions exhibit a faster rate of increase relative to numerical simulations. Figure 12 (c) shows that S_{max} increases with increasing V_L, and the trend closely matches the approximate linear relationship observed in empirical and analytical solutions. In addition, the numerical simulation results basically envelop those of empirical and analytical solutions, with field measurement falling between them.

In summary, the volume loss-equivalent method provides a broader range of S_{max} compared with the gap-controlled method. This means the gap parameter is more important than the volume loss when evaluating S_{max} using DCM. In practice, acquiring the gap or volume loss parameters individually is inadequate to accurately capture actual tunnel deformation characteristics. If both parameters are obtained, the tunnel convergence model can be derived more accurately, thereby allowing for more accurate evaluation of GSS. Nonetheless, possessing information of just one of these two parameters still enables a preliminary estimation of S_{max} and GSS trough.

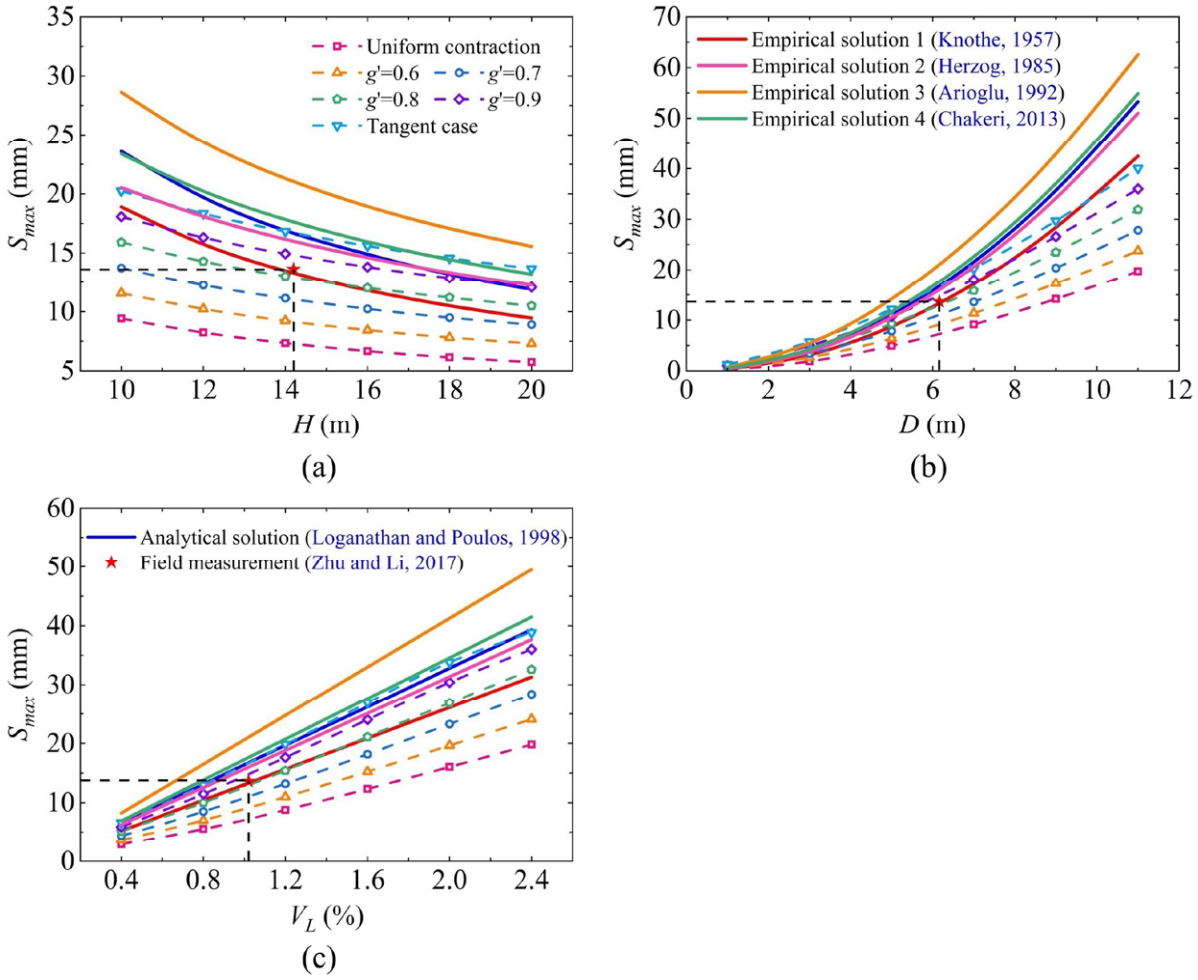

Figure 12: Variation of the maximum ground surface settlement with changing of (a) tunnel depth, (b) tunnel diameter and (c) volume loss in the volume loss-equivalent method.

6. DISCUSSION

6.1 ADVANTAGES AND LIMITATIONS OF PROPOSED METHOD

While the relationship between tunnel deformation and surface settlement has been studied by many researchers, this study extends these investigations by applying two numerical simulation-based approaches (the gap-controlled method and the volume loss-equivalent method) to systematically analyse the influence of tunnel convergence patterns on GSS troughs. The proposed 2D numerical method, based on the DCM, offers a probabilistic analysis of GSS during the initial stage of tunnel construction. Unlike conventional 3D numerical simulations that require detailed tunnelling information (e.g., excavation speed, thrust) and multiple sequential steps (e.g., application of face pressure, support removal, liner activation), the present method simplifies the process by directly incorporating tunnel convergence patterns. Figure 13 illustrates the steps of commonly used numerical methods for GSS evaluation. Figure 13 (a) outlines the analysis steps used in this study, while Figure 13 (b) and (c) summarize step-by-step 3D numerical simulation of tunnelling processes using FEM and FDM, respectively. As can be indicated, all methods start with establishing geostatic balance condition. Subsequently, 3D simulation of tunnelling activities follows multiple steps including applying face pressure, reducing support pressure and activating liner etc. These processes, while accurate, are often computationally intensive and time-consuming. In contrast, the proposed 2D numerical method requires fewer steps, thereby simplifying the simulation of tunnel excavation. By simplifying complicated tunnelling process into tunnel convergence patterns and incorporating geotechnical information along with data on the g or V_L, this method enables quick and probability analysis of GSS across various tunnel cross-sections. While maintaining satisfactory accuracy, this method effectively saves simulation time and improves computational efficiency. In addition, one potential engineering application is evaluating GSS in the early stages of a tunnel project utilizing limited information such as geotechnical properties, tunnel geometry, and tunnel convergence parameters (g or V_L). The determination of g and V_L is critical, as they significantly influence the derived tunnel convergence functions and tunnel convergence patterns.

Furthermore, different tunnelling methods, such as drill and blast, TBM, and New Austrian Tunnelling Method (NATM), can influence GSS in different ways. For instance, the drill and blast method has a higher potential for GSS due to the risk of over-excavation, as each blast can suddenly reduce stress at the excavation face, causing ground movement and localized settlement. In contrast, TBM tunnelling provides a more continuous and controlled excavation process (Wu et al., 2020; Yan et al., 2023). The managed excavation and immediate support installation result in lower GSS. For NATM, it tends to cause more significant and unpredictable GSS since the tunnel periphery is exposed for longer periods before the support is applied. For applying the method proposed in this study to tunnels constructed using the drill and blast approach as well as NATM, the tunnels need to be approximated as circle shapes, which can introduce errors due to the shape approximation. Additionally, in complex geotechnical conditions where the MC constitutive model fails to accurately describe soil behaviors, or when tunnel convergence is significant and exceeds the typical ranges, the proposed method need to be applied with caution.

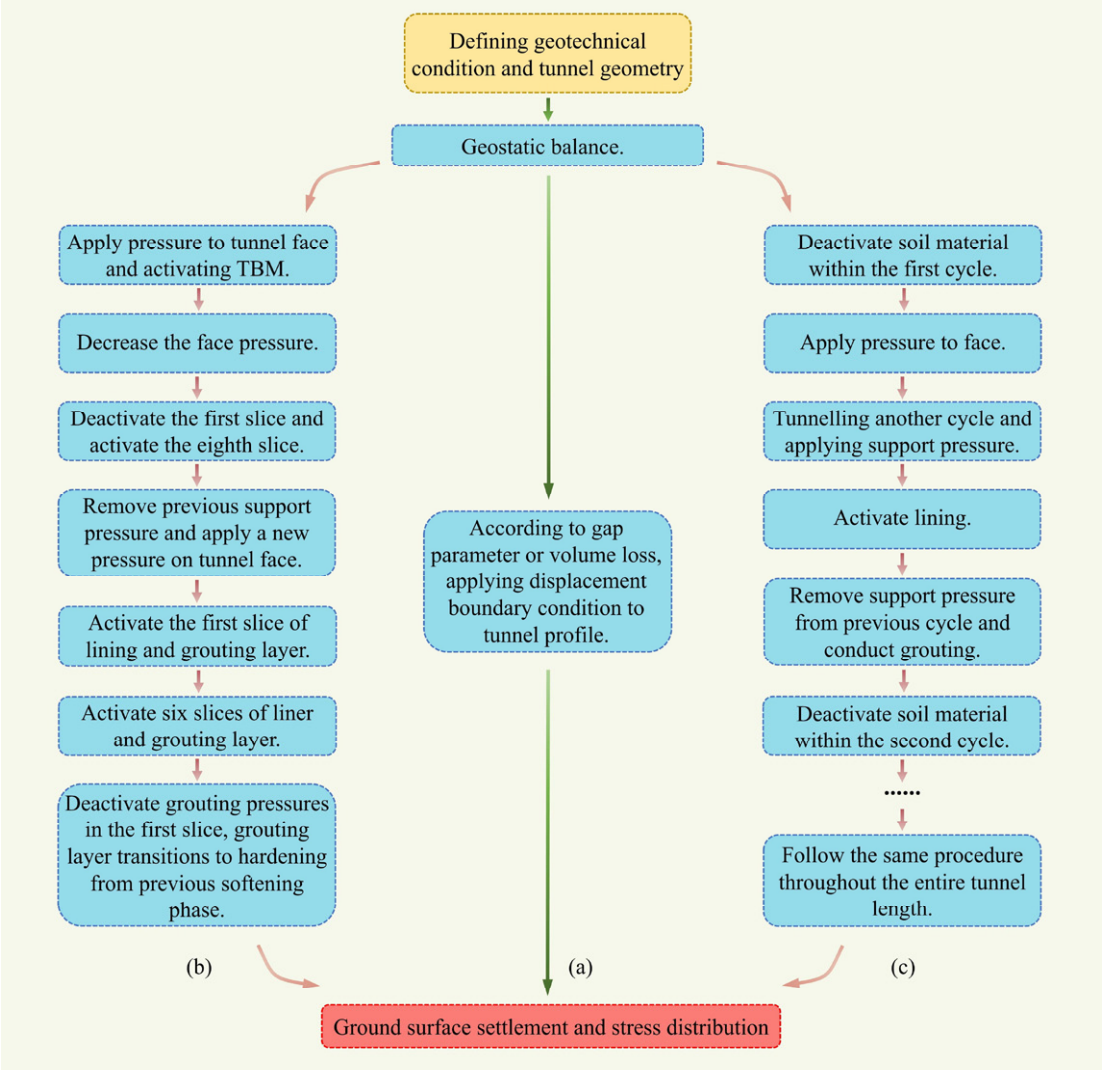

Figure 13: Comparison of proposed method with 3D simulation of tunnel excavation. (a) Simplified method in this study. (b) Step-by-step excavation in FEM (Li et al., 2019; Zhong et al., 2021). (c) Step-by-step excavation in FDM (Hao et al., 2022).

6.2 FUTURE DEVELOPMENT

In most tunnelling cases, ground deformation is relatively small, and the surrounding soil typically does not reach failure. Thus, the elastic response of soil is critical for analysing the GSS problem (Huang et al., 2017). The variation in Young's modulus contributes to changes in both the magnitude and width of ground settlement troughs (Zhang et al., 2021). The MC model, while widely used due to its simplicity, is primarily suited for problems involving large displacements where the nonlinearity of elastic behavior of soil is less important. This means the linear elastic response of MC model may falls short in accurately depicting soil behaviors in certain situations. For instance, over-consolidated clay exhibits highly nonlinear elastic before reaching failure (Grammatikopoulou et al., 2008). This nonlinearity cannot be captured by the linear elastic assumptions of the MC model, leading to potential inaccuracies in the analysis of GSS due to tunnelling in such soil conditions. Compared with MC, apply more advanced soil constitutive models such as Hardening Soil and Hardening Soil with Small Strain can enhance the assessment accuracy of tunnelling-induced GSS using DCM (Hejazi et al., 2008). Therefore, the development of User Subroutine (UMAT) is necessary for employing these models in ABAQUS. The efficacy of the proposed method in different soil constitutive models requires further exploration.

Furthermore, in numerical simulations, the assumption that soil material is homogenous and isotropic in each layer is often accepted for simplicity and efficiency. However, this assumption may not accurately reflect the complexity and variability of soil properties in real-world scenarios (Huang et al., 2015; Zhang et al., 2021). To address these challenges and achieve a more comprehensive analysis, it is suggested to incorporate a probability study. This can be achieved through the random fields of soil parameters, which considers the variability and uncertainty of soil properties. Consequently, it can offer more precise predictions of GSS associated with tunnelling activities.

7. CONCLUSION

This paper provides a simplified numerical method for the probability estimation of tunnelling-induced GSS. Various tunnel convergence models are proposed according to the g or V_L, respectively. Tunnel convergence is represented as a function of angle deviation. Employing these tunnel convergence functions in ABAQUS to make tunnel periphery experience targeted deformation, different resulting GSS troughs can be assessed. The region encompassed by these GSS troughs is considered as the probabilistic outcome of GSS. The effectiveness of proposed method is verified through case studies. From the analysis of results, the following conclusions can be made:

(1) Compared to 3D step-by-step tunnelling modelling that considers many factors such as face pressure, grouting pressure and grouting consolidation, the introduced approach eliminates the need for detailed material parameters and excavation specifics, thereby simplifying GSS analysis.

(2) The gap-controlled method is appropriate for instances where g is available. In cases that the V_L is obtained, DCM can operate on the principle of equivalent volume loss. Compared with the gap-controlled method, the volume loss-equivalent method provides a larger probabilistic region of GSS trough.

(3) The analytical method tends to overestimate S_{max} under loess conditions, as where Xi'an Metro Line 2 is located. In contrast, the proposed gap-controlled method can accurately describe the GSS trough both in shape and magnitude.

CRediT authorship contribution statement

Gang Niu: Conceptualisation, Software, Methodology, Writing - original draft. **Shaoeng Dai:** Data curation, Investigation, Methodology. **Yunhan Wang:** Validation, Visualisation. **Haoding Xu:** Validation. **Xuzhen He:** Supervision, Writing – review and editing.

8. REFERENCES

Addenbrooke, T. I., Potts, D. M., & Puzrin, A. M. (1997). The influence of pre-failure soil stiffness on the numerical analysis of tunnel construction. *Geotechniques*, *47*(3), 693–712.

Boldini, D., Losacco, N., Bertolin, S., & Amorosi, A. (2018). Finite Element modelling of tunnelling-induced displacements on framed structures. *Tunnelling and Underground Space Technology*, *80*, 222–231. https://doi.org/10.1016/j.tust.2018.06.019

Boubou, R., Emeriault, F., & Kastner, R. (2010). Artificial neural network application for the prediction of ground surface movements induced by shield tunnelling. *Canadian Geotechnical Journal*, *47*(11), 1214–1233. https://doi.org/10.1139/T10-023

Cao, L., Chen, X., Lu, D., Zhang, D., & Su, D. (2024). Theoretical prediction of ground settlements due to shield tunneling in multi-layered soils considering process parameters. *Underground Space (New)*, *16*, 29–43. https://doi.org/10.1016/j.undsp.2023.07.007

Cao, L., Zhang, D., Fang, Q., & Yu, L. (2020). Movements of ground and existing structures induced by slurry pressure-balance tunnel boring machine (SPB TBM) tunnelling in clay. *Tunnelling and Underground Space Technology*, 97. https://doi.org/10.1016/j.tust.2019.103278

Chakeri, H., Ozcelik, Y., & Unver, B. (2013). Effects of important factors on surface settlement prediction for metro tunnel excavated by EPB. *Tunnelling and Underground Space Technology*, 36, 14–23. https://doi.org/10.1016/j.tust.2013.02.002

Chen, R. P., Li, J., Kong, L. G., & Tang, L. jun. (2013). Experimental study on face instability of shield tunnel in sand. *Tunnelling and Underground Space Technology*, *33*, 12–21. https://doi.org/10.1016/j.tust.2012.08.001

Chen, R. P., Zhang, P., Kang, X., Zhong, Z. Q., Liu, Y., & Wu, H. N. (2019). Prediction of maximum surface settlement caused by earth pressure balance (EPB) shield tunneling with ANN methods. *Soils and Foundations*, *59*(2), 284–295. https://doi.org/10.1016/j.sandf.2018.11.005

Chen, Y. L., Shen, S. L., Zhou, A., & Zeng, Y. (2024). Novel model for evaluating ground settlement risk in slurry balance shield tunnel construction. *Tunnelling and Underground Space Technology*, *150*. https://doi.org/10.1016/j.tust.2024.105853

Cheng, C. Y., Dasari, G. R., Chow, Y. K., & Leung, C. F. (2007). Finite element analysis of tunnel-soil-pile interaction using displacement controlled model. *Tunnelling and Underground Space Technology*, *22*(4), 450–466. https://doi.org/10.1016/j.tust.2006.08.002

Chi, S.-Y., Chern, J.-C., & Lin, C.-C. (2001). Optimized back-analysis for tunneling-induced ground movement using equivalent ground loss model. *Tunnelling and Underground Space Technology* (Vol. 16).

Dias, D., & Kastner, R. (2013). Movements caused by the excavation of tunnels using face pressurized shields - Analysis of monitoring and numerical modeling results. *Engineering Geology*, *152*(1), 17–25. https://doi.org/10.1016/j.enggeo.2012.10.002

Do, N. A., Dias, D., Oreste, P., & Djeran-Maigre, I. (2014). 2D Tunnel Numerical Investigation: The Influence of the Simplified Excavation Method on Tunnel Behaviour. *Geotechnical and Geological Engineering*, *32*(1), 43–58. https://doi.org/10.1007/s10706-013-9690-y

Fargnoli, V., Boldini, D., & Amorosi, A. (2013). TBM tunnelling-induced settlements in coarse-grained soils: The case of the new Milan underground line 5. *Tunnelling and Underground Space Technology*, *38*, 336–347. https://doi.org/10.1016/j.tust.2013.07.015

Fargnoli, V., Gragnano, C. G., Boldini, D., & Amorosi, A. (2015). 3D numerical modelling of soil–structure interaction during EPB tunnelling. *Geotechnique*, *65*(1), 23–37. https://doi.org/10.1680/geot.14.P.091

Feng, X., Wang, P., Liu, S., Wei, H., Miao, Y., & Bu, S. (2022). Mechanism and Law Analysis on Ground Settlement Caused by Shield Excavation of Small-Radius Curved Tunnel. *Rock Mechanics and Rock Engineering*, *55*(6), 3473–3488. https://doi.org/10.1007/s00603-022-02819-6

Franza, A., Marshall, A. M., & Zhou, B. (2019). Greenfield tunnelling in sands: The effects of soil density and relative depth. *Geotechnique*, *69*(4), 297–307. https://doi.org/10.1680/jgeot.17.P.091

Franzius, J. N., Potts, D. M., & Burland, J. B. (2005). The influence of soil anisotropy and K0 on ground surface movements resulting from tunnel excavation. *Geotechnique*, *55*(3), 189–199.

Golpasand, M. R. B., Nikudel, M. R., & Uromeihy, A. (2016). Specifying the real value of volume loss (V L) and its effect on ground settlement due to excavation of Abuzar tunnel, Tehran. *Bulletin of Engineering Geology and the Environment*, 75(2), 485–501. https://doi.org/10.1007/s10064-015-0788-8

Grammatikopoulou, A., Zdravkovic, L., & Potts, D. M. (2008). The influence of previous stress history and stress path direction on the surface settlement trough induced by tunnelling. *Geotechnique*, *58*(4), 269–281. https://doi.org/10.1680/geot.2008.58.4.269Hao, D., Zhu, R., Wu, K., & Chen, R. (2022). Analysis of Ground Settlement Caused by Double-line TBM Tunnelling Under Existing Building. *Geotechnical and Geological Engineering*, *40*(2), 899–911. https://doi.org/10.1007/s10706-021-01934-5

Hejazi, Y., Dias, D., & Kastner, R. (2008). Impact of constitutive models on the numerical analysis of underground constructions. *Acta Geotechnica*, *3*(4), 251–258. https://doi.org/10.1007/s11440-008-0056-1

Hu, Y., Tang, H., Xu, Y., Lei, H., Zeng, P., Yao, K., & Dong, Y. (2024). Ground settlement and tunnel response due to twin-curved shield tunnelling in soft ground with small clear distance. *Journal of Rock Mechanics and Geotechnical Engineering*, *16*(8), 3122–3135. https://doi.org/10.1016/j.jrmge.2024.06.005

Huang, C., Du, H., Li, L., Ni, J., & Sun, Y. (2023). Application of tree-based methods in predicting the surface settlement arising from the tunnel excavation with large mix-shield. *Soils and Foundations*, *63*(6). https://doi.org/10.1016/j.sandf.2023.101379

Huang, H., Gong, W., Khoshnevisan, S., Juang, C. H., Zhang, D., & Wang, L. (2015). Simplified procedure for finite element analysis of the longitudinal performance of shield tunnels considering spatial soil variability in longitudinal direction. *Computers and Geotechnics*, *64*, 132–145. https://doi.org/10.1016/j.compgeo.2014.11.010

Huang, H. W., Xiao, L., Zhang, D. M., & Zhang, J. (2017). Influence of spatial variability of soil Young's modulus on tunnel convergence in soft soils. *Engineering Geology*, 228, 357–370. https://doi.org/10.1016/j.enggeo.2017.09.011

Huang, Z. K., Zhang, D. M., & Xie, X. C. (2022). A practical ANN model for predicting the excavation-induced tunnel horizontal displacement in soft soils. *Underground Space (China)*, *7*(2), 278–293. https://doi.org/10.1016/j.undsp.2021.07.009

Hussaine, S. M., & Mu, L. (2022). Intelligent Prediction of Maximum Ground Settlement Induced by EPB Shield Tunneling Using Automated Machine Learning Techniques. *Mathematics*, *10*(24). https://doi.org/10.3390/math10244637

Islam, M. S., & Iskander, M. (2021). Twin tunnelling induced ground settlements: A review. In *Tunnelling and Underground Space Technology* (Vol. 110). Elsevier Ltd. https://doi.org/10.1016/j.tust.2020.103614

Jallow, A., Ou, C. Y., & Lim, A. (2019). Three-dimensional numerical study of long-term settlement induced in shield tunneling. *Tunnelling and Underground Space Technology*, *88*, 221–236. https://doi.org/10.1016/j.tust.2019.02.021

Jin, D., Yuan, D., Ng, Y. C. H., & Pan, Y. (2022). Effect of an undercrossing tunnel excavation on an existing tunnel considering nonlinear soil-tunnel interaction. *Tunnelling and Underground Space Technology*, *130*. https://doi.org/10.1016/j.tust.2022.104571

Kim, D., Kwon, K., Pham, K., Oh, J. Y., & Choi, H. (2022). Surface settlement prediction for urban tunneling using machine learning algorithms with Bayesian optimization. *Automation in Construction*, *140*. https://doi.org/10.1016/j.autcon.2022.104331

Knothe, S. (1957). Observations of surface movements under influence of mining and their theoretical interpretation. *Proc European Conference on Ground Movement*, 210–218.

Lai, J., Zhou, H., Wang, K., Qiu, J., Wang, L., Wang, J., & Feng, Z. (2020). Shield-driven induced ground surface and Ming Dynasty city wall settlement of Xi'an metro. *Tunnelling and Underground Space Technology*, *97*. https://doi.org/10.1016/j.tust.2019.103220

Le, B. T., Nguyen, T. T. T., Divall, S., & Davies, M. C. R. (2023). A study on large volume losses induced by EBPM tunnelling in sandy soils. *Tunnelling and Underground Space Technology*, *132*. https://doi.org/10.1016/j.tust.2022.104847

Lee, K. M., Rowe, R. K., & Lo, K. Y. (1992). Subsidence owing to tunnelling. I. Estimating the gap parameter. *Can. Geotech. J.*, 29(6), 929–940.

Li, C., Zhong, Z., He, G., & Liu, X. (2019). Response of the ground and adjacent end-bearing piles due to side-by-side twin tunnelling in compound rock strata. *Tunnelling and Underground Space Technology*, *89*, 91–108. https://doi.org/10.1016/j.tust.2019.03.018

Lin, Q., Tian, Y., Lu, D., Gong, Q., Du, X., & Gao, Z. (2021). A prediction method of ground volume loss variation with depth induced by tunnel excavation. *Acta Geotechnica*, *16*(11), 3689–3707. https://doi.org/10.1007/s11440-021-01295-6

Ling, X., Kong, X., Tang, L., Zhao, Y., Tang, W., & Zhang, Y. (2022). Predicting earth pressure balance (EPB) shield tunneling-induced ground settlement in compound strata using random forest. *Transportation Geotechnics*, *35*. https://doi.org/10.1016/j.trgeo.2022.100771

Liu, L., Zhou, W., & Gutierrez, M. (2022). Effectiveness of predicting tunneling-induced ground settlements using machine learning methods with small datasets. *Journal of Rock Mechanics and Geotechnical Engineering*, *14*(4), 1028–1041. https://doi.org/10.1016/j.jrmge.2021.08.018

Loganathan, B. N., & Poulos, H. G. (1998). Analytical prediction for tunneling-induced ground movements in clays. *Geotech. Geoenviron. Eng.*, *124*(9), 846.

Losacco, N., & Viggiani, G. M. B. (2019). Class A prediction of mechanised tunnelling in Rome. *Tunnelling and Underground Space Technology*, *87*, 160–173. https://doi.org/10.1016/j.tust.2019.02.020

Ma, M., Liu, W., Qian, C., Deng, G., & Li, Y. (2016). Study of the train-induced vibration impact on a historic Bell Tower above two spatially overlapping metro lines. *Soil Dynamics and Earthquake Engineering*, *81*, 58–74. https://doi.org/10.1016/j.soildyn.2015.11.007

Ma, S., Liu, Y., Lv, X., Shao, Y., & Feng, Y. (2018). Settlement and Load Transfer Mechanism of Pipeline Due to Twin Stacked Tunneling with Different Construction Sequences. *KSCE Journal of Civil Engineering*, *22*(10), 3810–3817. https://doi.org/10.1007/s12205-018-0302-5

Mahmoodzadeh, A., Mohammadi, M., Daraei, A., Farid Hama Ali, H., Kameran Al-Salihi, N., & Mohammed Dler Omer, R. (2020). Forecasting maximum surface settlement caused by urban tunneling. *Automation in Construction*, *120*. https://doi.org/10.1016/j.autcon.2020.103375

Migliazza, M., Chiorboli, M., & Giani, G. P. (2009). Comparison of analytical method, 3D finite element model with experimental subsidence measurements resulting from the extension of the Milan underground. *Computers and Geotechnics*, *36*(1–2), 113–124. https://doi.org/10.1016/j.compgeo.2008.03.005

Miliziano, S., & de Lillis, A. (2019). Predicted and observed settlements induced by the mechanized tunnel excavation of metro line C near S. Giovanni station in Rome. *Tunnelling and Underground Space Technology*, *86*, 236–246. https://doi.org/10.1016/j.tust.2019.01.022

Miro, S., König, M., Hartmann, D., & Schanz, T. (2015). A probabilistic analysis of subsoil parameters uncertainty impacts on tunnel-induced ground movements with a back-analysis study. *Computers and Geotechnics*, *68*, 38–53. https://doi.org/10.1016/j.compgeo.2015.03.012

Moghaddasi, M. R., & Noorian-Bidgoli, M. (2018). ICA-ANN, ANN and multiple regression models for prediction of surface settlement caused by tunneling. *Tunnelling and Underground Space Technology*, *79*, 197–209. https://doi.org/10.1016/j.tust.2018.04.016

Möller, S. C., & Vermeer, P. A. (2008). On numerical simulation of tunnel installation. *Tunnelling and Underground Space Technology*, *23*(4), 461–475. https://doi.org/10.1016/j.tust.2007.08.004

Niu, G., He, X., Xu, H., & Dai, S. (2023). Tunnelling-induced ground surface settlement: A comprehensive review with particular attention to artificial intelligence technologies. *Natural Hazards Research*. https://doi.org/10.1016/j.nhres.2023.11.002

Noubissi, C., Taherzadeh, R., Puel, G., & Lopez-Caballero, F. (2024). An Optimized methodology of back-analysis and sensitivity analysis for the settlement evaluation: Case study on a TBM on the Metro Line 12 extension in the Paris region. In *Computers and Geotechnics* (Vol. 167). Elsevier Ltd. https://doi.org/10.1016/j.compgeo.2023.106043

Paraskevopoulou, C., & Diederichs, M. (2018). Analysis of time-dependent deformation in tunnels using the Convergence-Confinement Method. *Tunnelling and Underground Space Technology*, *71*, 62–80. https://doi.org/10.1016/j.tust.2017.07.001

Park, K. H. (2005). Analytical solution for tunnelling-induced ground movement in clays. *Tunnelling and Underground Space Technology*, *20*(3), 249–261. https://doi.org/10.1016/j.tust.2004.08.009

Peck, R. B. (1969). Deep excavations and tunneling in soft ground. *Proceedings of the 7th International Conference on Soil Mechanics and Foundation Engineering*, 225–290.

Peng, J. bing, Huang, Q. bing, Hu, Z. ping, Wang, M. xiao, Li, T., Men, Y. ming, & Fan, W. (2017). A proposed solution to the ground fissure encountered in urban metro construction in Xi'an, China. *Tunnelling and Underground Space Technology*, *61*, 12–25. https://doi.org/10.1016/j.tust.2016.09.002

Pourtaghi, A., & Lotfollahi-Yaghin, M. A. (2012). Wavenet ability assessment in comparison to ANN for predicting the maximum surface settlement caused by tunneling. *Tunnelling and Underground Space Technology*, *28*(1), 257–271. https://doi.org/10.1016/j.tust.2011.11.008

Rowe, R. K., Lo, K. Y., & Kack, G. J. (1983). A method of estimating surface settlement above tunnel constructed in soft ground. *Canadian Geotechnical Journal*, *20*, 11–22.

Russo, G., Corbo, A., Cavuoto, F., & Autuori, S. (2015). Artificial Ground Freezing to excavate a tunnel in sandy soil. Measurements and back analysis. *Tunnelling and Underground Space Technology*, *50*, 226–238. https://doi.org/10.1016/j.tust.2015.07.008

Santos, O. J., & Celestino, T. B. (2008). Artificial neural networks analysis of São Paulo subway tunnel settlement data. *Tunnelling and Underground Space Technology*, *23*(5), 481–491. https://doi.org/10.1016/j.tust.2007.07.002

Shahin, H. M., Nakai, T., & Okuno, T. (2019). Numerical study on 3D effect and practical design in shield tunneling. *Underground Space (China)*, *4*(3), 201–209. https://doi.org/10.1016/j.undsp.2019.01.002

Shahin, H. M., Nakai, T., Zhang, F., Kikumoto, M., & Nakahara, E. (2011). Behavior of ground and response of existing foundation due to tunneling. *Soils and Foundations*, *51*(3), 395–409.

Shen, S. L., Elbaz, K., Shaban, W. M., & Zhou, A. (2022). Real-time prediction of shield moving trajectory during tunnelling. *Acta Geotechnica*, *17*(4), 1533–1549. https://doi.org/10.1007/s11440-022-01461-4

Shen, S. L., Wu, H. N., Cui, Y. J., & Yin, Z. Y. (2014). Long-term settlement behaviour of metro tunnels in the soft deposits of Shanghai. *Tunnelling and Underground Space Technology*, *40*, 309–323. https://doi.org/10.1016/j.tust.2013.10.013

Shiau, J., & Sams, M. (2019). Relating volume loss and greenfield settlement. *Tunnelling and Underground Space Technology*, *83*, 145–152. https://doi.org/10.1016/j.tust.2018.09.041

Song, X., Wu, H. N., Meng, F. Y., Chen, R. P., & Cheng, H. Z. (2023). Soil arching evolution caused by shield tunneling in deep saturated ground. *Transportation Geotechnics*, *40*. https://doi.org/10.1016/j.trgeo.2023.100966

Tang, L., & Na, S. H. (2021). Comparison of machine learning methods for ground settlement prediction with different tunneling datasets. *Journal of Rock Mechanics and Geotechnical Engineering*, *13*(6), 1274–1289. https://doi.org/10.1016/j.jrmge.2021.08.006Verruijt, A., & Booker, J. R. (1996). *Surface settlements due to deformation of a tunnel in an elastic half plane*.

Vu, M. N., Broere, W., & Bosch, J. (2016). Volume loss in shallow tunnelling. *Tunnelling and Underground Space Technology*, 59, 77–90. https://doi.org/10.1016/j.tust.2016.06.011

Wu, H. N., Shen, S. L., Chen, R. P., & Zhou, A. (2020). Three-dimensional numerical modelling on localised leakage in segmental lining of shield tunnels. *Computers and Geotechnics*, *122*. https://doi.org/10.1016/j.compgeo.2020.103549

Xie, X., Tian, H., Zhou, B., & Li, K. (2021). The life-cycle development and cause analysis of large diameter shield tunnel convergence in soft soil area. *Tunnelling and Underground Space Technology*, *107*. https://doi.org/10.1016/j.tust.2020.103680

Yan, T., Shen, S. L., & Zhou, A. (2023). GFII: A new index to identify geological features during shield tunnelling. *Tunnelling and Underground Space Technology*, *142*. https://doi.org/10.1016/j.tust.2023.105440

Yang, W., Zheng, J., Zhang, R., & Liu, H. (2021). An empirical model for characterizing 3D deformation at the face of shield tunnel in soft clay. *Tunnelling and Underground Space Technology*, 112. https://doi.org/10.1016/j.tust.2021.103862

Yang, W., Zheng, J., Zhang, R., & Liu, H. (2022). An analytical method for predicting equivalent gap parameter induced by 3D deformation at the face of shield tunnel in soft clay. *Tunnelling and Underground Space Technology*, 130. https://doi.org/10.1016/j.tust.2022.104736

Zakhem, A. M., & El Naggar, H. (2019). Effect of the constitutive material model employed on predictions of the behaviour of earth pressure balance (EPB) shield-driven tunnels. *Transportation Geotechnics*, *21*. https://doi.org/10.1016/j.trgeo.2019.100264

Zareifard, Mohammad Reza. (2019). Ground response curve of deep circular tunnel in rock mass exhibiting Hoek–Brown strain-softening behaviour considering the dead weight loading. *European Journal of Environmental and Civil Engineering*, 1–31.

Zhang, J. Z., Huang, H. W., Zhang, D. M., Zhou, M. L., Tang, C., & Liu, D. J. (2021). Effect of ground surface surcharge on deformational performance of tunnel in spatially variable soil. *Computers and Geotechnics*, *136*. https://doi.org/10.1016/j.compgeo.2021.104229

Zhang, J., Phoon, K. K., Zhang, D., Huang, H., & Tang, C. (2021). Deep learning-based evaluation of factor of safety with confidence interval for tunnel deformation in spatially variable soil. *Journal of Rock Mechanics and Geotechnical Engineering*, 13(6), 1358–1367. https://doi.org/10.1016/j.jrmge.2021.09.001

Zhang, K., Lyu, H. M., Shen, S. L., Zhou, A., & Yin, Z. Y. (2020). Evolutionary hybrid neural network approach to predict shield tunneling-induced ground settlements. *Tunnelling and Underground Space Technology*, *106*. https://doi.org/10.1016/j.tust.2020.103594

Zhang, P., Wu, H. N., Chen, R. P., Dai, T., Meng, F. Y., & Wang, H. B. (2020). A critical evaluation of machine learning and deep learning in shield-ground interaction prediction. *Tunnelling and Underground Space Technology*, *106*. https://doi.org/10.1016/j.tust.2020.103593

Zhang, P., Wu, H. N., Chen, R. P., & Chan, T. H. T. (2020). Hybrid meta-heuristic and machine learning algorithms for tunneling-induced settlement prediction: A comparative study. *Tunnelling and Underground Space Technology*, *99*. https://doi.org/10.1016/j.tust.2020.103383

Zhang, Z., & Huang, M. (2012). Boundary element model for analysis of the mechanical behavior of existing pipelines subjected to tunneling-induced deformations. *Computers and Geotechnics*, *46*, 93–103. https://doi.org/10.1016/j.compgeo.2012.06.001

Zhang, Z., Huang, M., & Zhang, M. (2011). Theoretical prediction of ground movements induced by tunnelling in multi-layered soils. *Tunnelling and Underground Space Technology*, *26*(2), 345–355. https://doi.org/10.1016/j.tust.2010.11.005

Zhong, Z., Li, C., Liu, X., Fan, Y., & Liang, N. (2021). Analysis of ground surface settlement induced by the construction of mechanized twin tunnels in soil-rock mass mixed ground. *Tunnelling and Underground Space Technology*, *110*. https://doi.org/10.1016/j.tust.2020.103746

Zhou, J., Qi, H., Peng, K., Zhang, Y., & Khandelwal, M. (2024). Comprehensive review and future perspectives on prediction and mitigation of tunnel-induced ground settlement: A bibliometric analysis and methodological overview (2002–2022). *Tunnelling and Underground Space Technology*, *154*. https://doi.org/10.1016/j.tust.2024.106081

Zhu, B., Zhang, P., Lei, M., Wang, L., Gong, L., Gong, C., & Chen, F. (2023). Improved analytical solution for ground movements induced by circular tunnel excavation based on ground loss correction. *Tunnelling and Underground Space Technology*, *131*. https://doi.org/10.1016/j.tust.2022.104811

Zhu, C., & Li, N. (2017). Prediction and analysis of surface settlement due to shield tunneling for Xi'an Metro. *Canadian Geotechnical Journal*, *54*(4), 529–546. https://mc06.manuscriptcentral.com/cgj-pubs

CHADWICK GEOTECHNICS

Chadwick Geotechnics is a leading supplier of testing, drilling and engineering services to the Geotechnical, Civil and Environmental disciplines across Australia and throughout the Asia Pacific region.

Key capabilities include:

Field Engineering

- Construction Engineering Services
- Logging
- Factual Investigations & Reporting
- Earthworks Supervision (including Level 1)

Laboratory

- NATA Accredited
- Construction Materials Testing
- Triaxial and Consolidation Testing
- Thermal Resistivity Testing
- Remote Laboratory Establishment

Drilling

- Sonic/Solid/Percussion/Direct Push
- Geotechnical and Environmental Systems
- NDD (Non Destructive Digging)

Instrumentation

- Supply
- Installation
- Monitoring

Think Act Be Safe

bsi. AS/NZS 4801:2001 Occupational Health and Safety Management

Engineering • Laboratory • Drilling • Instrumentation

Head Office and VIC Laboratory: Melbourne QLD Laboratory: Sunshine Coast

www.chadwickgeotechnics.com.au | info@chadwickgeotechnics.com.au

BLACK
INSITU TESTING

GEOTECHNICAL TESTING SPECIALISTS

BLACK INSITU TESTING WAS FORMED IN 2008 AS A SPECIALISED CONE PENETRATION TESTING COMPANY.

The company founders are experienced geotechnical engineers who were motivated to create Black Insitu Testing by recognising a need for high quality CPT tests to aid accurate and economic geotechnical investigations.

In addition to CPT, we provide an extensive range of other insitu testing and soil sampling services. We have 9 CPT rigs that can access a wide range of site conditions.

Detailed information on our testing services and CPT rigs is available on our website

www.blackinsitutesting.com.au

TERRATEST

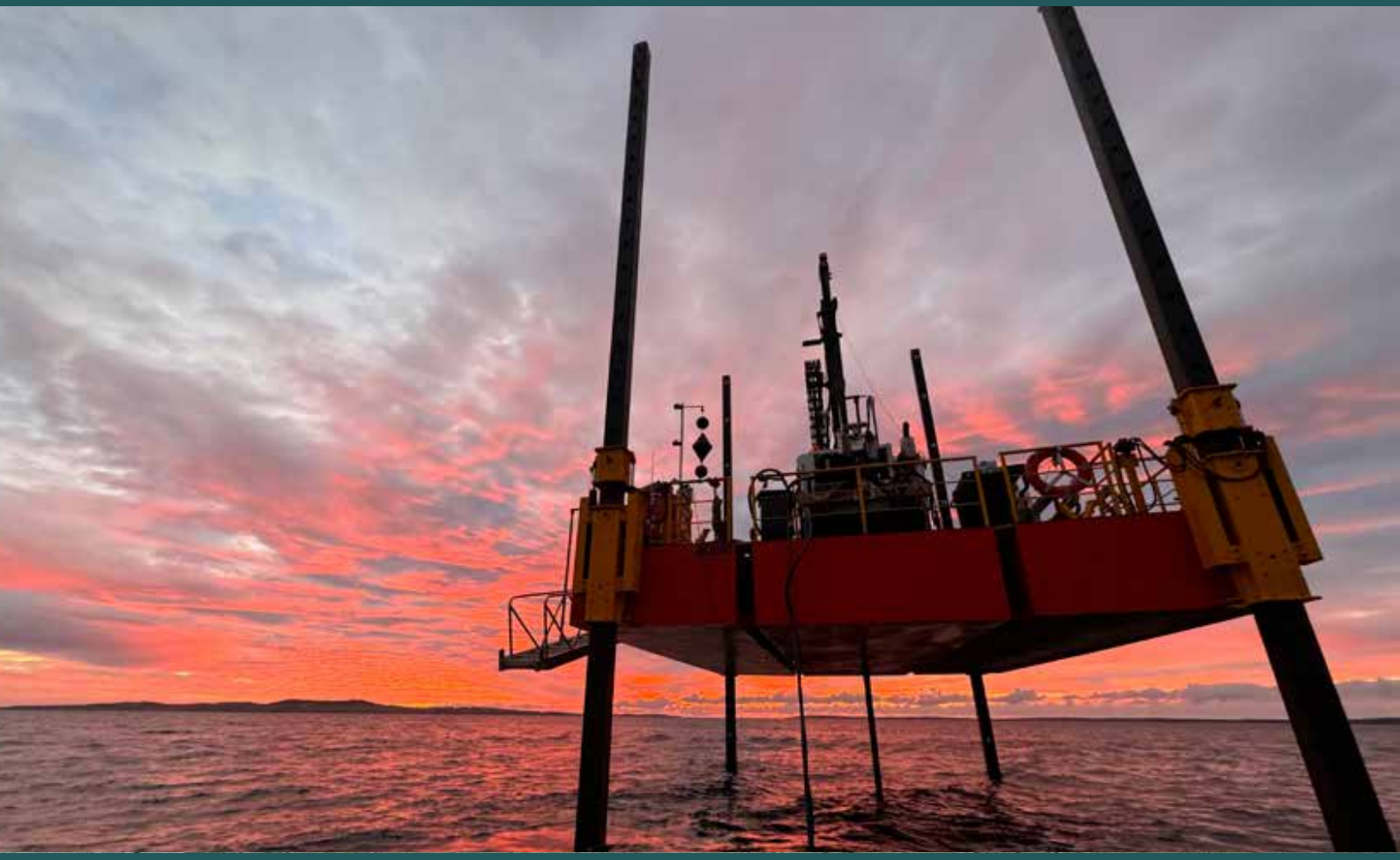

SITE INVESTIGATION DRILLERS

From the pint-sized XC to our powerful Sonic rig - from Queensland, Newcastle, Sydney, Melbourne and now Adelaide, Terratest has the tools to get the job done and the staff to ensure it's done safely.

Sydney

Simon Hamilton
E: simon@terratest.com.au
M: 0412 496 672

Newcastle

Tom Pilbro
E: tom@terratest.com.au
M: 0413 185 700

Queensland

Dave Coleman
E: dave@terratest.com.au
M: 0429 987 271

Victoria & South Australia

Simon Morris
E: smorris@terratest.com.au
M: 0429 199 445

Sonic

Simon Hamilton
E: simon@terratest.com.au
M: 0412 496 672

Environmental

Simon Hamilton
E: simon@terratest.com.au
M: 0412 496 672

terratest.com.au
1300 884 198

SUPPORT OF 26M HIGH SAND BACKFILL USING A ROCK PILLAR AND STRUCTURAL PROPS

Dino Sarac and Zhendong Li
Bechtel Australia, Brisbane, Australia. Fluor Corporation, Farnborough, UK (formerly Bechtel)

https://doi.org/10.56295/AGJ6114

ABSTRACT

Excavation of a deep underground station required support of high and narrow sand backfill that was placed by others during earlier construction of an adjacent 26m deep basement. The sand backfill was supported by a complex retaining system including a rock pillar and two levels of props. This paper describes design of the support system, monitoring results, retaining system operation and dismantling of the props.

The design employed a number of design methodologies developed from first principles including application of three methods for calculation of earth pressure from narrow sand backfill, using beam analogy for preliminary calculations of stresses in the rock pillar and of prop force, design criteria for assessment of stresses in the rock pillar and analyses of potential influence of temperature changes on prop forces and the rock pillar stresses. Construction and operation of the retaining system included systems for movement monitoring and prop force monitoring. The paper describes how monitoring results confirmed adequacy of design methodologies and enabled flexible operation of the retaining system when needed, such as more frequent adjustments of prop forces which was required due to higher than assumed degree of prop restraint. Dismantling of the propping system included its modification to suit construction methodology of the Station while monitoring results during that stage further indicated agreement with design assumptions.

1 INTRODUCTION

Construction of the deep underground stations for a transportation network involved vertical excavations to depths between 20m and 40m with a large proportion of the excavations in massive moderately weathered rock not requiring ground support, except in surficial soils and completely weathered rock, or when cavities were encountered. This paper presents a case history of a retaining system that was required due to the excavation proximity to sand backfill of a deep basement.

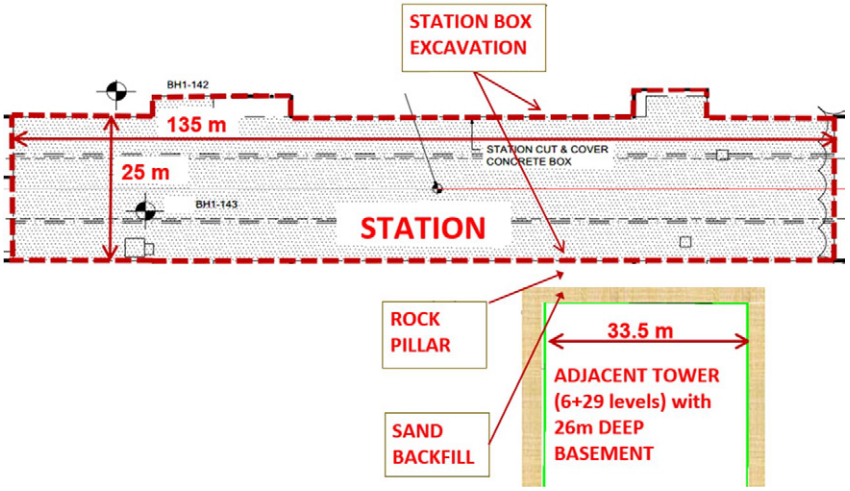

Figure 1: Layout (not to scale) – Station excavation, adjacent tower, sand backfill and rock pillar

Figures 1 and 2 present the excavation layout, location of the adjacent building with 6 basement levels and 29 level tower, sand backfill around the basement and a rock pillar between the excavation of the station main box and the sand. The excavation was 29m deep, depth of the sand backfill was 26m, sand width was 2.8m, and the width of the rock pillar formed by the excavation was 4.3m.

A temporary traffic deck for diversion of a major road extended over the edge of the excavation. The deck was supported on king posts within the station footprint installed as soldier piles before the excavation, and on strip footings and piles in the rock pillar, outside of the excavation. A pressurized 800mm potable water pipe ran all along the excavation and

presented additional risk to the stability. A slotted drainage pipe was installed around the basement before the sand was backfilled; the pipe drained into a pumped sump in the basement.

The adopted retaining system, including 2 levels of props spaced 10m vertically and between 5m and 7m centres horizontally (to avoid clash with the king posts), is shown on sketches and photos in Figures 2, 3 and 4.

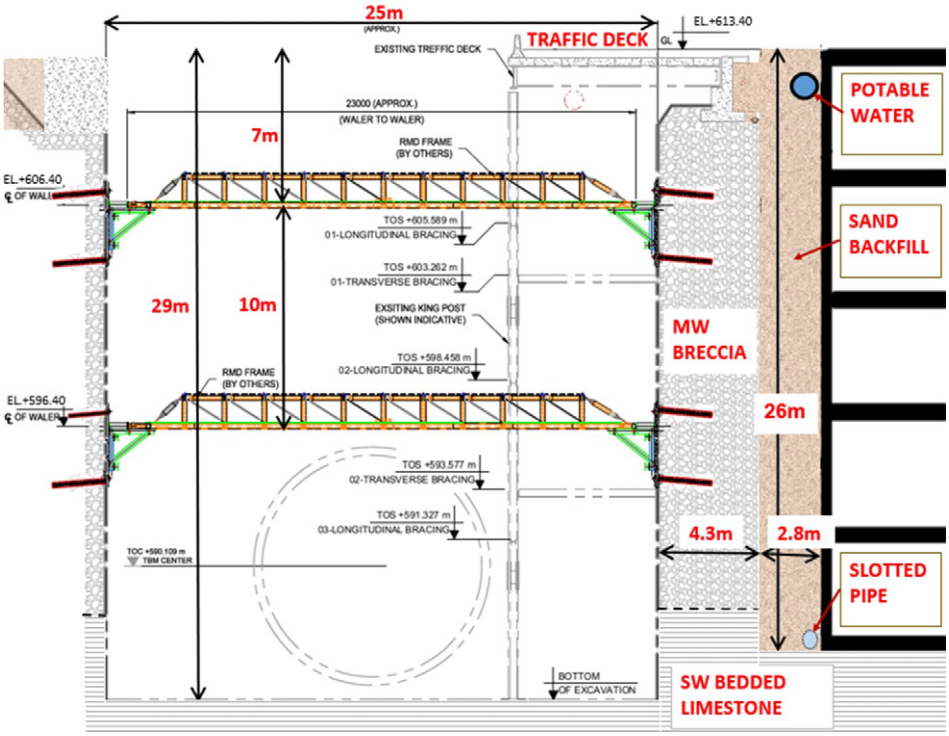

Figure 2: Excavation cross-section (not to scale)

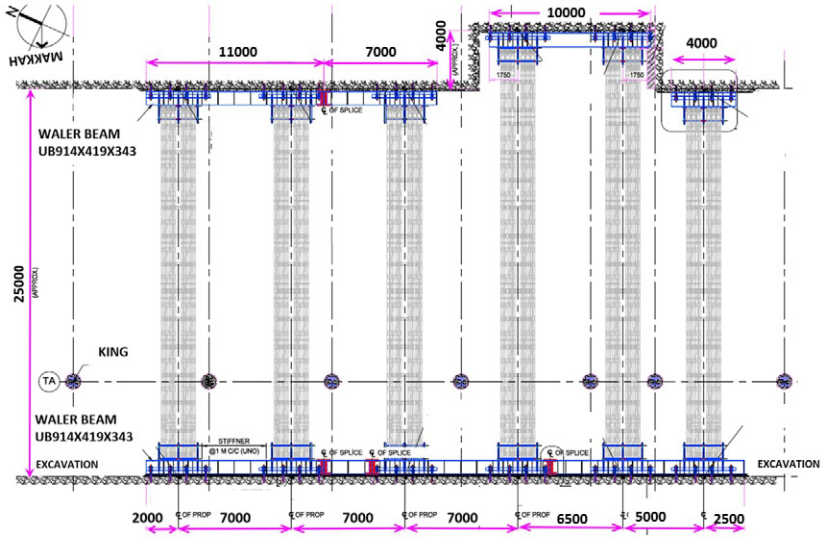

Figure 3: Layout was the same for upper and lower props (not to scale)

2 SUPPORT OF EXCAVATION OPTIONS

At the time when the design was prepared, behaviour of deep excavations along the transportation network was already well understood from other deep excavations in similar geological and geotechnical conditions. Vertical excavations down to depths of about 40m were self-supported, with limited remedial works required only when completely weathered zones or cavities were encountered. A typical deep station excavation is shown in Figure 5. Similar conditions were expected at the site, but the challenge was how to ensure stability of the rock pillar that would be subject to significant horizontal pressures from the backfilled sand.

Figure 4: Left – Excavation about 2m above excavation bottom; Right – base slab already casted

Figure 5: Another station excavation (30 m depth) in similar rock type (Breccia Limestone) and quality

A design of the support of excavation, that was provided by the project's design consultant, required the backfilled sand to be improved by jet grouting with intent to reduce sand gravity pressures on the rock pillar (with no allowance for any additional support of the rock pillar). However, there were major difficulties in implementing this solution including availability of suitably qualified contractors and equipment, high risk of damage to the basement and its water proofing, location of the potable water pipe which could obstruct drilling for the jet grouting, requirement to partially close traffic during the jet grouting and potential to increase horizontal pressures in the sand impacting the basement structure and stability of the rock pillar. Eventually, the jet grouting option was dismissed by project's geotechnical and construction teams due to the risk and unavailability of specialist contractors. At that time, the project's design consultant also provided a recommendation that propping of the rock pillar would be feasible.

Another option used in similar conditions for some shallower excavations was to fully excavate both sand and rock pillar, and expose the basement during construction of the station box. Although this would be much simpler than using props, it could not be implemented because of lack of information about the adjacent tower's structural design. Exposing one basement side would result in an unbalanced load on the tower due to sand pressure from the opposite basement side. It was anticipated that the friction on the sides of the basement and the base would be sufficient to resist the unbalanced force, but full structural assessment of the building structural system and its elements was also required, which was not feasible without detailed knowledge of the building. There was an additional risk of objections by the building owner that could not be quantified. This option would also require changes to traffic diversion plans and redesign of the traffic deck. Overall, this option was also dismissed by the project team.

Finally, it was decided to prop the rock pillar to ensure its stability, to enable uninterrupted traffic flow over the traffic deck, and to protect the adjacent structure. The retaining system design was prepared by the project geotechnical team.

3 GEOTECHNICAL MODEL, ROCK AND SAND PROPERTIES

No boreholes were available through the rock pillar before the excavation. The design relied on 3 boreholes that were drilled at between 60m and 200m distance, and on material properties adopted for geotechnical units that were project-wide, not site specific. Observations of rock exposures during early excavation stages assisted with confirmation of the initial material property assessments, which were further verified by engineering geology mapping as the excavation progressed.

A discussion of broader geological setting and these geological units is outside scope of this paper which is limited to properties relevant for the behaviour of the retaining system at the site. The subsurface conditions in the nearby boreholes indicated 2m to 3m of non-engineered fill overlying Breccia Limestone, to depths between 20m and 23m, over Bedded Limestone.

The Breccia Limestone was mostly cluster dominated, massive without discontinuities, moderately to slightly weathered (MW/SW) and medium strong. Poorly cemented, matrix dominated Breccia, would occur at random in limited extent, and was of low strength. The Bedded Limestone was horizontally bedded, typically without other discontinuities, slightly weathered (SW) and medium strong. From the findings in nearby boreholes, the contact between Breccia and Disturbed Limestone was expected to be close above the bottom of the rock pillar (26 m).

The encountered Breccia is shown in Figure 6. The excavated rock face exposes rock breaker traces and no noticeable fractures. Left image shows weak rock encountered in a very limited zone close to the surface; right image shows markings for anchor drilling to support prop brackets

Figure 6: Breccia Limestone

Groundwater level was measured in the 3 boreholes about 11m below the ground surface during the investigation (about 15m above the bottom of the rock pillar). The slotted drainage pipe at the bottom of the sand backfill (the basement drainage) was expected to fully drain the water and prevent saturation of the sand. To ensure no water pressure on the rock pillar, weep holes were additionally drilled through the rock pillar to drain any water from the sand. Therefore, no water pressure was taken into account for assessment of the rock pillar stability, its stresses and prop forces. No groundwater was encountered during drilling of the drainage holes nor drained through the holes into the excavation during the station construction.

Table 1 presents rock geotechnical properties based on the rock characterization that was carried out project wide by project's geotechnical consultant.

Hoek-Brown strength criterion (1997) was further used to develop and adopt rock mass properties for calculations and modelling in Table 2. Based on the excavation method using the rock breakers, and appearance of excavated surfaces, disturbance was considered to be minimal and Disturbance Factor D, Hoek et al. (2002), was assumed to be zero.

Potential bedding planes in the Bedded Limestone were assumed to be horizontal, have reduced shear strength and no tensile strength. Friction angle of 25° and zero cohesion were adopted according to suggestions by Barton and Choubey (1997) for a smooth rock joint.

For the sand backfill, average properties for loose sand were adopted: unit weight of 17kN/m^3, zero cohesion and friction angle of 30°.

Table 1: Adopted rock geotechnical properties

Parameter	Geotechnical Unit		Comment
	Breccia Limestone	Bedded Limestone	
Unit Weight, γ (kN/m3)	24	24	- median laboratory value(1) - 25th percentile value from gamma logging(1)
Intact Rock UCS, σ_{ci} (MPa)	15	20	- 10th percentile value was 14MPa for Breccia and 23MPa for Bedded Limestone (from UCS laboratory testing(1))
Geological Strength Index, *GSI*	75	75	- Estimated 75 - 90 from rock core and exposures - Adopted the lower bound value
Hoek-Brown Constant, m_i	19	10	- 19(2) is recommended by Hoek (2007) for clastic breccia and limestone, respectively.

Note: (1) Project-wide testing results.
(2) m_i value for breccias extends over a wide range, from values similar to sandstone to values used for fine grained sediments. The value adopted was considered to be representative for cluster dominated material.

Table 2: Rock mass properties

Parameter	Geotechnical Unit	
	Breccia Limestone	Bedded Limestone
Friction Angle, ϕ_m' (°)	44	46
Cohesion, c_m' (kPa)	400	600
Rock Mass UCS, σ_{cm} (MPa)	3.7	5.0
Tensile Strength, σ_{tm} (kPa)	120	300
Deformation Modulus, E_{rm} (MPa)	6000	8000

4 PRESSURE OF LIMITED WIDTH SAND

For the assessment purposes, the sand backfill width of 2.8m was adopted based on findings during drilling of 2 piles for the traffic deck support. The piles, that were 1m diameter, both encountered sand and rock during the drilling. Centres of these piles were at 2.3m distance to the basement; 0.5m was added to account for inability to accurately determine the sand width.

The lateral pressure from the sand backfill was estimated with three methods: initially a closed solution provided by Fan and Fang (2010) was used, followed by a check with limit equilibrium method of slices using SlopeW software, and finally using finite element method (FEM) and PLAXIS software.

4.1 FAN AND FANG (2010) CLOSED-FORM SOLUTION

Fan and Fang (2010) carried out parametric PLAXIS analyses for active pressure of limited width sand on basement retaining walls assuming wall translational movement. They provided a correlation between active pressure coefficient $K_{a(c)}$ for limited width of sand and $K_{a(Coulomb)}$ per Coulomb's conventional theory. The correlation was dependent on wall height/sand depth (H), sand width (b) and angle of inclination of sand zone away from the wall (β). Fan and Fang assumed that the friction angle between the basement wall and the sand was equal to the sand internal friction angle, which was also considered valid for the friction angle between the sand and the rock pillar. Their correlation is presented below and in Figure 7.

$$K_{a(c)}/K_{a(Columb)} = 0.23 + 3.11X - 3.68X^2 + 1.4X^3, where \quad (1)$$

$$0.05 < X < 0.92, \quad (2)$$

$$X = (b + H\tan(90° - \beta))/H \quad (3)$$

The rock pillar sand pressure was a special case of the above equation for vertical sand column, i.e. $\beta = 90°$:

$$X = b/H \tag{4}$$

Active pressures on the rock pillar were calculated using the above approach for the adopted backfill sand width of 2.8 m. The horizontal active pressures on the rock pillar were calculated for the friction angle between the rock pillar and the sand equal to the sand friction angle.

The active pressure horizontal force of 1017kN was obtained by integrating the horizontal active pressures.

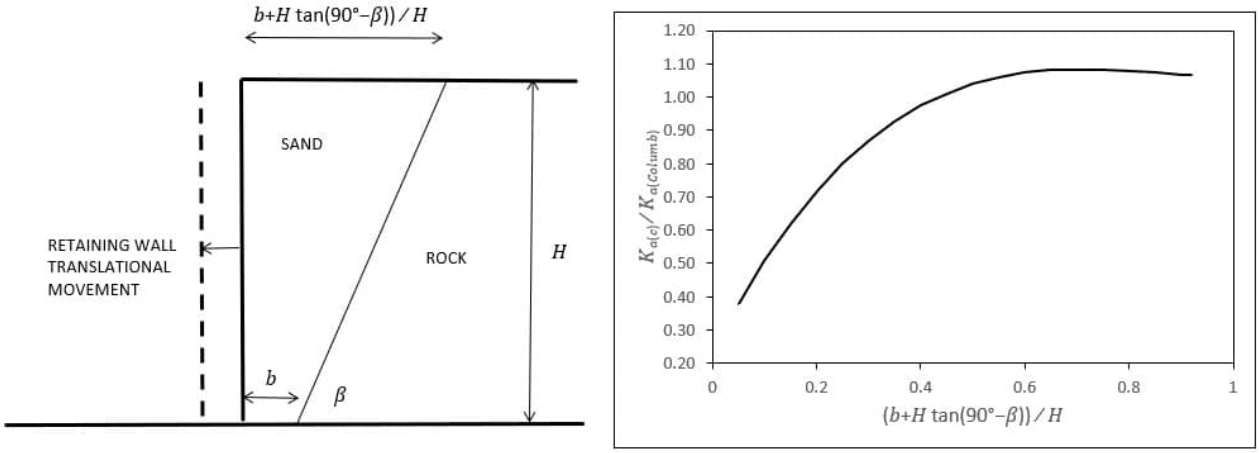

Figure 7: Active pressure coefficient for limited width sand per Fan and Fang (2010)

4.2 LIMIT EQUILIBRIUM METHOD

Bishop's method available in SlopeW program was used to check the active pressure horizontal force. Although method of slices and Bishop's method were not originally developed for calculating active pressure forces, it was considered that obtained values should be similar given that equilibrium of driving and resisting forces must be reached. An online example for SlopeW software by GEO-SLOPE International Ltd suggests a similar use of SlopeW for assessment of active and passive forces. The force was calculated by modelling the sand wedge and the active pressure force as shown in Figure 8, and by varying the force until a factor of safety of 1.0 was obtained. The force was applied at 10.4m above the bottom (about 40% of the wedge height as suggested by Fan and Fang (2010)) and at 30° angle to the horizontal, assuming friction between the rock pillar and sand of 30°. The horizontal component of the calculated force was 935kN/m. This force is about 8% lower than 1017kN obtained from the Fan and Fang solution and indicated a good agreement between the two methods.

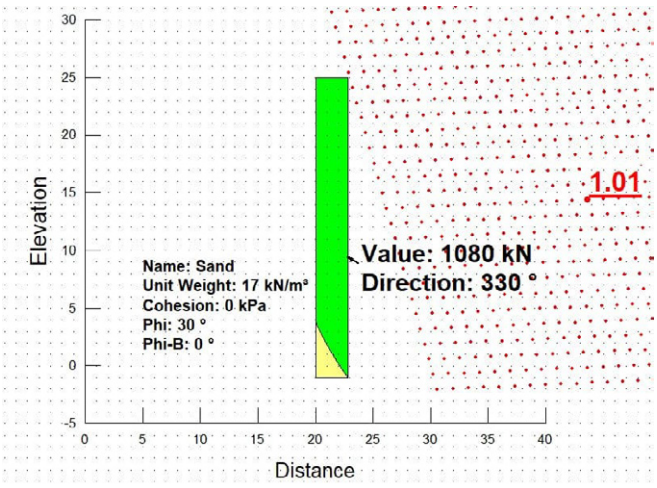

Figure 8: SlopeW model

It should be noted that SlopeW experienced numerical convergence problems for methods of slices that achieve equilibrium of both forces and moments, such as Morgenstern-Price, and that Bishop's method (only moment equilibrium satisfied) had to be used. It is likely that this was caused by a non-conventional shape of the sliding mass. This indicates

that caution should be exercised in using method of slices and SlopeW for limited width sliding mass without having an alternative method to check the results.

4.3 FINITE ELEMENT METHOD

Two-dimensional FEM analysis using PLAXIS was carried out at a later design stage to analyse the retaining system with two prop levels, and to assess temperature effects (FEM model in Figure 9). Sand pressure distribution was obtained by including interface elements and the sand pressure force was obtained by integration of the pressure. The model was run stage by stage to stimulate construction of the adjacent basement and the backfilling of the sand, after which the excavation of the station was simulated.

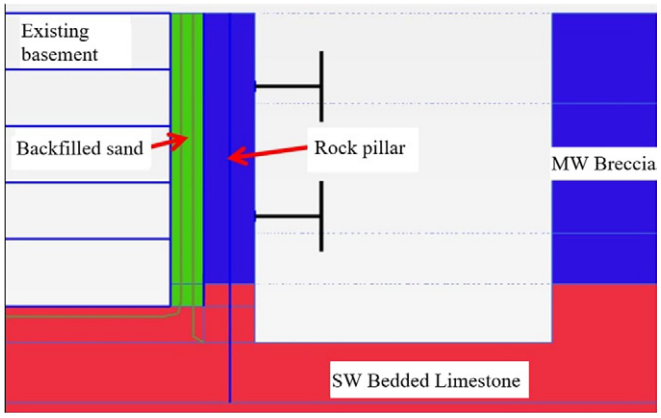

Figure 9: Finite element model

Figure 10 compares horizontal pressure at the rear side of the rock pillar from the FEM model and the pressure profile calculated with earth pressure coefficient $K_{a(c)}$ for limited width sand per Fan and Fang (2010). Coulomb's active pressure is also shown, i.e. full active pressure. The FEM and $K_{a(c)}$ pressure profiles were generally similar except at the top of the rock pillar, where FEM model produced a slightly higher lateral pressure than $K_{a(c)}$. This could be because of the relatively high stiffness of the rock pillar near the surface and incorporation of the propping system, resulting in soil pressures not fully relaxing to the active condition in the FEM model.

From the earth pressure profile in the FEM model, the corresponding total horizontal load was 1180kN/m, 16% higher than 1017kN/m based on the Fan and Fang closed-form solution. Coulomb's active pressure force for the full width sand was 1690 kN/m, 43% higher than the FEM force. If the full active force were used for the propping design, the prop capacity would have to be increased for about 40%, resulting in either larger props or increase in the number of props from 12 to 17 or 18.

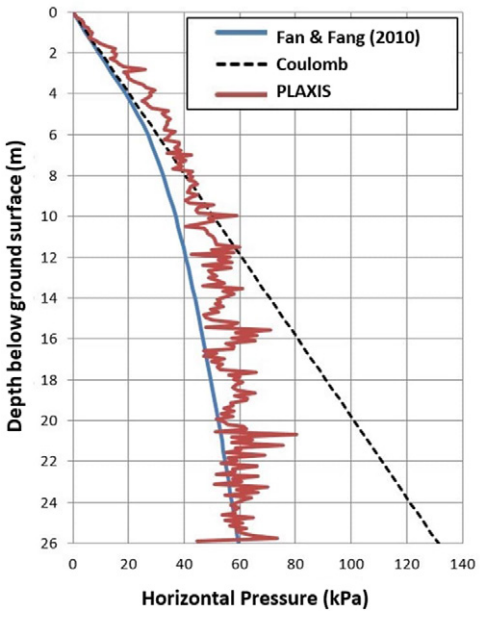

Figure 10: Comparison of sand horizontal pressures

5 ROCK PILLAR PRELIMINARY CHECKS (SIMPLE MODEL)

A preliminary assessment of the feasibility of the retaining system comprised of the rock pillar and props was carried out using an adopted beam analogy – i.e. assuming that the rock pillar is either a cantilever beam or a beam with hinged or fixed end supports, as shown in Figure 11. Soil pressures from Fan and Fang (2010) closed-form solution were then calculated as described under 4.1 and applied on the beam.

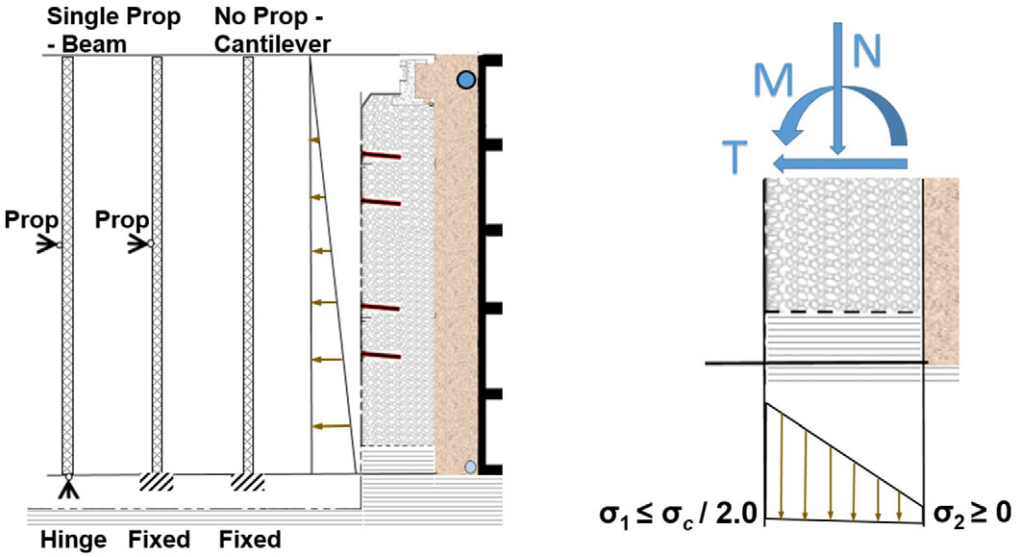

Figure 11: Rock pillar beam analogy and internal forces

A rock pillar without any propping was considered to be a cantilever which had to maintain full fixity at the base. A rock pillar with single prop was modelled as a beam supported at the prop level and at the bottom. The bottom support was expected to exhibit behaviour between hinged and fixed condition and the rock pillar was initially assessed by enveloping those 2 cases. A structural program was run to calculate beam internal forces, i.e. bending moments (M) and shear forces (T). These forces, together with vertical force (N), were used to calculate stresses in the rock mass as indicated on Figure 11. The vertical force was calculated taking into account weights (rock pillar and traffic deck) and vertical component of the sand pressure force. Beam reaction at the prop level was used to roughly estimate the propping force.

Design criteria adopted for these preliminary assessments of the rock pillar are presented in Table 3. Factors of safety were on the conservative side due to the preliminary nature of the assessment and impact on construction progress if a selected option was shown not to be feasible by later more detailed assessments. The design criteria were related to traditional structural and geotechnical approaches:

- Major stress σ_1 (compressive) was compared with rock mass uniaxial compressive strength σ_{cm}, not with intact uniaxial strength, to take into account rock mass effects.
- Factor of safety of 2.0 for the compressive stress was selected to reduce risk of cracking of the rock pillar face and was expected to maintain rock deformations mostly in the elastic range. An analogy with concrete behaviour is that stresses and strains are closely proportional when the stresses do not exceed approximately 50% of the concrete compressive strength (see Darwin et al. 2016).
- No tensile stress was allowed due to concern about ability of rock to develop tensile stresses (for example in case of presence of bedding planes) and from similar approach in design of concrete structures.
- Factor of safety of 2.0 for rock pillar shear was related to conventional factor of safety between 1.5 and 2.0 for sliding of retaining structures.

The cantilever option without any propping was dismissed due to high stresses in the rock pillar – compression of 4.1MPa and tension of 2.7MPa. This was not a surprise, given small width of the rock pillar comparing with the retained height, and that the rock pillar would essentially work as a gravity retaining wall.

For a prop at single level, compressive stresses were acceptable, of the order of 1MPa, but there was tension at the base of the rock pillar of the order of 200 kPa. This initial modelling did not include temperature effects. It was decided to proceed with FEM modelling, re-evaluate single-level prop option, and assess options with props at two levels.

Table 3: Design criteria

Condition	Failure Mode/ Location	Comparison	Criterion/ equation (1)
Rock pillar bending	Compressive stresses and cracking of compressed rock face	Major stress & Hoek-Brown (1997) uniaxial compressive strength of rock mass	$\sigma_1 \leq \sigma_{cm} \div 2.0$ (5) where $\sigma_{cm} = \sigma_{ci} s^a$ (6)
	Cracking due to tension	Minor stress – tension was conservatively not allowed although Hoek-Brown (1997) strength indicated tensile strength σ_t of 120 kPa	$\sigma_2 \geq 0$ (7)
Rock pillar shear	Mass rock (no bedding)	Shear stress in the rock pillar & rock mass shear strength using Hoek-Brown (1997) shear strength parameters	$\tau \leq (c_m' + \sigma_n \tan \varphi_m') / 2$ (8)
	Bedding planes	Shear stress on the bedding plane (bottom of rock pillar) & shear strength of smooth rock joint	$\tau \leq \sigma_n \tan 25°/2,$ (9) where σ_n is normal stress on bedding plane

Note: (1) Rock mass uniaxial compressive strength, cohesion and friction per values in Table 2.

6 TEMPERATURE EFFECTS ON SINGLE LEVEL PROPPING SYSTEM

The FEM model was used for detailed assessment of the retaining system behaviour including addressing influence of temperature changes on the retaining system. Climatic records indicated daily air temperature variation of up to 25ºC, with typical annual range between 5ºC and 50ºC. Local code for bridge design required temperature variation of 60ºC for structural design and that was included in design checks.

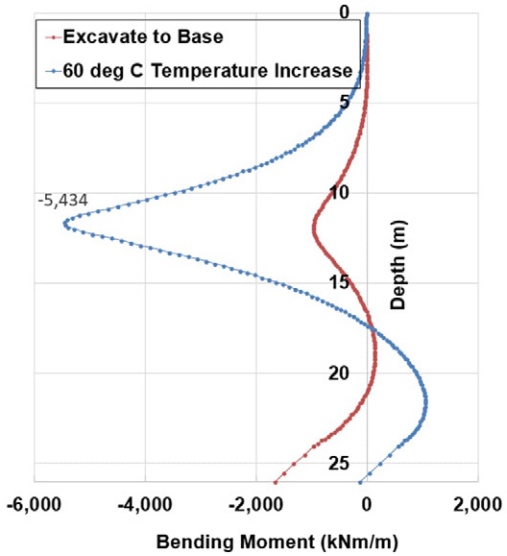

Figure 12: Rock pillar bending moment using beam analogy – single level prop at 11.5m depth

A flexible beam element was incorporated into the FEM model of the rock pillar providing bending moment and shear force distribution which enabled continued use of the beam analogy. Figure 12 presents the rock pillar bending moment for a single prop retaining system, with and without temperature effect (60ºC temperature increase).

For a prop installed at 11.5m depth, force of 670kN/m was calculated, i.e. 4020kN at 6m centres. However, potential daily temperature variation of 25ºC more than doubled this force. This analysis also indicated potentially severe effects of the temperature increase on the rock pillar performance. Major and minor stresses in the rock pillar were 530kPa and 150kPa (both compressive) following the excavation, but 1.9MPa and -1.2MPa (tension) when accounting for a temperature increase of 60 ºC. The results indicated that the large sand pressure force required very stiff props, which could further stress the rock pillar due to temperature forces, potentially resulting in fracturing of the rock and eventual "breaking" of the rock pillar.

To ensure no rock fracturing, a retaining system with 1 prop level would require automated jacks that would continuously adjust the propping force. It was not certain how much time it would require to obtain and install such system at the project location, the costs were relatively high, and there were additional concerns about ability to operate such system continuously over a longer period of time without having experienced personnel available at a short notice if troubleshooting or repairs were needed. This coupled with a general discomfort about having a single prop supporting a rock pillar of 26m height. In the end, a two-level propping option was adopted, which required less stiff props.

7 TWO LEVEL PROPPING SYSTEM

7.1 MODELLING APPROACH

Prop installation levels at 7m and 17m below ground level were selected to avoid large number of potential clashes between props and their hanging system with station permanent floors and traffic deck longitudinal and transversal bracing. There was no opportunity to optimize prop elevations due to these clashes. However, the selected prop levels were generally found to be well suited to the loading conditions.

The same structural truss was selected for both prop levels after preliminary calculation runs and some iterations due to impact of prop stiffness. The safe working load of props was 3720kN and average stiffness of the props was 50280kN/m. A steel thermal expansion coefficient of $12x10^{-6}$mm/mm/ºC was adopted. The total expansion/shrinkage for a free end 25m long steel prop, due to 60ºC temperature change, was 18mm. The load from 60ºC temperature increase assuming fully fixed ends was 5430kN. The props were assumed to have a restraint degree of 40% resulting in temperature load of 0.4x5430kN = 2172kN, or 362kN/m for props spaced at 6m spacing, for the 60ºC temperature increase. The restraint degree of 40% was assumed for design as an average value from a draft of new version of CIRIA C580 Guide (2003) which recommended 50% for stiff retaining walls in stiff soils, and 30% for flexible retaining walls in stiff soils. The 2003 Guide was later superseded by CIRIA C760 Guide (2017) which adopted the same restraint degree range as the draft.

It was decided to model temperature decrease of 40ºC, 30ºC and 20ºC by shortening of the upper prop of 12mm, 9mm and 6mm, respectively. This approach was conservative as it assumed full restraint (100%) of the prop, but it was considered necessary as stresses in the rock pillar could not be directly monitored in operation, and as there was uncertainty about the assumption of 40% prop restraint degree.

Preload force was used to control rock pillar movements and selected depending on prop installation temperature as shown in Table 4 with analyses Cases numbered 1 to 4.

Table 4: Prop Preload for prop installation temperature

Case	Installation Temperature (°C)	Preload (kN)
Case 1	0	100 (nominal)
Case 2	20	1200
Case 3	30	1800
Case 4	40	2000

Effects of temperature increase were investigated in the FEM model by increasing the axial prop force for load calculated using the change temperature, prop stiffness and the restraint factor. Temperature decrease was modelled by reducing the prop axial force to obtain the target shortening of 12mm, 9mm and 6mm. This included some iterations until the target shortening was obtained. The following example details the modelling sequence (an installation temperature of 30°C and a preload force of 1800kN):

1) Over-excavate for the basement construction,
2) Construct the basement,
3) Backfill with sand between the basement wall and basement excavation,
4) Excavate the station box to 8.0m below ground level (bgl.) to install the upper level prop,
5) Install the upper level prop at 7m bgl and preload to 1800kN,
6) Excavate the station box to 18m bgl to install the lower level prop,

7) Install the lower level prop at 17m bgl and preload to 1800kN,

8) Excavate to the final excavation level at 29m bgl,

9.1) Apply the additional axial load in the prop due to 30°C temperature rise by increasing the prop load from soil pressures, P_{soil}, to

$$P = P_{soil} + P_{temperature}\ , \tag{10}$$

where $P_{temperature}$ is 181kN/m from 30°C temperature increase, or

9.2) Continue from stage 8). Simulate temperature decrease of 30°C by reducing the axial loads in props to obtain movement of 9mm at the upper props and loss of prop load equivalent to the restraining force of 30°C in the lower prop.

7.2 ROCK PILLAR MAJOR STRESSES

The stress in the rock pillar was obtained directly from PLAXIS model. Table 4 presents all Cases analysed (4 installation temperatures), rock pillar stresses for excavation to 29m (bgl) and impact of temperature changes. The maximum compressive stresses were at the excavation face, and the tension stresses at rear/sand side, close to the bottom of the rock pillar. A subsequent numerical model run releasing the tension stresses for the case of a horizontal bedding plane presence, which would not be able to transfer tensile stress, did not result in significant increase of compressive stresses movements indicating that performance of the retaining system (rock pillar and struts) was not dependent on the ability of the rock to sustain and transfer tensile stress.

It was concluded that periodic adjustment of the jacking force would be required to control rock pillar stresses, and that these adjustments would depend on prop installation temperature and temperature changes during operation of the retaining system.

Table 5: Summary of temperature analyses

Analyses Case	Rock Pillar Stresses (1)			
	Tension	Factor of Safety	Compression	Factor of Safety
Case 1: Prop installed at 0ºC, preloaded to 100kN				
Excavate to 29m bgl	No tension	N/A	2.6MPa	1.9
60°C temperature increase	No tension	N/A	2.2MPa	2.3
Case 2: Install at 20°C, preloaded to 1200kN				
Excavate to 29m bgl	No tension	N/A	2.1MPa	2.4
Temperature increase for 40°C	No tension	N/A	1.8MPa	2.8
Temperature decrease for 20°C (6mm shortening)	122kPa	2.5	2.6MPa	1.9
Case 3: Prop installed at 30°C, preloaded to 1800kN				
Excavate to 29m bgl	No tension	N/A	2.1MPa	2.4
Temperature increase for 30°C	No tension	N/A	1.9MPa	2.6
Temperature decrease for 30°C (9mm shortening)	96kPa	3.1	2.9MPa	1.7
Case 4: Installed at 40°C, preloaded to 2000kN				
Excavate to 29m bgl	No tension	N/A	2.2MPa	2.3
Temperature increase for 20°C	No tension	N/A	2.1MPa	2.4
Temperature reduction for 40°C (12mm shortening)	218kPa	1.4	3.4MPa	1.5

Note: (1) The maximum stresses are close to the rock pillar bottom within Bedded Limestone.
The rock mass ultimate compressive strength of Bedded Limestone was 5MPa and tensile strength 300kPa, but tensile strength would be zero at bedding planes.

7.3 ROCK PILLAR SHEAR STRESS

Horizontal shear stress for checks of horizontal sliding through the rock pillar was calculated using shear force from the beam analogy for initial assessments, and later using average shear stress on horizontal plane from the FEM model (the 4 Cases from Table 5). The shear stress was compared with Hoek-Brown (1997) shear strength at the upper and lower prop levels, and assuming friction angle of 25º in Bedded Limestone at the bottom of the rock pillar. Minimum factor of safety for the 4 analysed cases varied between 2.8 and 3.4 at all locations, was considered adequate and not critical for performance of the retaining system.

7.4 MOVEMENTS TOWARDS THE EXCAVATION

Table 6 presents maximum movements of the rock pillar towards the excavation for Cases 1 to 4 (as described in Table 5). These results were compared with movement monitoring results in operation as confirmation that the rock pillar behaviour and stresses were within acceptable limits.

Table 6: Maximum rock pillar movements towards excavation (mm)

	Excavation to 26m bgl	Temperature Decrease
Case 1	9(1)	Not applicable
Case 2	5(2)	13(1)
Case 3	2(2)	14(1)
Case 4	1(2)	17(1)

Rock pillar movement pattern: (1) Rotation around bottom
(2) Roughly planar in the top 50%

8 PROPS, PROP FORCES AND FORCE MONITORING

The props had to be sized to resist both soil pressure and temperature load. The allowable axial load of the adopted truss was 3720kN. Each truss comprised six legs as shown in Figure 13.

As mentioned previously, the analyses were carried out assuming a 40% restraint degree. With this approach, the allowable prop load was exceeded only in the lower prop for Case 1 (Table 4), when there was temperature increase of 60ºC. For all other Cases, the maximum load was 3625kN in the upper prop, and 3247kN in the lower prop. Without temperature influence, the maximum load in both props was similar, about 2200kN.

The results indicated that, from perspective of allowable prop load, adjustments of prop forces in operation would not be required if the restraint degree was at about 40%, but would be required if it were higher as the prop loads were close to the allowable load.

Considering overall FEM modelling results, compressive and tension stresses in the rock pillar for cases of temperature decrease, and dependence of the prop axial force on temperature changes and degree of restraint, a jacking system was installed to enable manual control of the prop force. Each of the six truss legs had a jack, and the jacks were connected to a single pump which could apply same pressure (i.e. same force) to each jack (see Figure 13). One of the legs was fitted with a pressure cell for load monitoring, which was connected to a readout unit with a sound alarm set for cases when the allowable load was exceeded.

Shortly after upper level prop installation, a period of no advancement in excavation and variable night temperature was selected to assess degree of prop restraint by comparing theoretical load change from a ’cold’ to a ’warm’ night. The difference between the minimum measured loads during those nights was considered to reflect the temperature influence. Night temperature were selected to avoid any potential influence of sun exposure on steel temperature and prop force. The measured load change was between 60% and 80% of the fully fixed end load, i.e. the restraint degree was 60% to 80% - much higher than originally anticipated in the design.

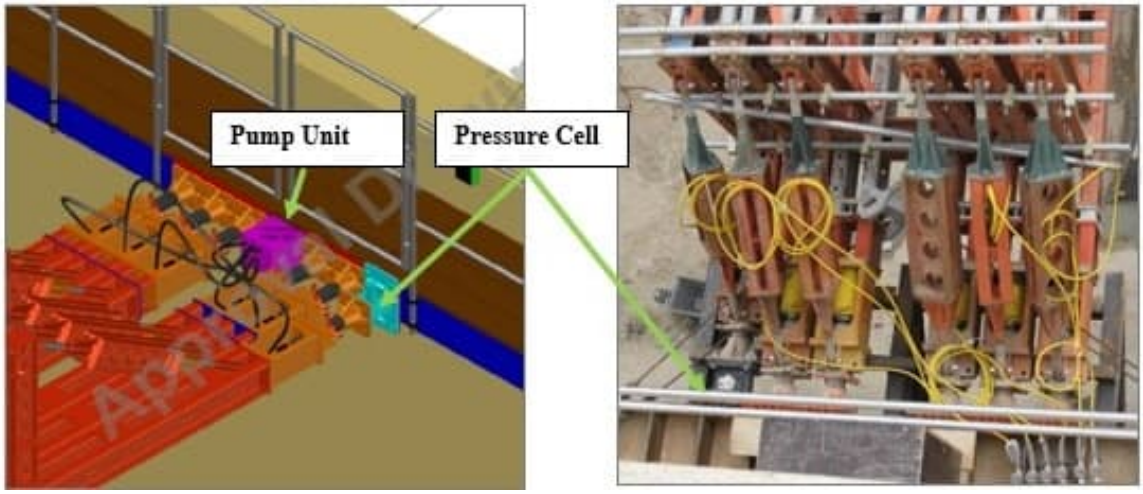

Figure 13: Props, system for load monitoring and adjustment

To account for this behaviour, the load in props was adjusted more frequently than anticipated. In general, once full excavation was reached, the load was maintained between 2100kN (close to the maximum prop load without temperature influence) and 3900kN (about 5% over the allowable prop load).

The load was adjusted 25 times over 80-week operation period, on average every three weeks. At times of abrupt weather changes, the load was adjusted within a few days following a previous adjustment. Figure 14 presents leg load (1/6 of total prop force) of an upper prop and recorded air temperature over the operation period.

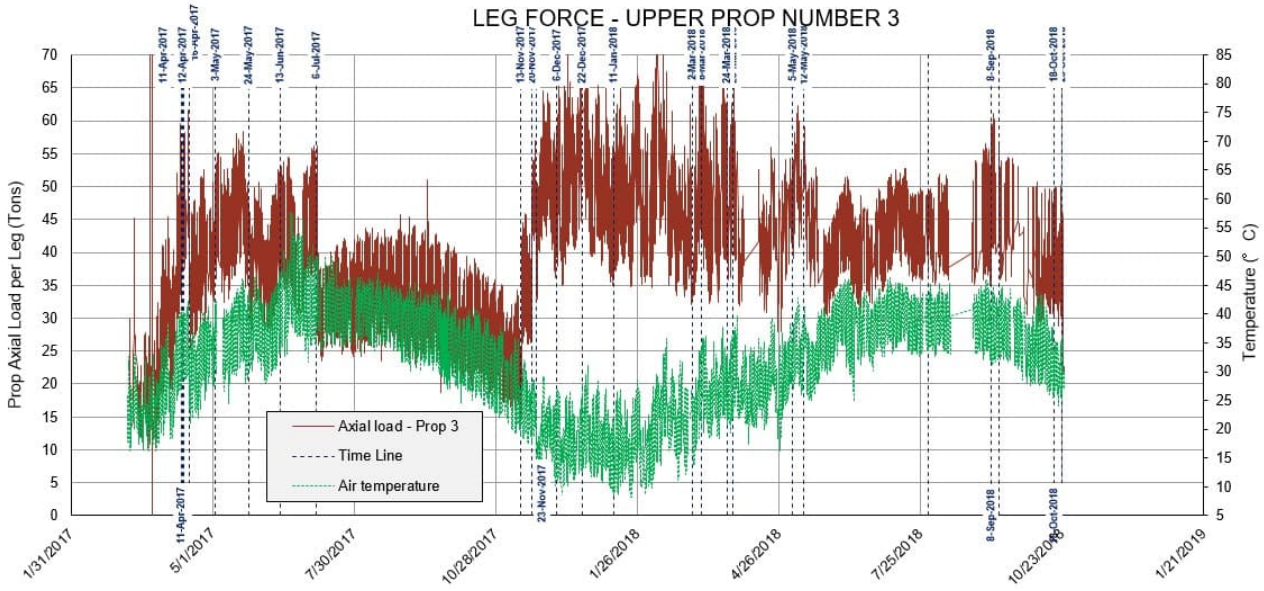

Figure 14: Prop force and air temperature

9 MOVEMENT MONITORING

Excavation movements were monitored using total stations and movement prisms mounted on excavation face. Each station excavation side (135m length x 29 m depth) had four prism rows starting from the top, spaced at 6m to 7m level difference. Each row had eight movement prisms. Some of these prisms were not available due to different obstructions during construction. Vector movements were monitored, but only horizontal movements towards the excavation were significant and are discussed further below. Position of prisms used for monitoring are indicated in Figure 15, and movements of the rock pillar are shown in Figure 16.

The maximum recorded movements of the rock pillar were in the range of 6mm to 7mm before movement monitoring had to be discontinued due to construction obstructions in May 2018. The last major increase in movements, of the order of 1mm, was observed in November 2017 which coincided with completion of the excavation but also with a significant drop in temperature when prop forces were allowed to reduce to about 1500kN. After jacking up of the prop forces, no

further movement was noticeable. These observed movements were somewhat higher than those predicted by the FEM model without temperature effects if the props were prestressed (1mm to 5mm depending on preload force), but lower than movements allowing for shortening of props due to temperature decrease (see Tables 5 and 6). Overall, the recorded movements were of the same order and close to the modelling results, confirming major assumptions of the design approach and that rock pillar stresses were within acceptable limits.

Movements of the excavation opposite side (rock mass) towards the excavation were of the order of 2 to 3mm.

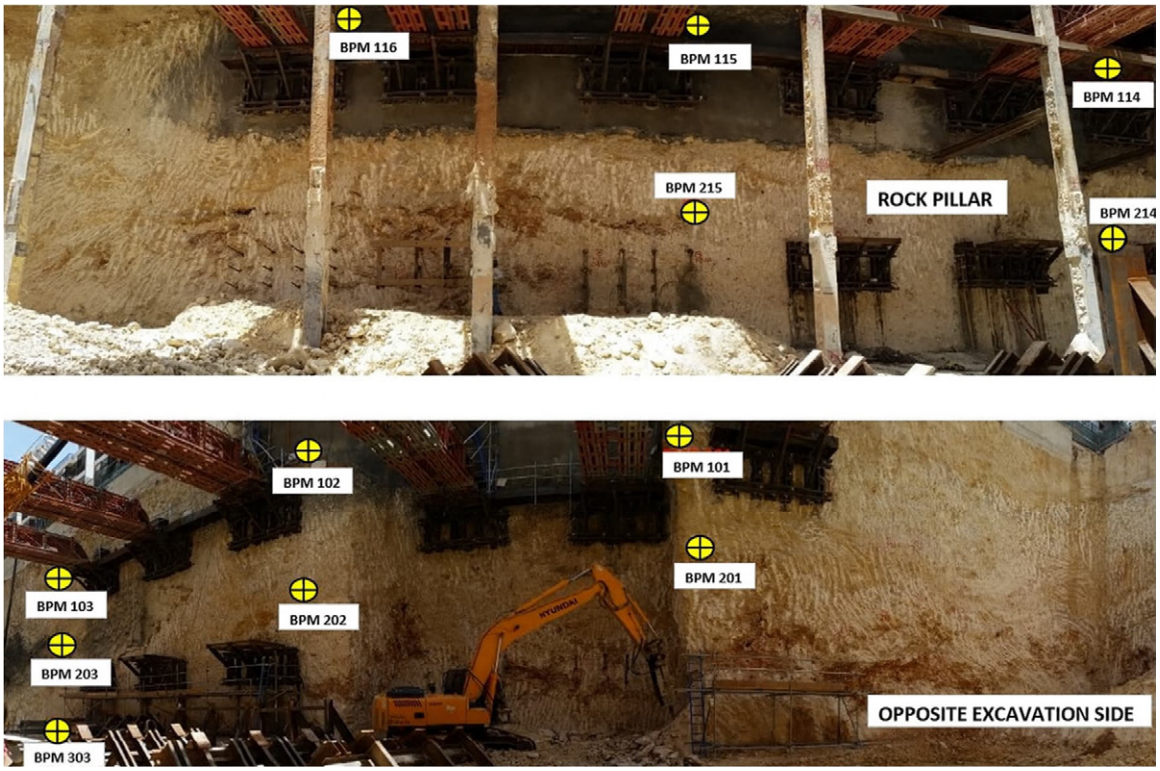

Figure 15: Monitoring prisms – rock pillar (top) and excavation opposite side (bottom) (upper props installed; brackets for support of lower props being installed)

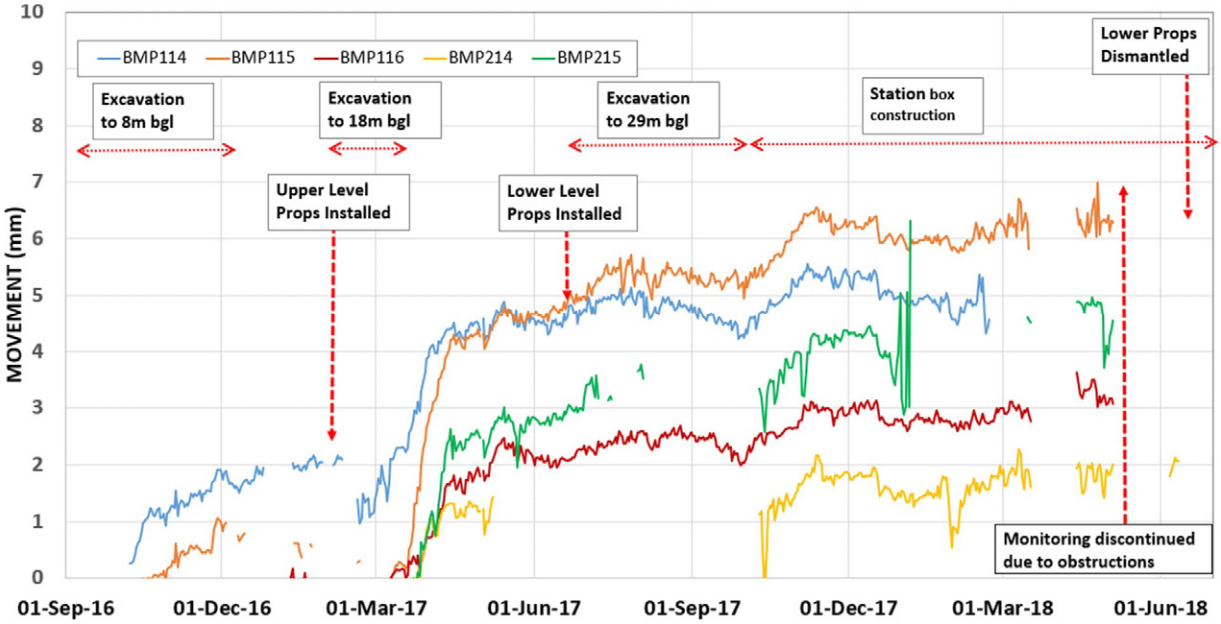

Figure 16: Movement of rock pillar prisms towards the excavation (daily median)

10 DISMANTLING OF THE PROPS

Lower props were dismantled following casting of one of the permanent slabs, which was only 300mm below the props. Unloading was carried out in a gradual manner, starting with 50% load reduction in a single prop which was maintained over 2 days. No increase of loading in the other props was observed either during this initial unloading, nor later during further reduction of load in other props. All the lower props were removed in a smooth process.

The initial plan for removal of the upper props was to cast permanent walls to the underside of the upper props, as a permanent slab was 3.4m below the props. However, this was not considered favourable by the construction team due to requirements for coupling a large number of wall reinforcement bars. Therefore, two trial reductions of prop force were carried out after casting the permanent slab, before the wall was constructed. Each trial consisted of a reduction of the prop force by about 50% in one of the props. However, during both trials, an instantaneous rise of the force was recorded in the remaining props, with the total force increase equal to the force reduction. This was a firm indication that the propping force was needed to control rock pillar behaviour and that removal of the props could lead to large deformations and potential rock pillar failure. Figure 17 includes 2 photographs at the time of the trial force reduction.

To facilitate early prop removal and the proposed construction sequence, an alternative solution with short inclined props against the permanent slab was developed as shown in Figure 17. The short inclined props were installed between a waler beam, which was part of the original system for distribution of loads between the rock pillar and props, and the penetration of the traffic deck column through the permanent slab. As the moment connection between the waler beam and the inclined prop could not be developed due to large forces, a vertical strut against the traffic deck had to be incorporated, utilizing the deck weight for reaction. This system was designed to carry a load equivalent to the prop load. Once the system was fully installed and shimmed to ensure tight connection, gradual reduction of the prop forces was carried out without any observed increase in load of props that were still in operation, and all the prop trusses were dismantled.

Figure 17: Excavation and retaining system during trial force reduction

11 CONCLUSION

The paper has outlined the design, operation, and dismantling of a retaining system consisting of a rock pillar and two levels of props, which successfully supported a 26m high sand column adjacent to critical infrastructure and an active traffic deck. The project addressed significant geotechnical and operational challenges, particularly the need to minimize risk to nearby structures and utilities.

Modelling the actual narrow sand column, validated by three independent methods, resulted in significant savings and a 40% reduction in required propping force compared to conventional approach using full sand width, demonstrating value of a design approach accounting for actual site conditions.

Three methods for assessment of the soil pressure for the narrow sand column were used: the Fan & Fang closed form solution, Bishop's limit equilibrium method of slices, and finite element method modelling. All three produced pressures of the same magnitude. Bishop's method showed satisfactory agreement with the Fan & Fang (2010) solution, differing 8% indicating that method of slices is acceptable for preliminary assessment of active pressures even in special conditions. The FEM results were 16% higher than the close-form solution, likely reflecting influence of retaining system stiffness. For the design of stiff or very stiff retaining systems, the impact of system stiffness on design stresses should therefore be considered in the design.

Assessment of stresses within the rock pillar employed both a beam analogy and FEM modelling, providing a robust basis for engineering the retaining system. The adopted design criteria for the rock pillar - limiting compressive stress to 50%

of the rock mass uniaxial compressive strength, eliminating tensile stress and limiting horizontal shear stress to 50% of the shear strength (rock mass and discontinuities where present) - were found to result in satisfactory pillar performance. Extensive FEM modelling of the influence of the temperature effects on the retaining system provided a good basis for decision making and supported the selection of a manually adjustable jacking system to control propping forces and design uncertainties.

The degree of restraint of 50%, as recommended in CIRIA C760 (2017, Guide for stiff retaining systems in soils), was found to be significantly lower than values observed and not applicable to excavations in rock. Monitoring indicated degrees of restraint of 60% to 80% with this range being recommended where props are supported by rock.

The agreement of movement and force monitoring results with predicted values, and instantaneous redistribution of the propping force into remaining props when the force was reduced in one of the props, demonstrated adequacy of the design methodologies and the FEM approach to capture interaction between the narrow sand column, the rock pillar and the props.

Finally, the use of permanent slab, traffic deck columns, and the deck provided propping action and facilitated early removal of temporary props before station walls reached the underside of the upper props. This was a practical solution adjusted to site conditions and construction staging, highlighting value of having design engineers closely involved in construction.

CRediT authorship contribution statement

Dino Sarac: Conceptualization, Formal analysis, Investigation, Methodology, Supervision, Writing – original draft, Writing - review and editing. **Zhendong Li:** Formal analysis, Investigation, Methodology, Software.

12 REFERENCES

Barton, N., and Choubey, V. (1997). The shear strength of rock joints in theory and practice. *Rock Mechanics,* 1/2, 1977, Vienna, Springer, 1-54.

Darwin, D., Dolan, C. W. and Nilson, A. H. (2016). Design of Concrete Structures. McGraw-Hill Education.

Fan, C. C. and Fang, Y. S. (2010). Numerical solution of active earth pressures on rigid retaining walls built near rock faces. *Computer and Geotechnics,* Vol 37, Issues 7-8, 1023-1029.

Gaba, A. R., Simpson, B., Powrie, W. and Beadman, D.R. (2003). Embedded retaining walls – guidance for economic design. CIRIA C580.

GEOSLOPE International Ltd. Comparison with Active and Passive Earth Pressures. *http://downloads.geo-slope.com/geostudioresources/examples/8/14/SlopeW/Comparison%20with%20active%20and%20passive%20earth%20pressures.pdf*

Hoek, E. (2007). Practical Rock Engineering. *https://www.rocscience.com/assets/resources/learning/hoek/Practical-Rock-Engineering-Full-Text.pdf*

Hoek, E. and Brown, E. T. (1997). Practical estimates of rock mass strength. *International Journal of Rock Mechanics and Mining Sciences,* Vol 34, No 8, 1165-1186.

Hoek, E., Carranza-Torres C. T. and Corkum, B. (2002). Hoek-Brown failure criterion-2002 edition. *Proceedings of the 5th North American Rock Mechanics Symposium*, Toronto, Canada: Vol 1: 267–273.

PROBEDRILL
GEOTECHNICAL SURVEY

The Leaders in Geotechnical Site Investigation

Excavator Platform CPT

CPT mounted to platform suitable for Excavator quick hitch

Ideal for hard to reach test locations

Up to 10t push

Seabed CPT

Pushing Capacity:
150kN (15 tonnes)
2.3m x 2.3m x 2.8m
(L x W x H); 5700kg
Testing Services:
CPTu; SCPTu; Ball CPT;
T-bar; DMT, Piston
Sampling (76mm dia x 3m)

Services:

- Electric Friction Cone Penetration Testing (CPT) including: 15cm (10t); 10cm (10t, 5t, 1t) cones.
- Piezocone (CPTu) and Dissipation testing
- Dilatometer (DMT) testing
- Seismic testing (SCPT & SDMT)
- Electrical Shear Vane Testing
- Dual Tube (Percussive) Soil sampler (50mm x 1000mm)
- Ball and T-bar testing
- Soil Sampling (25mm x 500mm; 35 x 1500mm)
- Water Sampling
- 50m, 32mm & 20mm Standpipe installation
- Vibrating Wire Piezometer installation (Single, Multiple; inverted)

New Services:

- Piston Sampler (60mm x 500mm)
- Multi-level VWP installation
- DGPS test location & Live data streaming
- Electronic Plate Load testing (up to 20 tonnes)

+61 8 9417 9933 · info@probedrill.com.au · www.probedrill.com.au

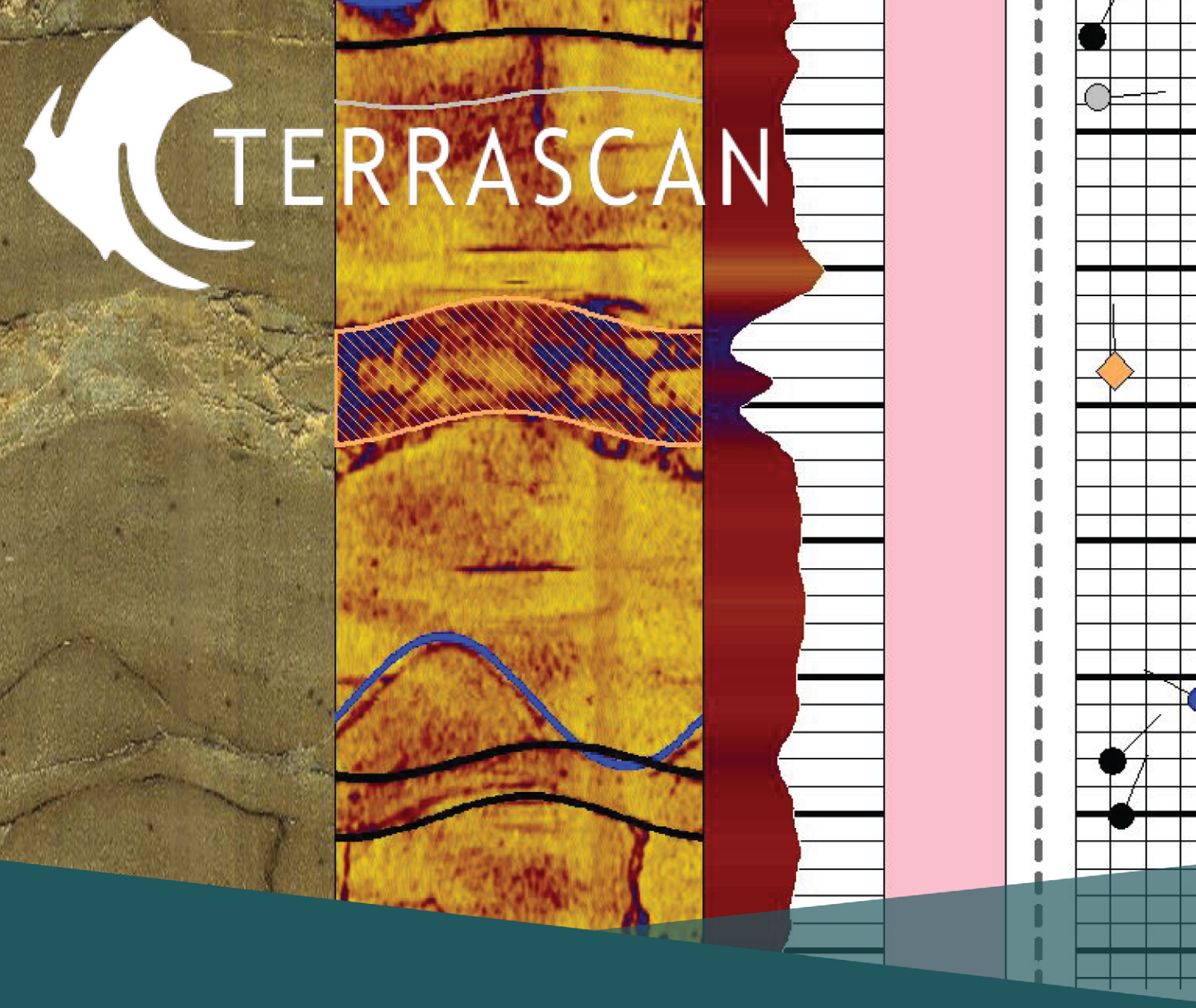

Providing Wireline & Geological services across Australia for the geotechnical and resource industries.

Contact us now to talk about your next project
wade@terrascangroup.com.au

TERRASCAN OFFERS

Downhole Wireline Geophysics

- Optical & Acoustic Televiewer
- Full Waveform Sonic (FWS)
- Resistivity
- Natural Gamma

Geological Services

- Core & Soil Logging
- Rig supervision
- Field Assistant

1300 884 198 | www.terrascangroup.com.au | 0408 723 340

GEOTECHNICAL CHALLENGES OF A DEEP BASEMENT EXCAVATION: A CASE STUDY

Michael Egan, Andrew Jackaman & Ali Parsa-Pajouh
JK Geotechnics, Sydney, Australia

https://doi.org/10.56295/AGJ6115

ABSTRACT

A 59 storey tower underlain by a 30m deep basement is currently under construction within the expanding central business district of Parramatta, NSW. The tower is surrounded by and abuts two multi-storey buildings with basement levels, a heritage listed church, a 100 year old water main, and is set back approximately 50m from the Parramatta River. A comprehensive site investigation program was carried out to characterise the complex geotechnical conditions of the site, including deep cored boreholes, insitu permeability testing and borehole imaging. Due to the challenging ground conditions encountered, proximity of the neighbouring structures and shallow groundwater, the shoring system consists of secant pile walls terminated above bulk excavation level in competent bedrock, below which a grout curtain extends approximately 50m below surface level to limit seepage inflows. An Instrumentation and Monitoring (I&M) program was implemented to assess actual basement wall movements against those predicted from the numerical analyses.

1 INTRODUCTION

Construction of a 198m high, 59 storey tower overlying nine basement levels is currently underway in Parramatta, NSW. Figure 1 presents a rendered image of the proposed tower. The site is roughly rectangular in plan area being approximately 48m long by 30m wide. The almost 100 year old 'St Andrew's Church' abuts the western site boundary. The original church hall and a five storey office building were located within the site. Due to heritage constraints, the front facade of the church hall needed to be retained as part of the development.

The tower is supported by a 900mm thick hydrostatic slab across Basement Level 9 (B9) with internal thickenings at the column locations, as well as eight 1.5m diameter (tower) piles integrated into the western basement wall. The deeper B10 lift core is supported by an approximately 2m thick hydrostatic slab. Over 200 micro-piles (200mm and 225mm diameter) and 50 vertical rock anchors installed below and tied into the B9 and B10 slabs resist hydrostatic uplift pressures.

The retention system consists of anchored and internally propped secant pile shoring walls that terminate within competent bedrock approximately 15m below ground surface level. Below the toes of the secant pile walls, the competent bedrock was cut vertically. To limit seepage inflows, a grout curtain extends below the toe level of the secant pile walls to a maximum depth of approximately 50m below ground surface; that is, approximately 20m below a B9 bulk excavation level (BEL) of RL-19.8m.

A comprehensive site investigation program was undertaken to assess the subsurface characteristics across the site. From the results of the investigations and cognisant of the many design and construction challenges, detailed numerical analyses were undertaken to model the ground-structure interactions of the shoring system, tower piles and hydrostatic slab, as well as a large diameter cast iron cement lined (CICL) water pipe. Geotechnical and structural instrumentation has been installed and is being monitored to confirm the analysis predictions.

This paper summarises the geotechnical challenges faced, the engineering solutions devised by the authors, and how they were incorporated into the project. The authors note this paper was originally published in the proceedings of the 14th Australia and New Zealand Conference on Geomechanics in Cairns, 2023. However, significant updates to the original paper (Egan, Jackaman and Parsa-Pajouh, 2023) have been made in this current version, including a more comprehensive discussion of the numerical analysis results, and back-analysis based on actual monitoring data.

2 GEOLOGY

The site is located approximately 20km west of the Sydney CBD and lies within relatively flat alluvial topography associated with the Parramatta River. The geology within and immediately surrounding the site comprises Quaternary alluvial soils, overlying Triassic-aged Hawkesbury Sandstone (i.e. at least 200 million years old). There is limited published information of the structural geology in the vicinity of the site, however various geological features (i.e. faults) are not uncommon in this part of western Sydney.

Figure 1: Rendered image of the proposed 59 storey tower (image courtesy of Woods Bagot)

3 GEOTECHNICAL INVESTIGATIONS

Due to site access constraints, the fieldwork for the investigations was carried out in a staged manner both pre and post demolition, as detailed below.

Stage 1 (Pre-Demolition): The preliminary investigation comprised the drilling of two cored boreholes to about 40m depth, and a 13m deep borehole down to the bedrock surface. Regular Standard Penetration Tests (SPT) were completed throughout the soil profile in the boreholes. A total of six, five-stage packer tests were completed in the two cored boreholes. Standpipe piezometers were installed in all three boreholes. Pump-out tests were completed in each standpipe piezometer. Data loggers monitored the groundwater recharge rate during borehole infiltration testing as well as the steady state groundwater levels over a five month period.

Stage 2 (Post-Demolition): The detailed investigation comprised the drilling of nine boreholes to depths ranging between about 13m and 60m. The six deeper cored boreholes were drilled to depths between about 40m and 60m, primarily to assess the levels at which seepage cut-off could be achieved, and to provide advice on the design of deep tensile elements required to resist hydrostatic uplift pressures acting on the lowest basement floor slabs. Regular SPT's were carried out throughout the soil profile in the boreholes. A total of fourteen, five-stage packer tests were carried out in four of the six cored boreholes. Three additional standpipe piezometers were installed into the three shallower boreholes for long-term groundwater monitoring. Four test pits were also excavated to confirm the footing details and foundations conditions below the abutting eastern wall of St Andrews Church.

At the time of demolition on the subject site, the neighbouring property to the north-east was being developed and their bulk excavation had just been completed. The neighbouring basement excavation was about 25m deep, set back at least 1.1m from the common boundary, and had been designed as a drained structure. Permission was granted by the developer of the neighbouring property to inspect the basement walls closest to the subject site. The shoring system within the neighbouring basement comprised anchored and internally propped secant pile walls that terminated approximately 14m below ground surface level and which were underlain by vertically cut sandstone rock faces. From observations within the neighbouring basement excavation, an approximately 2m thick, sub-horizontal shear zone (upper shear zone) was evident at approximately 18m depth. This shear zone was discontinuous in lateral extent and it was difficult to ascertain whether it was dipping into the subject site. As such, optical and acoustic televiewer imaging was carried out during the detailed investigation. The imaging was completed in two cored boreholes located in close proximity to the common boundary with the neighbouring property to assess the orientation of the upper shear zone.

Stage 3 (Detailed Design): A supplementary investigation was carried out and comprised the drilling of four additional cored boreholes to about 40m depth. The focus of the supplementary investigation was to provide updated and more specific advice on the design, construction and inspection of the heavily loaded tower piles located along the western shoring wall.

Laboratory soil aggression and point load strength index testing were carried out for each stage of investigation. Unconfined compressive strength tests were also attempted, but the results were considered to be unreliable based on a poor correlation with the abundance of point load tests completed, and the results were never reported.

4 GROUND MODEL

From the results of the geotechnical and hydrogeological investigations, the subsurface profile comprised fill overlying variable and interlayered alluvial soils to about 13m depth, then sandstone bedrock which contained localised horizontal shear zones and laminite beds. The alluvial soil profile consisted of silty/sandy clays and sands with various proportions of silt and clay fines. The upper sandstone profile was weathered but of limited thickness. The underlying sandstone was typically fresh and of medium, high and in some instances very high strength. The fresh laminite bed was also of medium to very high strength and was encountered below approximately 25m to 27m depth, and was about 4m thick. The sandstone and laminite bedrock were typically Class II/I (Pells et al., 1998) below 15m to 21m depth, with occasional laterally discontinuous bands of Class III to Class V rock between 1.4m and 4.2m thick.

In the north-eastern corner of the site, two of the cored boreholes encountered an upper shear zone (as discussed in Section 3) between approximately 17.5m and 19.5m depth. Within these boreholes, the upper shear zone manifested as fractured bedrock bound by two distinct sheared/crushed seams or no core zones. The shear seams encountered in one of the boreholes is shown in Figure 2.

The borehole imagery further confirmed the presence of the upper shear zone and indicated apertures within individual defects typically up to 8.5mm wide, however, aperture widths of between approximately 35mm and 100mm were also recorded; possibly widened due to drill flush water effects. These defects were mostly dipping down to the west and south-west; that is, into the proposed basement excavation. The fracturing/shearing observed in the cored boreholes was less extensive than anticipated following reinspection of the shear zone from within the neighbouring basement. In addition, the rock cores at similar depths within the remaining boreholes did not indicate any such features and it was inferred that the upper shear zone was laterally discontinuous to the south and west. A second, deeper shear zone, comprising closely spaced defects and no core zones, was also encountered in several other boreholes between about 38m and 46m depth.

Figure 2: Sandstone bedrock containing two distinct shear seams

A total of twenty, five-stage packer tests were completed as part of the preliminary and detailed investigations. The packer test results indicated that the insitu permeability of the sandstone and laminite bedrock typically ranged between about 0.01 to 9.0 Lugeons (uL) above 37.5m depth, but with a single result of 48uL. However, between 37.5m and 50m depth, the results generally indicated higher values between about 18uL and 133uL. Prior to dewatering commencing within the adjacent neighbouring basement, groundwater levels on the subject site fluctuated between approximately 5m and 6m depth, with a slight hydraulic gradient down to the north toward the Parramatta River. A summary of the encountered ground conditions is presented in Table 1.

Table 1: Simplified summary of the geotechnical model

Unit	Description	Top and Bottom of Unit (RL mAHD) [Unit Thickness (m)]
1. Fill	Variable silty/sandy clays and sandy soils generally assessed to be poorly compacted	9.6 to 6.3 [0.4 to 3.0]
2. Alluvial Soils	Alluvial clays of soft to hard strength and alluvial sands of very loose to dense relative density	9.1 to -3.5 [9.2 to 12.2]
3. Sandstone (See Note 1)	Highly to moderately weathered rock of very low or low strength (Class V and IV)	-2.3 to -11.6 [0.7 to 8.3]
4. Sandstone	Slightly weathered to fresh rock of medium, high or very high strength (Class III & II/I)	-3.9 to -17.6 [5.7 to 13.7]
5. Laminite	Fresh rock of medium, high or very high strength (Class II/I)	-15.9 to -21.6 [2.1 to 4.1]
6. Sandstone (See Note 2)	Fresh rock of medium, high or very high strength (Class II/I)	-17.3 to -50.8 [10.1 to 30.6]

[1] Unit 3 was overlain in places by a thin layer of extremely weathered sandstone which has been excluded from this summary.
[2] Unit 6 contained bands of Class III and IV rock up to 4.2m thick

5 GEOTECHNICAL STRATEGY

5.1 PRIMARY ISSUES

The following primary geotechnical and structural issues were identified for the proposed deep basement excavation:

- Transmission of ground borne vibrations from construction related activities causing settlement of the heritage listed St Andrews Church, which is supported on high level footings, partly founded in very loose and loose alluvial sands;
- Support of the church hall brick facade located inside the basement footprint at its southern end;
- Retention of the soil and weathered bedrock profiles, and limiting seepage inflows during construction and in the long-term;
- Deflection of the 100 year old, 900mm CICL water main, which was set back approximately 7.3m from the southern site boundary;
- Interaction of the proposed basement levels with the neighbouring basement structures, requiring a combination of temporary internal props and rock anchors to provide lateral support to the shoring system; and
- Stability of a 1.1m to 2.3m wide plinth of soil and rock located between the neighbouring 25m deep basement excavation and the northern side of the proposed 30m deep basement excavation.

The methodologies that were adopted to overcome the various design and construction issues are discussed in detail below.

5.2 ST ANDREW'S CHURCH

St Andrew's Church is located immediately behind the western basement wall. In order to reduce the risk of potential vibration induced settlement, jet grouting was carried out along the eastern side of the church (including short return distances along the northern and southern sides) in advance of the basement excavation. The process of jet grouting required a cementitious grout to be pumped into the underlying soils at high pressure, creating a soil-cement mix of greater strength than the insitu material. The grout was delivered via a small diameter nozzle. The drill rods were slowly extracted during grouting in an attempt to create closely spaced soil-cement columns of at least 1m diameter.

The high-pressure grout mix was injected into the soil profile to a target depth of approximately 9m, which correlated with the base of the very loose and loose alluvial sands below the church. To reduce the risk of damage, instrumentation was set up along the church facade to detect vertical movement of the walls during jet grouting. From the monitoring records, grouting pressures and in turn the soil-cement column diameters were reduced during the works in order to limit upward jacking forces along the base of the strip footings supporting the Church.

5.3 CHURCH HALL

The single storey church hall with an approximate 284m^2 plan area occupied the south-western portion of the basement footprint. Prior to the commencement of piling, the majority of the brick hall was demolished except for the southern facade, which had to be integrated into the ground and first floors of the proposed tower.

Following installation of the shoring piles and perimeter capping beams, the footings of the brick facade were strengthened, needled, and incorporated into a post-tensioned (PT) concrete ground floor slab. The PT slab was supported on the capping beams at the southern end of the site, and internally on six steel 'H' beam plunge columns (587mm diameter) socketed between 3.8m and 6.7m below BEL. The plunge columns were laterally braced off the basement shoring walls, underlying sandstone bedrock cut faces, and adjacent plunge columns as the excavation deepened. Figure 3 shows the PT slab and plunge columns supporting the hall facade at the southern end of the site.

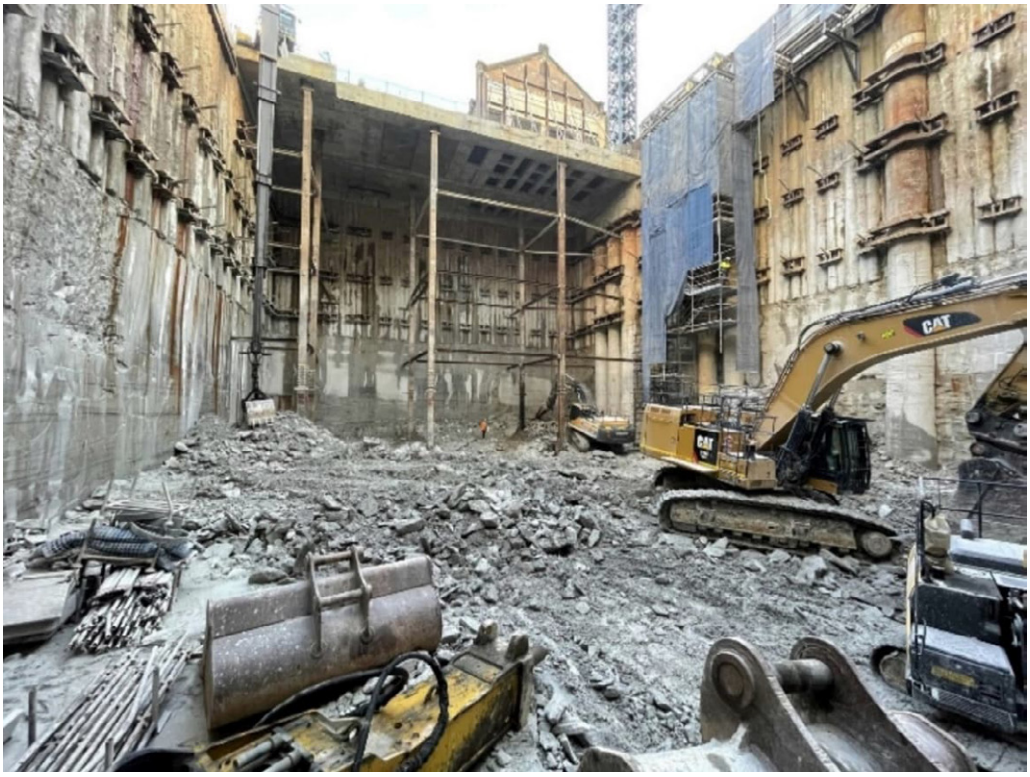

Figure 3: PT slab and plunge columns supporting the hall facade, looking south

5.4 RETENTION SYSTEM

Based on the results of the geotechnical investigations, including the long-term groundwater level monitoring and packer test results, a secant pile shoring wall was nominated to support the soil and upper weathered bedrock profiles. Diaphragm walls were also considered however, the limited site area and spatial constraints around the retained church hall facade rendered this option more costly than secant pile walls.

The 630mm diameter secant piles were installed by Bachy Soletanche Australia (BSA) using bored piling techniques with segmental casing. The secant piles were generally installed to approximately 15m depth below ground surface. In the vicinity of the rock plinth between the two deep basements, the hard piles were extended to 19.5m depth in order to engage and support the upper shear zone.

The secant pile walls were partly supported by three rows of temporary rock anchors (3 to 7 strands) between approximately 10m and 24m long, with maximum bond lengths into medium (or greater) strength bedrock of about 7m. Near the neighbouring basements at the northern end of the site, the anchors were complemented by internal props (up to four rows). The secant pile walls, temporary rock anchors and corner props are shown in Figure 4.

Below the toe level of the secant pile walls (i.e. below RL-5.5m), the sandstone and laminite bedrock was cut vertically. Regular inspections were completed during excavation to assess rock face stability and to design stabilisation measures, where necessary.

Six inclinometers were installed to progressively monitor the lateral deflections of the shoring walls and underlying vertically cut rock faces during bulk excavation. Load-cells were also utilised to measure the horizontal forces within three of the corner props in the north-eastern corner of the site.

5.5 GROUT CURTAIN

In order to control groundwater inflows, bedrock curtain grouting was carried out prior to the installation of the secant pile walls. From the results of the seepage analysis presented in Section 6.1 below, the grout curtain was installed to roughly 50m depth, with a 1.5m overlap between the top of the grout curtain and toe of the secant pile walls.

The adopted methodology comprised the drilling of 'primary' grout holes at approximately 6m centres, followed by intermediate 'secondary' grout holes. The primary and secondary holes (spaced 3m apart) were grouted until a satisfactory grout take was recorded and the closure criteria (less than 2uL) in the secondary grout holes was achieved. Inflatable rubber packers and digital flow meters/pressure gauges were utilised to assist the rock grouting process. Where closure of the open joints, seams etc. was not achieved, tertiary holes were drilled, grouted and tested. At several locations along the basement perimeter, quads, quaternary and quinary holes were required in order to achieve closure.

Within the north-eastern quadrant of the site, curtain grouting under pressure was abandoned due to connectivity of several persistent rock defects and leakage into the neighbouring 25m deep excavation. In one instance, grouting at 40m depth was leaking into the neighbouring basement at about 18m depth.

In total, approximately 340kL of grout was injected under pressure into the bedrock. For the remainder of the grout curtain adjacent to the neighbouring 25m deep basement, a method specification was designed including grout holes at 0.75m centres that were filled with grout under gravity only, and then progressively topped up, as required.

5.6 ROCK PLINTH

The 25m deep neighbouring basement to the north-east of the subject site is set back a minimum 1.1m, and extends at an oblique angle from the common boundary. The neighbouring retention system comprised anchored and internally propped secant pile walls underlain by vertically cut rock faces, similar to the subject site. In the long-term and adjacent to the subject site, the neighbouring secant pile walls are supported vertically and laterally by the four uppermost slabs, including ground floor, B1, B2 and B3. Concrete walls constructed directly in front of the rock faces and secant pile walls formed the permanent basement structure. Drainage provisions were reportedly installed behind the concrete walls.

As a result of the basement excavation on the subject site, a localised plinth of soil and rock would remain between the two basements. The primary geotechnical issue associated with a slender rock plinth was the possible reorientation and redistribution of the anticipated high horizontal stress field around the adjacent basements. It was assessed that a concentration of the horizontal insitu stresses could potentially cause the plinth of rock to crush and/or collapse during excavation within the subject site. Due to the presence of the unfavourably dipping upper shear zone above both BEL's, the potential collapse was expected to occur into the proposed excavation, however, there was also the potential that the plinth could at least partially collapse onto the back of the concrete wall within the neighbouring basement. Several options to mitigate the risk were devised and the option accepted by the neighbouring developer, as the plinth was located entirely within their property, was the provision of a narrow excavated slot between the two basement excavations to essentially remove the narrowest section of the plinth. It was expected that this slot would allow controlled stress relief within the bedrock profile during excavation of the proposed basement. The secant piles along the northern basement wall on the subject site were then returned in a northerly direction, on either side of the 3.2m wide slot, towards the neighbouring basement secant pile wall.

The faces of the return walls were progressively internally propped during excavation. Below the toes of the 19.5m deep hard piles, as discussed above, an approximately 1m wide slot in the bedrock was excavated down to the neighbouring BEL. The upper portion of the slot was excavated to the back of the neighbouring secant pile wall. The lower portion of the excavated slot exposed the toe of the neighbouring secant pile wall and back of the concrete wall. The excavated slot is shown in Figure 4 below.

Inclinometer monitoring of lateral movements during basement excavation confirmed that convergence into the excavated slot had occurred. For long-term restraint, the excavated slot was incrementally mass filled with concrete up to the ground surface, removing the internal braces as backfilling progressed. Drainage cells were also installed between the concrete backfill and neighbouring basement wall to continue to facilitate groundwater flow.

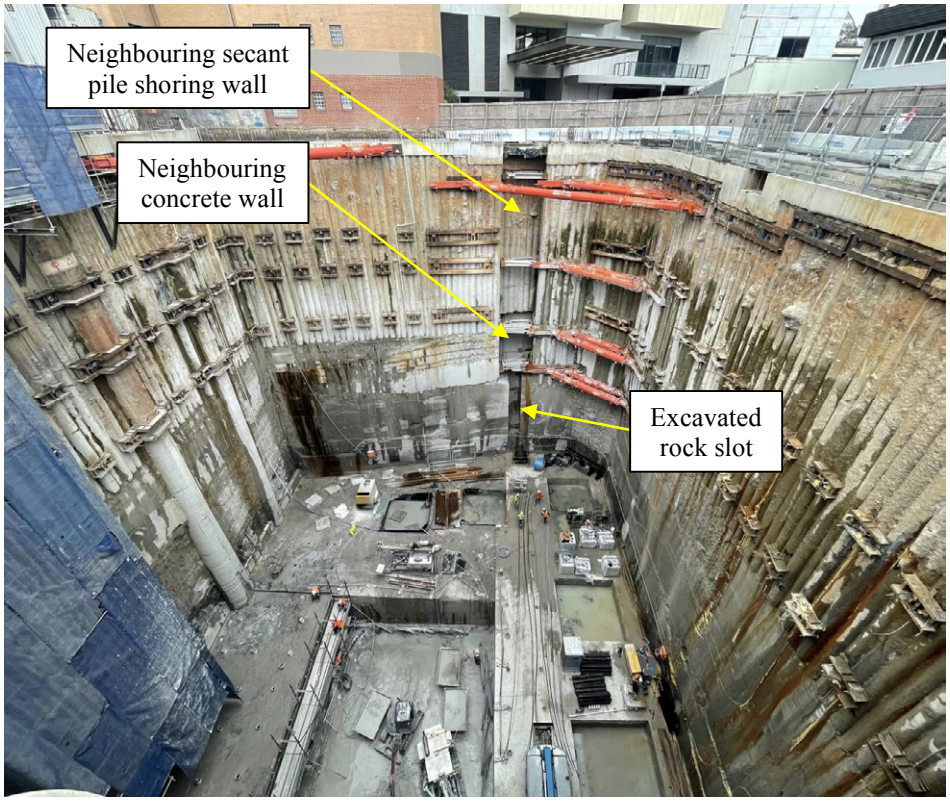

Figure 4: Rock slot extending toward the neighbouring basement walls, looking north

5.7 CICL WATER MAIN

An approximately 100 year old, 900mm diameter CICL water main was present a short distance behind the southern basement wall. The lateral deflection of the southern basement wall and of the water main itself were predicted by 2D & 3D finite element modelling. The deflections, joint pull-out, joint rotation, and tensile strain of the CICL water main were estimated from the results of our initial 2D analysis and using empirical relationships provided by various authors. The results were compared to the criteria outlined in Bracegirdle et al. (1986) as during the time of our analysis (i.e. nearly five years ago), the asset owner had no set criteria for assessment of a 900mm diameter pipe.

Due to the concerns raised by the asset owner in relation to the estimated high joint pull-out for the heritage listed pipe, as well as the anticipated delays with further analysis and obtaining approval to begin excavation, the design team (and the asset owner) ultimately decided to replace the section of pipe immediately adjacent to the proposed excavation, but with flexible connections with the retained portion of the original pipe. For this option, a more robust geotechnical assessment comprising 3D numerical modelling to predict the maximum displacement of the existing and new sections of pipe was carried out and the results provided to Warren Smith Consulting Engineers (WSce), who completed their own structural analysis of the water main. Due to the predicted lateral movements of the retention system from the 3D analysis, the new joint connections were approximately 15m beyond the eastern and western basement walls.

6 NUMERICAL ANALYSIS

Comprehensive 2D & 3D numerical analyses were carried out by the authors using PLAXIS (a software for finite element geotechnical analysis) for the following purposes:

- Predicting the potential seepage volumes into the proposed excavation during construction and in the long-term;
- Assessing the impact of the proposed deep excavation on the 900mm CICL water main;
- Predicting the shoring system behaviour and ground movements due to the proposed deep excavation; and
- Estimating the settlement, earth pressures and subgrade reaction modulus across the B9 hydrostatic slab and deeper B10 lift core slab.

The analysis of the tower piles and plunge columns was carried out by BSA on a D&C basis and is not included in this paper.

6.1 SEEPAGE ANALYSIS

The seepage analysis was carried out by developing a hydrogeological model based on the investigation results, specifications of the secant pile walls, details of the perimeter grout curtain extending below the toes of the secant pile walls, and the geometry of the basements both within and adjacent to the subject site. The permeability values adopted for the subsurface units based on the results of the borehole pump-out tests carried out in the soils, packer test results in the bedrock, well established correlations and experience with similar soils/rock, are presented in Table 2.

Table 2. Adopted permeability values for the various subsurface units

Geological Unit[1]	Permeability (m/sec)
1. Fill	Not Required
2. Alluvial Soils	2.0×10^{-4}
3. Sandstone	7.4×10^{-7}
4. Sandstone	6.0×10^{-7}
5. Laminite	6.0×10^{-7}
6a. Sandstone	4.0×10^{-7}
6b. Sandstone	5.4×10^{-6}
6c. Sandstone	2.7×10^{-9}

[1] Unit 6 sandstone was sub-layered due to the variability in the permeability test results

Based on the groundwater monitoring results within the subject site and available monitoring records within the neighbouring property to the north-east, the original groundwater level within the soil profile contained a slight hydraulic gradient down to the north from approximately RL4.2m at the southern end of the subject site, to RL2.9m at the northern end of the neighbouring property, adjacent to the Parramatta River. The water level of the adjoining non-tidal portion of the Parramatta River was taken to be approximately RL1.1m.

As groundwater levels within the subject site were partially being drawn down due to ongoing basement dewatering within the neighbouring property, the additional extracted water volumes from the long-term pumping were considered. The 3D seepage model was calibrated based on the reported daily groundwater pump-out rate in the neighbouring basement excavation of approximately 174m^3/day (i.e. equivalent to 2L/sec). The perimeter secant piles and grout curtain were then incorporated into the 3D seepage model. For the purpose of developing the model, an equivalent permeability of 0.02 uL for an assumed minimum 1m wide grout curtain, and an equivalent permeability of 0.002 uL for the secant pile walls, were adopted.

With the perimeter grout curtain cut-off at RL-41.0m, the 3D seepage analysis indicated a groundwater inflow into the basement excavation of about 5.7ML/year (i.e. 15.6m^3/day). Sensitivity analyses were completed to assess the impact of varying the toe level and equivalent permeability of the grout curtain. Based on these analyses, the inflow rates were very sensitive to the grout curtain toe level, mainly due to the more permeable sandstone layer (Unit 6b sandstone) being typically encountered between about RL-35m and RL-39m. From the sensitivity analyses, if the grout curtain was terminated above RL-35m, the rate of groundwater inflow into the excavation would be significantly higher at approximately 138m^3/day.

The actual seepage inflows which occurred between completion of bulk excavation and construction of the B9 hydrostatic slab were considerably less than predicted due to the effectiveness of the grout curtain and were readily controlled using submersible pumps.

6.2 CICL WATER MAIN ANALYSIS

The initial 2D analysis consisted of modelling the proposed southern basement shoring wall and two CICL water mains of 900mm and 150mm diameter. The pipes were set back approximately 7.3m and 12.6m from the southern site boundary, respectively with the pipe crowns at depths of approximately 2.5m (900mm diameter) and 1.0m (150mm diameter) below the road surface.

At the time of carrying out our initial analysis, no criteria existed for assessing the impact of construction related activities on 900mm diameter CICL pipes. Nevertheless, based on the results of the analysis, the expected lateral movements of the

900mm and 150mm diameter pipes, mid-length along the southern side of the proposed basement excavation, were in the order of approximately 32mm and 29mm, respectively.

As the analysed section was located mid-length along the southern side of the proposed basement excavation, and the analysis was carried out using PLAXIS 2D, the lateral movements were expected to be maximum, and possibly conservative values. Towards the eastern and western extremities of the basement excavation, the lateral movements were expected to be negligible as the southern secant pile basement wall would be buttressed by the eastern and western basement walls. Across the 30m width of the excavation, the predicted maximum curvature of both CICL pipes was in the order of 2.6mm/m. Figure 5 shows a heat map of the predicted lateral deflections of the shoring wall and pipes. A surcharge load of 20kPa along the road surface and adjacent footpath above the pipes was adopted in the model.

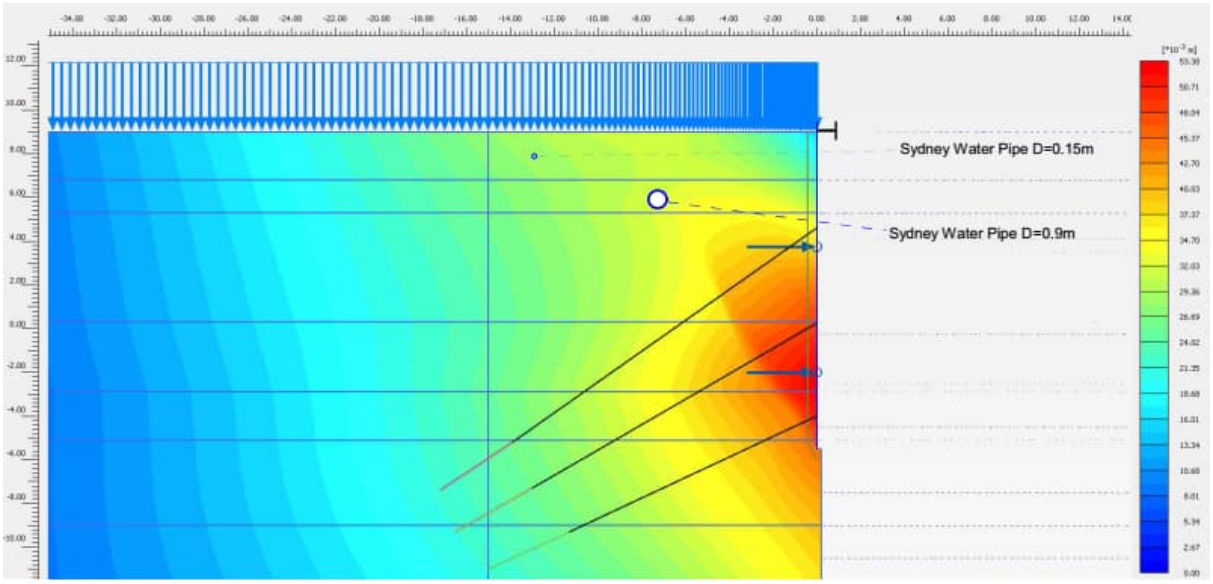

Figure 5: Heatmap of PLAXIS 2D results showing the lateral deflections of the anchored secant pile shoring wall

Following submission of our initial 2D analysis, further more rigorous assessments using the methodologies outlined in Bracegirdle et al (1996), Vorster et al (2005) and Vorster (2009) were carried out for the 900mm diameter CICL pipe only. Using these methods, the calculated empirical criteria (Smax/i), joint rotation (θ) and pipe strain (ε) were estimated as outlined in Table 3 below. The estimated lateral displacement of the pipe obtained from the 2D analysis was taken as the joint pull out (R).

Table 3. Empirical results for the 900mm diameter CICL water main

Factor	Allowable Values as Outlined in Bracegirdle et al. (1996)	Calculated Values
Empirical Criteria, $S_{max/i}$	0.012	0.0064
Joint Rotation, θ	1.5° (assuming lead-yard joints)	0.3°
Joint Pull Out, R	15mm (assuming lead-yard joints)	32mm
Cast Iron Pipe Tensile Strain, ε	>2000 με	570 με

The calculated values provided in Table 3 were below the permissible values outlined in Bracegirdle et al. (1996), with the exception of joint pull out. It is worth noting that Bracegirdle et al. (1996) stated *"again conservatively, it may be assumed that the maximum potential pull-out is equal to the maximum predicated horizontal ground displacement due to tunnelling for both longitudinal and transverse directions",* but no further discussion was given in the paper. As the lateral movement of the CICL pipe was expected to behave in a 'bell shaped' manner (i.e. Gaussian curve), the joint pull out was postulated to be less than predicted.

In addition to the numerical and empirical analyses outlined above, a monitoring plan and contingency action plan during basement excavation were prepared to support the Building Over or Adjacent to Our Stormwater Assets (BOA) submission to the asset owner. However, due their concerns, specifically that the "*level of deflection has a high potential to cause failure*", the BOA application for the proposed development was rejected. In response, the design team (and asset owner) cooperatively decided to replace the section of pipe adjacent to the proposed excavation.

A more robust 3D numerical model was developed to further assess the impact of the proposed development on the existing and replaced section of the 900mm diameter CICL pipe. The 3D model included detailed construction staging, the shoring system components including walers, rock anchors, corner props and the PT slab, as well as joints in the CICL pipe spaced at 3 feet centres. A snapshot of the 3D numerical model is shown in Figure 6.

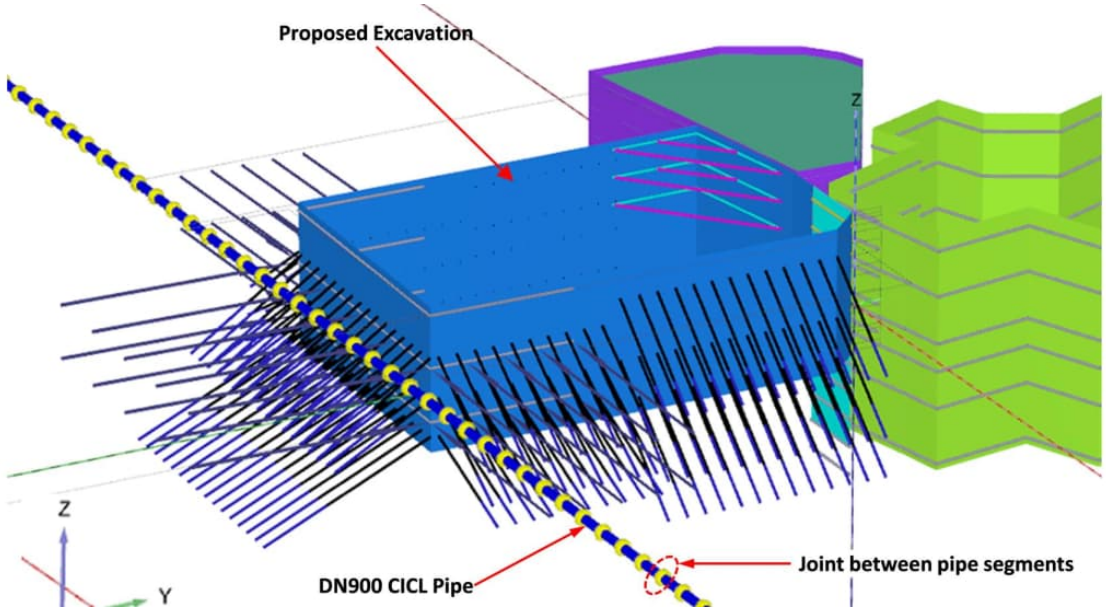

Figure 6: A snapshot of the 3D numerical model for the CICL water main analysis

The soil and rock parameters adopted in the numerical analysis were based on the results of the geotechnical investigations, past experience with similar materials and published literature (including Pells et al., 1998), and are presented in Table 4. A drained Mohr-Coulomb model was used to simulate the behaviour of the subsurface profile. Where soil/poor quality bedrock was in contact with the structural elements, a reduction factor (R_{inter}) of 0.67 was adopted. This was applied to the soil strength parameters to model the reduction in shear strength between the soils/poor quality bedrock and structural elements.

Table 4: Adopted soil and bedrock parameters in the numerical analysis

Parameter	Material [1]						
	1	2	3	4	5	6	7
γ (kN/m^3)	17	18	19	21	24	23	24
c' (kPa)	0	5	0	60	300	250	500
φ (°)	26	25	33	32	50	40	50
E (MPa)	5	10	20	80	900	2000	2000
v	0.35	0.3	0.3	0.3	0.25	0.15	0.2

[1] 1: Fill, 2: Alluvial Clay of Stiff to Very Stiff Strength, 3: Alluvial Sand of Medium Dense to Dense Relative Density, 4: Class V Sandstone, 5: Class III Sandstone, 6: Class II/I Laminite & 7: Class II/I Sandstone

The secant pile walls were modelled using plate elements representing only the hard (reinforced) piles, with an equivalent diameter and bending stiffness. This approach captures the primary structural role of the reinforced piles, which resist lateral earth pressures and control out-of-plane bending behaviour. In reality, in-plane bending transfer between adjacent secant piles is limited due to the presence of soft piles and the nature of loading conditions. To reflect this, no structural connection was introduced between adjacent plates, thereby avoiding artificial in-plane stiffening of the wall. Although inter-pile connections could be modelled using Custom Connection elements in PLAXIS 3D, this was not implemented due to the added complexity and computational cost. The selected modelling approach provided a practical balance between computational efficiency and structural realism under the governing loading conditions.

The initial stress field for the soil profile was modelled by the adopted K_o values relating horizontal and vertical stress. For the soil profile, K_o was calculated on the basis of the relationship $K_o = 1\text{-}\sin\text{Ø}$. The insitu stresses within the sandstone and laminite bedrock were simulated based on the well-recognised relationships proposed by Bertuzzi (2014).

The numerical model was run through a number of stages in an attempt to simulate the construction sequences, such as pre-development in order to generate the insitu stresses, construction of the retention system, application of ground surcharges and excavation to BEL. An initial 'greenfield' analysis was completed without the presence of the existing water main to conservatively assess the lateral displacements of the pipe assuming it moved entirely with the surrounding soils. A second 'ground-structure' model was developed and included the existing pipe adjacent to, and extending well beyond the subject site, to estimate the movement of the pipe for both rigid (i.e. continuous pipe) and free (i.e. semi-rigid) pipe joints (initially spaced at 3 feet centres).

The results of the geotechnical analysis indicated a total maximum displacement of the existing pipe due to the basement excavation was around 20mm, regardless of whether the pipe was or was not included in the model, and provided the basis for confirming the exact location where the water main would be replaced, which was approximately 15m beyond the eastern and western basement shoring walls. The results of the geotechnical analysis were then used by WSce to carry out their own structural assessment of the retained and replaced sections of pipe.

A first pass structural assessment used the predicted ground movements from the geotechnical 'greenfield' analysis to calculate the worst-case joint pull-out, joint rotation and strains in the existing pipe (i.e. assuming the pipe follows the ground movement) using the methods outlined in Bracegirdle et al. (1996). The interim criteria provided by the asset owner at the time of our analysis (i.e. 2.5mm for joint pull-out, 0.05° for joint rotation, and 40 με for tensile strain) was slightly exceeded but the impact on the retained sections of pipe was considered negligible. Similar methods were adopted for a second round of structural assessment using the predicted ground movements from the geotechnical 'ground-structure' analysis and were all well below the interim criteria outlined above.

Finally, the geotechnical 'ground-structure' analysis model was slightly modified and the estimated ground movements within a 'bounding box' approximately 4m x 4m in size around the CICL pipe was provided to WSce to assist with their design of the new pipe using Strand7 (a software for finite element structural analysis). The new section of pipe is Mild Steel Cement Lined (MSCL), of 900mm diameter and contains rubber ring joints (6m spacings) to facilitate future ground movements below/around the pipe.

6.3 RETENTION SYSTEM ANALYSIS

The 3D numerical model was developed further by including the narrow excavated slot between the two adjacent deep basements and updated shoring details to support the adjacent soil and weathered bedrock profiles. The assessment methodology, geotechnical parameters and excavation stages adopted for the analysis of the retention system were broadly similar to those outlined above for the CICL water main.

For comparative purposes, the maximum predicted lateral displacements of the shoring walls and underlying bedrock faces were reported at six inclinometer locations. After reaching BEL, the predicted lateral displacements into the proposed excavation at the inclinometer locations exceeded the maximum lateral predictions. It was postulated that the overpredictions of lateral movements were associated with the following:

- **Surcharge Loads** – Surcharges were applied immediately behind the western, eastern and southern shoring walls to simulate the additional loads from St Andrews Church and along the road/footpath surfaces. These surcharge loads were probably at the upper end of what may be expected for the church/roadways and would almost certainly increase the predicted shoring wall lateral displacements.
- **Elastic Modulus (Concrete)** – To account for long-term creep effects of the shoring system, a roughly 70% reduction of the modulus of elasticity of concrete was adopted based on advice provided by the structural engineer. It is likely that these long-term effects had not yet occurred and the concrete within the shoring system remained relatively stiff. A reduced concrete stiffness would increase the predicted shoring wall lateral displacements.
- **Elastic Modulus (Soil and Rock)** – The adopted modulus of elasticity for the soil and bedrock units were based on the results of the previous geotechnical investigations at the site, published literature and experience with similar materials. It is possible that the adopted geotechnical parameters were slightly conservative, particularly for the soil units. The underlying Class II/I sandstone and laminate bedrock exposed within the sides and base of the excavation may also have been closer to Class I rock parameters in some areas, i.e. greater stiffness. The slightly conservative soil and bedrock parameters would result in an increase and overestimation of the predicted shoring wall lateral displacements.

- **Groundwater** – The basement excavation was designed as a hybrid tanked system with secant pile shoring walls supporting the soil and weathered bedrock profiles to approximately 15m depth, below which was a grout curtain installed to approximately 50m depth, including a 1.5m overlap between the top of the grout curtain and toe of the secant pile walls. This system was very effective in reducing groundwater seepage inflows based on the low closure criteria achieved around much of the basement perimeter and only minor seepage inflows noted during basement excavation.

  During excavation, groundwater levels within the standpipe piezometers installed around the site were relatively stable within the soil profile. However, the groundwater level in one other standpipe piezometer sealed within the bedrock had been lowered by approximately 5m, which is surprising given the limited groundwater pumping required to maintain a dry basement. The lower groundwater level within the bedrock was attributed to the drainage occurring within the neighbouring basement to the north-east. It is possible that due to the lateral expanse and effectiveness of the grout curtain, the pore water pressures immediately behind the cut rock faces were reduced.

- **In-situ Stresses** – The in-situ stresses within the Class IV and better quality bedrock were estimated using the relationships proposed by Bertuzzi (2014). Recognising that these 'locked-in' stresses cannot be accurately simulated using the K_0 procedure or gravity loading alone, the following two-step approach was adopted in PLAXIS 3D to generate these stresses:

  - Step 1: Initial horizontal stresses proportional to vertical stress were generated using the K_0 procedure; and
  - Step 2: A subsequent plastic analysis stage was carried out by assigning a specified horizontal volumetric strain to the bedrock layers. This induced additional horizontal stresses, which were superimposed on the existing in-situ horizontal stresses calculated in Step 1.

  Based on the proximity of the nearby Parramatta River and neighbouring deep basement, as well as the presence of the upper shear zone and localised faults on the northern and southern elevations, it is possible that some of these 'locked in' stresses had already been released, both in geological time (i.e. Parramatta River) and in the past few years (i.e. due to the neighbouring development).

  A summary of the topographical effects on insitu stresses is presented in McQueen (2004). The author states that "*features such as valleys, coastal cliffs and paleochannels (bedrock channels infilled by recent alluvial or marine deposits) can realign the stress field and concentrate or reduce its magnitude*". The main geotechnical structures identified at the site were predominantly along the northern elevation (i.e. discontinuous sub-horizontal shear zone) and southern elevation (i.e. faulting), with the Parramatta River located approximately 50m to the north-west. Figure 7 and Figure 8 below show these geotechnical features. The identified geotechnical structures are likely related to variations in stress magnitude and possibly the formation of the Parramatta River. Lower in-situ stresses would result in an overestimation of the predicted shoring wall lateral displacements.

Figure 7: Upper shear zone exposed along the northern elevation

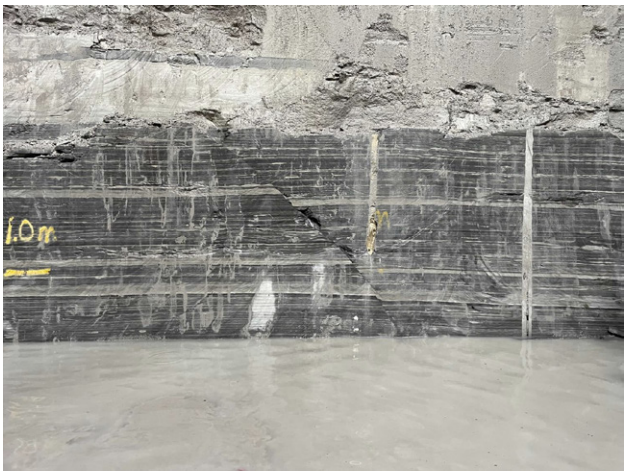

Figure 8: Localised fault within the laminite bed along the southern elevation

The geotechnical parameters and structural inputs adopted in the numerical model resulted in predicted maximum lateral displacements well above actual displacements measured during and following basement excavation. Back-analysis of the lateral displacements of the shoring wall and underlying bedrock was carried out considering the above issues.

Case 1 of the back-analysis considered no surcharge loads acting on the back of the secant pile shoring walls, a short term concrete modulus (instead of a long-term modulus) in the secant pile walls, and reduced insitu stresses (i.e. $\sigma_H = 2$ instead of $\sigma_H = 2.5MPa + 2\sigma_v$).

Case 2 of the back-analysis was similar to Case 1, but the groundwater level was lowered to below BEL to eliminate the groundwater pressure behind the shoring walls and excavation faces. This second case is obviously an extreme case and does not represent actual site conditions, but it is interesting to note the impacts of the reduced porewater pressure on the predicted lateral displacements. Reference should be made to Figures 9 and 10 below.

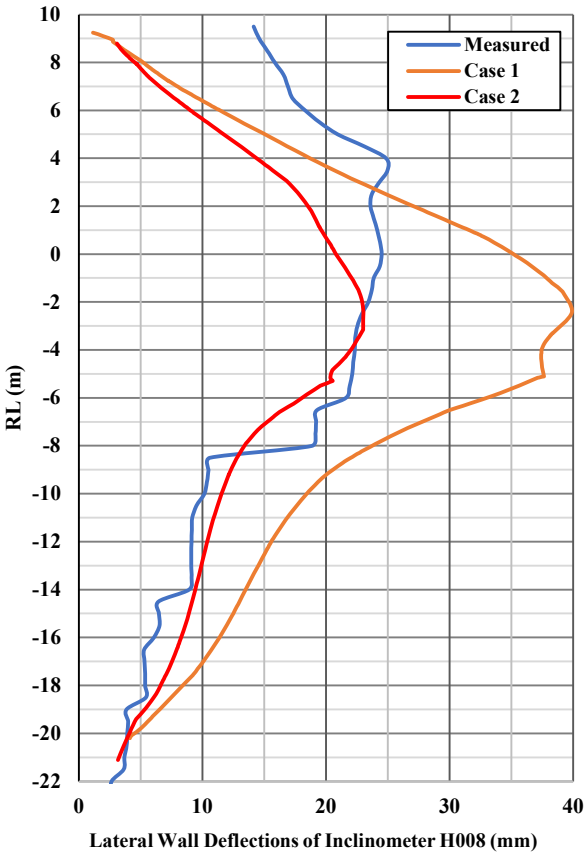

Figure 9: Measured and predicted a-axis lateral displacements

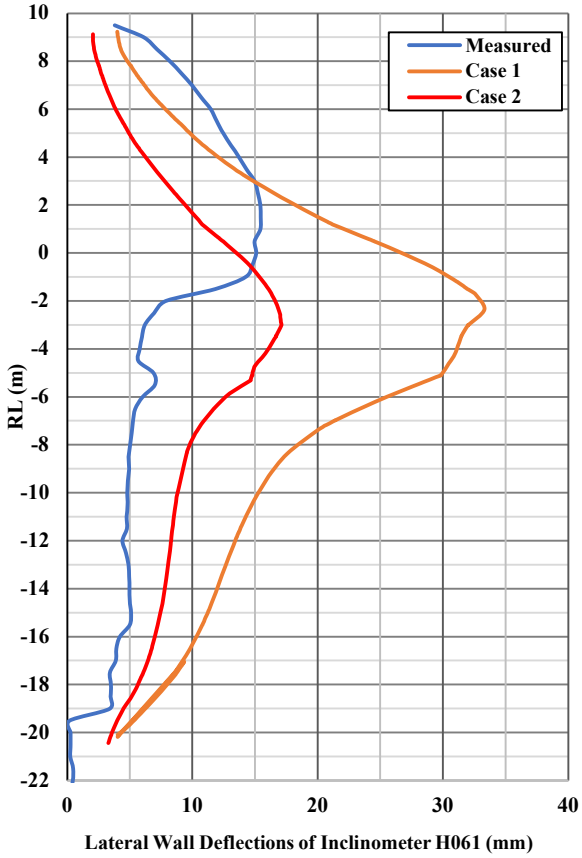

Figure 10: Measured and predicted a-axis lateral displacements

The above figures indicate that with reduced surcharge loads, insitu stresses and porewater pressures, and an increase in concrete stiffness, a better comparison with the actual lateral displacements can be made. Additional iterations of the back-analysis assessing variations in groundwater levels/pore pressures and in-situ stresses would potentially increase the accuracy of the model.

6.4 B9 HYDROSTATIC AND B10 LIFT CORE SLAB ANALYSIS

The developed 3D numerical model was also utilised to predict the settlements, earth pressures and subgrade reaction modulus values across the B9 and B10 slabs due to the application of building loads and anchor forces. The analysis was carried out by including the eight tower piles along the western shoring wall elevation and the more than 50 permanent and vertically drilled rock anchors installed below the B10 slab. The analysis did not consider the micro-piles installed below the B9 slab. The compressive building loads on the B9 columns and B10 lift core ranged between approximately 1.2MN and 113MN. The results of the analysis indicated maximum settlements below the B9 and B10 slabs of approximately 14mm, as shown in Figure 11 below.

The rock anchors (24 to 37 strands) installed to resist uplift forces on the B10 lift core ranged between 25m and 34m long and had been designed to resist jacking forces up to nearly 770 tonnes. As a result of the jacking forces on the B10 slab, additional 3D settlement analyses were undertaken and indicated maximum settlements up to approximately 5mm; a portion of this is in addition to the estimated settlements under the compressive building loads.

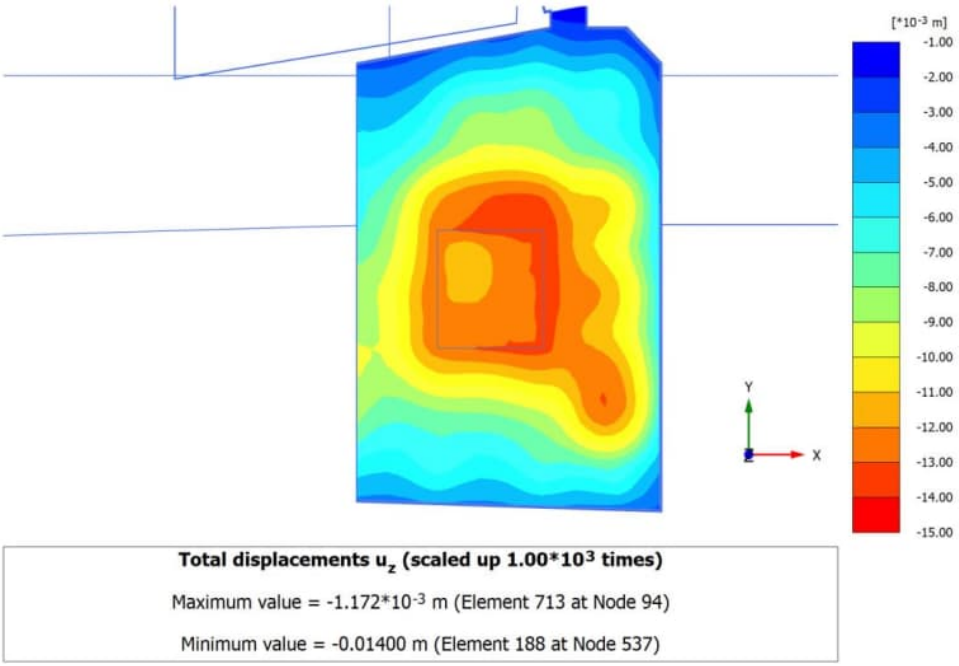

Figure 11: Heatmap of vertical settlement on the B9 & B10 hydrostatic slabs for a load combination of 1G + 1Q

The design head of water dictated the design of the micro-piles and vertical rock anchors to restrain the B9 & B10 hydrostatic slabs against uplift pressures. The design head of water was RL9.2m, which corresponds to a 1 in 100 year flood event with an additional 500mm freeboard. This level was similar to the original ground surface level across the site.

Prior to the commencement of the micro-pile and rock anchor design (completed by others), and in an effort to reduce the design head of water which was considered overly conservative, a detailed rainfall analysis of daily and antecedent rainfall (2 day to 90 day) events was prepared from available rainfall records for the period between 1 January 1832 and 28 March 2022. The rainfall data was obtained from the Bureau of Meteorology's (BOM) rainfall records for their nearby monitoring stations. A Gumbel probability plot showing the predicted return period for daily and antecedent rainfall events in Parramatta was prepared and is shown in Figure 12 below.

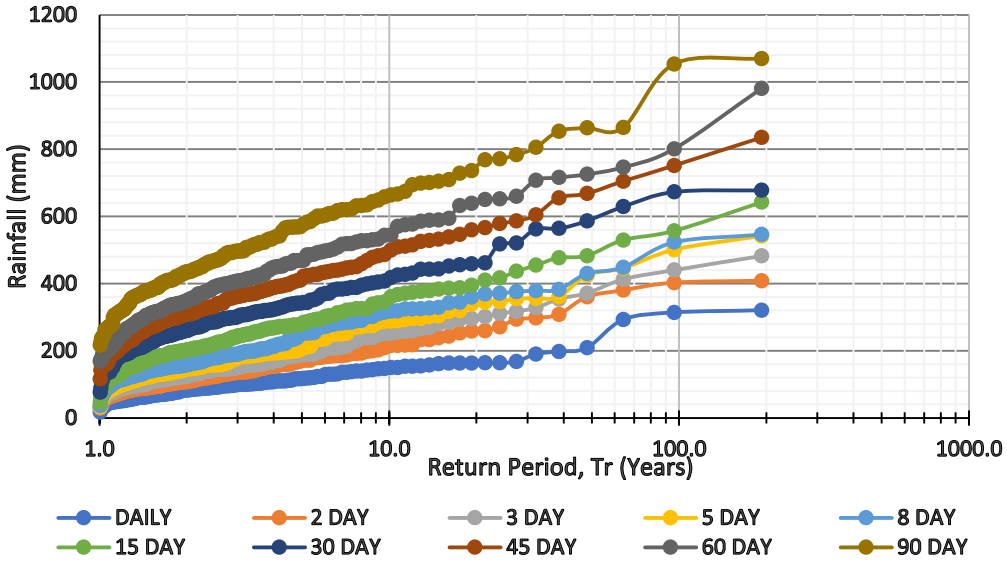

Figure 12: Probability plot of actual rainfall and antecedent rainfall between 1 January 1832 and 28 March 2022

Table 5 presents the long-term groundwater level data obtained from the three standpipe piezometers installed around the perimeter of the site against the return periods of various rainfall events.

Table 5: Historical daily and antecedent rainfall events during the groundwater level monitoring period

Date	Rainfall (mm)	Rolling Total No. of Days	Return Period (Years)	Highest Groundwater Level Recorded During Rainfall Event (RL mAHD)		
				JK107	JK108	JK109
10/2/2020	158.0	1	13.7	5.45	4.07	3.07
10/2/2020	260.0	2	21.3	5.45	4.07	3.07
10/2/2020	311.0	3	24.0	5.45	4.07	3.07
10/2/2020	360.6	5	38.4	5.45	4.07	3.07
14/2/2020	382.6	8	38.4	5.45	4.08	3.09[(2)]
17/2/2020	416.6	15	24.0	5.45	4.08	3.09[(2)]
9/3/2022	529.6	15	64.0	5.18	3.42	3.42
14/2/2020	462.0	30	21.3	5.45	4.08	3.09[(2)]
19/3/2022	586.8	30	48.0	5.74[(1)]	3.42	3.56
17/3/2020	515.4	45	12.0	5.45	4.08	3.09[(2)]
28/3/2022	668.2	45	48.0	5.99[(1)]	3.42	3.56
16/3/2020	570.0	60	10.7	5.45	4.08	3.09[(2)]
28/3/2022	716.2	60	38.4	5.99[(1)]	3.42	3.56
28/3/2022	864.6	90	64.0	5.99[(1)]	3.94	3.66

[1] The elevated groundwater levels recorded in JK107 between 14 March 2022 and 8 April 2022 were considered to be at least partially influenced by a leaking sewer pipe located adjacent to the monitoring well, as well as from ponded water above the protective cast iron Gatic cover.

[2] No groundwater levels were recorded between 13 February 2020 and 23 November 2021 due to a damaged water level data logger.

From Table 5, the highest recorded groundwater level at the site was RL5.99m (i.e. JK107). This level was recorded during a 1 in 38.4 year, 1 in 48 year & 1 in 64 year rainfall event for 45, 60 & 90 day rolling totals, respectively. As outlined above, the highest recorded groundwater level in JK107 was considered to be partially elevated due to a leaking sewer pipe and ponded water, which may have infiltrated into the standpipe piezometer. Notwithstanding this, for the historical daily rainfall events and recorded groundwater levels presented in Table 5, it was postulated that a 1 in 100 year rainfall event at the subject site could temporarily raise groundwater levels up to a maximum of approximately RL7.0m.

Cognisant that rainfall and flood events are different, there was no evidence based on the 3 years of groundwater level monitoring to suggest that groundwater levels (i.e. hydrostatic pressures) could rise above RL7.0m. It was further expected that groundwater levels across the site would be lower than any flood levels due to the relatively short duration of the flood events. Although there was significant evidence to suggest groundwater levels would not rise above RL7m, the design head of water for a 1 in 100 year flood event plus a 0.5m freeboard remained at RL9.2m, and the design of the micro-piles and vertical rock anchors to restrain the B9 & B10 hydrostatic slabs was carried out on this basis.

7 INSPECTION AND MONITORING PROGRAM

7.1 GEOTECHNICAL INSPECTIONS

Geotechnical inspections were completed during bulk excavation to: 1) identify potentially unstable wedges or blocks of rock that could detach from the vertically cut faces, 2) confirm the tower piles and internal slab thickenings were founded within sandstone bedrock suitable for the design ultimate bearing pressures, and 3) confirm the jet and rock grouting works were carried out in accordance with the design methodology.

During these inspections, the upper shear zone observed within the neighbouring basement excavation and confirmed during the detailed geotechnical investigation was encountered in the cut faces at the northern end of the basement excavation. The fractured, gouged and extremely weathered material within the shear zone was expected to soften and potentially spall/topple from the cut faces if left unsupported, both in the short and long-term. As a result, the upper shear zone was stabilised with reinforced shotcrete and rock bolts. Other potentially unstable blocks or wedges of rock that had been isolated by inclined joints and/or sub-horizontal partings, seams etc. were identified and removed from the cut faces, as necessary.

7.2 INSTRUMENTATION AND MONITORING

Regular inclinometer monitoring was carried out during and following the completion of bulk excavation, as outlined above. Load cells were also placed in three separate corner props (Prop No. S3 [Row 1], S7 [Row 2] and S9 [Row 3]) in the north-eastern corner of the site. The design working load of the props was 1215kN (S3), 1065kN (S7) and 2260kN (S9), respectively. Following their installation and during bulk excavation over the preceding months, the loads cells

indicated that the horizontal forces within the corner props were 75% (S3), 28% (S7) and 38% (S9) of their design working loads, possibly a result of the issues outlined in Section 6.3 above.

7.3 GEOTECHNICAL TESTING

Due to the heavily loaded tower columns and B10 lift core, six additional cored boreholes were completed from the B9 and B10 excavation levels in order to further assess the suitability of the foundation material (i.e. proof coring). Based on the results of the additional investigation, the foundation material below the B9 columns and B10 lift core was confirmed to comprise Class II/I sandstone, which was considered suitable for the design ultimate bearing pressure of 100MPa. A senior geotechnical engineer further inspected the footings prior to pouring concrete to confirm their bases had been adequately cleaned of all loose and water softened material.

8 CONCLUSIONS

This case study outlines many of the design and construction challenges that the project had encountered and were overcome, as well as touching on the numerical analysis of various structural elements and the inspection and monitoring program.

Numerical back analysis of the shoring system has been carried out due to the variability in the predicted and measured lateral displacements in order to better assess the ground-structure interactions. The overestimation of the predicted lateral displacements of the shoring walls and horizontal forces in the corner props is not unexpected due to the high surcharge loads applied behind the back of the shoring walls, the use of a long-term concrete modulus, a stiffer rock mass than initially assessed, and the possibility that some of the assumed 'locked in' insitu stresses had already been released, both in geological time (i.e. Parramatta River and through the shear zones) and in the past few years (i.e. due to the adjacent basement excavation).

9 ACKNOWLEDGEMENTS

The authors wish to acknowledge the significant contribution of the design team from Coronation Property, MN Builders (MNB), Robert Bird Group (RBG), Menard Oceania, BSA, WSce and JKG. In particular, the success of this project was in part attributed to the expertise provided by Andy Nahas, Domenic Pagano and Thomas Pagano of MNB, Mitch Starkey formerly of RBG, Mehdi Hajian formerly of BSA, Preneshin Govender and Belinda Madin of WSce, as well as Adrian Banks, Christopher Gorton, Howard Hughes, and Nick de Bie.

CRediT authorship contribution statement

Michael Egan: Formal analysis, Writing – original draft. **Andrew Jackaman:** Writing – review and editing. **Ali Parsa-Pajouh:** Writing – review and editing.

10 REFERENCES

Bertuzzi R., 2014. Sydney sandstone and shale parameters for tunnel design, *Australian Geomechanics Journal*, Vol 49, No 1.

Bracegirdle, A., Mair, R.J., Nyren, R.J. and Taylor, R.N., 1996. A methodology for evaluating potential damage to cast iron pipes induced by tunnelling, Geotechnical Aspects of Underground Construction in Soft Ground, pp. 659-664.

Egan, M., Jackaman, A. and Parsa-Pajouh, A., 2023. Geotechnical Challenges of a Deep Excavation in a Congested Urban Area, A Case Study from 8 Phillip Street, Parramatta, New South Wales. Proceedings of the 14th Australia and New Zealand Conference on Geomechanics.

McQueen L. B., 2004. Insitu Rock Stress and Its Effect in Tunnels and Deep Excavations in Sydney, *Australian Geomechanics Journal*, Vol 39, No 3.

Pells P. J. N., Mostyn G., and Walker B. F., 1998. Foundations on Sandstone and Shale in the Sydney Region, *Australian Geomechanics Journal*, Vol 33, Part 3.

Vorster, T.E.B., Klar, A., Soga, K. and Mair, R.J., 2005. Estimating the effects of tunnelling on existing pipelines, Journal of Geotechnical and Geoenvironmental Engineering, 131(11), pp.1399-1410.

Vorster, T.E.B., 2009. Designing for the effects of tunnelling on buried pipelines. Proceedings of the 17th International Conference on Soil Mechanics and Geotechnical Engineering, pp. 1842-1847.

NATURAL HAZARD PROTECTION? SURE!

Tested to the world's toughest standards and beyond, our systems provide the level of protection you need. Whether from rockfall, landslides, debris flows, or coastal erosion. Whether standard or special solutions. Learn more: **www.geobrugg.com**

MANUFACTURED IN **AUSTRALIA**

Geobrugg Australia Pty Ltd
300 Victoria Road | Malaga WA 6090
T +61 8 9249 9939
www.geobrugg.com.au

Regional offices
Sydney NSW, T +61 400 845 289
South Melbourne VIC, T +61 488 044 708
Brisbane QLD, T +61 488 044 003
Perth, WA +61 477 470 064

BRUGG
Geobrugg

Safety is our nature

IMPACT OF ZERO BOND TO ROCK ON SHOTCRETE LINING DESIGN

Erik Stefan Bernard[1] and John C. Braybrooke[2]

[1.] *Institute for Sustainable Industries and Liveable Cities (ISILC), Victoria University, Werribee, Australia*

[2.] *Douglas Partners, Geotechnical Consultants, Sydney, Australia*

https://doi.org/10.56295/AGJ6116

ABSTRACT

Shotcrete linings usually achieve good bond to the underlying rock substrate when first applied during construction. This bond usually remains sound through many years of service. However, in some cases the bond may be inadequate or diminish with the passage of time causing the lining to detach from the substrate. To prevent detachment, and possible collapse in these circumstances, a shotcrete lining needs to be secured in place using a secondary means of attachment which, in the case of linings on hard rock, usually comprises rock bolts with external cover plates or spider plates on the ends of bolts. The potential causes of bond loss are many both prior to spraying and in service. Testing of bond strength frequently leads to apparent 'zero bond' results that may reveal an actual absence of bond or may be an outcome of the coring and testing process. If bond is relied upon in design it is important to consider the significance of zero bond results rather than simply dismiss them as artefacts of the testing process. This paper considers how partial or total bond loss can be considered in shotcrete lining design.

1 INTRODUCTION

Shotcrete linings on hard rock tend to be relatively thin. This is because their function is usually limited to supporting potentially unstable ground between adjacent rock bolts and possibly acting as a canopy for diversion of groundwater to drains. Since rock bolts act as primary support to the ground, the structural loads imposed on the shotcrete lining are relatively small. Nevertheless, the lining is often required to support its own weight in addition to a small surcharge associated with locally unstable ground and excess groundwater pressure, while remaining serviceable throughout the design life of the tunnel (usually 100 years). Shotcrete is also frequently used for patch repairs and local coverage of features such as drains.

The capacity of a lining to support the relatively minor loads imposed on it can be enhanced if bond to the ground is maintained. Based on the method of shotcrete lining analysis described by Barrett and McCreath (1995), the governing mode of load resistance for a lining that is bonded to competent hard rock is likely to be shear in most cases. This is because flexural failure is highly unlikely when the lining is bonded to and acts in composite action with the substrate. To ensure a shear-based failure mode, satisfactory bond to the ground must be confirmed. This is normally done by testing the in situ bond strength between the lining and substrate at selected points throughout the works. However, experience has indicated that the measured in situ bond strength often falls below the required minimum, partly due to the inherently high variability in results, but also due to an apparent absence of bond in some locations evidenced by the high incidence of 'zero bond' results.

Zero bond results may indicate an actual absence of bond (e.g., Figure 1) or may be due to the coring and testing process. Simply dismissing zero bond results as an artefact of the testing process is an unconservative approach that would never be tolerated for other structural parameters such as compressive strength. One therefore needs to consider the causes of zero bond more thoroughly and investigate the effect that an actual absence of bond has on the structural resistance of a shotcrete lining.

2 THE SIGNIFICANCE OF ZERO BOND RESULTS

The use of pattern bolting and shotcrete has long been a common form of ground support in tunnels with authors such as Barton et al (1974) and Bieniawski (1974) summarising extensive case histories relating the degree of support required to various rock mass classification systems. These papers high-light that very thin (50mm +/-) layers of shotcrete are widely used in better rock mass conditions. The introduction of fibre reinforced shotcrete as a replacement for mesh reinforced shotcrete was accompanied by a change toward a more deterministic method of lining design and thickness estimation. Such an approach to the design of lining thickness was described by Barrett & McCreath (1995) who stated:

> "If adhesion is maintained, then the failure of the shotcrete will be controlled by direct shear. If adhesion is lost…then, and only then, does the flexural failure mechanism become kinematically possible".

Figure 1: Examples of delamination zones evident in core holes a) inside shotcrete, and b) at the shotcrete/substrate boundary, leading to zero bond strength results.

For the case of a shear-based resistance mode, the zone immediately around a loaded area is taken to support the load through direct tension between shotcrete and ground at the boundary around the unstable rock (Figure 2). Thus, shear failure of the lining will only occur if adequate bond in direct tension is present. If bond is inadequate the lining will suffer adhesion loss followed by failure in bending.

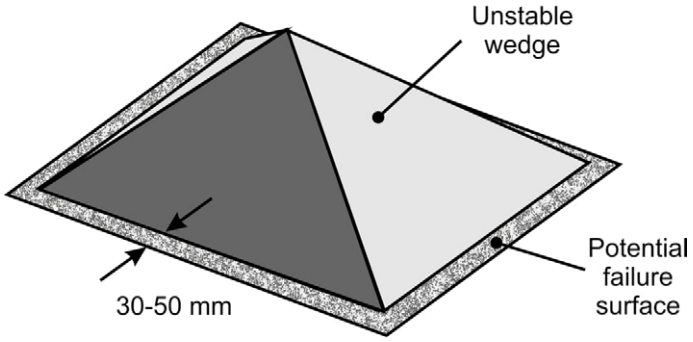

Figure 2: Bond failure zone around falling wedge, according to Barrett and McCreath (1995) based on work by Fernandez-Delgrado et al (1975) and Holmgren (1987).

The significance of adhesion is illustrated by the following example in which lining capacity is assessed according to the method by Barrett and McCreath (1995). For a lining of thickness t and orthogonal bolt spacing s, with shotcrete shear strength τ, the direct shear resistance V around a square failure zone (Figure 2) is found as

$$V = 4\tau st \quad (1)$$

The punching resistance V_p around surface-mounted bolt cover-plates or bolts with a positive means of attachment to the shotcrete such as mesh or handle-bar plates, is found as

$$V_p = 4\tau t(p + t) \quad (2)$$

where p is the plate perimeter length. In contrast, the flexural load resistance will depend on the moment resistance m of the shotcrete, which can be expressed as

$$m = f_t t^2/6 \quad (3)$$

for a flexural strength of f_t (taken at either first crack or post-crack). If the load is taken to act as a point load at the centre of a square yield-line failure zone, the load resistance P_{PL} will be

$$P_{PL} = 16m \quad (4)$$

but if the load is taken to act as a Uniformly Distributed Load (UDL), the load resistance P_{UDL} will be

$$P_{UDL} = 24m/s^2 \quad (5)$$

where the failure zone is taken to comprise a square with negative yield lines at the supports and positive yield lines across the diagonals. Importantly, the adhesive load resistance P_a along the perimeter of the unstable wedge is found as

$$P_a = 4sw_a f_b \quad (6)$$

where w_a is the width of the adhesion zone and f_b is the bond strength. It is presently assumed that the rock fails as a pyramid-shaped wedge with a 60° side inclination and density equal to 24 kN/m^3.

If we take τ = 2.0 MPa, f_t = 3.0 MPa, f_b = 0.5 MPa, cover plate side length to be 200 mm, and assume the adhesive width w_a around the unstable wedge to be equal to the thickness of the lining, we obtain the series of plots of Factor of Safety (FOS, based on unadjusted resistance/load) against bolt spacing s for the failure modes represented by Equations 1 to 6 shown in Figure 3. The direct shear resistance (solid black line) is clearly greater than the load to cause adhesive failure (red line) around the periphery of the unstable wedge. Punching around the cover plates offers a lower FOS but does not have an adhesive failure limit when the plates are on the outside of the shotcrete lining or are physically attached to the shotcrete. In contrast, the flexural modes of failure offer a lower degree of load resistance. For the case shown, adhesion to the substrate is maintained across the entire range of bolt spans so the lining can be taken to support the wedge in shear. However, there may be some problem with punching around the bolts for spacings greater than 2.2 m. Similarly, if the peripheral bond strength is diminished in some way then the likelihood of flexural failure is increased. A similar set of curves can be generated for other wedge shapes and failure zones.

The shear-based failure mode around unstable blocks and wedges observed by Fernandez-Delgrado et al (1975) and Holmgren (1987) (which subsequently formed the basis of the design method by Barrett and McCreath (1995)) requires that a satisfactory bond exists at the boundary to support the load. The ground load associated with an unstable wedge or block is supported by the bond at the shotcrete/rock interface around the perimeter of the loaded area (Figure 2). Holmgren (1987) approximated the highly loaded width of this zone to be about 30-50 mm while others have taken the critical width to be larger than this (Sjölander et al, 2021). If de-bonded areas exist within this highly loaded boundary zone, then only part of the perimeter is available to support the wedge or block. There is no way of identifying in advance whether the boundary of an unstable wedge will coincide with a de-bonded portion of a lining or not. It is therefore important that the *probable incidence* of de-bonded zones be identified, and that the impact of zero-bond areas be accounted for in estimating the average bond strength that can be used to calculate the carrying capacity of the lining.

As an example, assume that 100 bond tests are conducted in a length of tunnel lining using a laboratory-based test such as AS1012.24 [6] or the EFNARC Specification (1996). Assume 50% of the extracted cores produce a zero result (due either to an initial absence of bond or 'breakage' during drilling), but the remaining 50% of tests that resulted in an intact core indicate an average bond strength of 500 kPa. If the 'zero' results were, in fact, the result of poor drilling that led to breakage of the cores, then the 500 kPa estimate of bond strength could be valid. However, if the drilling was conducted in areas where some of the shotcrete had de-bonded from the substrate prior to drilling, the average bond strength may be 250 kPa rather than 500 kPa. It is therefore necessary to record all incidences of 'zero' results whenever *in situ* pull-tests are conducted or cores are extracted for testing in the laboratory and attempt to identify the cause of each zero result.

Table 1: Incidence of zero results in published coring programs, and recent Australian projects.

Sources	Method	Age	Surface Prep.*	No. of Cores	Zero results (%)
Malmgren et al (2005)	SS137342	2 yr	Grinding	45	44
	SS137342	2 yr	Hydro-scaling	25	12
NIOSH (2010)	Custom	7 d		185	5
Holter (2015)	Custom	14 d	Grinding	80	0
Sandstone	SS137342	17 yr	Grinding	85	53
	EN1542	17 yr	Grinding	24	50
	AS1012.21	4 yr	Grinding	127	53
	SS137342	4 yr	Grinding	28	78

* Surface preparation before testing

As shown in Table 1, the frequency of zero results can be very high and, as a consequence, will affect the average bond strength if the zero values are attributable to actual de-bonding of the lining. The data in Table 1 also suggests that the incidence of zero bond results increases with the age of the lining possibly indicating that a time-dependent process such as drying shrinkage or thermo-hygral cycling could be responsible for the apparent age-dependent bond loss.

3 SIZE EFFECT FOR BONDED LININGS

Shotcrete, rock, and the boundary between them are all quasi-brittle materials that are affected by the presence of flaws (whatever their scale). Fracture science has shown that as the size of a loaded member increases, it is more likely that points of weakness will exist within the zone subject to tensile stress with the result that the apparent mean strength will fall (Neville, 1996; Bažant and Planas, 1998; Pan et al, 2022). The high incidence of zero bond results obtained in field testing indicates that bond strength is a parameter that exhibits both considerable variability and frequent points of weakness (Table 1). Unfortunately, all the bond tests presently available for shotcrete linings were conducted using specimens of about the same size (64-75 mm diameter). It is therefore difficult to identify a size effect using these results. However, Shu et al (2024) conducted laboratory tests on samples of young concrete cast against old concrete to examine the relation between various factors and size effect. They found that for direct tension specimens of between 70 and 200 mm cross-sectional width there was an approximate 45 percent fall in mean tensile strength between the smallest and largest specimens for relatively smooth interfaces. Based on a Weibull model of statistical size effect, this would extrapolate to a 48 percent fall in tensile strength for members with a 1000 mm cross-sectional length relative to a 100 mm core test. If a Bažant model of energy-based size effect is used, then the fall in mean tensile strength will be about 53 percent for a 1000 mm wide tension zone compared to a 100 mm core test (2024).

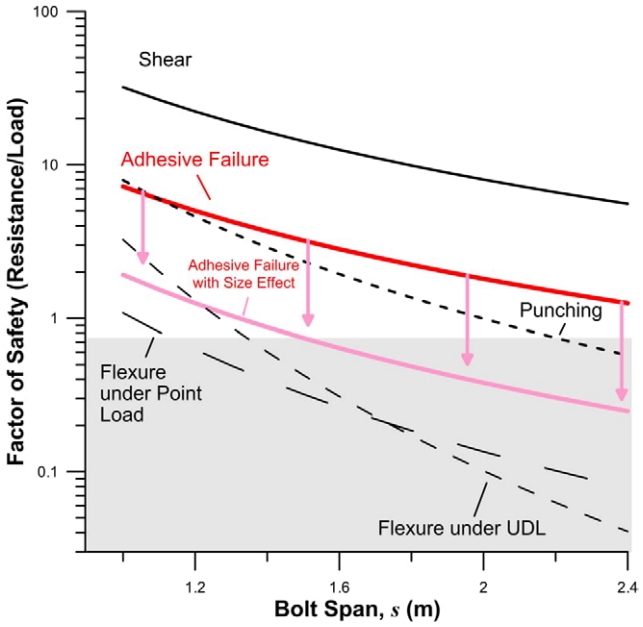

Figure 3: Factor of Safety on failure by various modes for a 75 mm thick shotcrete lining of between 1.0 and 2.4 m bolt span, calculated using method by Barrett and McCreath (1995).

As described later in this paper, there are numerous potential causes of zero or near-zero bond strength at the shotcrete/substrate boundary so their occurrence cannot be dismissed. Local flaws will diminish the effective bond strength of a large area of shotcrete loaded in tension. When local flaws affecting strength are present it is appropriate that size effect be accounted for by factoring down the mean bond strength obtained in tests as the size of the loaded boundary between shotcrete and substrate increases. For engineering assessments of bond in shotcrete linings we are generally not concerned with differences between statistical size effect, energy-based size effect, and other phenomena, thus a relatively simple size effect model is most appropriate. For a limited data set of bond specimens, the size-corrected tensile bond strength f_b for a wedge falling through a shotcrete lining (as per the Holmgren tests (1987) and Barrett and McCreath design method (1995)) can be approximately related to the apparent bond strength f_{test} obtained in testing by the simple expression $f_b = \alpha f_{test}$ in which α is a size correction factor of the form:

$$\alpha = \left(\frac{l}{l_0}\right)^{-\frac{1}{n}} \quad (7)$$

where l is the length of the side of an unstable wedge, l_0 is a characteristic reference length (e.g. the diameter of a tensile test core), and n is about 3 (see Bažant and Planas, 1998) depending on the characteristics of the process under consideration (for example, the heterogeneity of the material, the rate of strain, and duration of loading). Clearly, the proportion of 'zero bond' results obtained in bond tests on specimens of differing size will strongly influence the magnitude of n but insufficient information is presently available to determine the exact magnitude of n. Nevertheless, as an example, if $n = 3$ one can estimate that a bonded area of 1000 mm side length exhibits an average tensile strength f_b about 0.42 times the mean apparent tensile strength f_{test} obtained for a 75 mm diameter core extracted from the same area. Thus, using this bond strength adjusted for size effect the load to cause adhesive failure around an unstable wedge will be diminished, as shown by the pink line in Figure 3. In this case, when the bolt spacing exceeds 1.5 m, the lining will experience adhesion loss and flexural failure will occur in the lining.

The form of the size effect relationship for shotcrete bonded to a rock substrate should be examined in greater detail when more comprehensive information about the incidence of zero bond results and the effect of size becomes available.

4 THE SIGNIFICANCE OF ADHESIVE FAILURE

The widely used method of lining design by Barrett and McCreath (1995) is based on falling block tests conducted by Holmgren (1987) and Fernandez-Delgrado et al (1975). These tests examined the behaviour of shotcrete linings in response to the intrusion of falling blocks into a tunnel space. Some of their tests extended to examination of post-peak behaviour in which the bond strength in the zone around the periphery of a falling block was exceeded, a process now known as 'adhesive failure'. All such tests resulted in a rapid fall in load resistance as the shotcrete lining around the falling block proceeded to peel off the substrate. Following bond failure, the laboratory linings resisted load purely in flexure as they spanned between the edge of the falling block and the nearest point of support (such as a rock bolt, see Figure 4a). Since the flexural resistance of shotcrete linings is usually relatively low compared to shear resistance, the onset of adhesive failure leads to strongly deflection-softening behaviour and may result in the falling block breaking through the lining.

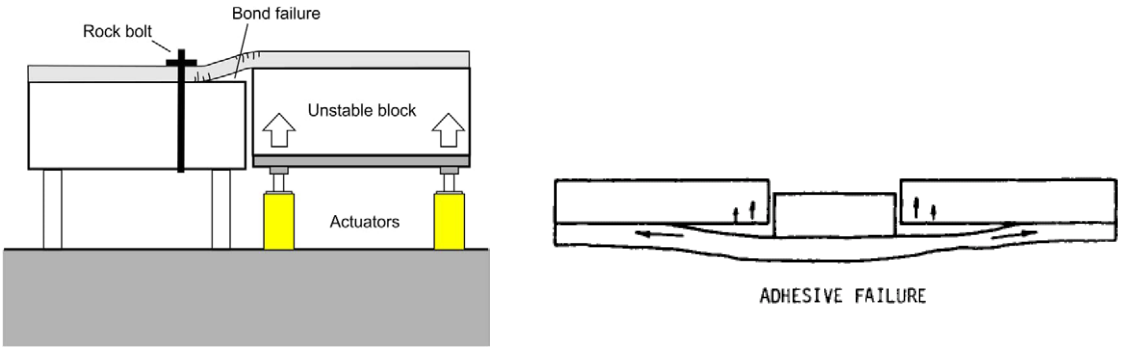

Figure 4: a) Adhesive failure in falling block test used by Holmgren (1987) to assess shotcrete lining capacity, and b) Fernandez-Delgrado et al (1975) tests to assess shotcrete lining capacity.

Adhesive failure primarily involves separation of the lining and substrate by peeling action (Figure 4b). Peeling is the process by which tensile failure occurs at an adhesive surface that is eccentrically loaded. Eccentric loading is known to have a deleterious effect on the apparent tensile strength of concrete; that is why bond tests such as EN1542 and SS137243 have been developed to eliminate eccentric loading and achieve an 'optimal' bond strength estimate (see the Appendix for a more detailed discussion of available bond test methods and their limitations). However, ground loads are usually applied to shotcrete in an eccentric manner with the result that a peeling mode of failure is more likely than direct tension. Moreover, peeling is more likely to occur at an interface of regular geometry (typical of excavations made using a road header or TBM) than irregular geometry (such as blasted rock surfaces) because geometrically regular surfaces exhibit fewer physical obstacles to the propagation of a long splitting crack.

The significance of peeling is that the load resistance that can be sustained by a lining suffering peeling-based adhesive failure is much lower than can be expected if the load was supported in direct tension at the bonded interface. Although tests of peeling resistance between concrete surfaces are rare, peeling between concrete and bonded fibre board has been

examined by several researchers and found to result in an approximate 80-90% fall in apparent tensile bond strength compared to direct tension (Dai et al, 2007; Alam et al, 2012; and Zhang 2014). It is therefore reasonable to conclude that a lining subject to adhesive failure will support very little residual load at the substrate boundary and instead will primarily resist load through flexure between the falling wedge and points of anchorage (such as rock bolts with plates on the outside of the shotcrete, handle-bar plates, etc).

The bond strength at the shotcrete/substrate interface in regions beyond the 30-50 mm wide boundary around a falling wedge cannot be relied upon for residual support due to the low resistance of the peeling mode of failure that would be induced in these areas. Moreover, it is self-evident that a pre-existing de-bonded area adjacent to a falling wedge will degrade the load resistance of the lining because it will promote peeling action rather than resistance in direct tension. For these reasons, the magnitude of bond strength achieved at the periphery of a potentially unstable block must be maintained during the life of a lining. Zones of de-bonded lining will increase the likelihood that an unstable block will coincide with low-resistance zones thereby increasing the likelihood of a flexural mode of failure. Since it is not possible to predict in advance where zones of weak bond may exist, it is prudent to control this risk by either applying a size effect factor to the bond strength or designing the entire lining as if no bond exists anywhere at the shotcrete/substrate boundary.

5 POSSIBLE CAUSES OF POOR BOND

Bond between shotcrete and a substrate such as rock is achieved by chemical and physical means as soon as the shotcrete is sprayed onto the surface. Long-term bond is created by hydration of the cementitious components within shotcrete paste forming tensile linkages with the substrate material, and by physical interlock between the hardening cement and the rough substrate surface. Under ideal conditions, the high speed of impact between an impinging jet of shotcrete and the substrate combined with the relatively high strength typically achieved by a shotcrete paste produce a bond between lining and substrate of between 0.5-2.0 MPa in direct tension (Hahn and Holmgren, 1979). However, the actual bond strength achieved will vary with many factors, including the composition and surface roughness of the substrate, the strength of the shotcrete and substrate, cleanliness of the substrate, and quality of spraying. If bond is relied upon for effective operation of a lining or retention of local shotcrete features such as patch repairs or drains, it is important that the designer understands the factors that influence long term retention or loss of bond to the substrate.

5.1 DISRUPTION OF BOND DURING CONSTRUCTION

There are numerous factors that can potentially reduce or eliminate the bond between shotcrete and its substrate during construction. Based on the authors' many years of experience in lining construction and inspection, these detrimental factors can be summarised as:

Insufficient cleanliness of the substrate. Even though the rock is usually washed prior to spraying it is inevitable that there will be some areas which will remain contaminated with dust and other unconsolidated material that limit the development of effective bond.

Surface contamination with oils, other hydrocarbons, or set accelerator. This often occurs during spraying due to leaks from machinery and poor control of accelerator.

Variations in the *roughness of the substrate*. This depends on rock type and excavation techniques. Friable rocks such as shale or schist will exhibit very poor adhesion due to fragmentation within the rock.

Deleterious *mineral composition* of the substrate. In rock, the presence of clay, mica, talc, or chlorite minerals may lead to expansive reactions or poor adhesion, resulting in degraded bond strengths.

Poor spraying technique. The spraying nozzle should always be perpendicular to the substrate surface and at an optimum distance from the surface, normally between 1-2 metres. However, if in some areas the nozzle happens to be further away the shotcrete will impact the substrate at a lower velocity thus affecting adhesion. In other areas where the nozzle is too close the shotcrete will exhibit excessive rebound. Both these processes can diminish the bond achieved.

Seepage of groundwater from the rock. Groundwater seepage should be controlled and channelled away from the area of work prior to the application of shotcrete to the substrate. Excessive groundwater that is not channelled away may compromise adhesion in that area.

Excessive dosage of set accelerator in the shotcrete can have a substantial detrimental effect on bond. Excessive use of set accelerator can also produce layers of weak shotcrete within the lining (Figure 1) that act both as potential delamination surfaces and channels for water ingress through the completed lining. Excessively accelerated shotcrete that hardens before it impacts the substrate is more likely to bounce off and interfere with the motion of trailing airborne concrete particles further reducing the effectiveness of compaction.

Poor mixing of the supplied concrete that creates lenses of hydration stabiliser or paste-free material within the as-placed material can lead to sloughing and detachment of wet shotcrete.

Poor mix designs that lead to low cohesion within the shotcrete also diminish bond to the substrate; this can cause internal detachment of the wet lining from the substrate (which is hard to detect) or fall-outs.

Bond disruption may also occur due to ground movement in the vicinity of the newly sprayed shotcrete lining. Ground movement may be caused by relief of pre-existing stresses in the ground because of excavation of the tunnel space, or by break out of the ground or nearby temporary shotcrete structures as part of the excavation process. For example, the practice of spraying a primary shotcrete lining close to the face during double- or triple-heading excavation sequences and then breaking out parts of the temporary shotcrete to complete the excavation is highly likely to disrupt the bond between the ground and the adjacent primary lining. Similarly, a heading and bench excavation in a high horizontal stress environment will cause additional convergence of the sidewalls. In an excavation with a flat roof this can induce pressure within a thin shotcrete lining in the roof, causing it to shear or buckle. In these circumstances it is prudent to either remove the compromised shotcrete and apply a new lining to the rock or include a secondary means of attachment between the primary shotcrete lining and ground (such as handle-bar plates or spider plates on the ends of the rock bolts) to anticipate the bond disruption likely during the excavation sequence. Surface preparation techniques also influence the achievement and retention of bond in local repairs (Bissonette, et al, 2012; Reny, 2013).

Regardless of the cause, the outcome of bond disruption is areas of low or non-existent bond between the shotcrete lining and substrate that can affect the load resistance and serviceability of the lining. The size of de-bonded areas can range from a few square centimetres to several square metres.

5.2 BOND DISRUPTORS SPECIFIC TO ROAD HEADERS

There are several phenomena that occur during excavation of ground using road headers that warrant special attention. Each of these phenomena are associated with the characteristic grooves that are left in the surface of the rock following excavation by road header (Figure 5).

*Formation of Cracks in Grooves***.** The high compressive stress applied to the rock face at the tip of each excavation pick can generate cracks within the rock that remain after the pick has passed. These cracks can then act as initiation points for the growth of larger cracks if the face of the rock is subject to sustained tensile stress.

*Rock Flour in Grooves***.** The high compressive stress acting at the tip of each excavation pick can also grind the constituents of the rock into a flour that remains as a loose surface coating to the more competent rock underneath. Recent investigations of mature shotcrete linings on sandstone excavated by road header have revealed grooves in the substrate filled with silica flour. This material requires careful cleaning to remove but this clearly does not occur in all cases.

*Accumulation of Over-spray in Grooves***.** Even if the surface of the excavated rock is carefully cleaned prior to spraying, the spraying process itself can lead to over-spray associated with the shotcrete jet accumulating as loose debris in adjacent grooves (Figure 5). This over-spray consists of small loose particles that rapidly dry out and form an unconsolidated layer at the base of each groove that later acts as an initiation point for cracks.

5.3 IN-SERVICE DISRUPTION OF BOND

Even if good bond is initially achieved between shotcrete and substrate, in-service conditions can degrade the magnitude of bond strength or extend the size of existing de-bonded regions. Among the most important contributing factors to in-service bond disruption are:

Ground movement. On-going ground movement following the initial re-distribution of stress that accompanies excavation may occur in some cases due either to nearby excavations or changes in ground conditions such as time-dependent loss of strength of thin layers under stress (Oliveira and Diederichs, 2017) or creep of highly stressed ground.

Drying shrinkage. Shotcrete exhibits a high degree of inherent drying shrinkage that is often made worse by poor curing practices. Experience has shown that most shotcrete tunnel linings experience significant shrinkage cracking. Differential shrinkage between the surface and interior parts of a lining can induce curling at cracks and other boundaries that may lead to de-bonding (Sjölander and Ansell, 2017). This is a slow process that can take years to manifest itself.

Thermohygral Cycling. Seasonal variations in temperature and humidity can drive thermal or moisture gradients between a shotcrete lining and its substrate that generate shear stresses at the boundary between these elements. This type of

environmental cycling can exacerbate crack widths (Holter, 2015) and promote progressive de-bonding by a similar mechanism to that associated with drying shrinkage (Silfwerbrand, 1997).

Chemical and physical degradation of the shotcrete or substrate. Excavating a tunnel through ground introduces oxygen to a previously anaerobic environment. This will lead to chemical changes, including acidification of some minerals, that may subsequently attack the shotcrete lining and substrate rock. The shotcrete may also chemically interact with the ground because of the introduction of an alkaline material to a previously acidic environment. Both these processes can potentially reduce the magnitude of the bond strength achieved early in the life of a lining.

Crystal growth in the zone between lining and substrate. The drained nature of most tunnels, and the drying environment typical of many tunnels with forced ventilation, act to draw moisture out of the surrounding ground. Dissolved minerals such as mirabilite, epsomite, and halite can thereby be transported from the ground to the tunnel lining with this moisture. Upon evaporation, the expansive pressure associated with growth of crystals precipitating from solution can steadily destroy porous materials and prise a lining away from its substrate (Hunter, 2026).

Sustained Tension. Materials such as concrete exhibit a reduced tensile strength when loaded in sustained tension due primarily to the slow growth of cracks (Rüsch, 1960). If a significant tensile or shear stress is applied to a lining boundary for a sustained period of time the apparent bond strength will diminish.

Weak Planes in Substrate. The achievement of a strong bond to the substrate is of little value if the substrate itself includes de-bonded internal planes. This is often the case in layered rocks where weak strata (or bedding planes) may exist immediately inside an apparently competent surface. Thin layers of shale, mudstone, and other weak materials within an otherwise competent rock mass or schistose foliation can lead to low tensile strengths that render the bond between shotcrete and substrate irrelevant.

Any of these processes can take years to progressively de-bond a lining from its substrate, so the presence of a strong bond soon after construction does not guarantee that bond will persist throughout the life of a lining. The fact that so many potential degradation mechanisms exist supports the requirement for a means of effectively assessing bond at any point in the life of a shotcrete lining if bond is relied upon to support a load (including self-weight).

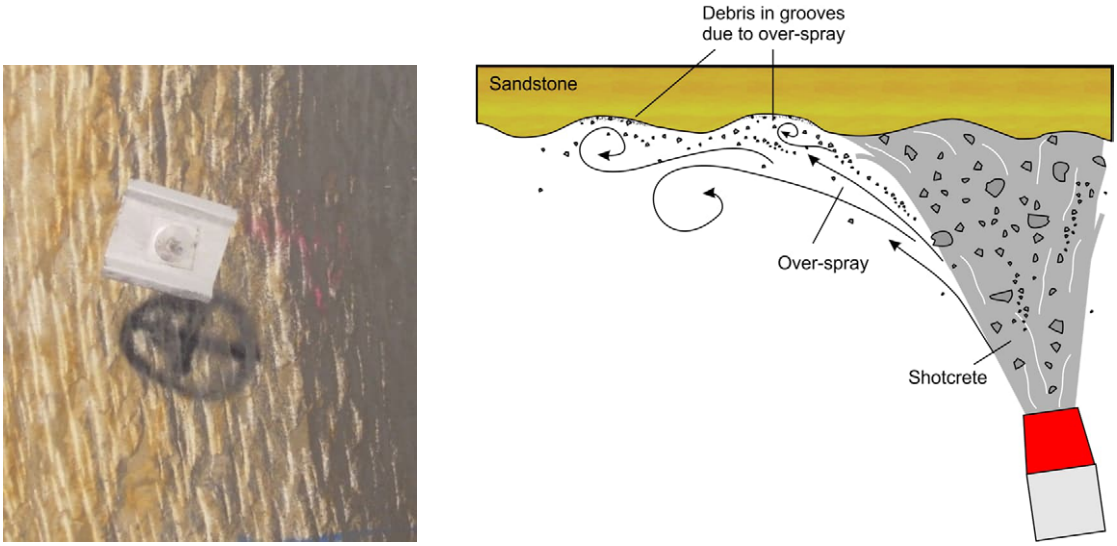

Figure 5: a) Accumulation of loose over-spray in pick grooves, and b) adjacent to an active spraying area.

6 THE INCIDENCE OF ZERO RESULTS

One of the realities of bond testing is the frequent occurrence of so-called ‘zero’ results. These ‘zero’ results may be caused by an actual absence of bond at the shotcrete/substrate boundary or may be caused by breakages induced by the drilling and testing process. The high frequency of ‘zero’ results is illustrated by the data in Table 1 which shows the zero rate in published studies and tests conducted in various tunnels.

When investigating bond strength every ‘zero’ result should be recorded and investigated to identify whether it indicates a true area of de-bonding or not. Hammer sounding prior to coring is useful in identifying whether de-bonded zones are likely to be present. If gaps are observed in the core hole either at the boundary with the substrate or within the lining

then the 'zero' result must be counted as valid (Figure 1). An endoscope may be useful for this purpose. Even if a gap is not visible at the substrate boundary, profuse dripping of water after coring may indicate that a narrow delamination plane exists.

As previously identified, zones of delamination or de-bonding may be associated with sand lenses within the shotcrete, sloughing of wet shotcrete, layers of excessive set accelerator dosage, ground movement, layers of dirt and debris that were not cleaned off prior to spraying, or other contaminants such as spillage of construction polymers or oils. These phenomena can often be identified by close examination of the broken surfaces of the extracted core. Each of these factors may not result in an actual gap within the shotcrete or at the substrate boundary but can produce a zero or near-zero bond strength result that must be included in any estimation of average bond strength.

Problems during drilling of a core can lead to breakage and an apparent 'zero' result even for very strongly bonded shotcrete. A poorly anchored drill rig can either shake or shift position during drilling, or the drill rig may be bumped or stop functioning properly, leading to a change in drill inclination and increase in friction during operation. Cores can also be broken when the drill barrel is withdrawn upon completion of drilling. While evidence of poor drilling may sometimes be found in the form of a wavy or discontinuous core barrel surface, it is seldom possible to be certain about the actual cause of breakage.

7 SUMMARY

Experience with bond measurement from numerous hard rock tunnelling projects has demonstrated that bond between a shotcrete lining and its substrate can be disrupted by many factors both during construction and over the service life of a lining. This can result in a high proportion of 'zero' bond results when conducting tests in the field. Considerable difficulty usually occurs in distinguishing whether these 'zero' results are artefacts of the sampling process or whether they represent true areas of de-bonding.

The high incidence of zero bond results in field testing raises concerns about the effect local flaws have on the effective tensile bond strength of a shotcrete lining around a potential falling rock wedge. Since bond to the substrate affects the mode of failure that the lining will exhibit in response to the falling wedge (shear or flexure), and these two modes of failure typical exhibit substantially different peak load resistance, the existence of areas of zero bond between a lining and its substrate can influence the load resistance of a lining.

Given the significance of de-bonding to load bearing capacity, the most effective means of addressing the difficulties of assessing and accounting for the high variability and frequent occurrence of 'zero' bond strength is to either account for de-bonding by including a size effect factor on bond strength, or assume that bond is non-existent and design all thin linings on hard rock to resist load primarily through bending rather than shear. As described by Barrett and McCreath (1995), this requires points of attachment between the lining and rock to exist in the form of rock bolts with cover plates *over* the lining, or spider plates with adequate resistance to punching shear *within* the lining, so that the flexural resistance of the lining can be exploited.

CRediT authorship contribution statement

Erik Stefan Bernard: Conceptualisation, Formal analysis, Writing - original draft. **John C. Braybrooke:** Data curation, Investigation, Writing – review & editing.

REFERENCES

Alam, M.S., Kanakubo, T., and Yasojima, A., 2012. "Shear-Peeling Bond Strength between Continuous Fiber Sheet and Concrete", *ACI Structural Journal*, V. 109, No. 1, January-February 2012, pp75-82.

ASTM C1583, "Standard Test Method for Tensile Strength of Concrete Surfaces and the Bond Strength or Tensile Strength of Concrete Repair and Overlay Materials by Direct Tension (Pull-off Method)", ASTM International, West Conshohocken, PA.

ASTM D7234, "Standard Test Method for Pull-Off Adhesion Strength of Coatings on Concrete Using Portable Pull-Off Adhesion Testers", ASTM International, West Conshohocken, PA.

Australia Standard AS1012 "Methods of testing concrete, Part 24: Determination of the tensile bond strength of concrete - Repairs and strengthening systems", Standards Australia, Sydney.

Barrett, S. & McCreath, D.R., 1995. "Shotcrete Support Design in Blocky Ground - Towards a Deterministic Approach", *Tunnels and Deep Space*, 10(1), pp79-88.

Baźant, Z.P. and Planas, J., 1998. *Fracture and Size Effect in Concrete and Other Quasibrittle Materials*, CRC Press, Boca Raton.

Bissonnette, B., Vaysburd, A.M. and von Fay, K.F., 2012. "Best Practices for Preparing Concrete Surfaces Prior to Repairs and Overlays", *Report Number MERL 12-17*, U.S. Department of the Interior, Bureau of Reclamation.

British Standard EN 1542, "Products and systems for the protection and repair of concrete structures – Test methods – Measurement of bond strength by pull-off", British Standards Institute.

Dai, J., Ueda, T. and Sato, Y., 2007. "Bonding Characteristics of Fiber-Reinforced Polymer Sheet-Concrete Interfaces under Dowel Load", *Journal of Composites for Construction*, ASCE, Vol. 11, No. 2, April 1, 2007.

EFNARC, 1996. *European Specification for Sprayed Concrete*.

EFNARC, 1999. *European Specification for Sprayed Concrete*, Guidelines for Specifiers and Contractors.

Fernandez-Delgrado, G., Mahar, J.W., and Parker, H.W., 1975. "Structural Behavior of Thin Shotcrete Liners Obtained from Large Scale Tests", *Shotcrete for Underground Support*, Proceedings of the Engineering Foundation Conference, Tidewater Inn, Easton, Maryland, USA, October 4 - 8, 1975, ACI Publication SP-54. pp399-442.

Hahn, T. and Holmgren, J. 1979, "Adhesion of Shotcrete to various types of Rock Surfaces", in *Proceedings of the 4th International Congress on Rock Mechanics*, Montreux, pp421-429.

Holmgren, J., 1987. "Bolt-anchored, steel-fibre-reinforced shotcrete linings", *Tunnelling and Underground Space Technology*, Vol. 2, Issue 3, pp319-333

Holter, K.G., 2015. "Performance of EVA-Based Membranes for SCL in Hard Rock", Rock Mechanics and Rock Engineering, DOI 10.1007/s00603-015-0844-5

Hunter, A., 2025. "Management of Acid Sulfate Rock in a Sydney Road Tunnel", *Australian Geomechanics Journal*, Vol. 60, No. 1, pp37-58.

ISO 4624, 2023. "Paints and varnishes — Pull-off test for adhesion", *International Organization for Standardization*, Geneva.

Malmgren, L., Nordlund, E. and Rolund, S., 2005. "Adhesion strength and shrinkage of shotcrete," *Tunnelling and Underground Space Technology*, 20, pp33–48.

Neville, A.M., 1996. *Properties of Concrete*, Fourth Edition, Longman.

Norwegian Concrete Association, 2015. "Sprayed Concrete for Rock Support". *Publication No. 7*.

Oliveira, D. and Diederichs, M.S., 2017 "Tunnel support for stress induced failures in Hawkesbury Sandstone", *Tunnelling and Underground Space Technology*, Vol. 64, April, pp10-23.

Pan, J., Zhong, W., Wang, J., and Zhang, C., 2022. "Size effect on dynamic splitting tensile strength of concrete: Mesoscale modelling", *Cement and Concrete Composites*, Vol. 128, April 2022, 104435.

Reny, S., 2013. "Surface Preparation for Shotcrete Repair", *Shotcrete*, Spring 2013, pp28-30.

Rüsch, H., 1960. "Researches Toward a General Flexural Theory for Structural Concrete", *Journal of the American Concrete Institute*, 57-1, July 1960, pp1-28.

Seymour, B., L. Martin, C. Clark, M. Stepan, R. Jacksha, R. Pakalnis, M. Roworth, C. Caceres, 2010. "A Practical Method of Measuring Shotcrete Adhesion Strength," *Materials Science*, pp1-9.

Shu, Y., Shen, Z., Zhang, H., Gan, L., Xu, L., Sun, Y., Yu, J., and Wang, R., 2024. "Size effect on tensile bonding strength between new and old concrete", *Journal of Building Engineering*, 97, 110739.

Silfwerbrand, J., 1997. "Stresses and strains in composite concrete beams subject to differential shrinkage", *ACI Structural Journal*, Vol. 94, No. 4, pp347-353.

Sjölander, A. and Ansell, A., 2017. "Numerical Simulations of Restrained Shrinkage Cracking in Glass Fibre Reinforced Shotcrete Slabs", *Advances in Civil Engineering* Volume 2017, Article ID 8987626, pp11

Sjölander, A., Ansell, A. and Malm, R., 2021 "Variations in rock support capacity due to local variations in bond strength and shotcrete thickness", *Engineering Failure Analysis* 128, 105612.

Swedish Standard SS137342, "Concrete testing - Hardened concrete, shotcrete and plaster - Adhesion strength", Swedish Institute for Standards, Stockholm.

Zhang, W., 2014. Study on Bond and Peeling Characteristics between CFRP Plates and Concrete under Fatigue Loading, *Master's Thesis*, University of Tsukuba.

APPENDIX

BOND ASSESSMENT METHODS

Given the numerous possible causes of bond degradation outlined in this paper, and the significance of bond loss to lining behaviour, it is often necessary to quantify the degree of de-bonding that may arise or quantify the magnitude of bond strength remaining to support potentially unstable ground especially if shear resistance is relied upon in the lining. Methods of detecting and measuring bond strength have therefore been developed and are described below.

A1.1 HAMMER TESTING

Tapping the surface of a shotcrete lining to detect hollow internal zones is a partially effective means of identifying de-bonded zones but is prone to subjectivity and error. The method is sometimes known as the Norwegian Hammer method of sounding because it was first described in the Norwegian Concrete Association Publication No. 7 titled "Sprayed Concrete for Rock Support". It involves tapping the surface of a shotcrete lining with a light hammer and listening for 'drumminess'. Unfortunately, there are spurious causes of drumminess (such as the presence of drainage elements within the lining or delamination of the underlying substrate) and different operators vary in their opinion of what constitutes a drummy sound. Despite this, there is general agreement that a drummy sound is an indicator that de-bonding may be present.

A1.2 BOND STRENGTH MEASUREMENT

While hammer testing can identify areas of de-bonding, it cannot identify the magnitude of bond strength. To measure bond strength it is necessary to conduct a pull-test on a sample that includes the shotcrete/substrate boundary.

Bond strength is commonly assessed between concrete and overlying membranes such as floor coverings and shotcrete. Test methods for floor coverings (such as bonded flooring materials) are more widely used than for shotcrete so the tests and equipment used for shotcrete have often been adapted from test methods originally developed for floor coverings and repair media. The most common methods used for these applications include EN 1542, ASTM C1583, and ASTM D7234 which are all primarily used to assess overlays and repairs to a concrete surface. These tests are carried out *in situ* and numerous manufacturers have developed equipment which can be used to conduct this test. However, these methods are primarily intended to test geometrically smooth and regular surfaces, so the proprietary equipment available for this test method usually cannot accommodate the uneven surfaces typical of shotcrete linings. Similarly, ISO 4624 is an internationally recognised method used to measure the adhesive strength of paints and varnishes on various substrates using a metallic dolly with pivoting pin. For a concrete substrate, it recommends a sample diameter of 100 mm. In contrast to these in situ tests, AS1012.24 is an Australian standard that involves drilling a core through a concrete overlay and into the substrate to extract an intact core that is subsequently tested in tension in a laboratory. Several variants of this method exist in other countries.

Test procedures specific to the assessment of the tensile strength of shotcrete bonded to a substrate include the EFNARC European Specification for Sprayed Concrete, 1996 (Section 10.6). This specification covers the assessment of the tensile strength of shotcrete bonded to a substrate, but it lacks detail regarding how the procedure is actually implemented. Oddly, it includes both *in situ* testing and laboratory testing of an extracted sample but does not preference either. This procedure was followed by a second edition in 1999 that differed in several respects from the 1996 edition but introduced the recommendation for a minimum of six cores to be tested 'from the same general area of the works' to calculate one estimate of bond strength.

Swedish Standard SS137342 is the only actual standard in existence specifically for testing the bond between a layer of shotcrete and its substrate. It differs significantly from earlier guidelines and specifications in that it requires a double-core bit to drill an over-sized round groove around the primary core so that a chuck can be mounted concentrically over the sample to be pulled (Figure A1). This method is more detailed and better thought-out than the EFNARC specification for ensuring that eccentric loading is eliminated from the load train.

Figure A1: In situ testing of bond strength using a) drilled concentric core holes, b) mounting of a glued dolly to the end of a partially drilled core, and c) pull-testing, similar to the SS137243 test method.

The method by Seymour et al (2010) is not a standard but is a recommendation produced by NIOSH in North America. It uses a pull-pin drilled and glued into the end of a partially drilled core instead of the tension chuck required by SS137243 but is otherwise very similar to the Swedish method.

As part of research conducted into the behaviour of shotcrete sprayed over a waterproofing layer, Holter (2015) used a variation on the method by Seymour et al (2010) and ISO 4624 that incorporated an abrasive disk to grind a flat reference surface into the shotcrete face around the core. A concentric jack was then placed on the perpendicular surface to pull the core via a central pin and measure *in situ* bond strength (Figure A2). Expanding pins and epoxy grouting of the pin are both possible.

In general, the methods listed above can be divided into *in situ* tests, which are all based on pull-tests of a core drilled through the boundary between shotcrete and substrate, and laboratory-based tests in which an intact core sample comprising both the shotcrete lining and substrate is extracted and moved to a laboratory and tested in tension after preparation of the ends. Among the *in situ* tests, some use a dolly (or 'rondell') comprising a round metallic disk bonded to the end of the core to exert tension during testing, while others rely on an expanding pin or threaded metallic pin glued into a hole drilled through the centre of the core (usually before coring) to impart tension. The pin-based method avoids the problem of debonding due to a weak surface on the face the shotcrete, while the dolly-based method avoids potential breakage of the core due to splitting. The pin-based method is probably superior for longer cores (with a length/diameter greater than unity) while the dolly method is better for thin linings in which the length/diameter ratio is less than unity. When using a dolly it is necessary to grind away the weakest surface layers of shotcrete before starting the process of coring and gluing.

A1.3 CORE BREAKAGE

The laboratory-based tensile tests of bond strength suffer the problem that the core must be broken off at some point in the substrate so the sample can be extracted for transportation to the lab. This is almost always done by hammering a wedge into one side of the core slot, which introduces an eccentric load to the core resulting in flexural failure. This can lead to breakage at the shotcrete/substrate boundary for weakly bonded specimens, after which the sample cannot be tested. Thus, a positive bias is introduced into the statistical record because the weaker bond strength samples end up being discarded due to breakage and are thereafter excluded from further consideration.

Similarly, cores that break off during coring cannot be tested using either the *in situ* or laboratory-based methods. These samples are then discarded and seldom recorded as 'zero' results. It is usually quite difficult to determine whether a core that supposedly 'broke' during drilling was, in fact, broken off as a result of the drilling process, or was de-bonded from the substrate prior to drilling. This ambiguity may be partially clarified by tapping the surface before drilling to detect drumminess, but an absence of drumminess does not confirm the presence of bond because small areas of de-bonding often do not sound drummy. Even if a weak bond is present, the elimination of weak specimens by 'breakage' during drilling introduces a positive bias to the population of surviving samples.

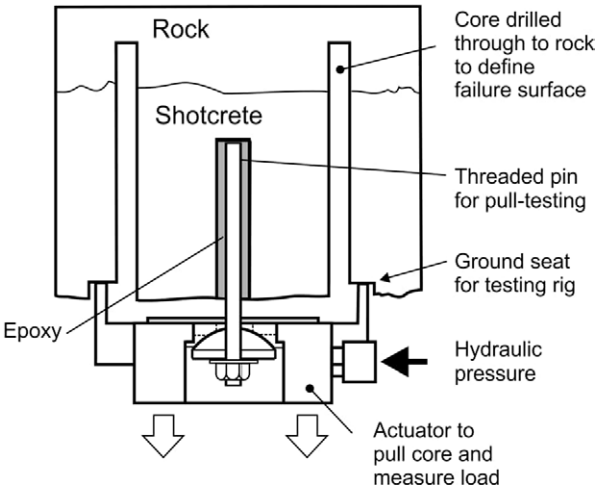

Figure A2: Test configuration similar to that described by Holter (2015) for pull-testing with drilling and surface grinding completed prior to installation of pull-pin in central hole.

The 1999 EFNARC recommendation (Section G9.5) for six samples to be tested in 'the same general area of the works' to calculate one estimate of bond strength does not provide any guidance on whether to include 'zero' results in the average bond strength estimate or not. The common practice in the field is to assume 'zero' results are caused by drilling problems, discard these samples, and keep drilling until the required number of non-zero results or intact samples are obtained. This clearly introduces a positive bias to the distribution of recorded results.

AGS Members' Photography

AUSTRALIAN GEOMECHANICS SOCIETY

You too can publish your photos in *Australian Geomechanics*

We are inviting all our members to submit photos for publication in Australian Geomechanics to showcase the top class work being undertaken in our industry.

All selected photos will be published with acknowledgment of the photographer, their affiliation and with a caption describing the photo.

If you would like to promote your project and your work in this way, please submit your high resolution digital images via email to our Editor at: editor@australiangeomechanics.org

Please include:

- Name of the Photographer.
- Affiliation of the Photographer.
- A caption describing the image.
- Authorisation from end client.

Our Editor will select photos for publication.

By submitting your photo, you grant your permission for the Australian Geomechanics Society to publish the photograph in *Australian Geomechanics*. The AGS Photography Release Form needs to be completed to formalise agreement. It will be provided if submissions are selected for publication.

Photographs selected for publication will be at the sole discretion of the Australian Geomechanics Society.

ERRATUM

Goodall, S.J. and Merifield, R. S. (2023). Working Platforms and Bearing Capacity Assessments of Sand Overlying Clay Using Finite Element Limit Analysis, *Australian Geomechanics*, Volume 58, Number 3, pp 117-139. [DOI: https://doi.org/10.56295/AGJ5835]

Please replace Tables 2, 3, 4 and 6 on pages 125, 126, 127 and 137 respectively:

Table 2: Values of ultimate bearing capacity ($q_u/B\,\gamma$) rough rigid footings φ' = 35 °

D/B	$s_u/\gamma B$	Ultimate bearing capacity ($q_u/B\,\gamma$)			
		Square Footing (*L/B* = 1.0)	**Rectangular Footing (*L/B* = 2.0)**	**Rectangular Footing (*L/B* =5.0)**	**Strip Footing (*L/B* = ∞)**
0.25	0.56	3.43	3.28	3.17	2.90
	1.11	5.78	5.75	5.64	5.31
	1.67	7.68	7.83	7.80	7.51
	2.22	9.48	9.97	9.97	9.60
	2.78	11.10	11.74	11.84	11.59
0.5	0.56	5.24	4.54	4.11	3.53
	1.11	7.71	7.06	6.68	5.96
	1.67	9.50	9.09	8.71	8.04
	2.22	11.03	10.76	10.65	9.87
	2.78	12.41	12.14	12.25	11.57
1.0	0.56	12.21	9.27	7.41	5.61
	1.11	15.43	12.50	10.40	8.46
	1.67	17.53	14.72	12.97	10.72
	2.22	18.73	16.63	14.88	12.55
	2.78	19.46	17.47	16.75	14.22
2.0	0.56	18.93	19.11	18.44	11.84
	1.11	18.53	19.11	19.10	15.99
	1.67	18.64	18.37	18.62	16.67
	2.22	18.67	18.81	19.39	16.57
	2.78	18.65	19.13	20.27	16.55
Uniform Sand	-	18.98	19.06	18.92	16.53

Table 3: Values of ultimate bearing capacity ($q_u/B\,\gamma$) rough rigid footings φ' = 40 °

D/B	$s_u/\gamma B$	Ultimate bearing capacity ($q_u/B\,\gamma$)			
		Square Footing (*L/B* = 1.0)	**Rectangular Footing (*L/B* = 2.0)**	**Rectangular Footing (*L/B* =5.0)**	**Strip Footing (*L/B* = ∞)**
0.25	0.56	4.03	3.73	3.44	3.17
	1.11	6.92	6.60	6.28	5.85
	1.67	9.57	9.29	8.88	8.38
	2.22	11.95	11.71	11.55	10.88
	2.78	14.18	14.11	13.91	13.21
0.5	0.56	6.93	5.59	4.82	4.01
	1.11	10.22	8.88	8.03	6.85
	1.67	13.26	11.67	10.62	9.59
	2.22	15.74	14.77	13.01	12.04
	2.78	17.87	16.57	15.69	14.40
1.0	0.56	17.55	12.74	9.28	6.69
	1.11	23.92	17.53	13.61	10.39
	1.67	27.79	21.31	17.27	13.55
	2.22	31.68	24.77	20.60	16.35
	2.78	34.73	27.16	23.35	18.99
2.0	0.56	55.80	39.00	25.58	14.45
	1.11	54.17	51.31	34.55	20.97
	1.67	55.06	50.87	40.84	26.21
	2.22	56.79	52.35	46.20	29.81
	2.78	54.60	52.66	49.93	33.51
Uniform Sand	-	54.81	50.12	49.05	40.91

Table 4: Values of ultimate bearing capacity ($q_w/B\gamma$) rough rigid footings φ' = 45 °

D/B	$s_w/\gamma B$	Ultimate bearing capacity ($q_w/B\ \gamma$)			
		Square Footing (*L/B* = 1.0)	**Rectangular Footing (*L/B* = 2.0)**	**Rectangular Footing (*L/B* =5.0)**	**Strip Footing (*L/B* = ∞)**
0.25	0.56	4.63	4.12	3.78	3.37
	1.11	8.12	7.36	6.90	6.29
	1.67	11.17	10.55	9.92	9.04
	2.22	14.35	13.48	12.64	11.88
	2.78	17.26	16.35	15.68	14.58
0.5	0.56	8.71	6.66	5.48	4.50
	1.11	13.24	10.73	9.18	7.78
	1.67	17.24	14.49	12.81	10.89
	2.22	20.65	18.08	15.90	13.76
	2.78	24.10	20.90	18.68	16.64
1.0	0.56	24.23	16.56	11.56	7.83
	1.11	33.18	23.66	17.43	12.32
	1.67	40.43	29.34	22.13	16.27
	2.22	46.99	33.88	26.22	19.54
	2.78	52.69	37.76	30.15	23.29
2.0	0.56	88.12	53.79	33.58	17.44
	1.11	119.00	75.77	46.82	25.71
	1.67	138.97	88.43	56.74	32.40
	2.22	154.82	99.95	64.86	38.26
	2.78	164.78	108.82	71.78	43.62
Uniform Sand	-	193.57	160.25	141.75	112.51

Table 6: Summary of input and results for Fundex 3500 piling rig example

Inputs	Input Values	
	Load Case 1	**Load Case 2**
Applied Pressure	261 kPa	270 kPa
Design Length, L	3.5 m	2.9 m
Width of Load, B	0.9 m track width	1.3 m padfoot width
Thickness of Platform, D from BRE (2004)	First pass check ~ 1 m (based on BRE (2004))	First pass check ~ 1 m (based on BRE (2004))
L/B	3.9 (check L/B = 2.0 to 5.0)	2.2 (check L/B = 2.0)
D/B	1.1 (check D/B = 1.0)	0.77 (check D/B = 0.5 to 1.0)
φ'	45°	
γ	21 kN/m^3	
s_u	15 kPa	
$s_u/\gamma B$	0.79	0.55
$q_u/B\gamma$	~ 14.2 to 19.8	~ 6.6 to 16.5
q_u	~ 270 kPa to 370 kPa This is noting that L/B is 3.9, using linear interpolation indicates an ultimate bearing capacity of about 330 kPa. This gives a FoS of about 1.26 which would not be considered acceptable for Load Case 1 if using the BRE (2004) loading factors as a guide.	~ 180 kPa to 450 kPa This is noting that D/B = 0.77, using linear interpolation indicates an ultimate bearing capacity of about 325 kPa. This gives a FoS of 1.20 which would be considered acceptable for Load Case 2 if using the BRE (2004) loading factors as a guide.
Summary	The proposed thickness of 1 m is not considered suitable for Load Case 1, and consideration should be given to increasing the thickness. By trial and error it can be shown that a working platform of about 1.2 m thickness would satisfy a minimum FoS of 1.6, which would normally be accepted for Load Case 1 (if using BRE (2004) load factors as a guide).	

The online version of the paper accessible from australiangeomechanics.org has been corrected and is available for download.

Please note that this is a typographical error only and the charts and conclusions within the paper based on these tables are not affected.

The authors sincerely apologises to the readers for the error.

JOIN THE AUSTRALIAN GEOMECHANICS SOCIETY

AUSTRALIAN GEOMECHANICS SOCIETY

Visit the Australian Geomechanics Society website to learn more about under-graduate and post-graduate student membership:

https://geomechanics.org.au/become-an-ags-member/

Geomechanics is the application of engineering and geological principles to the behaviour of the ground and ground water and the use of these principles in civil, mining, offshore and environmental engineering in the widest sense.

The Australian Geomechanics Society was founded in 1970. Its origins lie in the National Committee of Soil Mechanics of the Institution of Engineers, Australia established in 1953 and the call for a corresponding society in rock mechanics. In 1973 the society was expanded to include the third discipline of engineering geology and has remained substantially unchanged since that date.

The society is affiliated with:

- International Association of Engineering Geology and the Environment
- International Society for Soil Mechanics and Geotechnical Engineering
- International Society for Rock Mechanics

The AGS produces *Australian Geomechanics* the newsletter and journal of the Society and specialty conferences, symposia, seminars and workshops, including the four-yearly ANZ Geomechanics conference. *Australian Geomechanics* is published four times a year. The AGS is jointly sponsored by the Institution of Engineers Australia and the Australasian Institute of Mining and Metallurgy.

EDITORIAL POLICY

Australian Geomechanics is published quarterly, in March, June, September and December, by the *Australian Geomechanics* Society. The magazine is edited and produced by the Australian Geomechanics Society. It provides a journal and news magazine for matters of interest to the Australian geotechnical community. The statements made or opinions expressed do not necessarily reflect the views of the AGS.

Whilst the authors of papers retain copyright, submission of a paper for publication implies that the author gives AGS permission to copy and distribute papers in hardcopy format as well as in electronic format. Furthermore, permission is given for the sale of individual papers or compilations by AGS to benefit AGS members as well as for the supply of paper abstracts to third parties so that papers can be catalogued and made findable in bibliographic databases.

All technical papers submitted to *Australian Geomechanics* should be accompanied by a signed AUTHOR DECLARATION FORM which can be downloaded from the AGS website: https://australiangeomechanics.org/wp-content/uploads/2019/05/AG-author-declaration-form.pdf

No technical paper will be processed unless the form is submitted.

Material will be accepted at any time and published in the next available issue.

The Editorial Panel of *Australian Geomechanics* seeks contributions for future editions. The following comments are offered to assist would-be contributors.

Contributions can include: refereed technical papers; technical papers or notes; or news items and reports.

Technical papers can be refereed to ensure that they are of a standard similar to those published in international geotechnical journals. Authors should aim for a maximum overall length of no more than 10 pages, although shorter papers or technical notes are particularly welcome. Authors should indicate if they want their submission to be refereed; the status of the paper will be indicated on publication.

Refereed technical papers should be original and:

- Papers on geotechnical engineering, engineering geology and environmental geomechanics. Papers should be topical, practically oriented and preferably of national interest. Case studies describing innovative geotechnical work are particularly encouraged.
- Papers on geotechnical or geoscience research undertaken in Australia or of relevance to *Australian Geomechanics*. These should clearly indicate their practical relevance and limitations.
- Authoritative reviews of aspects of geotechnical practice or aspects of geotechnical education.

Technical papers or notes can be: Items as above but submitted for rapid publishing. These will not be refereed but will be reviewed. They will be accepted at the discretion of the editorial panel. The intention is to provide a source for rapid dissemination of technical material to the geotechnical community.

- Discussions on papers published in previous editions.
- News items and reports can be: Items describing significant projects, instructive failures, conferences, courses or other matters of general interest to the Australian geotechnical community.
- Geotechnical book reviews.
- Letters to the Editor.

It is preferable for contributors to submit formatted text, tables and figures in electronic format using Microsoft Word on Windows or Mac compatible hardware. If containing equations a PDF file should also be submitted.

It is preferable that submitted papers are presented in a specific format, detailed below. Papers that have not been properly formatted prior to submission, and are provisionally accepted, will be returned to authors to address peer review comments and proper formatting. A formatted template for technical papers in *Australian Geomechanics* is available for download from the AGS website: https://australiangeomechanics.org/journal/editorial-policy/

Details of the correct journal format are:

- Single column format on A4 paper.
- Left and right margins of 20 mm.
- A top margin of 30 mm and a bottom margin of 25 mm.
- 10 point character size of Times New Roman font with single (normal) line spacing.
- Text should be formatted to have 6 pt after paragraphs and after headings.
- No indent at the beginning of paragraphs.
- Title of Paper in 14 point Times New Roman, bold, uppercase, and centred in column.
- Main headings numbered 1, 2, 3…. etc. in 12 point Times New Roman, bold, upper-case and centred in the column.
- Sub-headings numbered 2.1, 2.2, 2.3 … etc. in 10 point Times New Roman, bold, upper-case and left justified.
- Minor headings numbered 2.1.1, 2.1.2 … etc. in 10 point Times New Roman, bold, lower-case and left justified

- Items in bulleted or numbered lists should not be separated by a line, but should be indented by 10 mm.
- Formulae typed and numbered (1), (2), (3) … etc. and centred in the column.
- Captions for figures should be placed beneath the item and numbered Figure 1.
- Captions for tables should be placed above the item and numbered Table 1:
- Figures and tables should be referred to in the text as Figure 1, Table 1, etc.
- Figures and tables should be centred in the column.
- Do NOT use page numbers, these will be added later.
- In text citation according to the Harvard system of author (year) or (author, year) as appropriate. Multiple references should be separated by semicolons (author 1, year 1; author 2, year 2)
- References should be listed at the end of the paper in alphabetical order using the Harvard system: Author (year) title, publication, volume, pages, publisher with a 10 mm hanging indent and no blank line between each.
- Underlining should be avoided and symbols shown in italics.

FIGURES AND TABLES

All the journal is published in colour.

Where possible figures and tables should be placed at the correct position in the text. Figures should be imported into the document as a single image and not constructed in the word document. These should be sharp and of the correct size for incorporation into the finished document. The width of these must be less than or equal to the width of the text column (165 mm).

Where images are included in the paper they should be sent as a separate JPEG file to improve the picture resolution.

Photographs should preferably be good contrast gloss prints and of the correct size for incorporation directly into the copy. Please ensure that all such items are clearly marked to indicate position in paper.

EDITORIAL CONTACTS

The Editor is Hugo Acosta-Martinez, and the Editorial Panel consists of the Executive and State Chapter Representatives on the AGS National Committee.

The process of submission, peer review, discussion, re-submission, approval etc. of technical papers, is conducted using the peer review platform Scholastica. Technical papers should be submitted via:

Submit Manuscript button on the AGS Scholastica website:
https://ags.scholasticahq.com
or
Submit using Scholastica button on the AGS website:
https://australiangeomechanics.org/journals/

Correspondence other than submission of, and queries about, technical papers, may be emailed to:

Editor, *Australian Geomechanics*
E-Mail editor@@geomechanics.org.au

ADVERTISING RATES

Every three months, *Australian Geomechanics* reaches more than 2000 professional geotechnical engineers and engineering geologists spread throughout Australia. Most of these are associated with significant site investigations, construction and computer analysis. So *Australian Geomechanics* provides a very targeted delivery for advertising.

Advertising rates include GST and from the 1st January 2020 are:

SIZE*	ONE ISSUE	TWO ISSUES	FOUR ISSUES
Cover Page	$1330	$1920	$3330
Full Page	$1030	$1760	$2640
Half Page	$530	$990	$1320
Quarter Page	$300	$480	$740

The prices quoted are for advertisements supplied in digital form as print resolution (240dpi or more) PDF, JPG or TIFF files.

* Files should be supplied at correct size with at least 3 mm bleed for designs that print to the edge of the page.

A4 Portrait – Width: 210 mm x Height: 297 mm (+bleed)
Half A4 Landscape – Width: 210 mm x Height: 148.5 mm (+bleed)
Half A4 Column – Width: 105 mm x Height: 297 mm (+bleed)
Quarter A4 Column – Width: 105 mm x Height: 148.5 mm (+bleed)

Inserts into an individual mail-out of *Australian Geomechanics* can be accepted at a minimum charge of $1330 (including GST).

Advertising queries should be addressed to:

Sara Lanesman, Email: *lanesman@optusnet.com.au*

ADVERTISEMENT DESIGN

If required AGS can arrange the design of adverts for *Australian Geomechanics*. The advertiser shall provide logo (high resolution), heading, text content, other images (photos) and style guide (if advertiser has one), otherwise styles and colours will be made similar to company's website styles or other provided media.

AGS will provide 1-2 design options and allow for two revisions of the chosen concept.

AD SIZE	APPROX. MAXIMUM WORD COUNT	COST
Full Page	250	$350
Half Page	150	$250
Quarter Page	75	$150

If design is required, material should be submitted no later than the first business day of February for the March issue, May for June, August for September and November for the December issue.